ORNL-5422
Distribution
Category UC-77

Contract No. W-7405-eng-26

METALS AND CERAMICS DIVISION

HTGR FUEL RECYCLE DEVELOPMENT PROGRAM (189a 0H045)

General Support – Task 800

POSTIRRADIATION EXAMINATION OF RECYCLE TEST ELEMENTS FROM THE PEACH BOTTOM REACTOR

T. N. Tiegs and E. L. Long, Jr.

Date Published: December 1978

OAK RIDGE NATIONAL LABORATORY
Oak Ridge, Tennessee 37830
operated by
UNION CARBIDE CORPORATION
for the
DEPARTMENT OF ENERGY

DISCLAIMER

CONTENTS

POSTIRRADIATION EXAMINATION OF RECYCLE TEST ELEMENTS FROM THE PEACH BOTTOM REACTOR

T. N. Tiegs and E. L. Long, Jr.

ABSTRACT

The Recycle Test Elements were a series of tests of High-Temperature Gas-Cooled Reactor fuels irradiated in Core 2 of the Peach Bottom Unit 1 Reactor. They tested a wide variety of fissile and fertile fuel types of prime interest when the tests were designed. The fuel types included UO_2, UC_2, $(2Th,U)O_2$, $(4Th,U)O_2$, ThC_2, and ThO_2. The mixed thorium-uranium oxides and the pure thorium oxide were tested as Biso-coated particles only, while the others were tested as both Biso- and Triso-coated particles. The Biso coatings on the fissile kernels contained the fission products inadequately but on the fertile kernels they did so acceptably. The results from accelerated and real-time tests on the particle types agreed well.

In particles with kernels made of UC_2 the high-yield rare-earth fission products migrated out of the kernel and down the temperature gradient. In Triso-coated particles, these fission products accumulated at the SiC, which caused graphitization of the inner LTI and corrosion of the SiC.

Kernels made of UO_2 showed an unacceptable amount of migration up the temperature gradient. In Biso-coated particles kernels migrated at average temperatures as low as 1298 K (1025°C) and at burnups of 53.7% FIMA.

Slight amoeba was observed with kernels made of $(2Th,U)O_2$ irradiated at average temperatures of 1423 K (1150°C) and burnups of 21.7% FIMA. On the other hand, the $(4Th,U)O_2$ kernels showed no amoeba in any of the recycle test elements.

The ThC_2 particles performed adequately at moderate temperatures and burnups (<1523 K, 1250°C, and 3.0% FIMA), but amoeba was observed under more severe conditions. On the other hand, the ThO_2 kernels performed well and showed no amoeba, even at a highest average temperature of 1698 K (1425°C) and burnup of 3.1% FIMA.

---

1. INTRODUCTION

The Recycle Test Elements (RTE) were a series of tests of High Temperature Gas-Cooled Reactor (HTGR) fuel irradiated in Core 2 of the

Peach Bottom Unit 1 Reactor. The work was a cooperative effort between Oak Ridge National Laboratory (ORNL) and General Atomic Company (GA), as part of the National HTGR Fuel Recycle Development Program.[1] Fuel was fabricated for the RTE series by both ORNL and GA.[2–5]

The RTEs were designed to replace standard Peach Bottom Reactor Core 2 fuel elements. But in place of the annular fuel compacts, six graphite bodies contained the fuel rods in a "telephone dial" arrangement (Fig. 1.1). A detailed description of the design and assembly of the experiments is presented in ref. 2. Operation of the Peach Bottom Reactor[6] and irradiation of the RTE series[7–10] has been reported previously.

The fuels irradiated were those of prime interest at the time the tests were designed. These included both sol-gel oxide fuels fabricated at ORNL[3–5] and carbide fuels fabricated at GA.[2] Many changes have occurred in the HTGR recycle program since the RTE series was planned and the fuel fabricated.[11] Although most of the fuel

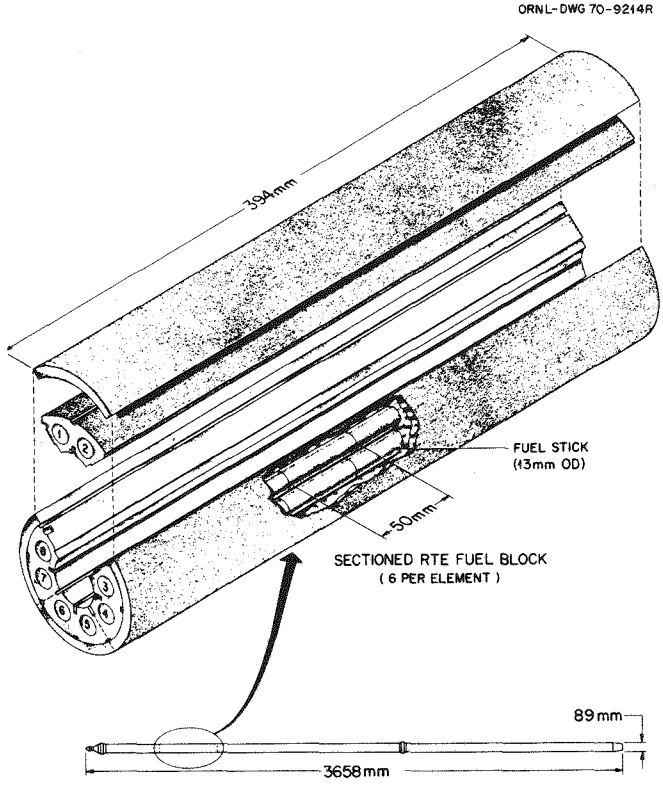

Fig. 1.1. Recycle Test Element Showing End View of Single Fuel Body.

types in the RTE series have been eliminated from consideration by results from irradiation testing under accelerated conditions, examination of the fuel was important because it was necessary to show that the results from real-time testing, that is, the RTE series, were comparable to those from accelerated testing of the same fuel.

A summary of the properties typical of the various particle batches is presented in Table 1.1. Detailed descriptions of the properties can be found in refs. 2 and 3. The particles were formed into fuel rods approximately 12.45 mm (0.490 in.) in diameter and 54.4 mm (2.14 in.) long by the slug-injection method. The matrix material for the ORNL fuel rods was 15V coal tar pitch mixed with approximately 35 wt % AXM or 35–40 wt % graphite flour. The coal tar pitch and graphite flour came from Allied Chemical Company and Poco Graphite, Inc., respectively. The matrix material used for the GA fuel rods was a blend of 27 to 30% natural flake graphite flour and 70 to 73% coal tar pitch.

After fabrication the green fuel rods were carbonized and heat treated by one of three methods. Some rods were carbonized and heat treated in individual graphite holders. Some were packed in graphite flour and placed in the graphite fuel bodies. And some were loaded directly into the fuel bodies, carbonized, and heat treated in place.

The irradiation and postirradiation examination schedule of the RTEs is outlined in Table 1.2. Elements RTE-2 and -4 through -8 were charged into the Peach Bottom Reactor on July 14, 1970. In April 1971, RTE-7 was withdrawn and RTE-1 (renamed FTE-11) was inserted; RTE-4 was withdrawn in April 1972. RTE-2 was withdrawn in September 1973 and the remaining elements were withdrawn after reactor operations ceased on October 31, 1974.

The postirradiation examination (PIE) of RTE-4 and -7 has been reported previously.[3,9,12] Summaries of the postirradiation examinations of the remaining elements have been published.[13,14] This report plus refs. 2 and 3 complete the reporting of the recycle test element program.

Table 1.1. Summary of Particle Characteristics From Recycle Test Elements

Particle Batch[a]	Kernel			Coater Type[b]		Buffer Coating		iLTI Coating			SiC Coating		oLTI Coating		
	Type	Mean Diameter (μm)	Density (Mg/m^3)	(mm)	(in.)	Mean Thickness (μm)	Density (Mg/m^3)	Thickness	Density (Mg/m^3)	BAF[c] or OPTAF	Mean Thickness (μm)	Density (Mg/m^3)	Mean Thickness (μm)	Density (Mg/m^3)	BAF[c] or OPTAF
PR-54	$(4Th,U)O_2$	343.2	10.10	130	5	72.1	1.103	N.A.[d]			N.A.		73.2	1.94	N.D.[e]
PR-55	$(4Th,U)O_2$	343.2	10.10	130	5	72.1	1.103	N.A.			N.A.		81.1	1.90	N.D.
PR-56	$(4Th,U)O_2$	355.0	10.10	130	5	73.5	1.101	N.A.			N.A.		129.1	1.91	N.D.
PR-57	$(4Th,U)O_2$	355.0	10.10	130	5	73.5	1.101	N.A.			N.A.		134.6	1.92	N.D.
PR-60	$(2Th,U)O_2$	352.9	10.18	130	5	76.3	1.159	N.A.			N.A.		123.2	1.91	N.D.
PR-61	$(2Th,U)O_2$	352.9	10.18	130	5	76.3	1.159	N.A.			N.A.		122.2	1.91	N.D.
PR-66	$(2Th,U)O_2$	347.1	10.02	130	5	87.0	1.72	N.A.			N.A.		128.6	1.86	N.D.
PR-67	$(2Th,U)O_2$	347.1	10.02	130	5	87.0	1.172	N.A.			N.A.		141.1	1.85	N.D.
Mixed 1,2,3	UO_2	75–125	∿10.5	38	1.5	∿54	∿1.4	N.A.			N.A.		∿60	1.89	N.D.
OR-1256 -1257 -1258	ThO_2	350–500	10.0	38	1.5	∿44	∿1.1	N.A.			N.A.		63	N.D.	N.D.
Mixed A	ThO_2	N.D.	N.D.	38	1.5	41–45	N.D.	N.D.			N.A.		60–74	1.99	N.D.
PR-47	ThO_2	409.7	9.96	130	5	55.6	1.26	N.A.			N.A.		77.1	1.93	N.D.
PR-48	ThO_2	409.7	9.96	130	5	55.6	1.26	N.A.			N.A.		62.2	1.94	N.D.
PR-50	ThO_2	390.9	9.89	130	5	51.4	1.33	N.A.			N.A.		70.9	1.91	N.D.
PR-51	ThO_2	390.9	9.89	130	5	51.4	1.33	N.A.			N.A.		69.8	1.91	N.D.
4000-307	UC_2	99	10.43			51	1.30	21	1.81	1.04	20	3.21	32	1.73	1.03
4000-309	UC_2	98	10.57			47	1.34	N.A.			N.A.		74	1.84	1.02
4000-274	UO_2	111	N.D.			∿70	N.D.	N.A.			N.A.		∿60	N.D.	<1.09
4000-306	ThC_2	384	8.86			48	1.13	23	1.85	1.05	23	3.20	41	1.79	1.04
4000-225	ThC_2	350	8.84			49	1.21	N.A.			N.A.		66	1.88	1.08
4000-226	ThC_2	356	8.80			58	1.17	N.A.			N.A.		71	1.88	1.06
4000-273	ThO_2	410	N.D.			55	1.26	N.A.			N.A.		75	1.94	<1.09
4000-325	UC_2	93	10.43			50	1.29	22	1.82	1.21	20	3.19	27	1.71	1.11
4000-340	UC_2	95	10.44			45	1.34	N.A.			N.A.		73	1.78	1.14
4000-355	UO_2	201	N.D.			53	1.29	27	1.79	1.21	23	3.20	37	1.80	1.07
4000-319	ThC_2	387	8.78			54	1.15	32	1.85	1.09	27	3.21	36	1.86	1.09
4000-323	ThC_2	351	8.78			56	1.24	N.A.			N.A.		67	1.85	1.10
4000-339	ThO_2	410	9.95			62	1.32	N.A.			N.A.		81	1.78	1.09

[a] Batches with numbers beginning with 4000- were fabricated by GA; all others were fabricated by ORNL.

[b] ORNL particles were coated either in a 0.13-m-diam (5-in.) coater bath or in a 0.05-m-diam (1.5-in.) coater bath using a core gas distributor.

[c] Bacon Anisotropy Factor (BAF.) or Optical Anisotropy Factor (OPTAF) for particles in RTE-1.

[d] N.A. signifies not applicable.

[e] N.D. signifies not determined.

Table 1.2. Irradiation and Postirradiation Examination Schedule of Recycle Test Elements

Element	Date Charged into Reactor	Date Discharged from Reactor	Postirradiation Examination Time Period	Equivalent Full-Power Days	Maximum Fast-Neutron Exposure, >0.18 MeV (n/m^2)	Maximum Fuel Burnup, FIMA (%)
RTE-1 (FTE-11)	April 1971	Oct. 1974	June 1976—Sept. 1976	650	3.0×10^{25}	49.6
RTE-2	July 1970	Sept. 1973	Dec. 1973—April 1974	701	3.1	45.6
RTE-4	July 1970	April 1972	July 1972—Dec. 1972	385	1.9	31.8
RTE-5	July 1970	Oct. 1974	Jan. 1976—May 1976	897	4.1	58.7
RTE-6	July 1970	Oct. 1974	July 1975—Nov. 1975	897	4.2	59.8
RTE-7	July 1970	April 1971	July 1971—Dec. 1971	525	1.2	20.0
RTE-8	July 1970	Oct. 1974	April 1975—July 1975	897	4.2	60.0

2. POSTIRRADIATION EXAMINATION OF RECYCLE TEST ELEMENT-7

Recycle Test Element-7 was irradiated in core location E10-06* of Peach Bottom Core 2 from 0 to 252 Effective Full-Power Days. This test element contained a variety of fissile and fertile fuel combinations, as summarized in Table 2.1. Results from an early examination have been reported previously.[3]

The irradiation conditions were analyzed under subcontract by GA. Summaries of the power history, heavy-metal burnup, and neutron fluence are presented in Tables 2.2, 2.3, and 2.4, respectively. The time-averaged temperatures and temperature envelopes for the entire element are presented in Figs. 2.1 through 2.8. Maximum burnup was 20% FIMA (Fissions per Initial Metal Atom); fast fluence (E >0.18 MeV) was 1.16×10^{25} n/m^2; and fuel temperature was 1575 K (1300°C).

From previous results[3] we concluded that the fuel particles all performed satisfactorily. The only indication of potential difficulty was the presence of numerous cracks in the outer Low-Temperature Isotropic coating (oLTI) of fuel rod RTE-7-3-7-3.* Additional metallography on the same particle type but at a lower flux position, that is, fuel rod RTE-7-5-5-5, showed no failed oLTI coating. The fast-neutron fluences (E >0.18 MeV) of the two positions differed: 1.16×10^{25} n/m^2 versus 0.78×10^{25} n/m^2. The cracks were evidently caused by fast-neutron-induced dimensional changes in the pyrocarbon.

Further metallographic examination revealed that a slight reaction had occurred at the interface between the inner Low-Temperature Isotropic coating (iLTI) and the SiC on the cold side of the fissile particles. This reaction formed graphite flakes that extended about 3 μm from the inner surface of the SiC into the iLTI. The reaction also resulted in a slight attack on the inner surface of the SiC layer to a depth of 1 to 2 μm. That this reaction appeared on the cold side of

---

*RTE-W-X-Y-Z: W = Experimental Test Element; X = Graphite Body in Element (1 Bottom, 6 Top); Y = Hole in Body; Z = Fuel Rod in Hole (1 Bottom).

Table 2.1. Fuel-Loading Scheme for Recycle Test Element-7

Body	Hole	Fissile Fuel		Fertile Fuel		Carbonization Procedure for Bonded Rods
		Particle Type	Batch	Particle Type	Batch	
1,2,3	1,2	UO_2 Biso	4000-274	ThC_2 Biso	4000-226	CGT[a]
	3,4	$(2Th,U)O_2$ Biso	PR-60	ThC_2 Biso	4000-225	PGF[b]
	5,6	UO_2 Biso	Mixed 2,3[c]	ThO_2 Biso	Mixed A	PGF
	7,8	UC_2 Triso	4000-307	ThC_2 Triso	4000-306	CGT
4	1,2	UO_2 Biso	4000-274	ThC_2 Biso	4000-226	CGT
	3,4	UO_2 Biso	Mixed 3	ThO_2 Biso	4000-273 (PR-47)	
	5,6	UC_2 Biso	4000-309	ThO_2 Biso	Mixed A	PGF
	7,8	$(2Th,U)O_2$ Biso	PR-60	ThC_2 Biso	4000-225	PGF
5,6	1,2	$(4Th,U)O_2$ Biso	PR-57-1, -6[d]	ThC_2 Biso	4000-225	PGF
	3,4	$(2Th,U)O_2$ Biso	PR-61	ThO_2 Biso	PR-48[e]	PGF
	5,6	UC_2 Triso	4000-307	ThC_2 Biso	4000-226	CGT
	7,8	UO_2 Biso	Mixed 2	ThO_2 Biso	PR-51	PGF

[a] Carbonized in covered graphite tray.

[b] Carbonized in packed graphite flour.

[c] Fuel stack RTE-7-3-5 was a combination of batches Mixed 2 and Mixed 3; fuel stack RTE-7-3-6 used batch Mixed 3; batch Mixed 2 was used in all others.

[d] Fuel stack RTE-7-5-2 used batch PR-57-6; all others used PR-57-1.

[e] Fuel rod RTE-7-5-4-1 was a combination of batches PR-47 and PR-50; all others used PR-48.

Table 2.2. Recycle Test Element-7 Power, Flow, and Flux History

Interval Reference Equivalent Full-Power Time		Thermal Analysis					Nuclear Analysis					
		Irradiation Interval[a]	Absolute Radial Power	Relative Padial Power	Coolant Relative Radial-Power Factor	TRICUSP Channel Flow	Real Time[b]	Gage Power	Flux in Groups[c] from Gage, n/m²s				
From EFPD	To EFPD	(d)	(kW)			(kg/s)	(d)	(kW)	1A[d]	1B	2	3	4
0.00	26.99	28.84	103.66	0.794	0.971	0.0316	28.84	103.66	3.66×10^{17}	0.64×10^{17}	7.27×10^{17}	1.20×10^{17}	3.87×10^{17}
26.99	62.71	38.84	104.71	0.802	0.981	0.0336	38.84	104.71	3.79	0.67	7.59	1.25	3.97
62.71	68.57	7.50	87.47	0.802	0.978	0.0325	7.50	87.47	3.20	0.56	6.40	1.05	3.39
68.57	202.06	140.94	106.62	0.807	0.985	0.0328	140.94	106.62	3.88	0.68	7.77	1.28	4.15
202.06	252.41	53.62	107.16	0.818	0.990	0.0343	60.00	95.78	3.50	0.62	7.08	1.16	3.99
Sum/Time-Weighted Average		269.74	105.60	0.807	0.984	0.0331	276.12	103.17	3.74	0.66	7.51	1.24	4.04
Root Mean Square			3.27	0.007	0.005	0.0008		5.00	0.18	0.03	0.34	0.06	0.15

[a] Time at nonzero power used in thermal analysis.

[b] Real calendar days used in nuclear analysis. Some short-term zero-power periods are included.

[c] *The energy ranges for the flux groups follow:*

Group 1A: 14.96 MeV ≥ E ≥ 0.18 MeV or 2.40 pJ ≥ E ≥ 28.84 fJ
Group 1B: 0.18 MeV ≥ E ≥ 8.65×10^4 eV or 28.84 fJ ≥ E ≥ 13.86 fJ
Group 2: 8.65×10^4 eV ≥ E ≥ 17.60 eV or 13.86 fJ ≥ E ≥ 2.82 aJ
Group 3: 17.60 eV ≥ E ≥ 2.38 eV or 2.82 aJ ≥ E ≥ 0.38 aJ
Group 4: 2.38 eV ≥ E ≥ 0 or 0.38 aJ ≥ E ≥ 0

[d] Group 1A, the fast-flux group, has been modified from the Gage output by a factor of 0.85. This accounts for the Peach Bottom energy cut-off of 8.65×10^4 eV instead of 0.18 MeV.

Table 2.3. Recycle Test Element-7 Burnup: Fissions per Initial Metal Atom

Fuel Body	Fuel Rod	Core Height (mm)	Fertile FIMA (%)	Fissile FIMA (%)	Mixed FIMA (%)
1	1	688	0.007	4.659	0.601
	2	742	0.020	7.594	0.987
	3	797	0.038	10.507	1.375
	4	851	0.059	13.407	1.764
	5	906	0.083	15.176	2.010
	6	960	0.106	16.740	2.230
Mean		824	0.052	11.347	1.495
Range/RMS		327	0.035	4.233	0.570
2	1	1082	0.126	17.620	2.360
	2	1136	0.145	18.358	2.471
	3	1190	0.160	18.829	2.544
	4	1244	0.173	19.200	2.603
	5	1299	0.183	19.488	2.649
	6	1353	0.189	19.689	2.680
Mean		1217	0.163	18.864	2.551
Range/RMS		325	0.022	0.706	0.109
3	1	1477	0.194	19.863	2.706
	2	1530	0.195	19.964	2.720
	3	1583	0.195	20.035	2.729
	4	1636	0.192	19.964	2.717
	5	1690	0.188	19.823	2.696
	6	1743	0.182	19.556	2.656
Mean		1610	0.191	19.868	2.704
Range/RMS		319	0.005	0.156	0.024
4	1	1873	0.175	19.258	2.612
	2	1927	0.168	18.936	2.565
	3	1981	0.160	18.553	2.509
	4	2035	0.152	18.151	2.451
	5	2089	0.143	17.695	2.385
	6	2143	0.133	17.220	2.315
Mean		2008	0.155	18.302	2.473
Range/RMS		324	0.014	0.700	0.102
5	1	2267	0.121	16.655	2.233
	2	2321	0.109	16.045	2.145
	3	2375	0.098	15.352	2.046
	4	2429	0.086	14.578	1.937
	5	2483	0.075	13.735	1.819
	6	2537	0.064	12.980	1.713
Mean		2402	0.092	14.891	1.982
Range/RMS		324	0.020	1.274	0.180
6	1	2664	0.053	12.258	1.612
	2	2718	0.039	11.566	1.511
	3	2772	0.026	10.876	1.412
	4	2825	0.017	10.212	1.319
	5	2879	0.009	9.552	1.228
	6	2933	0.003	8.898	1.139
Mean		2799	0.024	10.560	1.370
Range/RMS		323	0.017	1.147	0.161
Grand Mean		1810	0.113	15.639	2.096
Grand Range/RMS		2299	0.064	4.123	0.581

Table 2.4. Recycle Test Element-7 Fast- and Thermal-Neutron Fluences

Fuel Body	Fuel Rod	Core Height (mm)	Fluence, n/m^2	
			Fast, >0.18 MeV	Thermal, <2.38 eV
1	1	688	0.358×10^{25}	0.428×10^{25}
	2	742	0.503	0.538
	3	797	0.624	0.641
	4	851	0.734	0.741
	5	906	0.829	0.838
	6	960	0.905	0.929
Mean		824	0.659	0.686
Range/RMS		327	0.187	0.171
2	1	1082	0.972	1.015
	2	1136	1.027	1.086
	3	1190	1.070	1.138
	4	1244	1.106	1.177
	5	1299	1.128	1.196
	6	1353	1.144	1.211
Mean		1217	1.074	1.137
Range/RMS		325	0.060	0.068
3	1	1477	1.155	1.222
	2	1530	1.159	1.227
	3	1583	1.160	1.229
	4	1636	1.158	1.228
	5	1690	1.149	1.223
	6	1743	1.138	1.216
Mean		1610	1.153	1.224
Range/RMS		319	0.008	0.005
4	1	1873	1.123	1.206
	2	1927	1.103	1.192
	3	1981	1.079	1.174
	4	2035	1.051	1.150
	5	2089	1.022	1.119
	6	2143	0.991	1.081
Mean		2008	1.062	1.154
Range/RMS		324	0.046	0.043
5	1	2267	0.955	1.036
	2	2321	0.916	0.990
	3	2375	0.875	0.941
	4	2429	0.831	0.891
	5	2483	0.785	0.838
	6	2537	0.732	0.782
Mean		2402	0.849	0.913
Range/RMS		324	0.076	0.087
6	1	2664	0.678	0.728
	2	2718	0.626	0.678
	3	2772	0.559	0.628
	4	2825	0.487	0.583
	5	2879	0.406	0.544
	6	2933	0.299	0.514
Mean		2799	0.509	0.613
Range/SD		323	0.129	0.074
Total Mean		1810	0.884	0.954
Total Range/RMS		2299	0.257	0.253

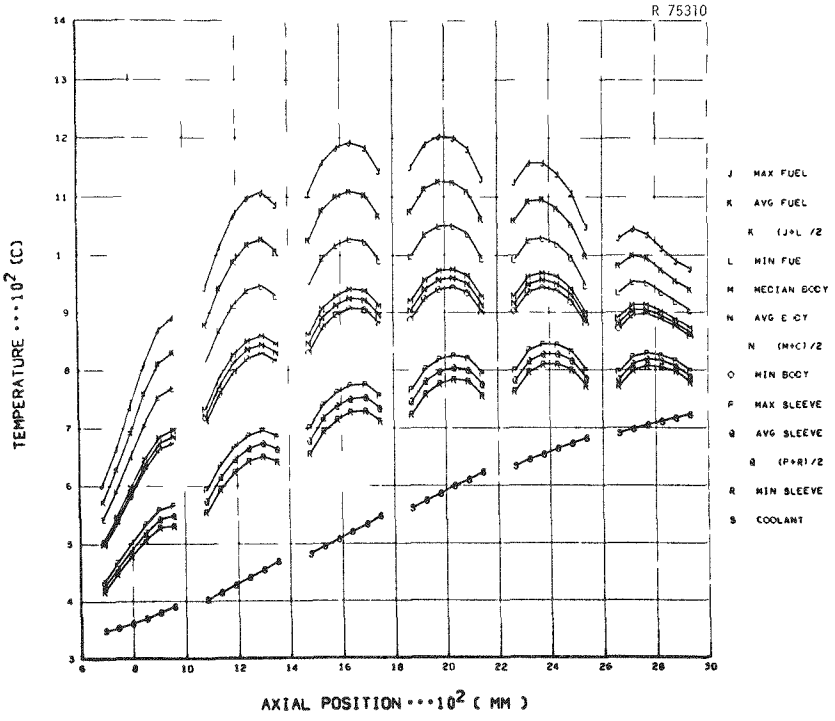

Fig. 2.1. Recycle Test Element-7 Time-Averaged Temperatures: Bodies 1–6, Holes 1–2.

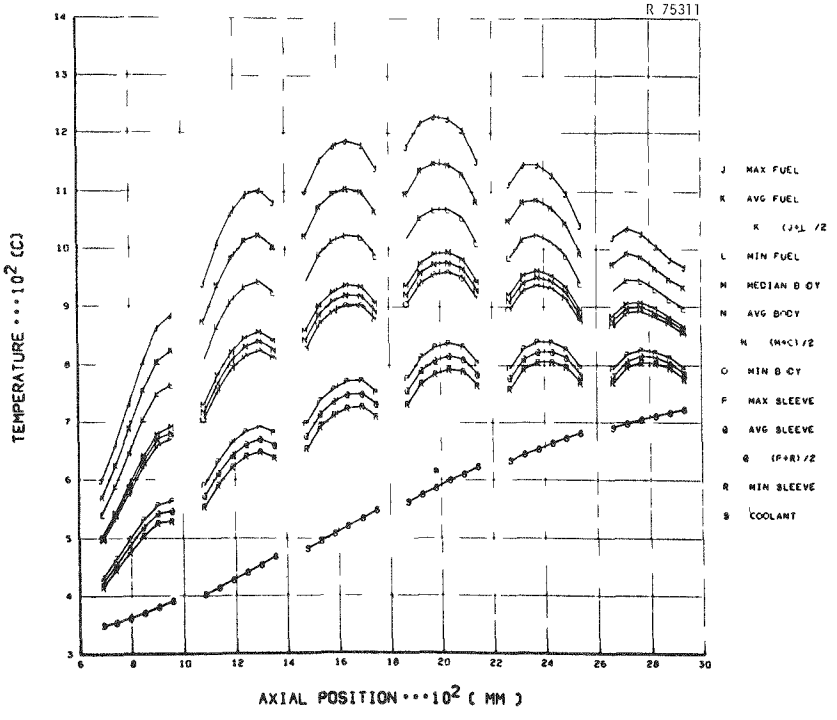

Fig. 2.2. Recycle Test Element-7 Time-Averaged Temperatures: Bodies 1–6, Holes 3–4.

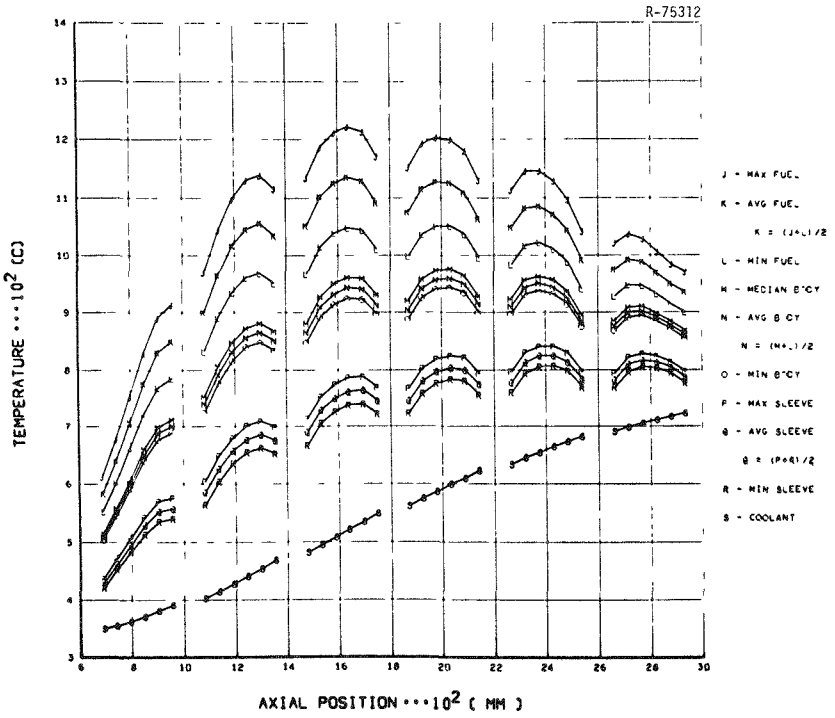

Fig. 2.3. Recycle Test Element-7 Time-Averaged Temperatures: Bodies 1–6, Holes 5–6.

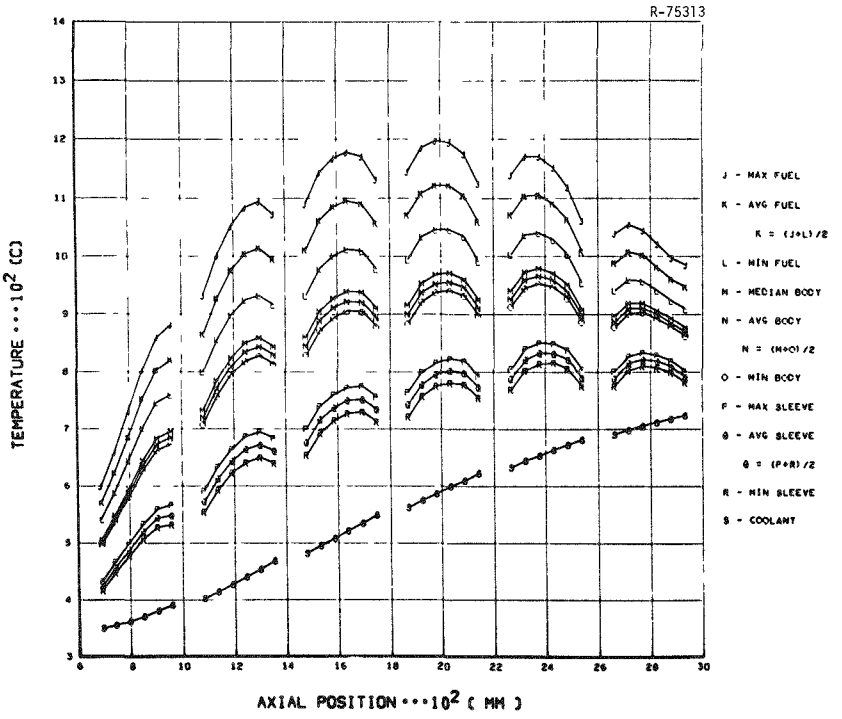

Fig. 2.4. Recycle Test Element-7 Time-Averaged Temperatures: Bodies 1–6, Holes 7–8.

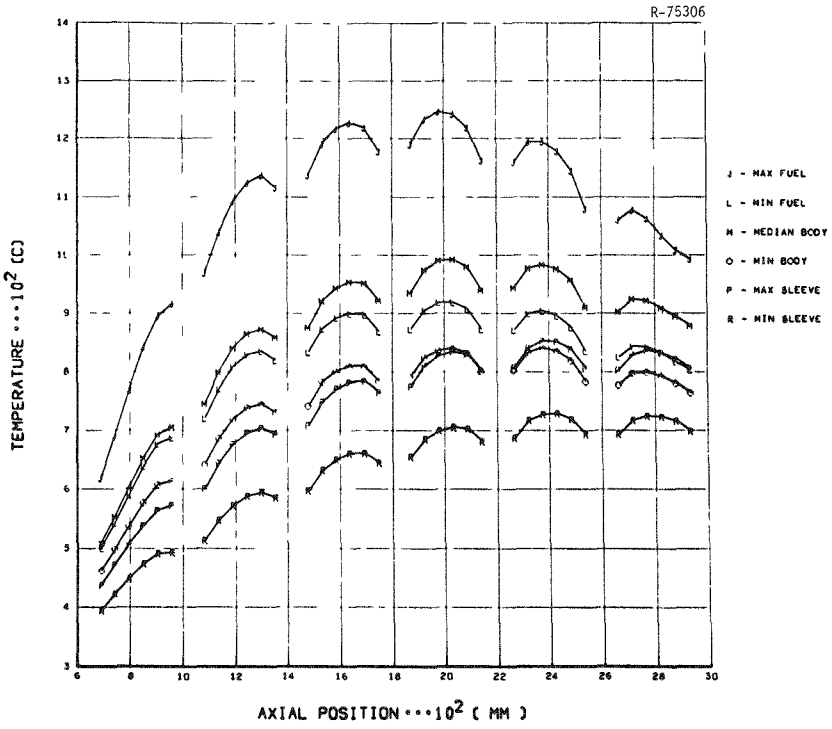

Fig. 2.5. Recycle Test Element-7 Temperature Envelope: Bodies 1–6, Holes 1–2.

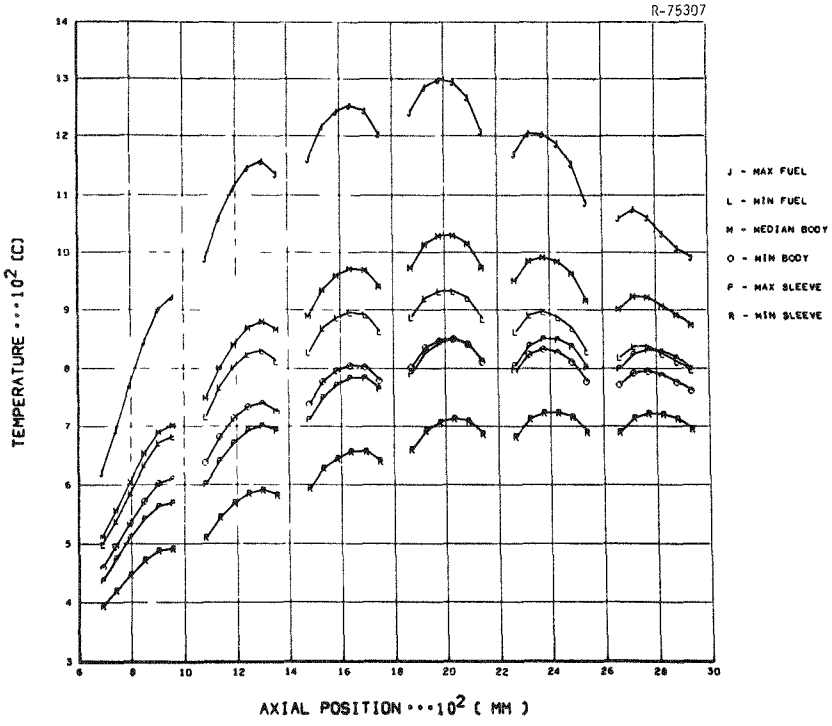

Fig. 2.6. Recycle Test Element-7 Temperature Envelope: Bodies 1–6, Holes 3–4.

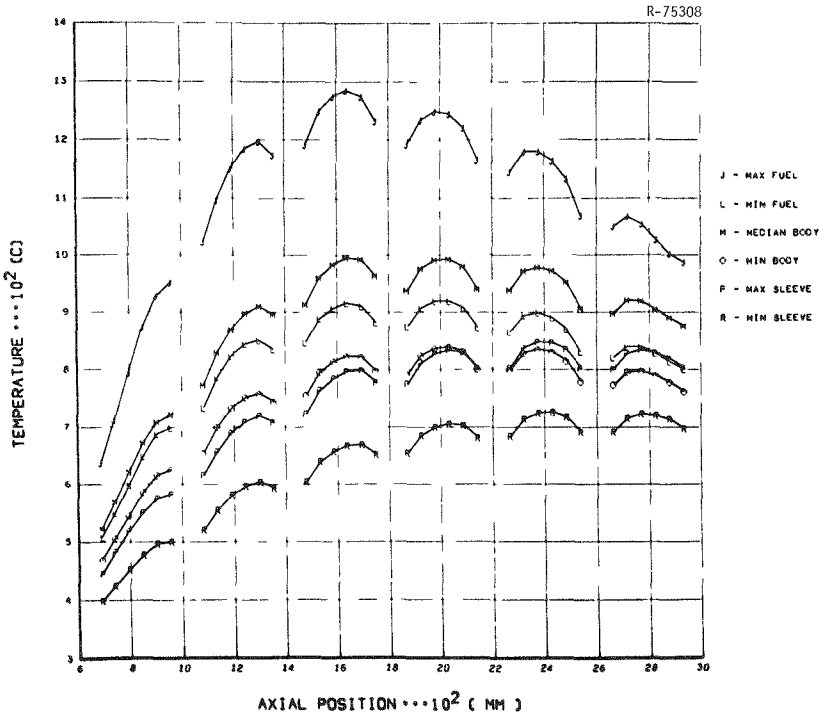

Fig. 2.7. Recycle Test Element-7 Temperature Envelope: Bodies 1—6, Holes 5—6.

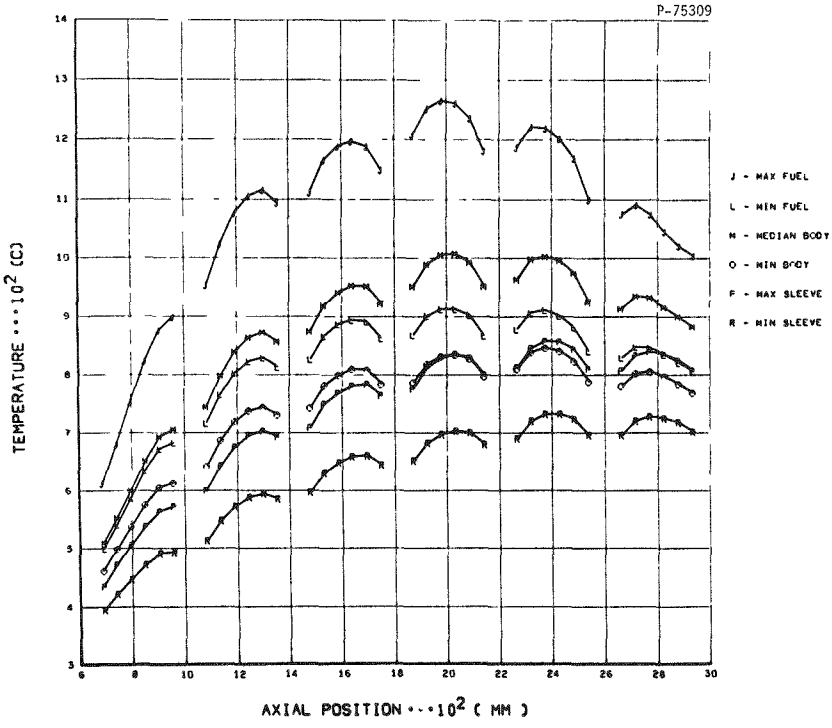

Fig. 2.8. Recycle Test Element-7 Temperature Envelope: Bodies 1—6, Holes 7—8.

the particles suggests that the rare-earth fission products were responsible for it.[15] The graphitized region adjacent to the SiC is shown in Fig. 2.9.

One fissile particle appeared to have failed by a pressure-vessel-type failure mechanism (Fig. 2.10). The rather low burnup of the particle — 13.7% FIMA — makes this observation surprising.

Additionally the dimensional changes in the rods from RTE-7 exceeded those predicted by extrapolation of data at higher exposure from accelerated tests. The dimensional analysis of Sect. 10 will discuss this result further.

3. POSTIRRADIATION EXAMINATION OF RECYCLE TEST ELEMENT-4

Recycle Test Element-4 was irradiated in core location B10-06* from 0 to 385 EFPD. The fuel-loading combinations are shown in Table 3.1. Preliminary results[3] from an early visual and dimensional examination have been reported previously. The metallographic examination was delayed until the capability to polish carbide fuels was established.

The nuclear and thermal evaluations of this element were also performed by GA. Summaries of the power history, heavy-metal burnup, and neutron fluence are given in Tables 3.2, 3.3, and 3.4. The time-averaged temperatures and temperature envelopes for the entire element are presented in Figs. 3.1 and 3.2. The radial temperature profile at the maximum fuel temperature achieved is presented in Fig. 3.3. As shown, the maximum fuel temperature does not occur at the center line of the fuel rod but shifts toward the central axis of the element.

Maximum burnups were 30.9, 4.9, and 0.6% FIMA for the fissile, mixed Th-U, and fertile particles, respectively. The highest fuel temperature and fast-fluence exposure ($E > 0.18$ MeV) were 1325°C and 1.92×10^{25} n/m^2, respectively. These irradiation conditions were more severe than those encountered in RTE-7 and resulted in different irradiation behaviors observed in the metallographic examination.

---

*See ref. 6 for core location.

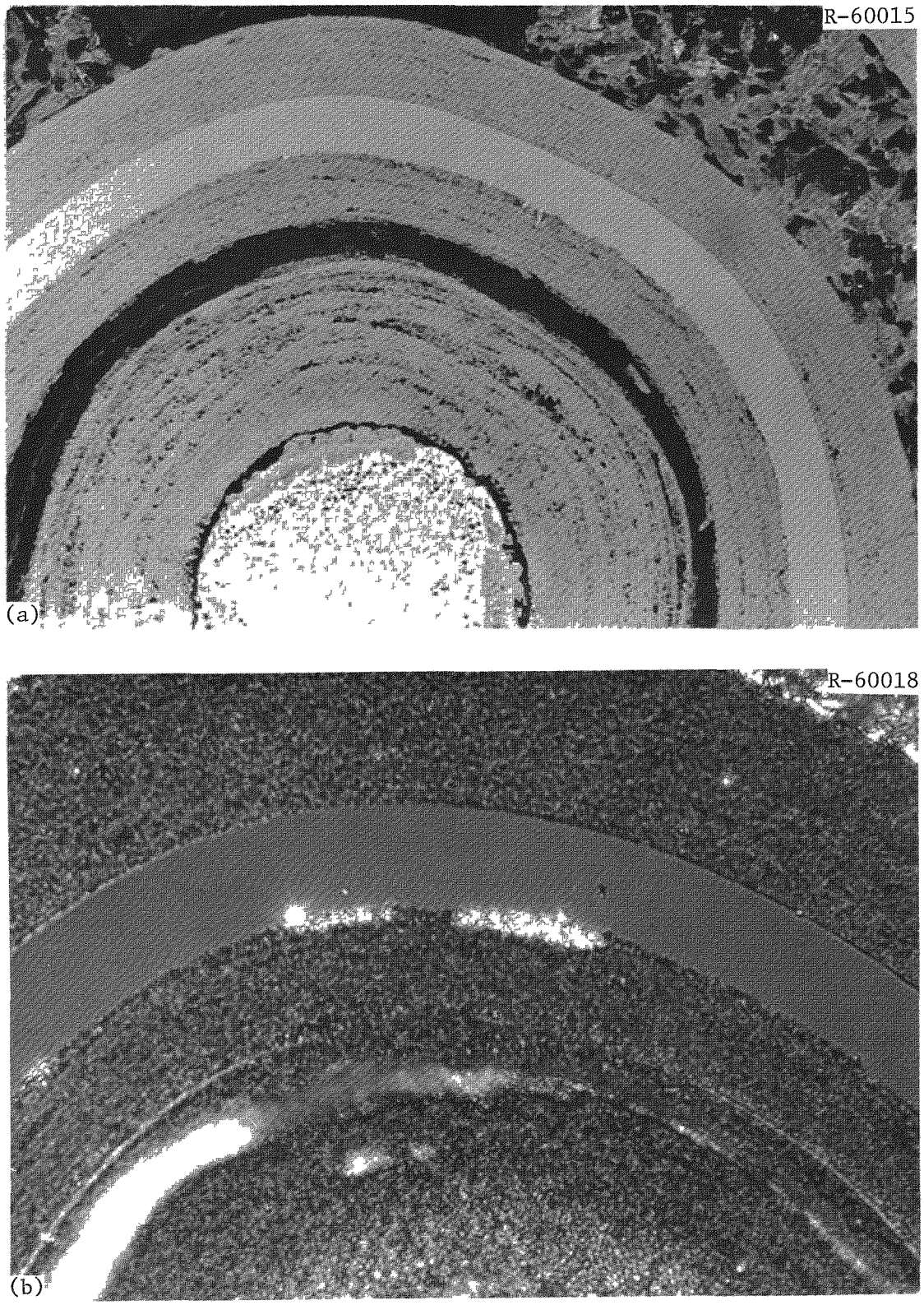

Fig. 2.9. Reaction on Cold Side of Triso-Coated UC_2 Particle from RTE-7-5-5-5. (a) Bright field. (b) Polarized light. 500×.

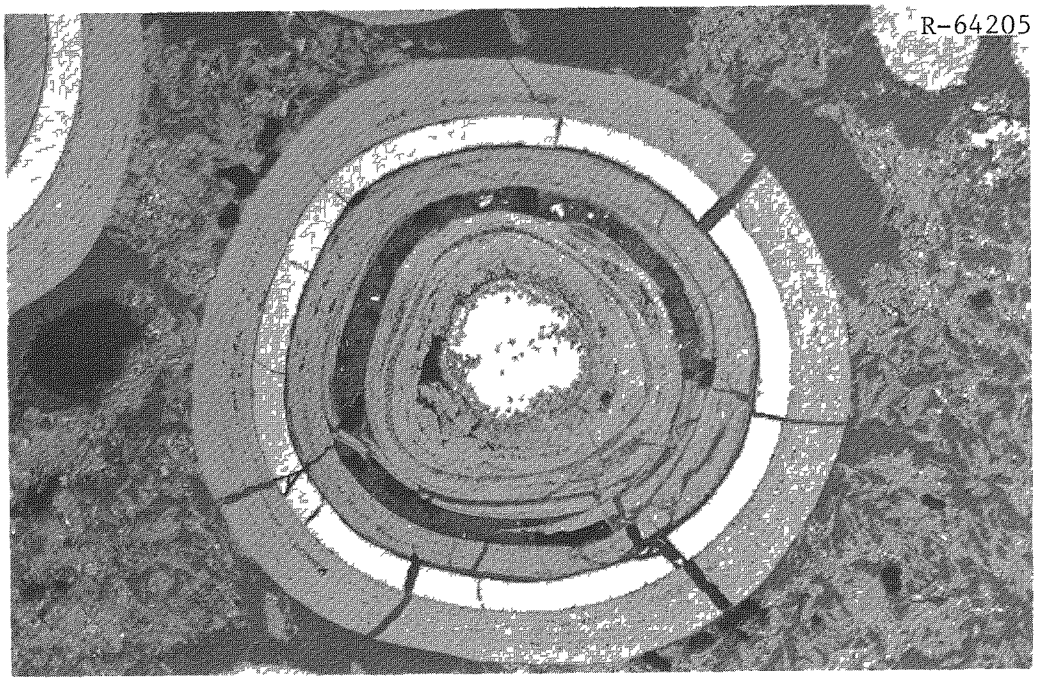

Fig. 2.10. Pressure-Vessel-Type Failure Observed in RTE-7-5-5-5. 250×.

Table 3.1 Fuel-Loading Scheme for Recycle Test Element-4

Body	Fissile Fuel		Fertile Fuel		Fuel-Bed Type
	Particle Type	Batch	Particle Type	Batch	
1	UC_2 Biso	4000-309	ThC_2 Biso	4000-226	Bonded Rods[a]
2	UC_2 Triso	4000-307	ThC_2 Biso	4000-225	Blended Bed[b]
3	$(4.2Th,U)O_2$ Biso	PR-54	ThC_2 Biso	9T-980-BL	Blended Bed[b]
4	UC_2 Triso	4000-307	ThC_2 Biso	4000-226	Bonded Rods[a]
5	$(2Th,U)O_2$ Biso	PR-61	ThC_2 Biso	4000-225	Bonded Rods[c]
6	UC_2 Biso	4000-248	ThC_2 Biso	4000-225	Blended Bed[b]

[a] Carbonized in fuel body.

[b] Blended beds contain calcined graphite powder as a bed stabilizer to prevent segregation.

[c] Carbonized in packed graphite flour.

Table 3.2. Recycle Test Element-4 Power, Flow, and Flux History

Interval Reference Equivalent Full-Power Time		Thermal Analysis							Nuclear Analysis				
		Irradiation Interval[a]	Absolute Radial Power	Relative Radial Power	Coolant Relative Radial-Power Factor	TRICUSP Channel Flow	Real Time[b]	Gage Power	Flux in Groups[c] from Gage, n/m^2s				
From EFPD	To EFPD	(d)	(kW)			(kg/s)	(d)	(kW)	1A[d]	1B	2	3	4
0.00	26.99	28.84	112.80	0.864	1.093	0.0312	28.84	112.80	4.10×10^{17}	0.72×10^{17}	8.11×10^{17}	1.34×10^{17}	4.43×10^{17}
26.99	62.71	38.84	112.54	0.862	1.091	0.0332	38.84	112.54	4.21	0.74	8.39	1.38	4.49
62.71	68.57	7.50	93.46	0.857	1.086	0.0322	7.50	93.46	3.54	0.63	7.07	1.16	3.83
68.57	202.06	140.94	113.23	0.857	1.086	0.0324	140.94	113.23	4.35	0.77	8.53	1.40	4.66
202.06	252.41	53.62	110.04	0.840	1.066	0.0341	60.00	98.35	3.78	0.67	7.64	1.25	4.39
252.41	252.41	0.00	109.12	0.833	1.057	0.0341	0.00		0.00	0.00	0.00	0.00	0.00
252.41	298.00	48.99	106.70	0.822	1.041	0.0329	56.40	92.68	3.43	0.61	7.03	1.15	4.20
298.00	342.95	50.19	102.20	0.818	1.038	0.0329	55.62	92.23	3.55	0.63	7.24	1.19	4.34
342.95	385.44	44.83	107.63	0.814	1.032	0.0335	46.98	102.69	3.88	0.68	7.92	1.30	4.97
Sum/Time-Weighted Average		413.75	109.65	0.842	1.067	0.0328	435.12	104.26	3.96	0.70	7.92	1.30	4.51
Root Mean Square			4.34	0.019	0.023	0.0007		8.94	0.35	0.06	0.57	0.09	0.24

[a] Time at nonzero power used in thermal analysis.

[b] Real calendar days used in nuclear analysis. Some short-term zero-power periods are included.

[c] The energy ranges for the flux groups follow:

Group 1A: 14.96 MeV $\geq$ E $\geq$ 0.18 MeV or 2.40 pJ $\geq$ E $\geq$ 28.84 fJ
Group 1B: 0.18 MeV $\geq$ E $\geq$ 8.65×10^4 eV or 28.84 fJ $\geq$ E $\geq$ 13.86 fJ
Group 2: 8.65×10^4 eV > E > 17.60 eV or 13.86 fJ > E > 2.82 aJ
Group 3: 17.60 eV $\geq$ E $\geq$ 2.38 eV or 2.82 aJ $\geq$ E $\geq$ 0.38 aJ
Group 4: 2.38 eV $\geq$ E $\geq$ 0 or 0.38 aJ $\geq$ E $\geq$ 0

[d] Group 1A, the fast-flux group, has been modified from the Gage output by a factor of 0.85. This accounts for the Peach Bottom energy cut-off of 8.65×10^4 eV instead of 0.18 MeV.

Table 3.3. Fissions per Initial Metal Atom for Recycle Test Element-4

Fuel Body	Fuel Rod	Core Height (mm)	Fertile FIMA (%)	Fissile FIMA (%)	Mixed FIMA (%)
1	1	689	0.020	7.441	1.044
	2	743	0.060	12.098	1.721
	3	797	0.115	16.723	2.407
	4	850	0.178	21.309	3.094
	5	904	0.248	24.193	3.553
	6	958	0.319	26.765	3.969
Mean		823	0.157	18.088	2.631
Range/RMS		322	0.104	6.758	1.021
2	1	1083	0.379	28.156	4.213
	2	1137	0.436	29.384	4.431
	3	1190	0.483	30.129	4.574
	4	1243	0.522	30.747	4.694
	5	1297	0.553	31.204	4.783
	6	1350	0.575	31.548	4.849
Mean		1217	0.491	30.195	4.591
Range/RMS		321	0.068	1.153	0.217
3	1	1479	0.590	31.826	4.901
	2	1534	0.594	32.006	4.929
	3	1588	0.596	32.156	4.952
	4	1643	0.586	32.041	4.927
	5	1698	0.574	31.849	4.891
	6	1752	0.556	31.417	4.815
Mean		1616	0.583	31.883	4.902
Range/RMS		328	0.014	0.237	0.044
4	1	1874	0.536	30.947	4.733
	2	1928	0.514	30.429	4.643
	3	1982	0.491	29.827	4.539
	4	2036	0.466	29.183	4.429
	5	2090	0.438	28.459	4.305
	6	2143	0.409	27.713	4.177
Mean		2009	0.476	29.426	4.471
Range/RMS		323	0.043	1.111	0.191
5	1	2269	0.373	26.804	4.021
	2	2324	0.337	25.837	3.856
	3	2378	0.300	24.714	3.670
	4	2432	0.265	23.480	3.469
	5	2486	0.230	22.118	3.251
	6	2541	0.196	20.890	3.052
Mean		2405	0.283	23.974	3.553
Range/RMS		326	0.061	2.051	0.335
6	1	2664	0.162	19.716	2.861
	2	2718	0.121	18.595	2.670
	3	2773	0.080	17.479	2.481
	4	2827	0.052	16.406	2.309
	5	2881	0.027	15.335	2.140
	6	2935	0.009	14.279	1.978
Mean		2800	0.075	16.968	2.407
Range/RMS		325	0.053	1.856	0.301
Grand Mean		1812	0.344	25.089	3.759
Grand Range/RMS		2300	0.196	6.623	1.079

Table 3.4. Recycle Test Element-4 Thermal- and Fast-Neutron Fluences

Fuel Body	Fuel Rod	Core Height (mm)	Fluence, n/m^2	
			Fast, >0.18 MeV	Thermal, <2.38 eV
1	1	689	0.596×10^{25}	0.742×10^{25}
	2	743	0.827	0.923
	3	797	1.024	1.101
	4	850	1.202	1.274
	5	904	1.354	1.443
	6	958	1.479	1.604
Mean		823	1.080	1.181
Range/RMS		322	0.303	0.295
2	1	1083	1.588	1.756
	2	1137	1.675	1.884
	3	1190	1.749	1.982
	4	1243	1.813	2.060
	5	1297	1.851	2.097
	6	1350	1.882	2.128
Mean		1217	1.760	1.985
Range/RMS		321	0.102	0.130
3	1	1479	1.902	2.153
	2	1534	1.913	2.165
	3	1588	1.919	2.173
	4	1643	1.920	2.174
	5	1698	1.909	2.168
	6	1752	1.892	2.157
Mean		1616	1.909	2.165
Range/RMS		328	0.010	0.008
4	1	1874	1.869	2.141
	2	1928	1.839	2.117
	3	1982	1.802	2.088
	4	2036	1.755	2.045
	5	2090	1.708	1.991
	6	2143	1.661	1.924
Mean		2009	1.773	2.051
Range/RMS		323	0.072	0.075
5	1	2269	1.603	1.843
	2	2324	1.540	1.759
	3	2378	1.471	1.671
	4	2432	1.397	1.579
	5	2486	1.320	1.485
	6	2541	1.234	1.384
Mean		2405	1.427	1.620
Range/RMS		326	0.126	0.157
6	1	2664	1.143	1.285
	2	2718	1.051	1.189
	3	2773	0.941	1.101
	4	2827	0.819	1.021
	5	2881	0.681	0.951
	6	2935	0.495	0.897
Mean		2800	0.855	1.074
Range/RMS		325	0.220	0.134
Total Mean		1812	1.467	1.679
Total Range/RMS		2300	0.423	0.454

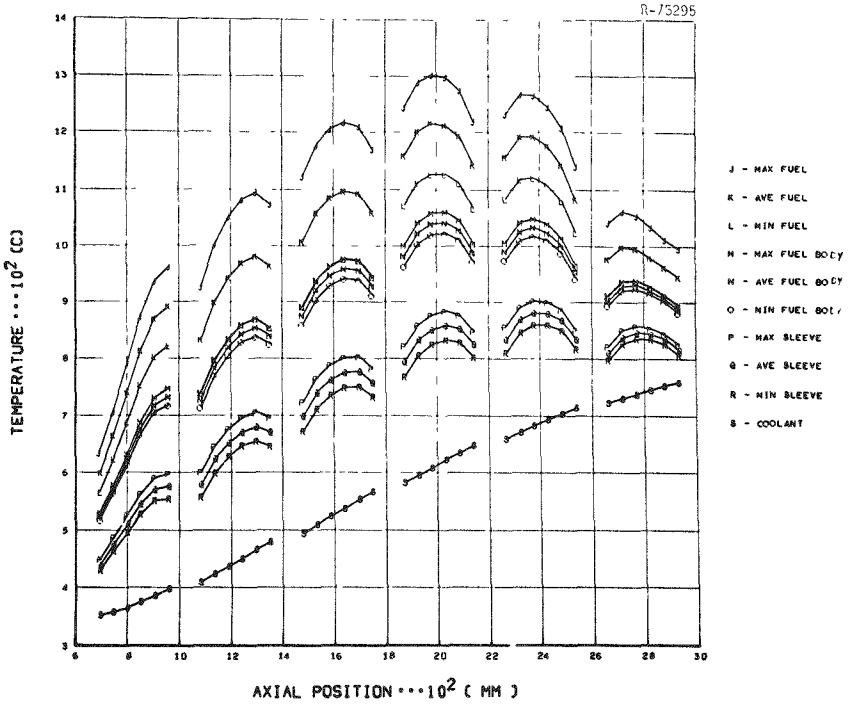

Fig. 3.1. Recycle Test Element-4 Time-Averaged Temperatures: Bodies 1–6.

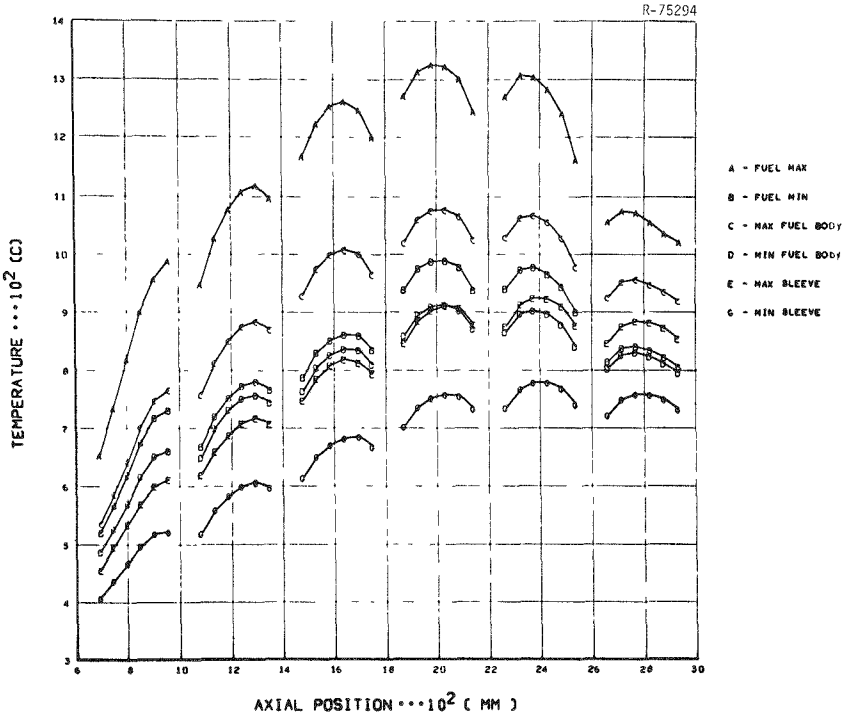

Fig. 3.2. Recycle Test Element-4 Temperature Envelope: Bodies 1–6.

ORNL-DWG 78-19953

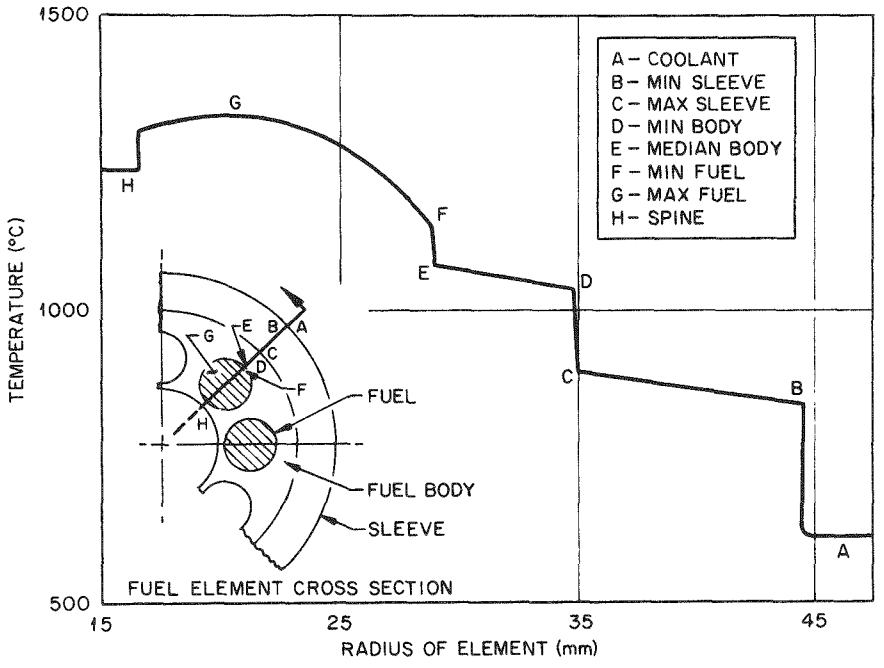

Fig. 3.3. Recycle Test Element-4 Radial Temperature Profile at Peak Temperature of Fuel Rod for Time Interval 69-202 EFPD and Core Height 1944 mm.

A metallographic section was taken from fuel rod RTE-4-4-1-3, which contained Triso-coated dense UC_2 and Biso-coated ThC_2. Its maximum time-averaged fuel temperature during irradiation was 1300°C, and it achieved a burnup of 29.2% FIMA. Examination of the transverse section revealed no evidence of amoeba in either the UC_2 or the ThC_2 particles. Typical fissile and fertile particles are shown in Fig. 3.4.* However, of 526 Triso-coated UC_2 particles, 3% had SiC coatings with straight-line fractures, while in 1% the oLTI had failed. This same batch (4000-307) of Triso-coated UC_2 particles was also in RTE-7, where the oLTI of the particles behaved similarly.

Further examination of these fissile particles under polarized-light illumination revealed that the iLTI had graphitized on the cold side of the particle, as indicated by high optical activity (Fig. 3.5).

*Note: In all the metallographic particle micrographs presented, the temperature gradient increases from left to right.

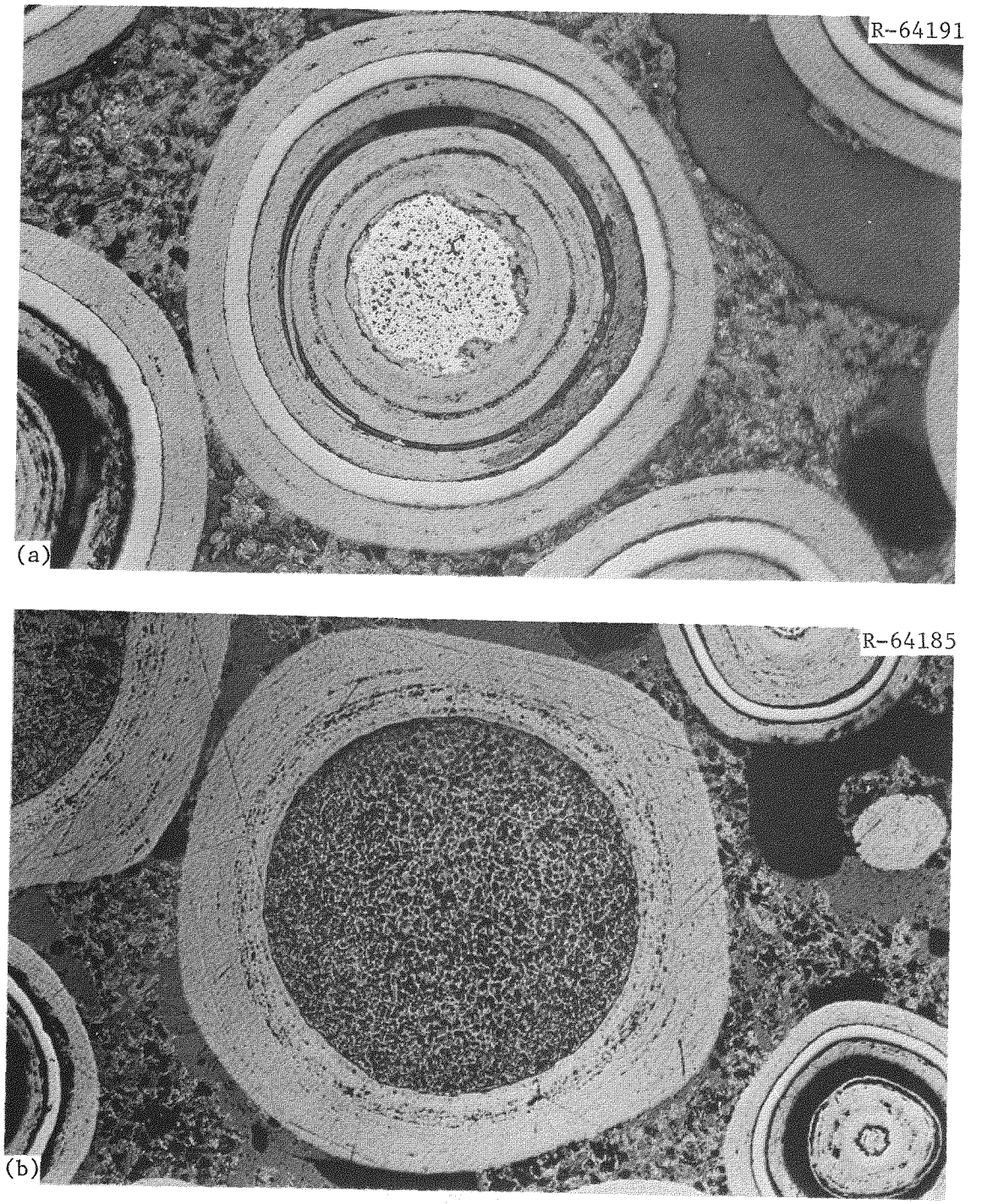

Fig. 3.4. Typical Particles from RTE-4-4-1-3. (a) Triso UC_2 fissile particle. 250×. (b) Biso ThC_2 fertile particle. 150×.

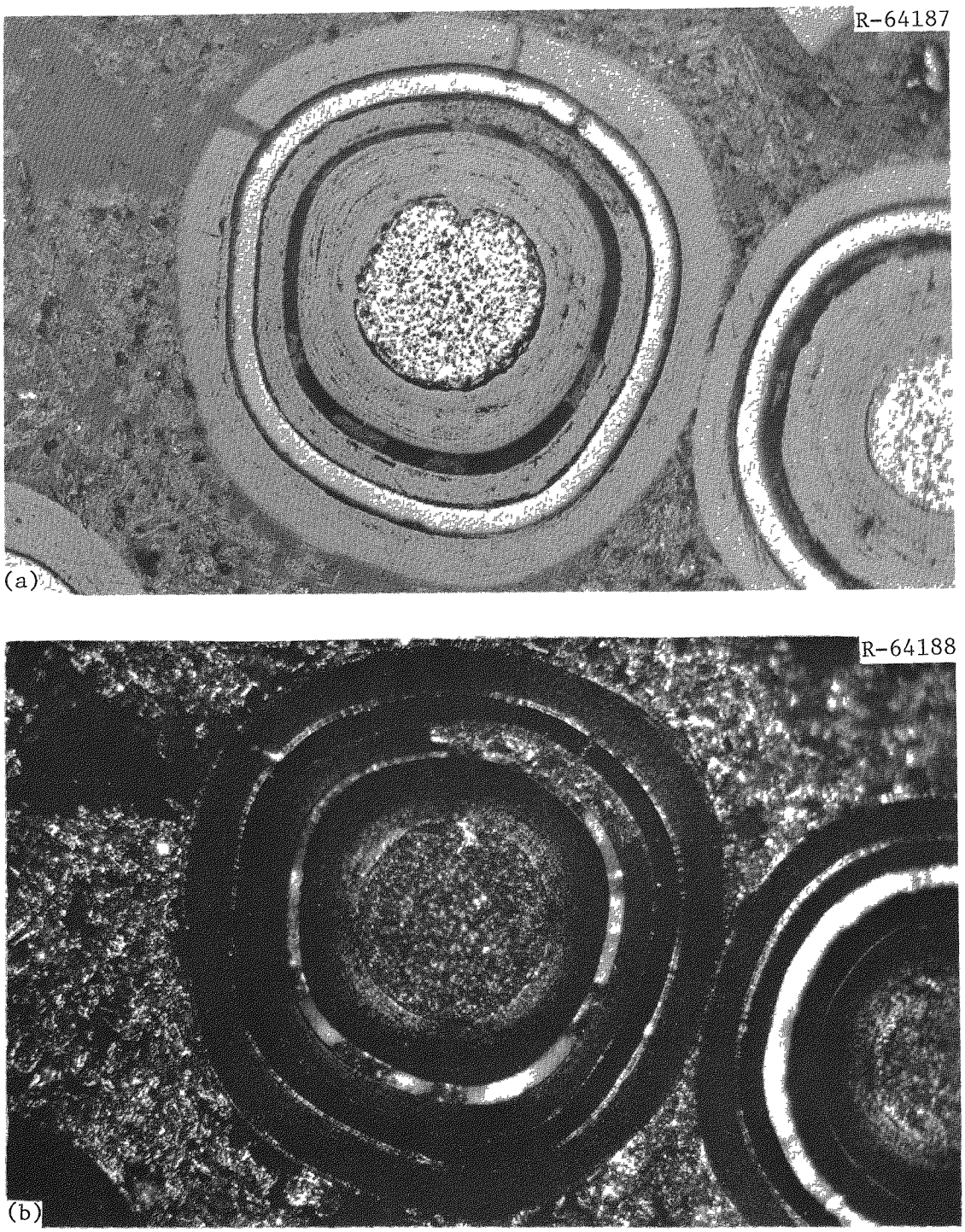

Fig. 3.5. Triso UC_2 Particle from RTE-4-4-1-3 Showing Graphitization of the iLTI Coating. 250×. (a) Bright field. (b) Polarized light.

In addition the inner surface of the SiC had corroded to a depth of 5 μm. This behavior was observed over the entire metallographic cross section. Electron microprobe analysis showed the graphitized regions of the iLTI contained the high-yield rare earth fission products La, Ce, Pr, and Nd, as presented in Fig. 3.6. Similar results on dense UC_2 irradiated under accelerated conditions[16,17] have been observed previously. Evidently the rare earths are able to migrate out of the kernel and down the temperature gradient. Further migration is stopped by the SiC, causing an accumulation in the iLTI, which results in graphitization of the iLTI and corrosion of the SiC.

Matrix-particle interaction was also observed in fuel rod RTE-4-4-1-3. Approximately 10% of the fissile particles contained tears that extended about halfway through the outer coatings, as shown in Fig. 3.7. This was the first example of matrix-particle interaction observed in fuel rods carbonized in an RTE graphite fuel body. This fuel rod received a fast-fluence exposure (E >0.18 MeV) of 1.8×10^{25} n/m^2, or about 25% of the exposure expected in a commercial HTGR.

Body 2 contained a blended bed of Triso-coated dense-UC_2 fissile particles (batch 4000-307) and Biso-coated ThC_2 fertile particles. Body 2 and body 4 were comparable because their fuel rods contained the same fuel system. While the fissile particles came from the same batch, the fertile particles came from different ones, although all fertile particles from all batches were ThC_2. The microstructure of the blended bed resembled that of the coated particles contained in the fuel rods, with one exception. Graphitization of the cold side of the iLTI was found in the fissile particles across the entire cross section of the fuel rod in body 4 (Fig. 3.5), whereas this effect was not observed in any of the particles in the loose-bed sample. The metallographic sample was taken from the middle of the stack from hole 1. The maximum fuel temperature for that position was 1110°C, about 200°C cooler than at RTE-4-4-1-3. The burnups were comparable. The migration of the rare-earth fission products evidently depends very much on temperature, and occurs at a relatively slow rate at temperatures below 1100°C. Typical particles from body 2 are shown in Fig. 3.8.

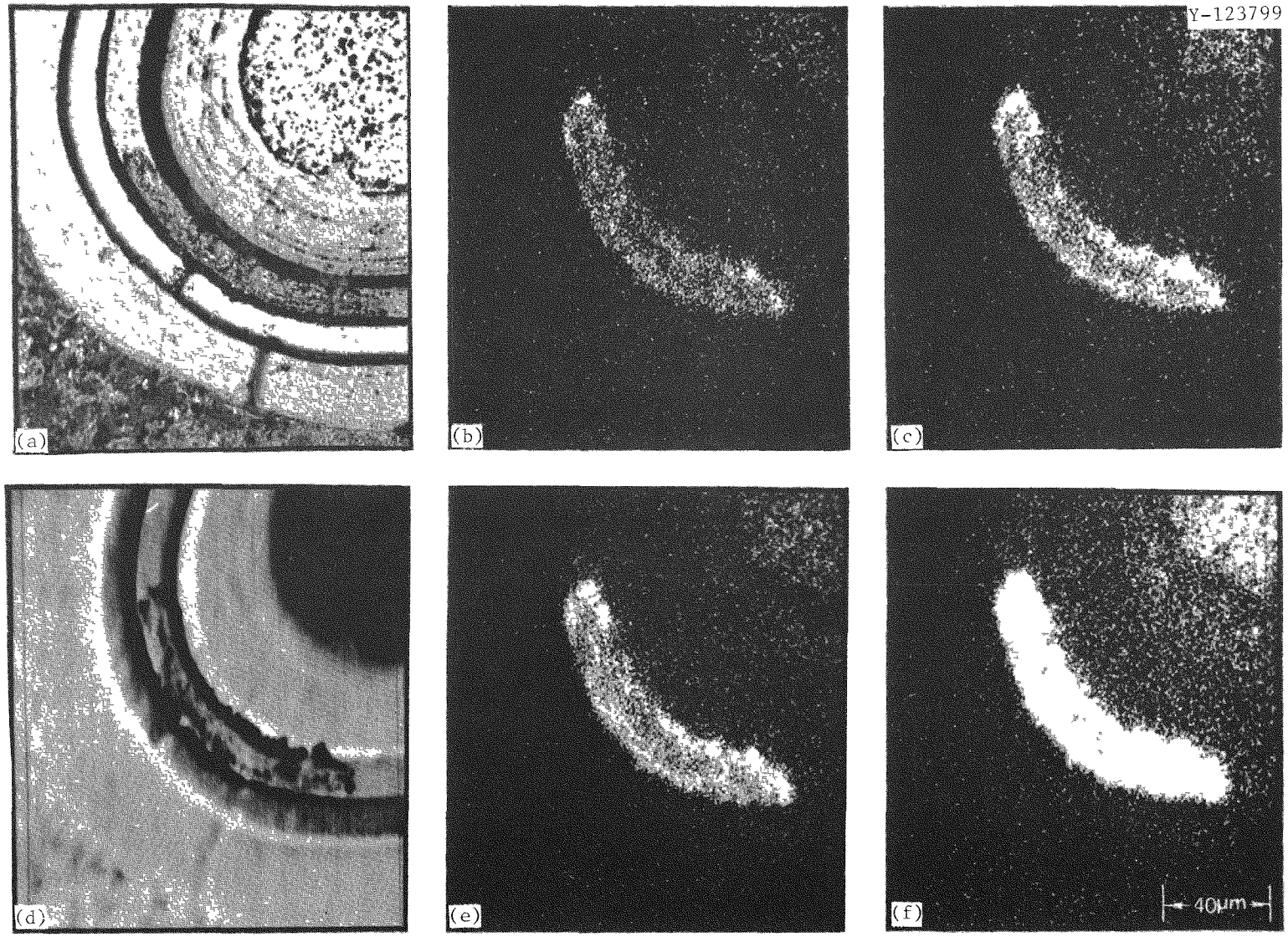

Fig. 3.6. Rare-Earth Fission Products Found on Cold Side of Triso-Coated Dense-UC_2 Kernel from RTE-4. (a) Optical Micrograph. (b) La Lα. (c) Pr Lα. (d) Backscattered electrons. (e) Ce Lα. (f) Nd Lα.

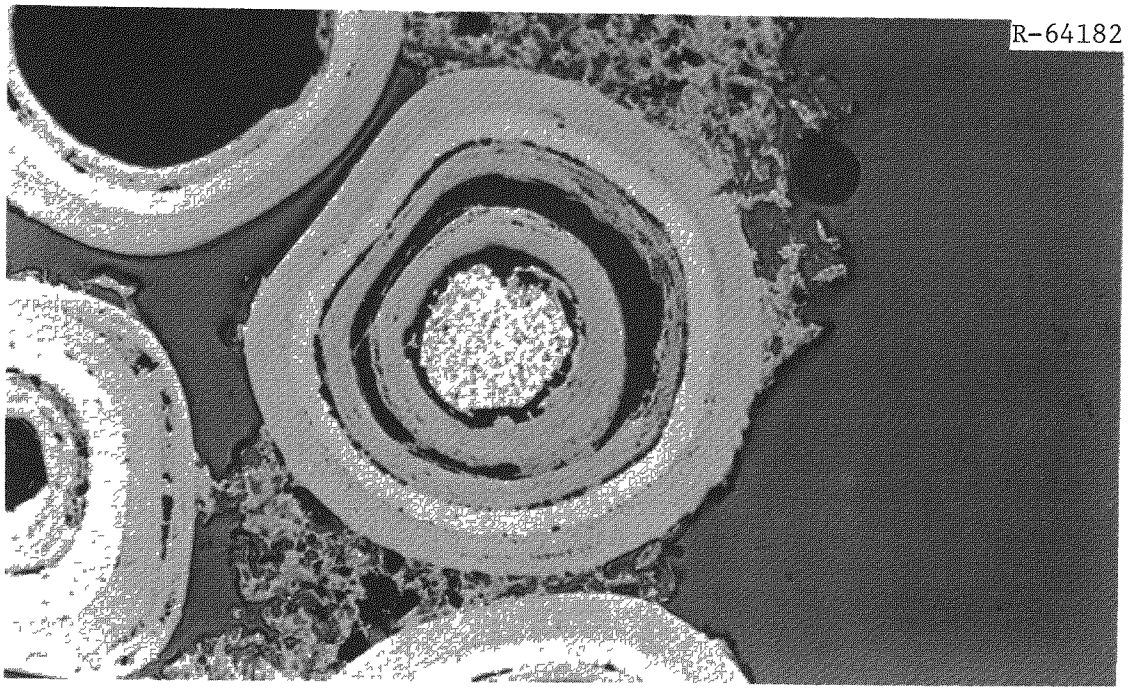

Fig. 3.7. Matrix-Particle Interaction Involving Triso UC_2 Particles from RTE-4-4-1-3. 200×.

Fuel rod RTE-4-1-1-3, which contained Biso-coated UC_2 and ThC_2, was also metallographically examined. Its maximum time-averaged temperature was 800°C and it achieved burnups of 16.7 and 0.1% FIMA in the fissile and fertile particles, respectively. No particles were observed to have failed as a result of the irradiation test. However, two of the Biso coatings had broken during fabrication. We found no evidence of amoeba in either the UC_2 or the ThC_2 kernels. Although none of the coatings showed indications of potential failure, the coatings on the UC_2 kernels contained sooty regions that delineated layers in the pyrocarbon. Also, the outer layers of many particles contained cracks that extended 20 to 30 μm into the coatings. Typical fissile particles from this fuel rod, RTE-4-1-1-3, are shown in Fig. 3.9. The fertile ThC_2 particles appeared identical to those from RTE-4-4-1-3 (Fig. 3.4).

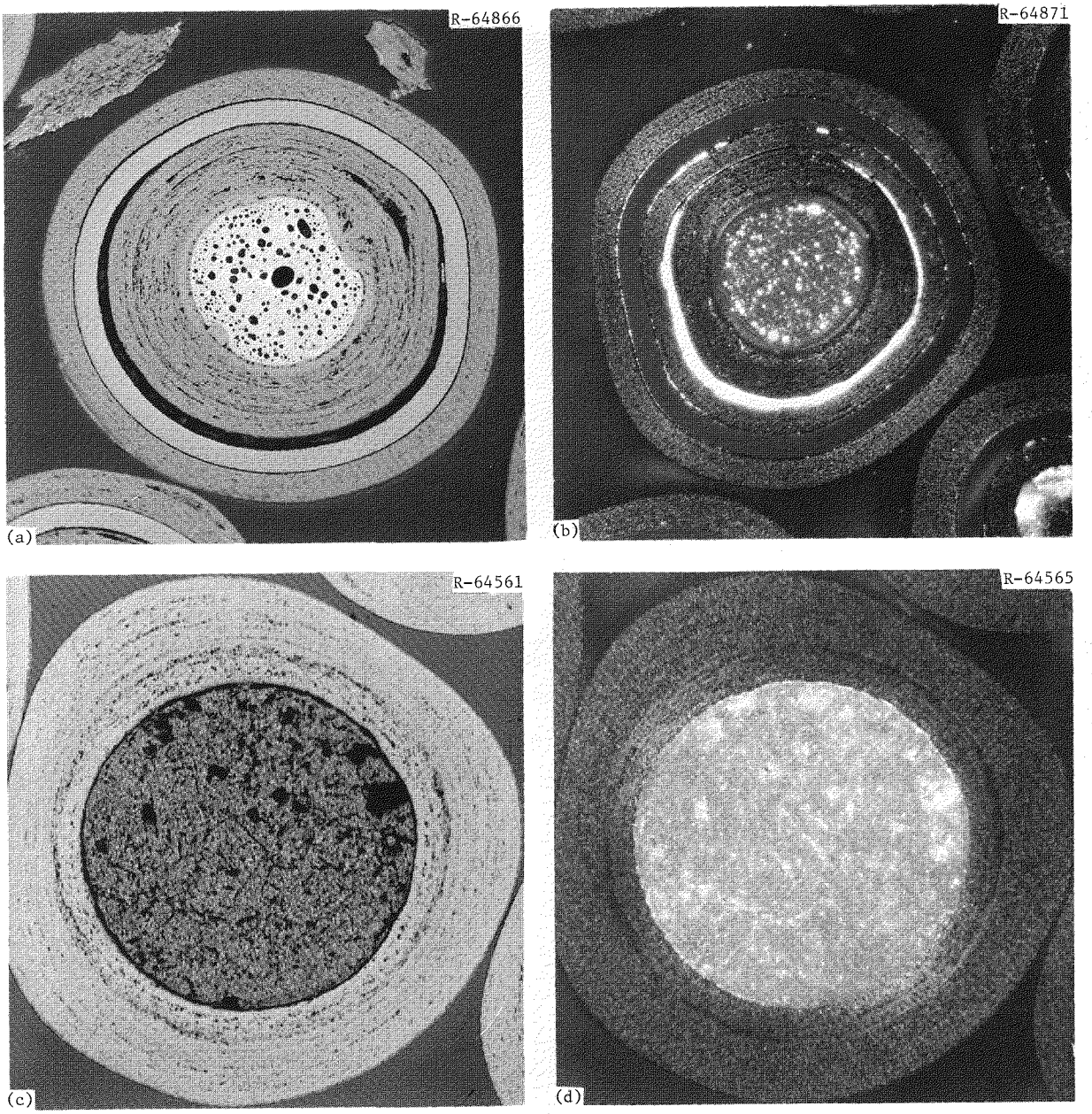

Fig. 3.8. Typical Particles from RTE-4-2. (a) Triso UC_2 fissile particle. Bright field. 250×. (b) Same. Polarized light. (c) Biso ThC_2 fertile particle. Bright field. 200×. (d) Same. Polarized light. Reduced 29%.

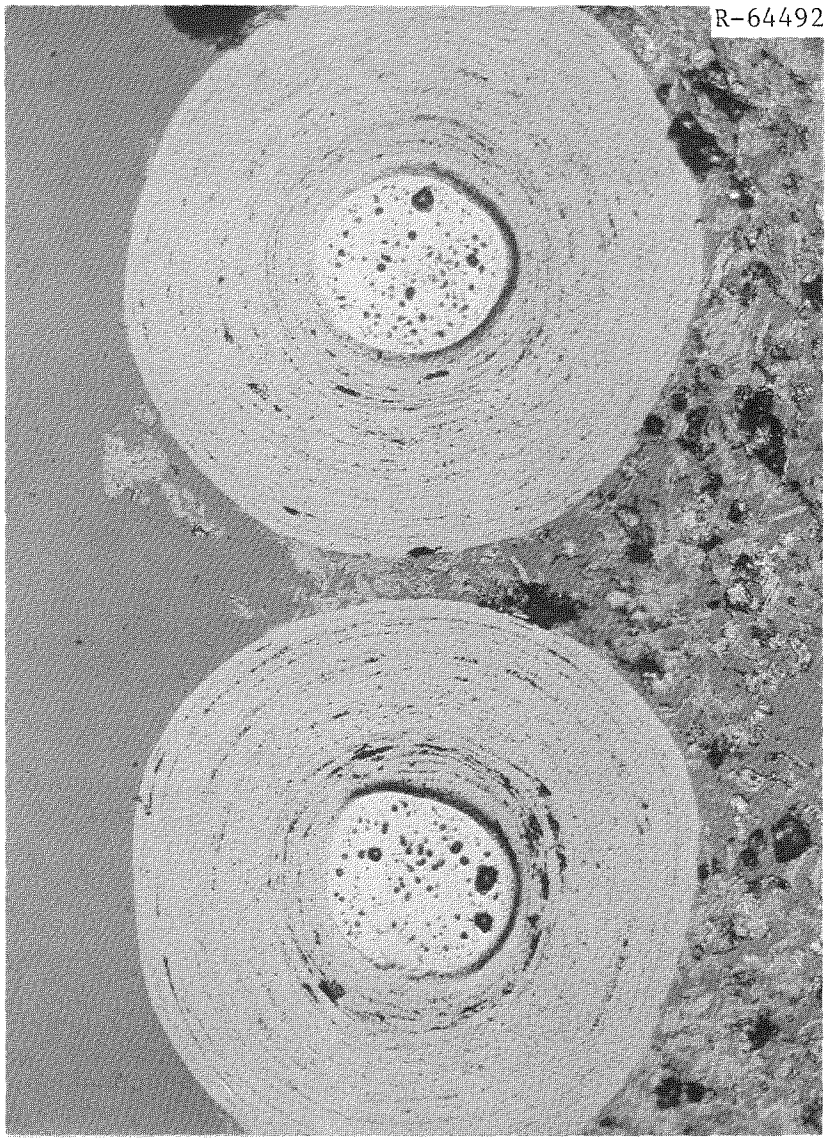

Fig. 3.9. Typical Fissile Particles from RTE-4-1-1-3. 250×.

Electron microprobe examination of the Biso-coated UC_2 from body 1 detected the rare-earth fission products — La, Pr, Ce, and Nd — contained in the kernel and buffer coating (Fig. 3.10). These results indicate that the rare earths migrate out of the kernel into the buffer but diffuse very little into the LTI coating. The maximum fuel temperature — 820°C — was considerably lower than that — 1320°C — observed in body 4, in which rare-earth migration was high. Also, because these particles were at the end of the element where the

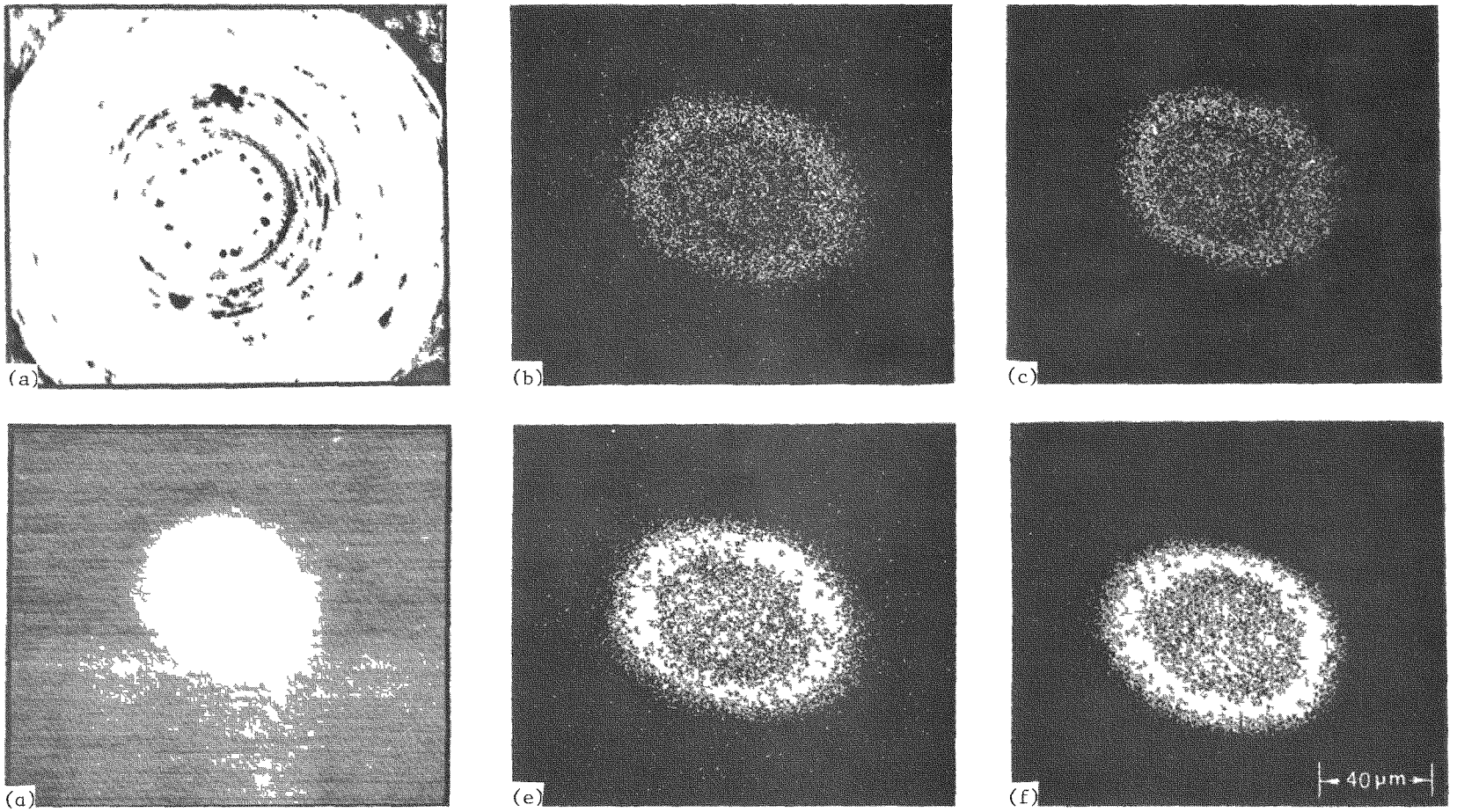

Fig. 3.10 Rare-Earth Fission Products Found in a Biso-Coated Dense UC_2 Kernel from RTE-4, Body 1. (a) Optical micrograph. (b) La Lα. (c) Pr Lα. (d) Backscattered electrons. (e) Ce Lα. (f) Nd Lα.

thermal-neutron fluxes (E <2.38 eV) were much lower, the heat generation by individual particles was lower. Again these results point to the large temperature-dependence of the rare earth behavior.

The electron microprobe was also used to determine the behavior of cesium in the Biso-coated UC_2 particles from body 1 (Fig. 3.11). Cesium was observed in all areas of the particle, but whether it migrated out of the particle could not be determined. Even at the low burnups and temperatures encountered by these fuel particles, cesium migration was extensive. These results point to the need for a SiC coating on fissile particles to contain the cesium during irradiation.

The blended bed in body 6 contained Biso-coated UC_2 and ThC_2. This fuel system was also used in body 1, although the particles came from different batches. A metallographic section was prepared with particles from the middle of the stack from hole 1. These particles operated at a maximum time-averaged temperature of 1050°C and maximum burnups of 17.5 and 0.1% FIMA for the fissile and fertile particles, respectively. The microstructural features of the particles from body 6 resembled those of the particles from body 1 in that no amoeba was detected and no indications of potential failure were found in either the fissile or the fertile particles. Typical particles are shown in Fig. 3.12. The short radial cracks noted in the peripheral regions of the Biso coating on the UC_2 kernels in the fuel rods from body 1 were also present in the loose-particle sample (Fig. 3.13), indicating that the cracks probably resulted from a coating problem rather than from a rod fabrication problem.

The fuel system contained in the fuel rods in body 5 consisted of Biso-coated $(2Th,U)O_2$ and ThC_2. The metallographic section was taken from fuel rod RTE-4-5-1-3, which operated at a maximum time-averaged fuel temperature of 1260°C and obtained burnups of 3.7 and 0.3% FIMA in the fissile and fertile particles, respectively. Examination of the transverse section from this fuel rod revealed neither amoeba nor evidence of potential failure of either the fissile or the fertile particles. A typical fissile particle is shown in Fig. 3.14. These particles closely resembled their counterparts from the same

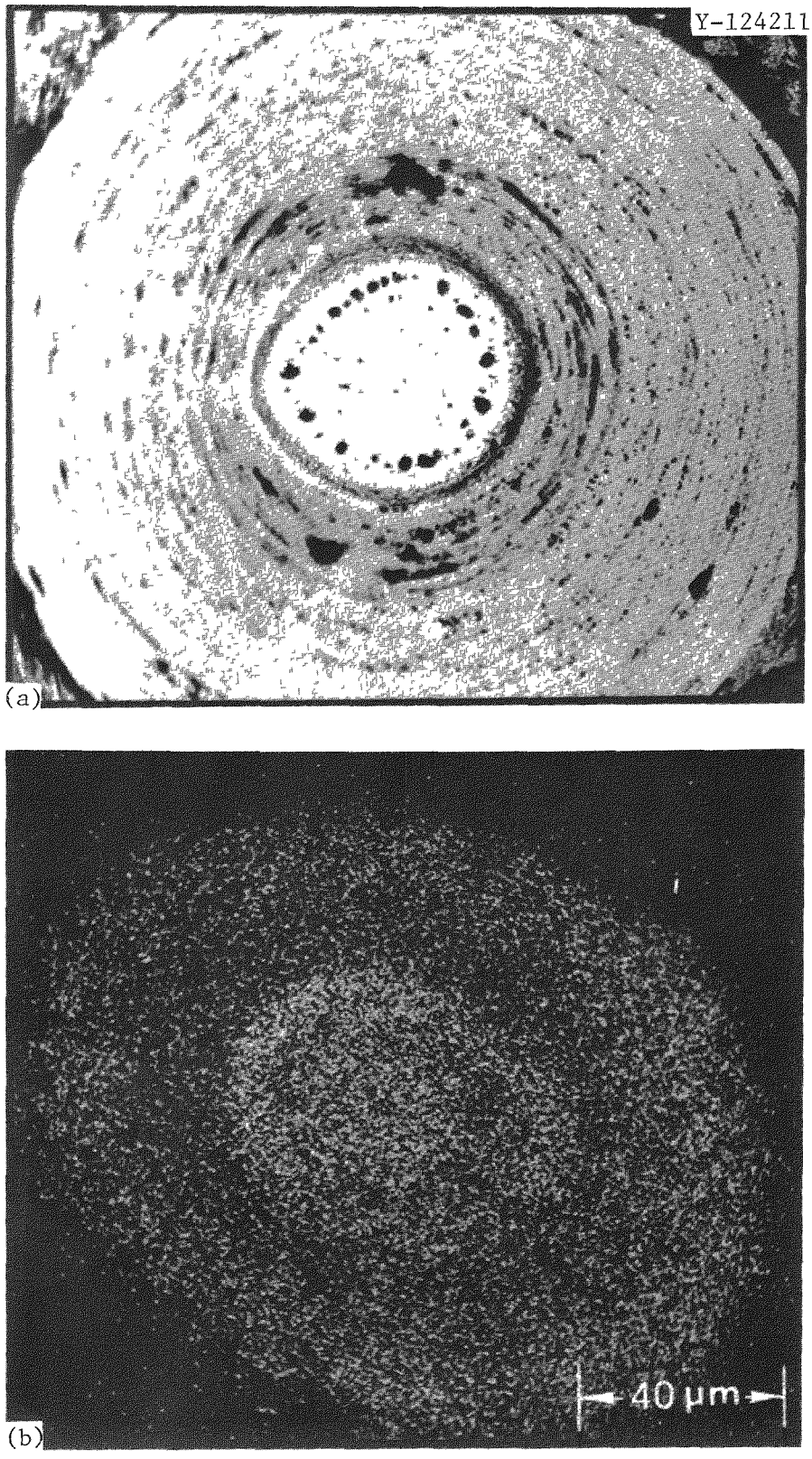

Fig. 3.11. Distribution of Cesium in a Biso-Coated Dense UC_2 Kernel from Recycle Test Element-4, Body 1. (a) Optical micrograph. (b) Cesium Lα.

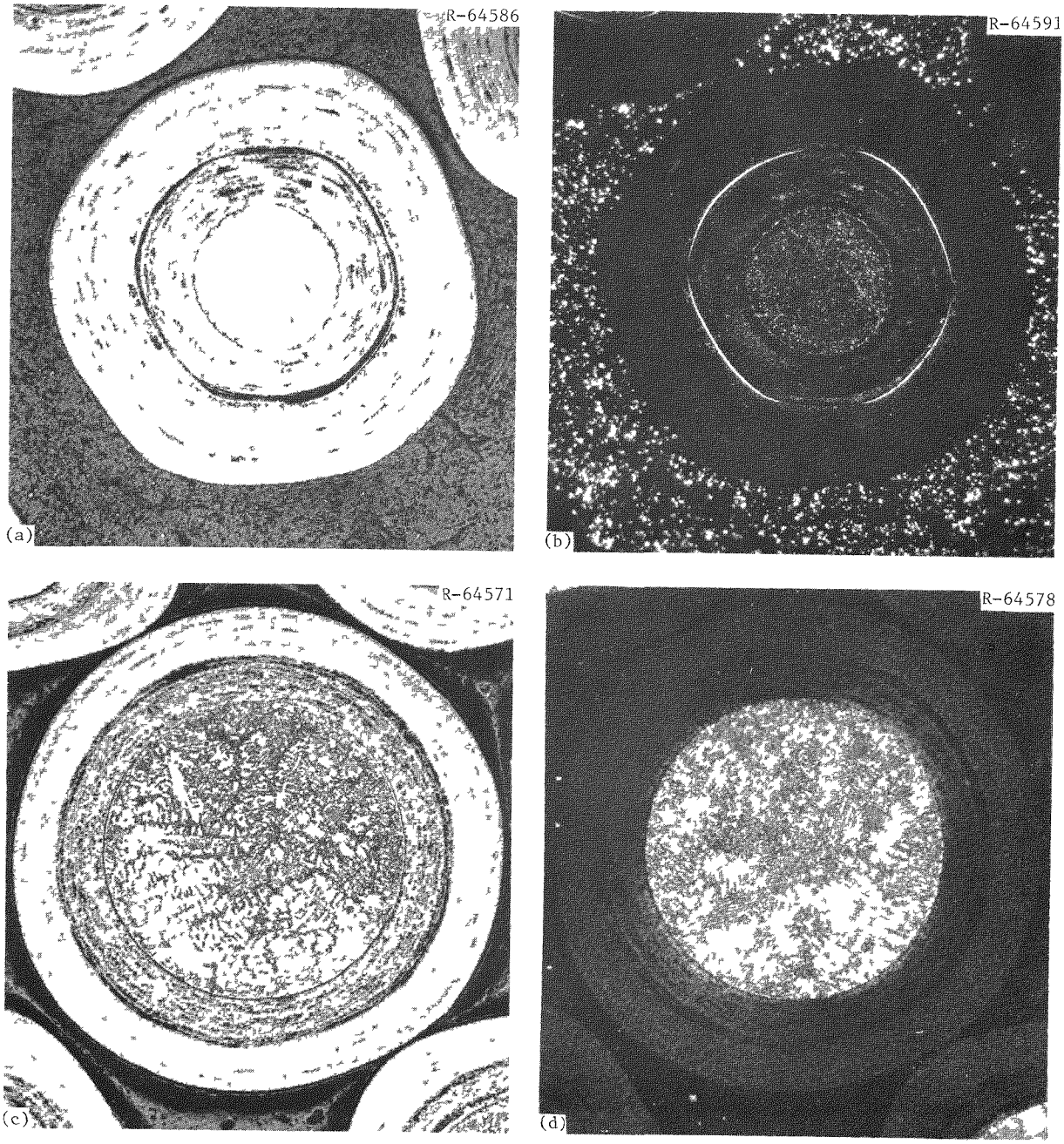

Fig. 3.12. Typical Particles From RTE-4-6. (a) Biso UC_2 fissile particle. Bright field. 250×. (b) Same. Polarized light. (c) Biso ThC_2 fertile particle. Bright field. 150×. (d) Same. Polarized light. Reduced 23.5%.

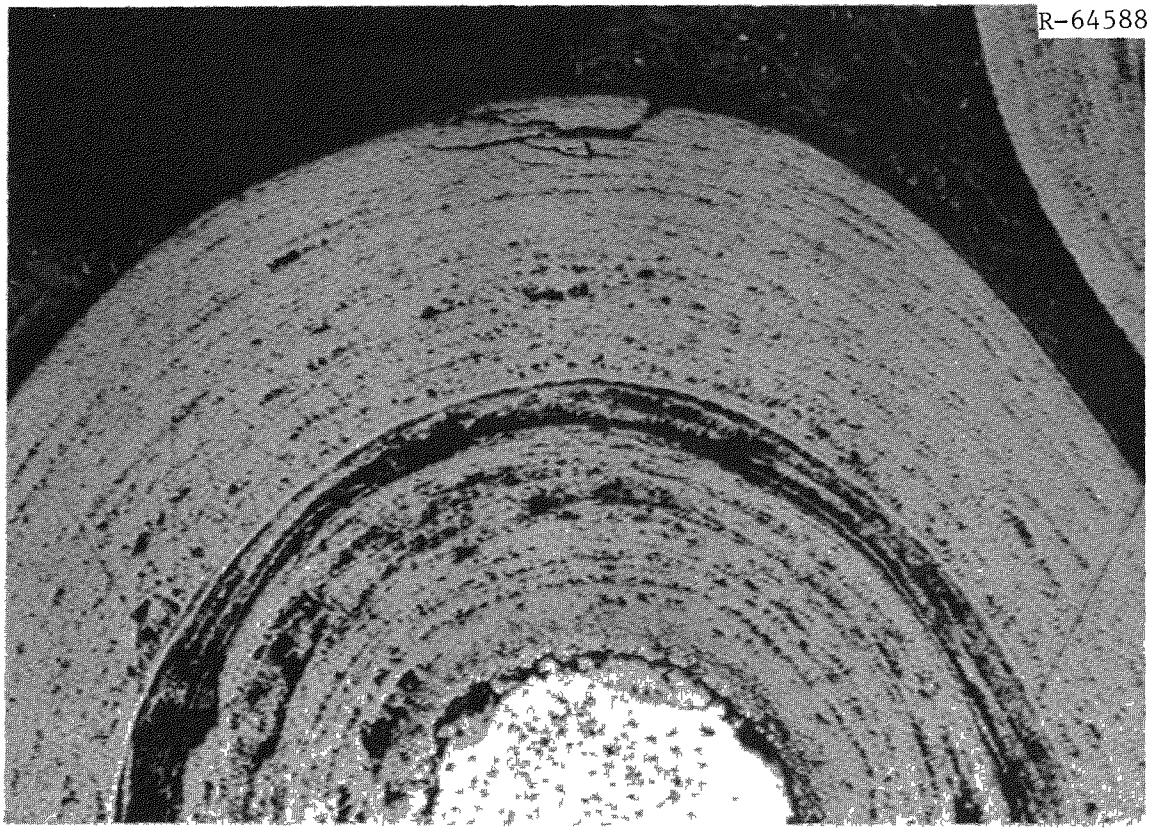

Fig. 3.13. Appearance of Short Radial Cracks in Outer Low-Temperature Isotropic Coating on the Biso UC_2 Particles from RTE-4-6. 750×.

batch irradiated in RTE-7. Furthermore, the fertile particles also appeared identical to others from the same batch of Biso-coated ThC_2 in body 2 (Fig. 3.9).

Body 3 contained a blended bed of Biso-coated $(4Th,U)O_2$ and ThC_2 particles. The metallographic sample was prepared with particles from hole 1, in the middle of the stack, which operated at a maximum time-averaged fuel temperature of 1210°C, and achieved burnups of 5.0 and 0.6% FIMA in the fissile and fertile particles, respectively. No amoeba was evident in either the fissile or fertile particles. Nor was any indication of potential failure discerned. Typical fissile and fertile particles are shown in Fig. 3.15.

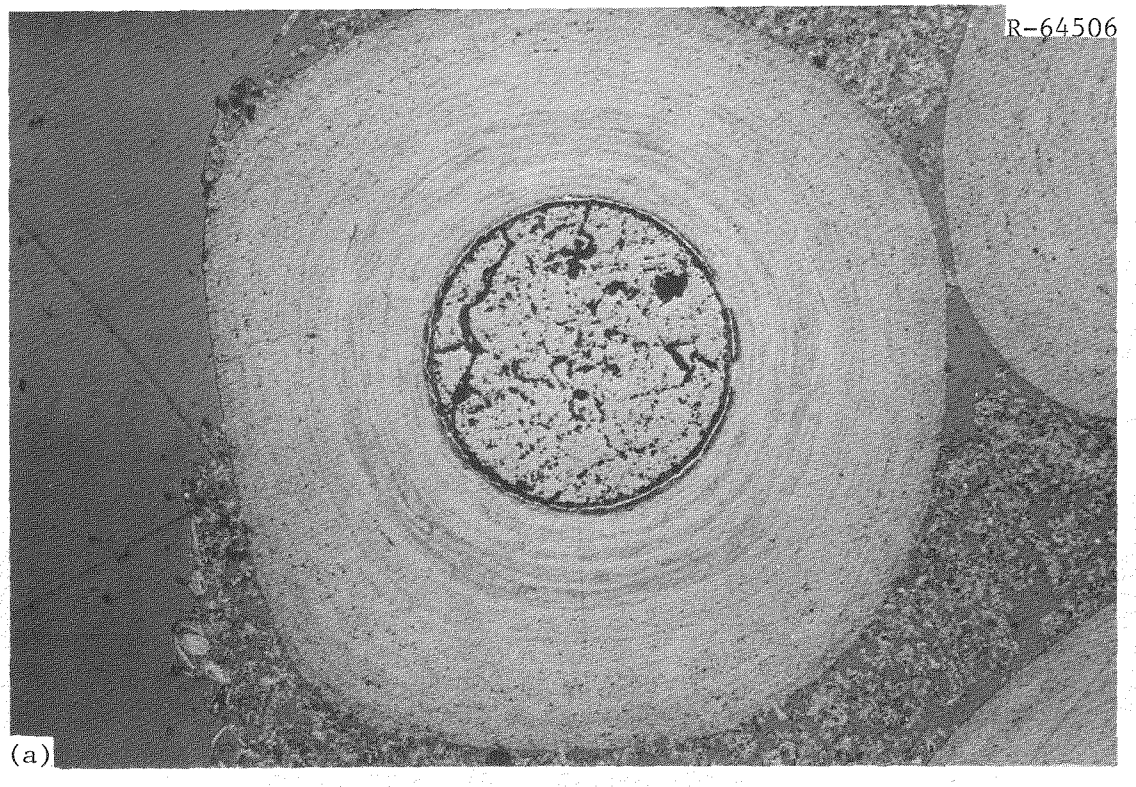

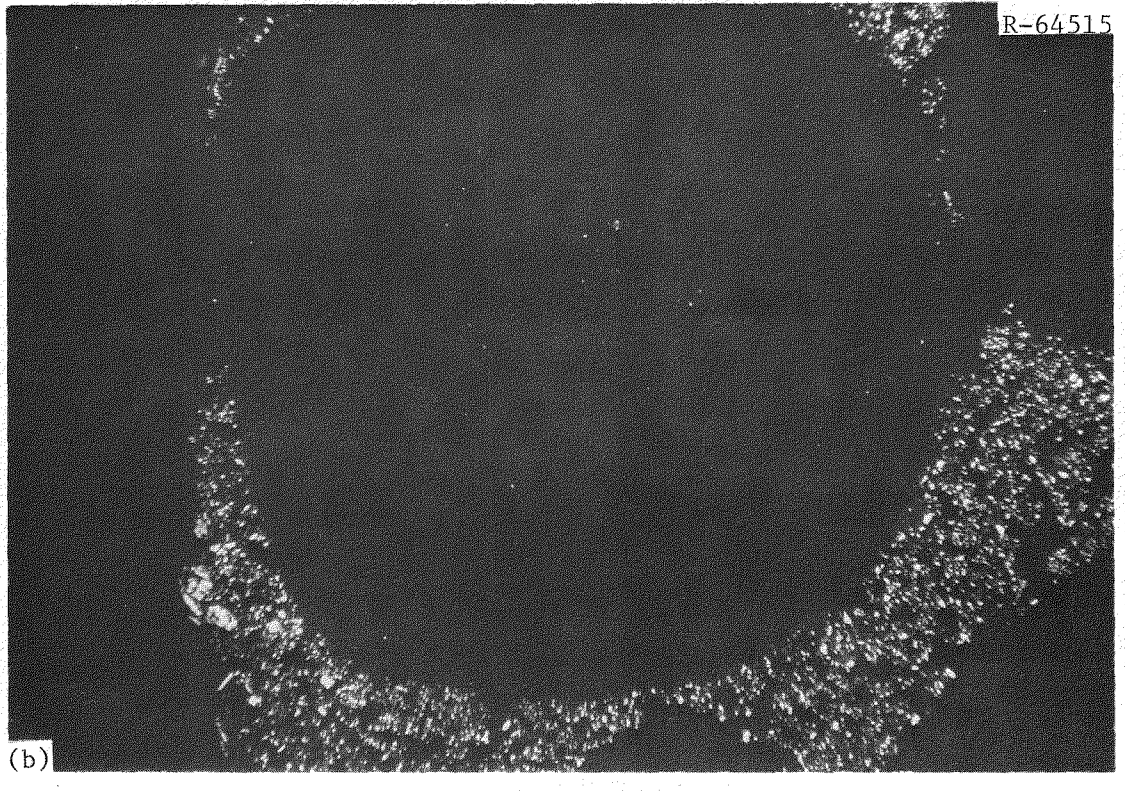

Fig. 3.14. Typical Biso $(2Th,U)O_2$ Fissile Particles From RTE-4-5-1-3. 150×. (a) Bright field. (b) Polarized light.

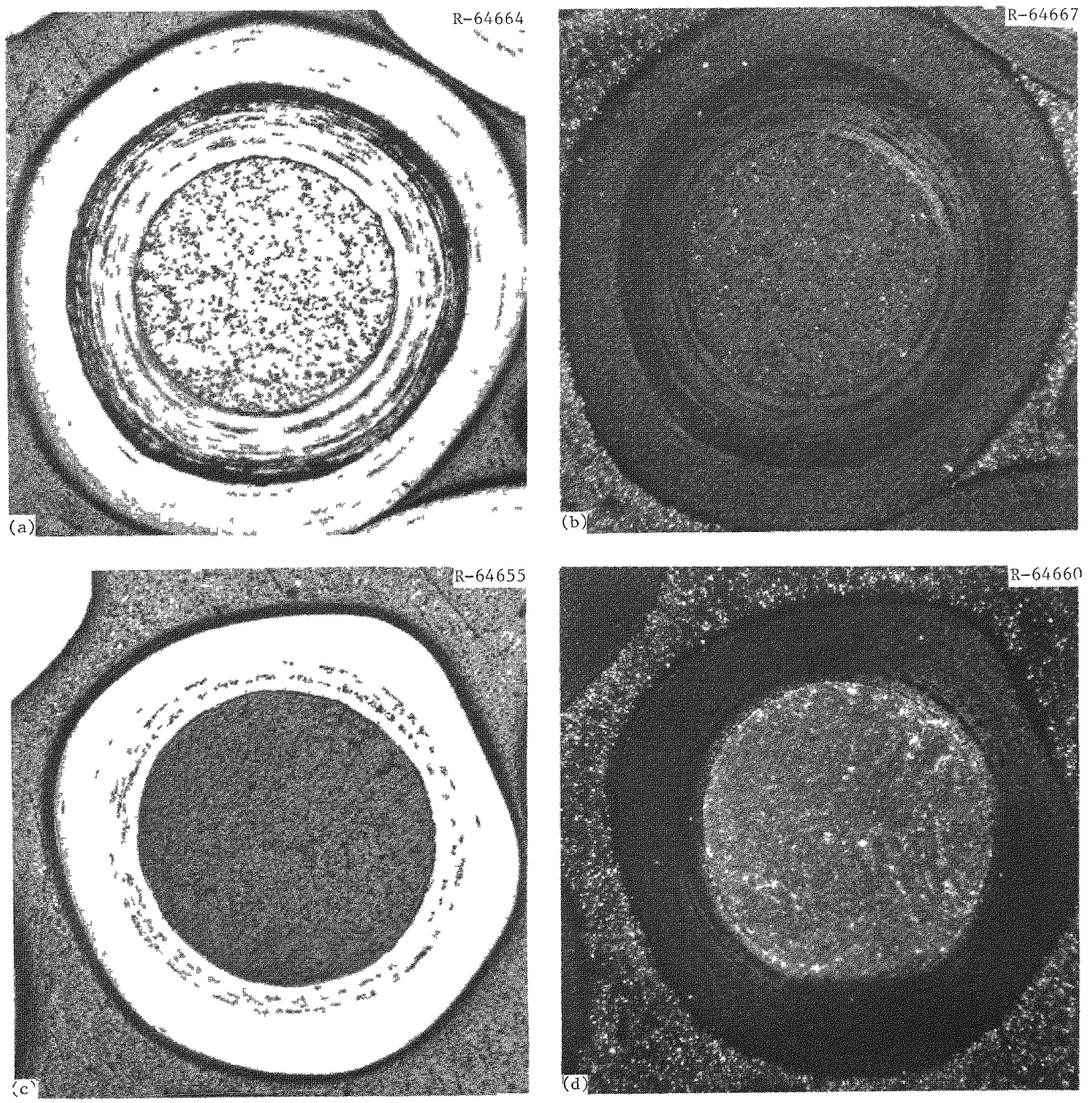

Fig. 3.15. Typical Particles From RTE-4-3-1. 150×. (a) Biso $(4Th,U)O_2$ fissile particle. Bright field. (b) Same. Polarized light. (c) Biso ThC_2 fertile particle. Bright field. (d) Same. Polarized light. Reduced 27.5%.

4. POSTIRRADIATION EXAMINATION OF RECYCLE TEST ELEMENT-2

Recycle Test Element-2 was irradiated in core location F07-06 of Peach Bottom Core 2* from 0 to 701 EFPD. It contained a variety of fissile and fertile fuel combinations, as summarized in Table 4.1. The only PIE results previously published are a summary in the Gas-Cooled Reactor Program Annual Progress Report.[13]

Summaries of the power history, heavy-metal burnup, and neutron fluence performed by GA are presented in Tables 4.2, 4.3, and 4.4, respectively. The time-averaged temperatures and temperature envelopes for the entire element are presented in Figs. 4.1 and 4.2.

Maximum burnups were 45.6, 1.7, and 10.5% FIMA for the fissile, fertile, and mixed thorium-uranium particles, respectively. The highest fuel temperature and fast fluence exposure (E >0.18 MeV) were 1663 K (1390°C) and 3.1×10^{25} n/m^2, respectively. Again the irradiation conditions faced by RTE-2 were more severe than those faced by the two elements previously discussed.

The element was received at ORNL in March 1974 and disassembly started in mid-April. The overall appearance of the element was excellent, with no evidence of any localized regions of corrosive attack. A sooty deposit was present in the region of the lower spacer-ring of the graphite sleeve (Fig. 4.3). This sooty deposit rubbed off easily, exposing the as-machined surface. Similar deposits were observed on the other test elements. After the upper and lower graphite reflector sections were cut off, the six graphite fuel bodies were pushed out of the graphite sleeve. The appearance of the fuel bodies was excellent, with no signs of surface corrosion.

A representative number of fuel rods — about 40% — were removed by tapping the graphite bodies on the hot-cell floor. As in the previous recycle test elements and other irradiation tests,[18] the fuel rods carbonized in the graphite fuel bodies — bodies 4 and 6 — were considerably more difficult to remove than those carbonized before being loaded in the graphite fuel body — body 2.

---

*See ref. 6 for description of core location.

Table 4.1. Fuel-Loading Scheme for Recycle Test Element-2

Body	Fissile Fuel		Fertile Fuel		Fuel-Bed Type
	Particle Type	Batch	Particle Type	Batch	
1	UC_2 Biso	4000-248	ThC_2 Biso	4000-225	Blended Bed[a]
2	$(2Th,U)O_2$ Biso	PR-66	ThC_2 Biso	9T-980-3L	Bonded Rod[b]
3	UC_2 Triso	4000-307	ThC_2 Biso	4000-225	Blended Bed[a]
4	UC_2 Biso	4000-309	ThC_2 Biso	4000-226	Bonded Rod[c]
5	$(4.2Th,U)O_2$ Biso	PR-55	ThC_2 Biso	9T-930-BL	Blended Bed[a]
6	UC_2 Triso	4000-307	ThC_2 Biso	4000-226	Bonded Rod[c]

[a]Blended beds contained calcined graphite powder as a bed stabilizer to to prevent segregation.

[b]Carbonized in packed graphite flour.

[c]Carbonized in graphite fuel body.

The general appearance of the fuel rods carbonized in the bodies was good, with only slight evidence of debonding of the particles at the surface (Fig. 4.4). Most fuel rods had separated at the original rod interfaces, but in a few instances, two fuel rods had stuck together (Fig. 4.5). The two fuel rod segments bowed noticeably. This made its removal from the graphite body even more difficult. "Sooty" regions were noted along the fuel rods from body 4. The rods from body 6 were free of surface deposits. The sooty regions of the fuel rods from body 4 were rust-colored. As Table 4.1 shows, the fuel rods from body 4 contained a Biso-Biso fuel system, while those from body 6 contained a Triso-Biso system and operated at lower temperatures. We also noted that the graphite spine sample from body 4 was more radioactive — about 5 rad at 0.61 m (2 ft.) — than that from body 6, which was 200 mrad. The spine sample from body 3 contained a Triso-Biso fuel system and operated at temperatures comparable to those of body 4; its radiation level was also 200 mrad. These surface deposits will be discussed further in the metallography section, which describes evidence that the deposits resulted from problems in the rod fabrication and not from different fission-product behavior.

Table 4.2. Recycle Test Element-2 Power, Flow, and Flux History

Interval Reference Equivalent Full-Power Time		Thermal Analysis					Nuclear Analysis					
		Irradiation Interval (d)	Absolute Radial Power (kW)	Relative Radial Power	Coolant Relative Radial-Power Factor	TRICUSP Channel Flow (kg/s)	Real[b] Time (a)	Gage Power (kW)	Flux in Groups[c] from Gage, n/m^{2}s				
From EFPD	To EFPD								1A[a]	1B	2	3	4
0.00	26.99	28.84	99.36	0.761	0.848	0.0321	28.84	99 36	3.3032×10^{17}	0.5829×10^{17}	6.7009×10^{17}	1.0902×10^{17}	3.1741×10^{17}
26.99	62.71	38.84	105.62	0.809	0.902	0.0339	38.84	105.62	3.6010	0.6355	7.3206	1.1909	3.4195
62.71	68.57	7.50	85.39	0.783	0.875	0.0329	7.50	85.39	2.9487	0.5204	5.9947	0.9743	2.8294
68.57	202.06	140.94	107.68	0.815	0.912	0.0331	140.94	107.68	3.6899	0.6512	7.5224	1.2236	3.5851
202.06	252.41	53.62	106.50	0.813	0.918	0.0346	60.00	95 19	3.3236	0.5865	6.8135	1.1065	3.4300
252.41	252.41	0.00	106.11	0.810	0.919	0.0346	0.00		0.0000	0.0000	0.0000	0.0000	0 0000
252.41	298.00	48.99	98.78	0.761	0.864	0.0336	56.40	85 80	2.9528	0.5211	6.0526	0.9818	3.1659
298.00	342.95	50.19	101.45	0.812	0.924	0.0333	55.62	91 55	3.2218	0 5686	6.6257	1.0746	3.4827
342.95	385.44	44.83	113.32	0.857	0.983	0.0337	46.98	108 12	3.6891	0.6510	7.5339	1.2239	4.2682
385.44	385 44	0.00	113.98	0.862	0.990	0.0337	0.00		0.0000	0.0000	0.0000	0.0000	0.0000
385.44	499.59	141.93	95.05	0.847	0.975	0.0304	145.87	92.47	3.1573	0.5572	6.4538	1.0479	3.7371
499.59	564.07	72.69	106.17	0.858	0.995	0.0344	80.59	95.75	3.3079	0.5837	6.8991	1.1210	4.2132
564.07	610.25	49.63	117.21	0.903	1 053	0 0338	51.56	115.68	3.9925	0.7046	8.3621	1.3607	5.2581
610.25	701.23	98.73	117.67	0.915	1.074	0.0329	98.73	117.65	4.0213	0.7096	8.4192	1.3713	5.7284
Sum/Time-Weighted Average		776.73	105.76	0.839	0.960	0.0329	811.87	101.36	3.4806	0.6142	7.1627	1.1643	4.0041
Root Mean Square			7.82	0.044	0.066	0.0013		10 09	0.3380	0.0596	0.7394	0.1215	0.8115

[a] Time at nonzero power used in thermal analysis.

[b] Real calendar days used in nuclear analysis. Some short-term zero-power periods are included.

[c] The energy ranges for the flux groups follow:

Group 1A: 14.96 MeV $\geq$ E $\geq$ 0.18 MeV or 2.40 pJ $\geq$ E $\geq$ 28.84 fJ
Group 1B 0.18 MeV $\geq$ E $\geq$ 8.65×10^{4} eV or 28.84 fJ $\geq$ E $\geq$ 13.86 fJ
Group 2· $8\ 65 \times 10^{4}$ eV $\geq$ E $\geq$ 17.60 eV or 13.86 fJ $\geq$ E $\geq$ 2.82 aJ
Group 3. 17.60 eV $\geq$ E $\geq$ 2.38 eV or 2.82 aJ $\geq$ E $\geq$ 0.32 aJ
Group 4: 2.38 eV $\geq$ E $\geq$ 0 or 0.38 aJ $\geq$ E $\geq$ 0

[d] Group 1A, the fast-flux group has been modified from the Cage output by a factor of 0.85 This accounts for the Peach Bottom energy cut-off of 8.65×10^{4} eV instead of 0.18 MeV.

Table 4.3. Fissions per Initial Metal Atom for Recycle Test Element-2

Fuel Body	Fuel Rod	Core Height (mm)	Fertile FIMA (%)	Fissile FIMA (%)	Mixed FIMA (%)
1	1	688	0.115	13.387	2.854
	2	742	0.279	19.797	4.307
	3	797	0.448	25.856	5.691
	4	851	0.618	31.762	7.045
	5	906	0.789	35.326	7.916
	6	960	0.958	38.460	8.697
Mean		824	0.534	27.431	6.085
Range/RMS		327	0.289	8.763	2.035
2	1	1082	1.122	40.142	9.175
	2	1136	1.271	41.567	9.587
	3	1190	1.392	42.512	9.878
	4	1244	1.490	43.323	10.123
	5	1299	1.567	44.025	10.329
	6	1353	1.623	44.538	10.479
Mean		1217	1.411	42.684	9.928
Range/RMS		325	0.173	1.494	0.445
3	1	1477	1.671	44.990	10.611
	2	1530	1.692	45.311	10.694
	3	1583	1.709	45.570	10.761
	4	1636	1.715	45.528	10.757
	5	1690	1.707	45.350	10.714
	6	1743	1.674	44.930	10.601
Mean		1610	1.695	45.280	10.690
Range/RMS		319	0.017	0.244	0.064
4	1	1873	1.634	44.452	10.470
	2	1927	1.589	43.930	10.327
	3	1981	1.541	43.440	10.188
	4	2035	1.493	42.960	10.051
	5	2089	1.426	42.101	9.820
	6	2143	1.355	41.199	9.578
Mean		2008	1.506	43.014	10.072
Range/RMS		324	0.095	1.097	0.301
5	1	2267	1.265	40.156	9.291
	2	2321	1.169	39.019	8.980
	3	2375	1.061	37.704	8.623
	4	2429	0.953	36.226	8.232
	5	2483	0.845	34.608	7.813
	6	2537	0.741	32.991	7.396
Mean		2402	1.006	36.784	8.389
Range/RMS		324	0.181	2.471	0.653
6	1	2664	0.639	31.380	6.983
	2	2718	0.535	29.720	6.558
	3	2772	0.432	28.046	6.131
	4	2825	0.331	26.341	5.699
	5	2879	0.231	24.649	5.270
	6	2933	0.134	22.979	4.848
Mean		2799	0.384	27.186	5.915
Range/RMS		323	0.173	2.875	0.730
Grand Mean		1810	1.089	37.063	8.513
Range/RMS		2299	0.523	8.363	2.13

Table 4.4. Recycle Test Element-2 Thermal- and Fast-Neutron Fluences

Fuel Body	Fuel Rod	Core Height (mm)	Fluence, n/m^2	
			Fast, >0.18 MeV	Thermal, <2.38 eV
1	1	688	0.973×10^{25}	1.150×10^{25}
	2	742	1.354	1.439
	3	797	1.660	1.727
	4	851	1.938	2.013
	5	906	2.180	2.295
	6	960	2.373	2.565
Mean		824	1.746	1.865
Range/RMS		327	0.479	0.485
2	1	1082	2.545	2.820
	2	1136	2.688	3.038
	3	1190	2.807	3.209
	4	1244	2.909	3.350
	5	1299	2.976	3.429
	6	1353	3.029	3.495
Mean		1217	2.826	3.224
Range/RMS		325	0.168	0.234
3	1	1477	3.071	3.548
	2	1530	3.096	3.580
	3	1583	3.112	3.605
	4	1636	3.118	3.620
	5	1690	3.107	3.621
	6	1743	3.091	3.614
Mean		1610	3.099	3.598
Range/RMS		319	0.016	0.026
4	1	1873	3.065	3.597
	2	1927	3.026	3.561
	3	1981	2.979	3.512
	4	2035	2.918	3.441
	5	2089	2.857	3.353
	6	2143	2.794	3.249
Mean		2008	2.940	3.452
Range/RMS		324	0.094	0.121
5	1	2267	2.705	3.119
	2	2321	2.610	2.981
	3	2375	2.507	2.833
	4	2429	2.390	2.679
	5	2483	2.266	2.519
	6	2537	2.128	2.346
Mean		2402	2.435	2.746
Range/RMS		324	0.197	0.264
6	1	2664	1.980	2.173
	2	2718	1.830	2.005
	3	2772	1.642	1.850
	4	2825	1.436	1.714
	5	2879	1.199	1.595
	6	2933	0.871	1.500
Mean		2799	1.493	1.806
Range/RMS		323	0.376	0.232
Total Mean		1810	2.423	2.782
Total Range/RMS		2299	0.665	0.767

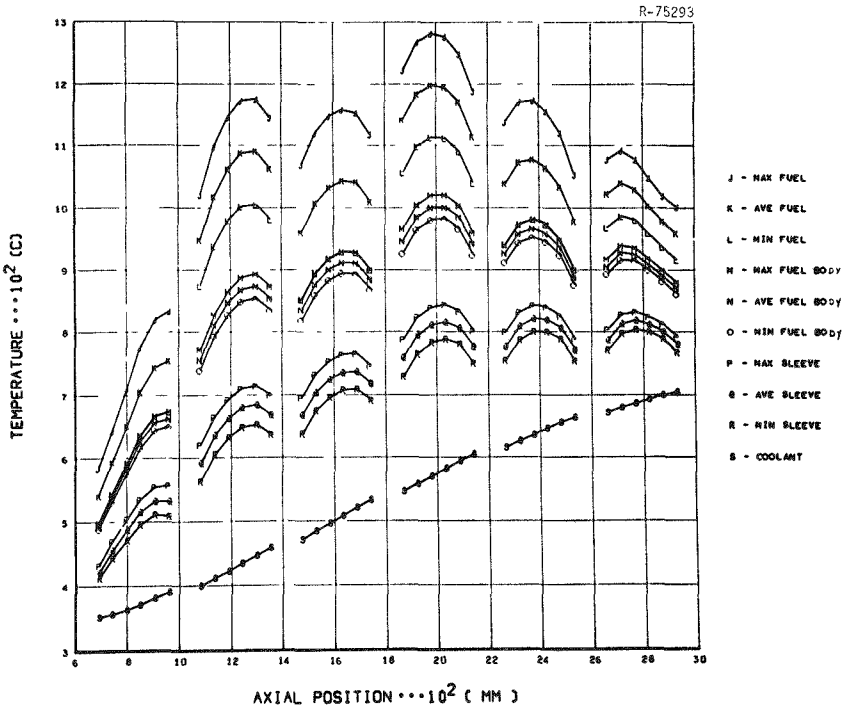

Fig. 4.1. Recycle Test Element-2 Time-Averaged Temperatures: Bodies 1–6.

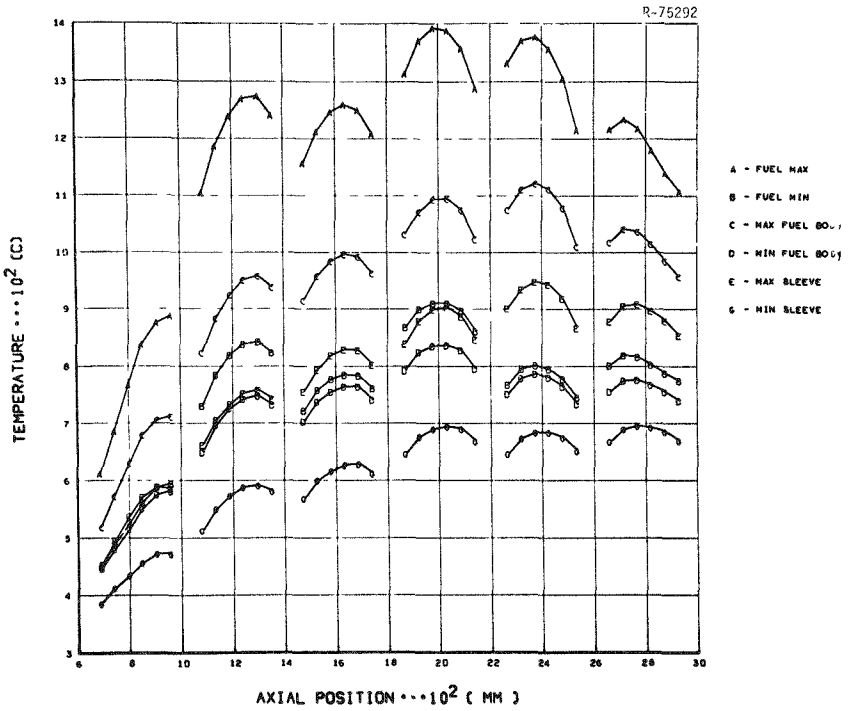

Fig. 4.2. Recycle Test Element-2 Temperature Envelope: Bodies 1-6.

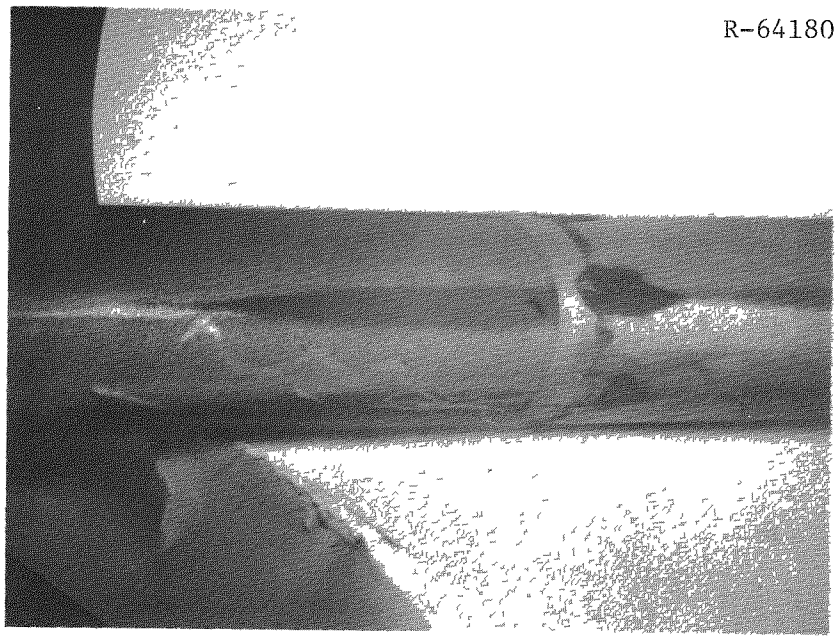

Fig. 4.3. Sooty Deposit Near Lower Spacer-Ring on RTE-2 Graphite Sleeve. 3×.

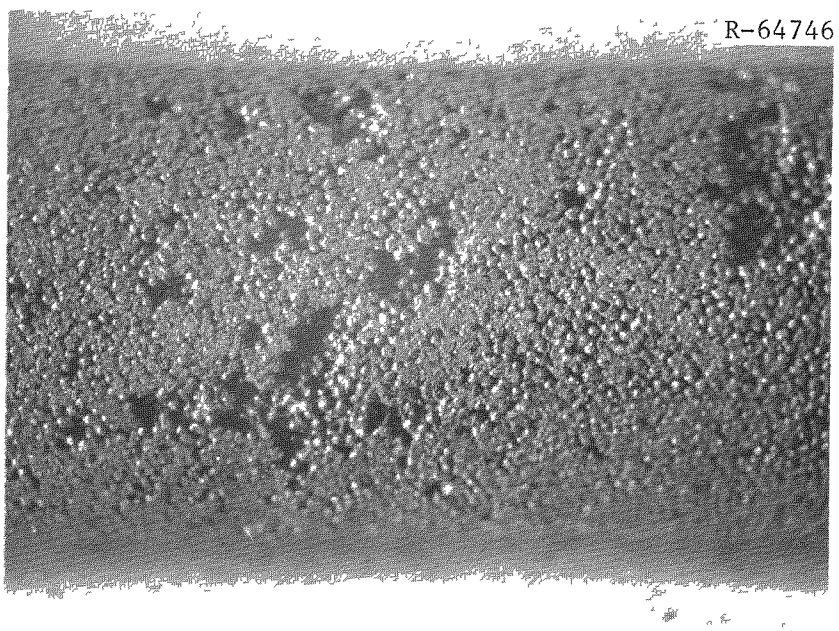

Fig. 4.4. Slight Debonding on Surface of Rods From RTE-2-6. 5×.

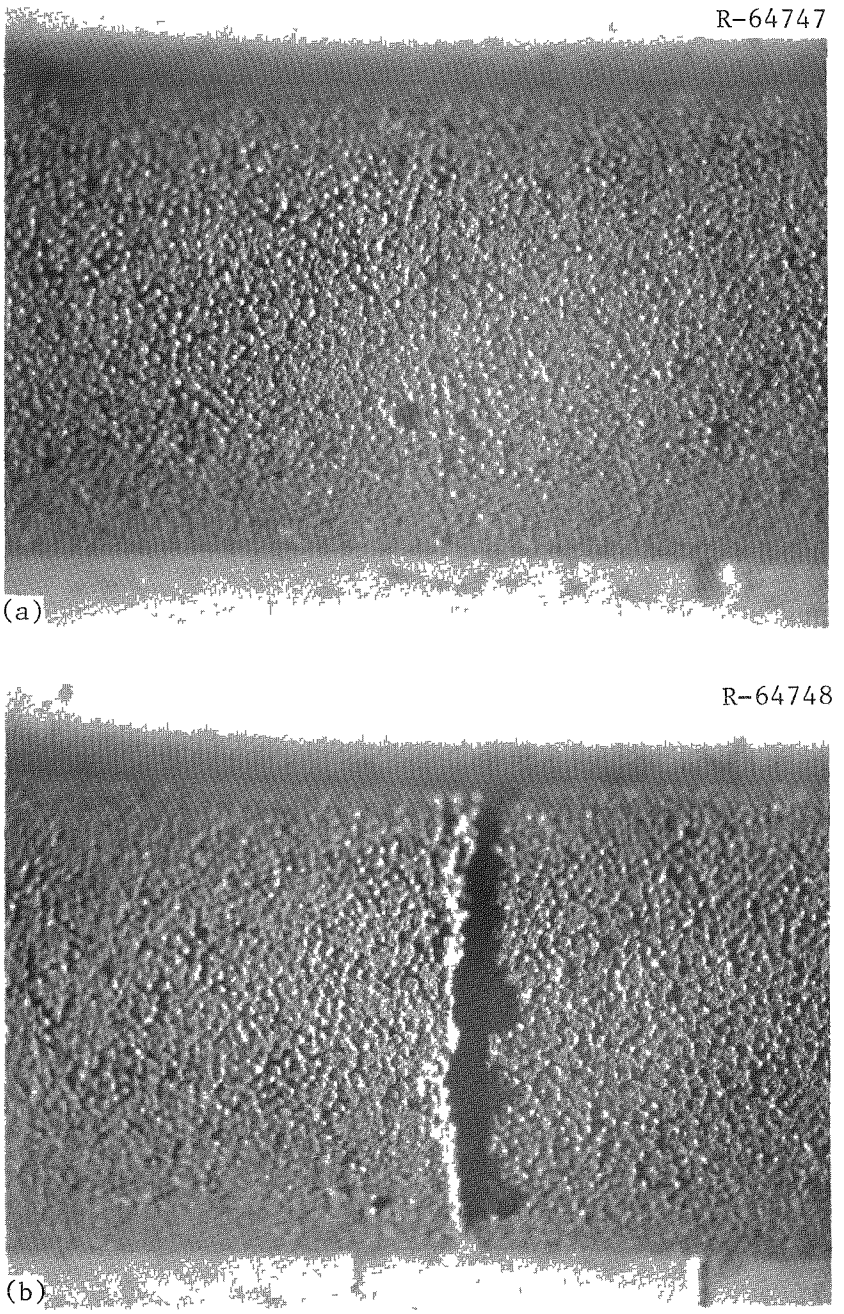

Fig. 4.5. Comparison of Rods From RTE-2-6. 5×. (a) Two rods bonded together. (b) Two nonbonded rods.

The ORNL fuel rods carbonized before loading in graphite body 2 were easily removed. The general appearance of the fuel rods was excellent, with only slight evidence of debonding (Fig. 4.6). Of 24 fuel rods removed from this body, three were found broken near mid-length. The breaks were "clean," and examination of the fracture surfaces revealed no broken coatings.

The differences between observations of the rods carbonized in the graphite fuel bodies and of those that were not indicate a bond of some kind was established between the fuel rod and graphite body when the rods were carbonized in the body. This would explain differences in the ease of rod removal and in the appearance of the rod surfaces.

The blended beds from bodies 1, 3, and 5 were sampled by a vacuum pickup system. All samples were obtained from hole 1 of each body. The loose fissile and fertile particles from body 1 were themselves found to be faceted. We also noted several doublets (Fig. 4.7). We discovered that the particles from body 3 were also faceted and we saw several broken particles and doublets, as well (Fig. 4.8). Samples from body 5 also contained faceted particles and doublets, and we observed a few broken particles (Fig. 4.9).

R-64742

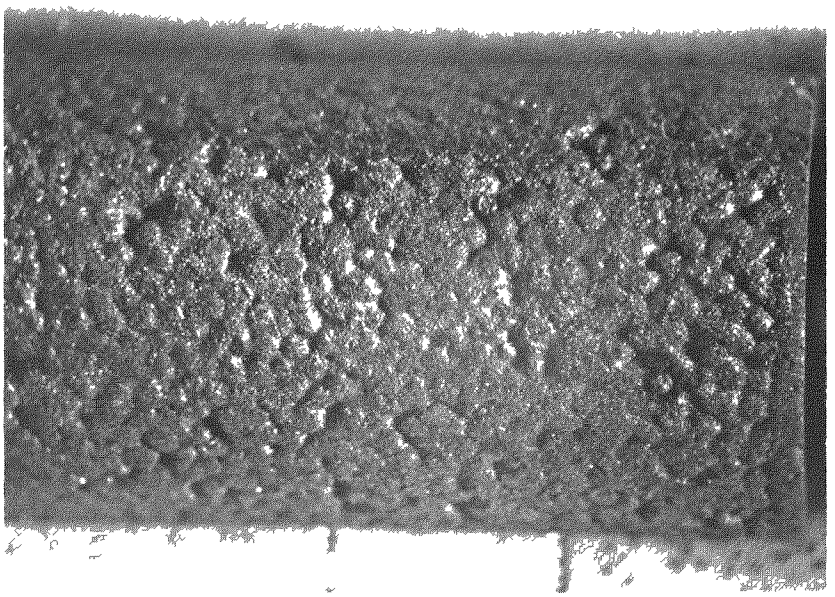

Fig. 4.6. Appearance of Rods from RTE-2-2. 5×.

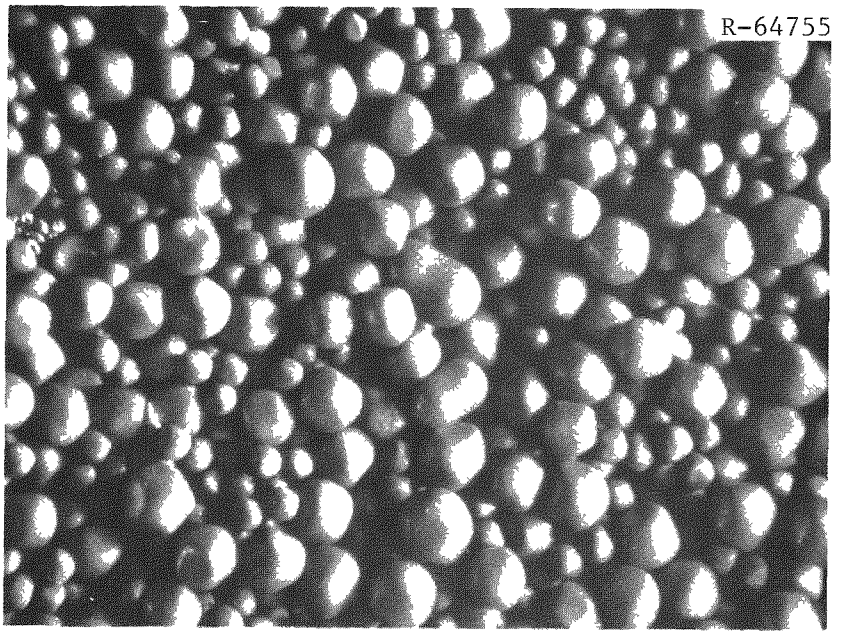

Fig. 4.7. Typical Biso UC_2 Fissile (Small-Diameter) and Biso ThC_2 Fertile (Large-Diameter) Particles from RTE-2-1-1. 14×. Doublets and facets are present in these particles.

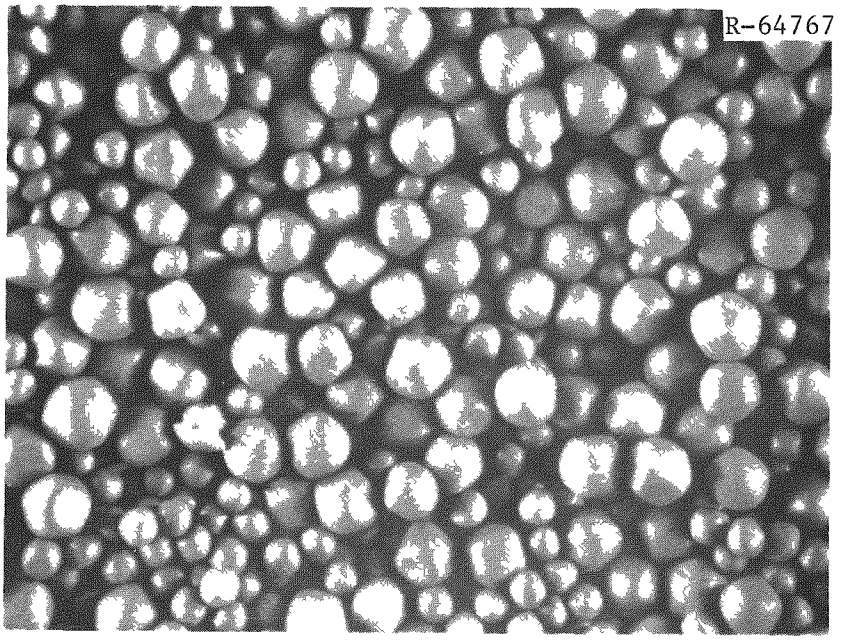

Fig. 4.8. Typical Triso UC_2 Fissile (Small-Diameter) and Biso ThC_2 Fertile (Large-Diameter) Particles from RTE-2-3-1. Note broken particle in lower left hand corner. 14×.

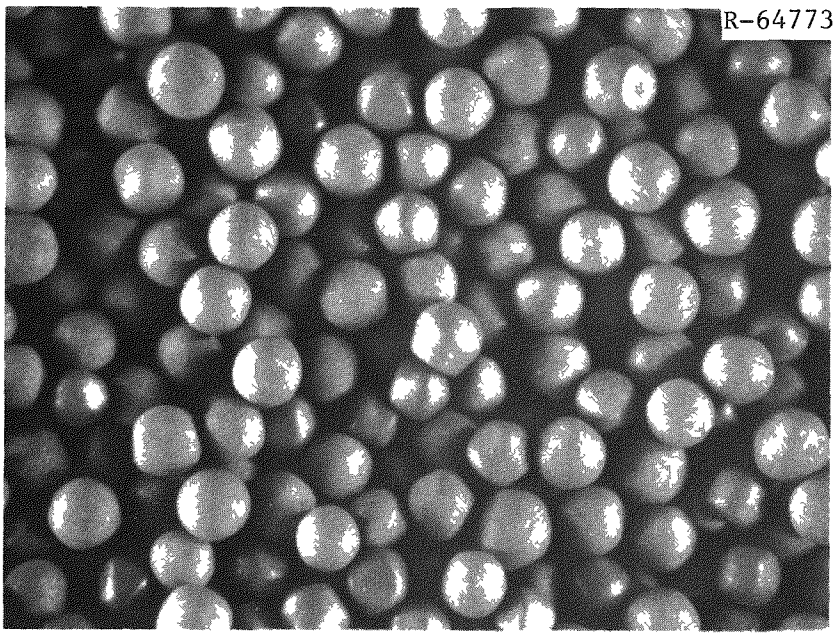

Fig. 4.9. Typical Biso $(4.2Th,U)O_2$ Fissile and Biso ThC_2 Fertile Particles from RTE-2-5-1. 14×.

Transverse sections through fuel rods from bodies 2, 4, and 6 were prepared for metallographic examination. In each case, samples were taken from the maximum-temperature region of each body.

In the two rods examined from body 2 — RTE-2-2-1-2 and RTE-2-2-1-6 — we observed no coating failures or indications of them in the Biso-coated $(2Th,U)O_2$ or ThC_2 particles. We found no evidence of kernel migration in either the fissile or the fertile particles. The low irradiation temperature (the time-averaged temperature was 1020°C) would lead to very low kernel-migration coefficients, so the kernels would not be expected to migrate.[19] Figure 4.10 shows typical particles.

No failures were found upon examination of 611 UC_2 Biso fissile particles (batch 4000-309) from fuel rod RTE-2-4-1-1 from the high-temperature region of body 4. The only significant change noted in the coatings on the fissile particle was densification and an accompanying increase in the anisotropy of the buffer layer. The buffer coating of the same batch of particles irradiated in RTE-4 body 1 showed some

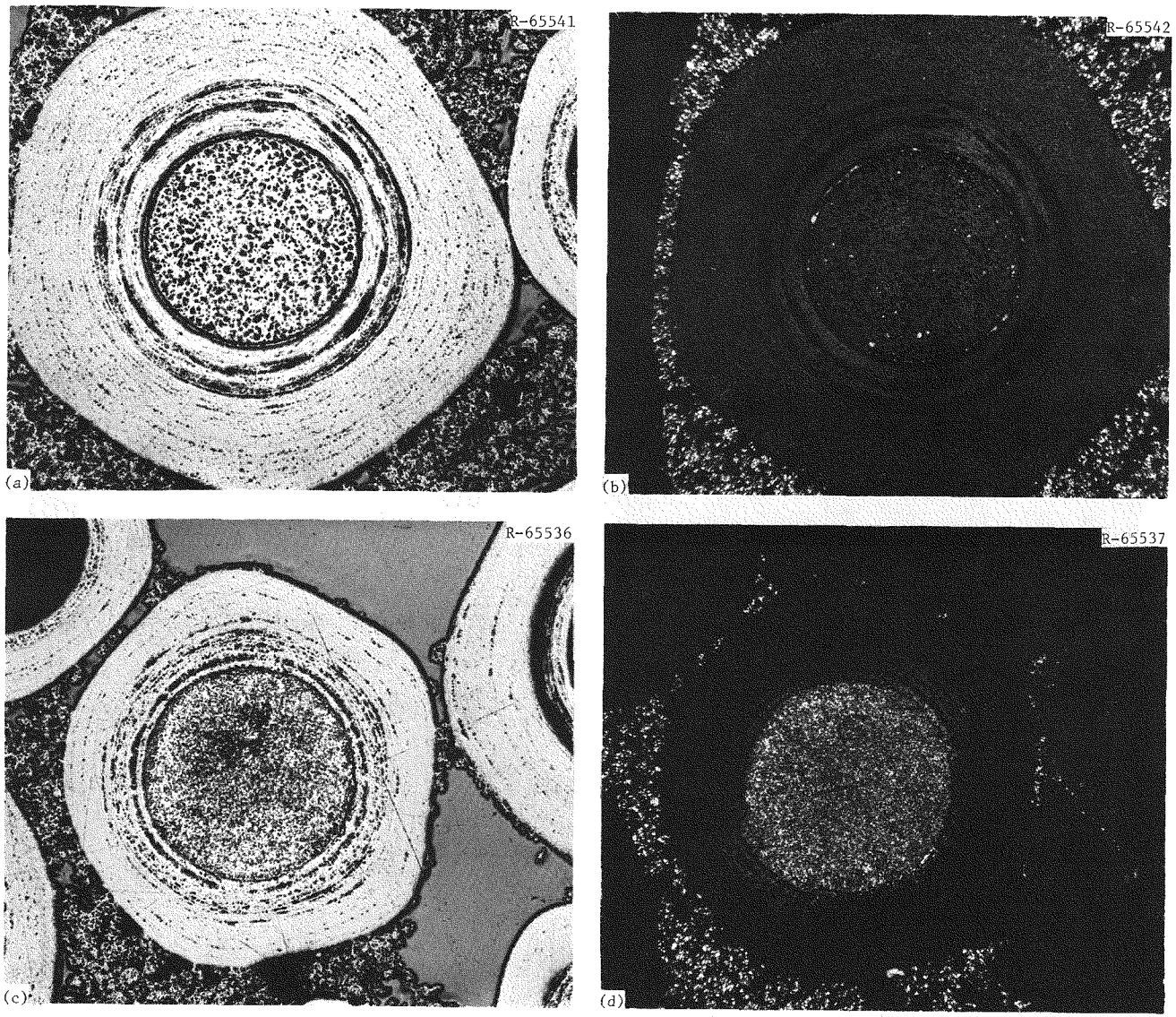

Fig. 4.10. Typical Particles From RTE-2-2-1-6. 150×. (a) Biso $(2Th,U)O_2$ fissile particle. Bright field. (b) Same. Polarized light. (c) Biso ThC_2 fertile particle. Bright field. (d) Same. Polarized light. Reduced 34%.

anisotropy, but it was not as great as in RTE-2. Electron microprobe examination of the particles from RTE-2 showed migration of the rare-earth fission products Nd, La, Pr, and Ce into the buffer coating. The higher temperatures (1498 vs 1093 K, 1225 vs 820°C) and burnups (44.5 vs 16.7% FIMA) attained by the particles in RTE-2 as compared to those in RTE-4 may have increased the content of the rare earths in and consequently, the optical activity of the buffer coating. Optical activity of pyrocarbon caused by the rare earths has been observed previously.[15–17] We found no failures in the ThC_2 Biso fertile particles in RTE-2-4-1-1. We saw no evidence of migration of either the fissile or fertile kernels. Typical particles are shown in Fig. 4.11.

We examined 433 UC_2 Triso fissile particles (batch 4000-307) from fuel rod RTE-2-6-1-1 and found four particles with failed PyC and SiC coatings. The oLTI coatings, as well, had failed on 14 particles (Fig. 4.12). The failures were mechanical ones and were in the form of radial cracks. Tears that indicated matrix-particle interaction were present in the oLTI layers of about 25% of the particles.

In the fissile particles across nearly the entire diameter of fuel rod R-2-6-1-1, we noted graphitization of the cold side of the iLTI. Graphitization of the iLTI is associated with the collection of rare-earth fission products on the cold side of fissile particles, as the previous section on RTE-4 shows. The attack of the SiC by fission products was not measureable. The average fuel temperature was 1298 K (1025°C) during irradiation. We found no failures among the Biso ThC_2 fertile particles. We also found no evidence of kernel migration in either the fissile or fertile particles. Typical particles from RTE-2-6-1-1 are shown in Fig. 4.13.

Samples were taken from the maximum-temperature region of each of the bodies containing the blended beds and were examined metallographically. A sample from body 5 was found free of unusual microstructural features and its Biso $(4.2Th,U)O_2$ particles achieved 9.2% FIMA. This sample operated at a maximum time-averaged temperature of 1443 K (1170°C), and its Biso $(4.2Th,U)O_2$ particles achieved 9.2% FIMA. We saw no evidence of migration of either the $(4.2Th,U)O_2$ fissile or the

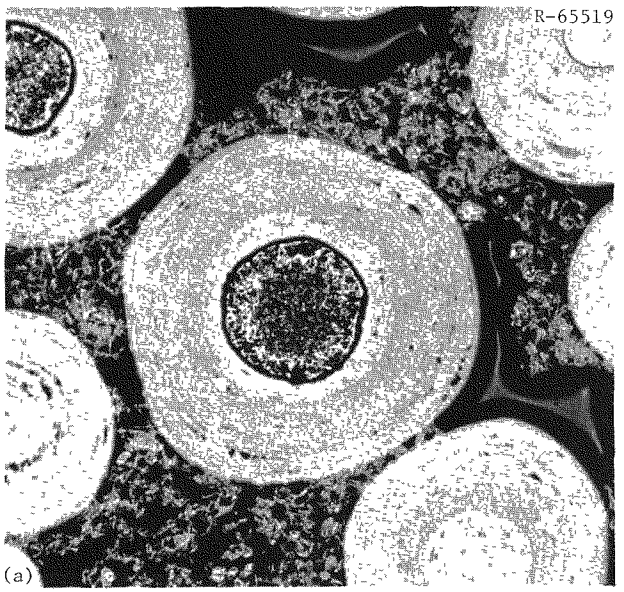

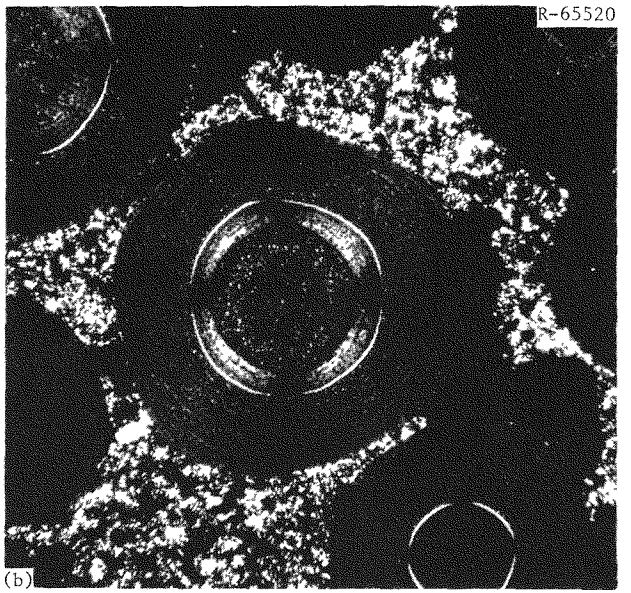

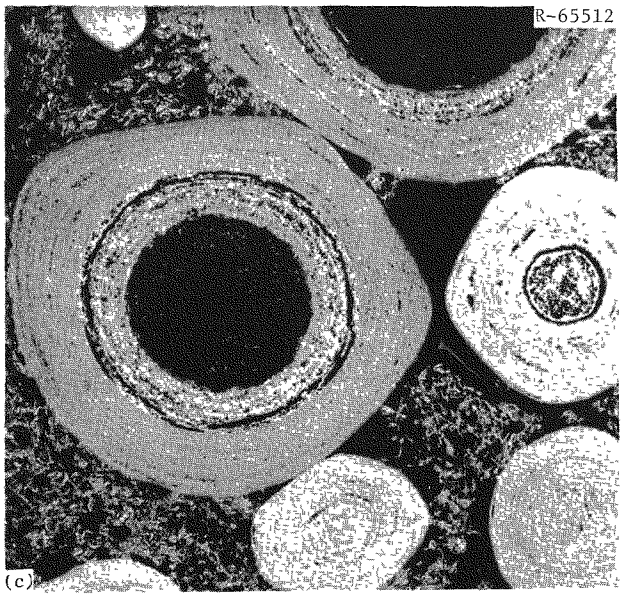

Fig. 4.11. Typical Particles from RTE-2-4-1-1. (a) Biso UC_2 fissile particle. 200×. Bright field. (b) Same. Polarized light. (c) Biso ThC_2 particle under bright field. 150×. Reduced 28.5%.

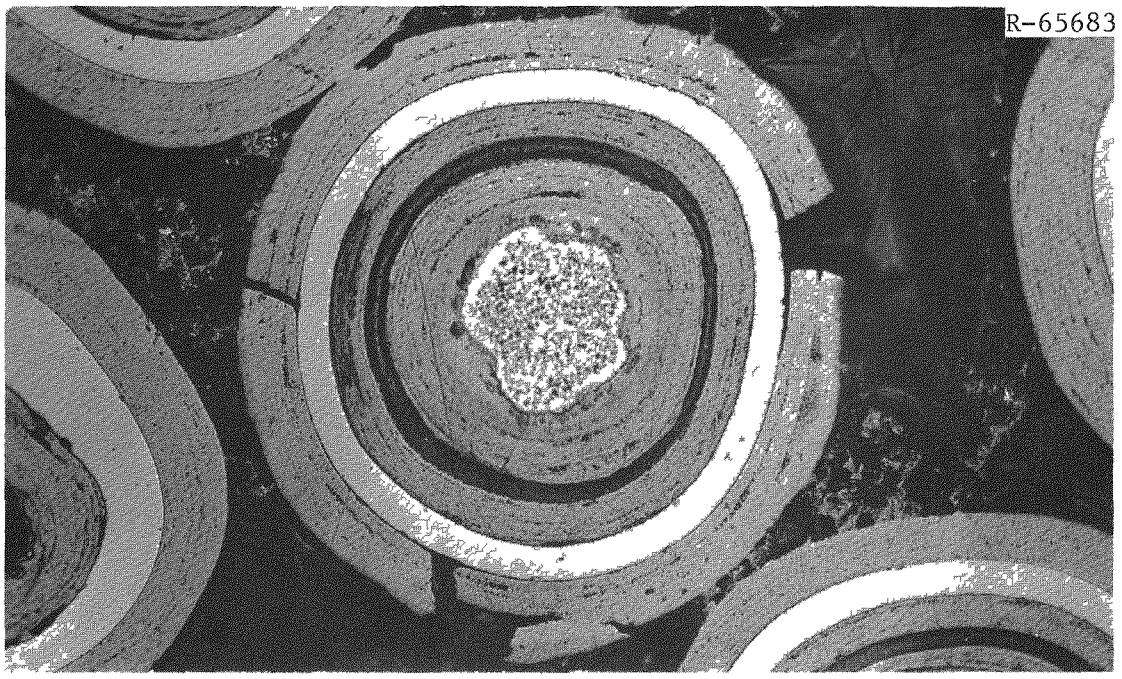

Fig. 4.12. Failure of the oLTI Coating of Triso UC_2 Fissile Particle from RTE-2-6-1-1. 250×.

Biso-coated ThC_2 fertile kernels, nor any indication of failure or potential failure of either the fissile or fertile particles. Typical particles from 2-5-1 are shown in Fig. 4.14.

Examination of the Biso UC_2 fissile particles from body 1 revealed no unexpected changes or failures. The maximum burnup in these particles was 38.5% FIMA and the maximum time-averaged temperature was 1113 K (840°C). The kernels contained numerous relatively small fission gas bubbles and showed no evidence of migration. Polarized light clearly revealed a thin (3- to 4-μm) sealer coat that had been put on the buffer coating before deposition of the oLTI coating. The sealer coat did no harm to the coatings. In addition, optical anisotropy of the buffer coat was not evident in the batch 4000-248 particles, but it was in the Biso UC_2 particles from batch 4000-309. However, the irradiation temperature may have been low enough to prevent sufficient fission-product migration out of the kernel. Examination of the Biso ThC_2 fertile particles revealed no evidence of kernel migration or coating failure. Typical particles from RTE-2-1-1 are shown in Fig. 4.15.

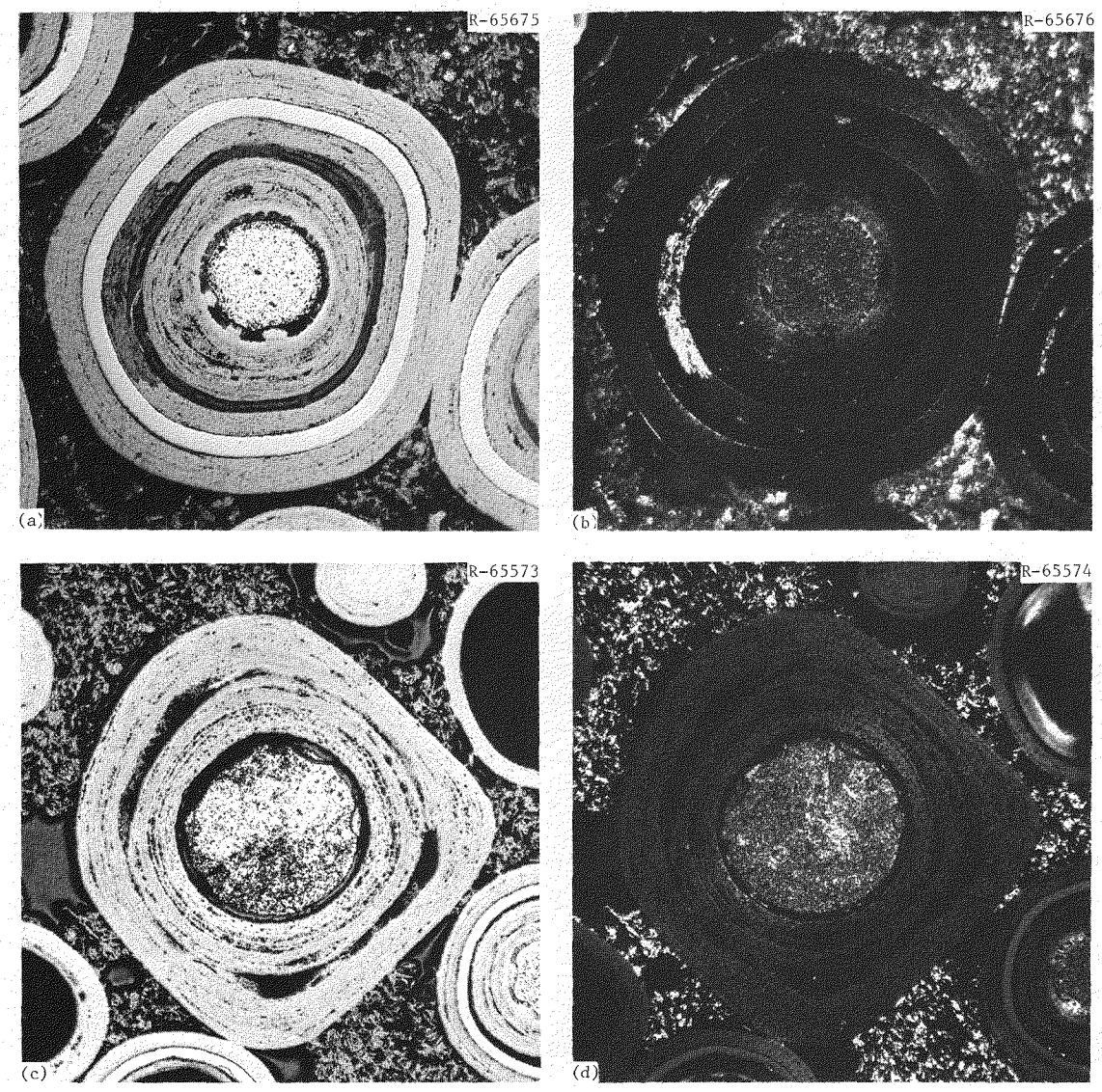

Fig. 4.13. Typical Particles from RTE-2-6-1-1. (a) Triso UC_2 fissile particle 400 μm from outer surface. Bright field. 250×. (b) Same, polarized light. (c) Biso ThC_2 fertile particle, midradius. Bright field. 150×. (d) Same, polarized light. Reduced 34%.

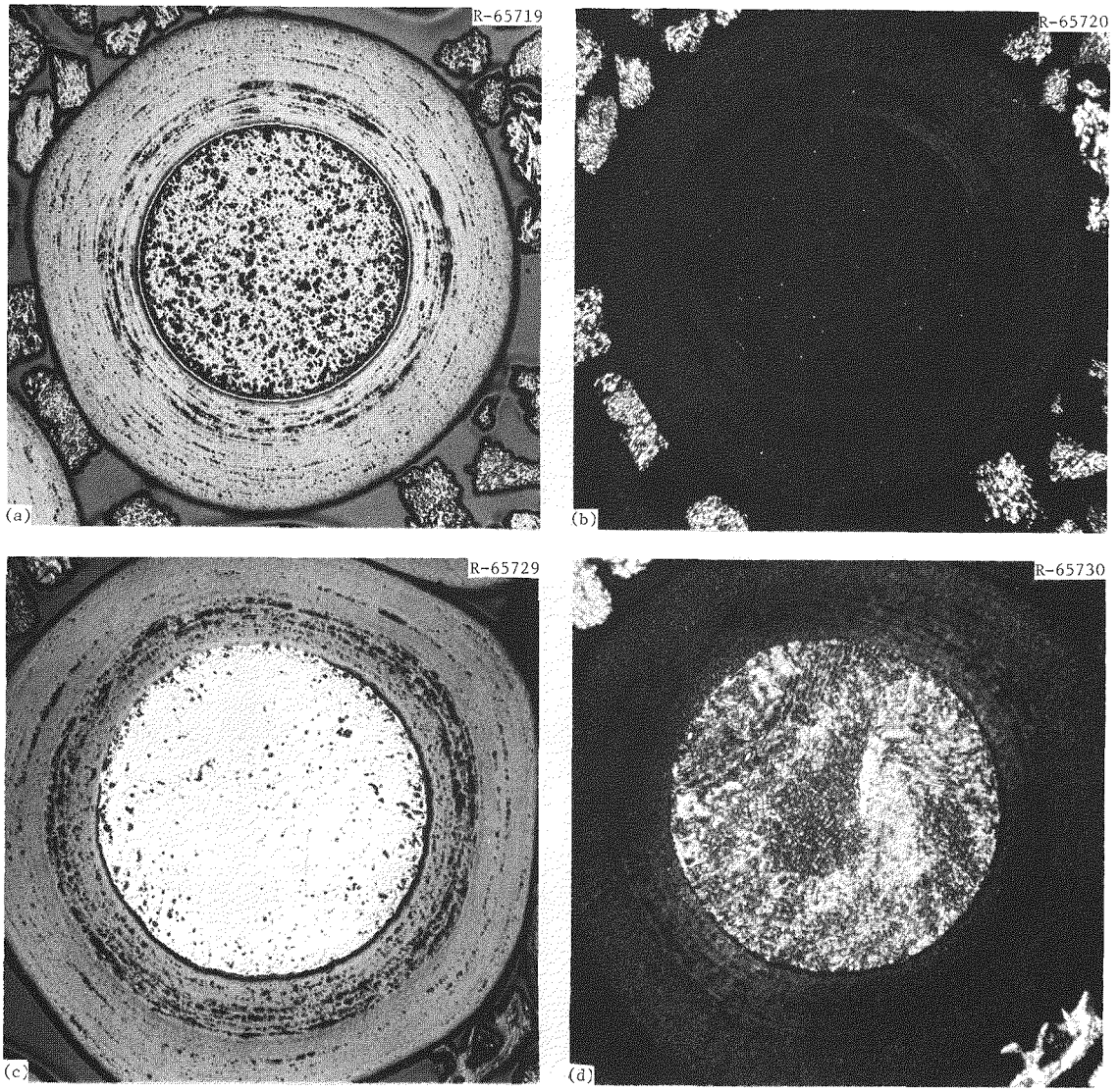

Fig. 4.14. Typical Particles from Maximum-Temperature Region of RTE-2-5-1. (a) Biso $(4.2Th,U)O_2$ fissile particle. 150×. Bright field. (b) Same. Polarized light. (c) Biso ThC_2 fertile particle. 200×. Bright field. (d) Same. Polarized light. Reduced 36%.

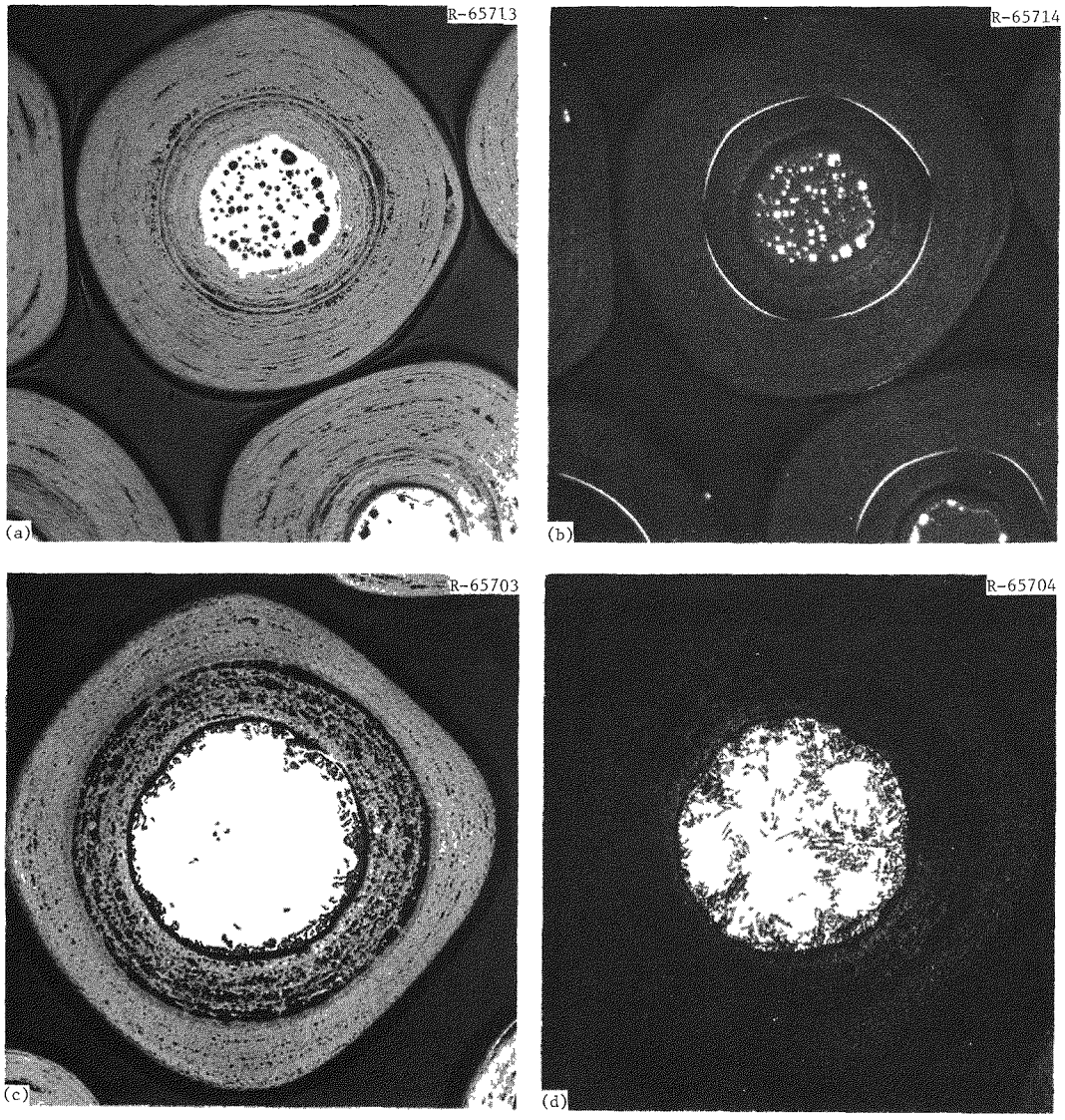

Fig. 4.15. Typical Particles from Maximum-Temperature Region of RTE-2-1-1. (a) Biso UC_2 fissile particle. 250×. Bright field. (b) Same. Polarized light. (c) Biso ThC_2 fertile particle. 200×. Bright field. (d) Same. Polarized light. Reduced 37.5%.

The Triso UC_2 particles from body 3 showed many similarities to the particles bonded in rods from body 6. A count of 472 Triso coatings revealed that 17 SiC coatings (3.6%) had failed. Statistically, this represents a failure fraction range of between 2.8 and 5.4% at a 95% confidence level. The failures were in the form of straight-line radial cracks. Viewing the coatings under polarized light showed that the failures were associated with graphitized regions in the iLTI layers. The apparent graphitization of the iLTI has been associated with the accumulation of the rare-earth fission products on the cold side of the particle. This behavior has been observed previously[15–17] and occurred in the same batch of fissile particles used in the fuel rods in body 6 of this element. No tears in the outer surface regions were seen in any of the fissile particles. The absence of tears supports the matrix-particle interaction observed for the fuel rods contained in body 6 of this element. Examination of the Biso ThC_2 fertile particles revealed no evidence of kernel migration or coating failures. Typical fissile particles from RTE-2-3-1 are shown in Fig. 4.16.

5. POSTIRRADIATION EXAMINATION OF RECYCLE TEST ELEMENT-5

Recycle Test Element-5 was irradiated in core location C10-06* from 0 to 897.4 Effective Full-Power Days of Peach Bottom Core 2. Table 5.1 identifies the type of fuel loading combinations in the element. In addition, 12 fuel samples made from six types of graphite filler were located in the spine positions in bodies 2 and 4. Table 5.2 shows the graphite fillers and fuels used in the spine samples.

The nuclear and thermal evaluations of this element were also performed by GA. Summaries of the power history, heavy-metal burnup, and neutron fluence are given in Tables 5.3, 5.4, and 5.5, respectively. The time-averaged temperatures and temperature envelopes for the entire element are presented in Figs. 5.1 through 5.8. Since the heavy-metal loadings in — and, therefore, the power production from — fuel

*See ref. 6 for core location.

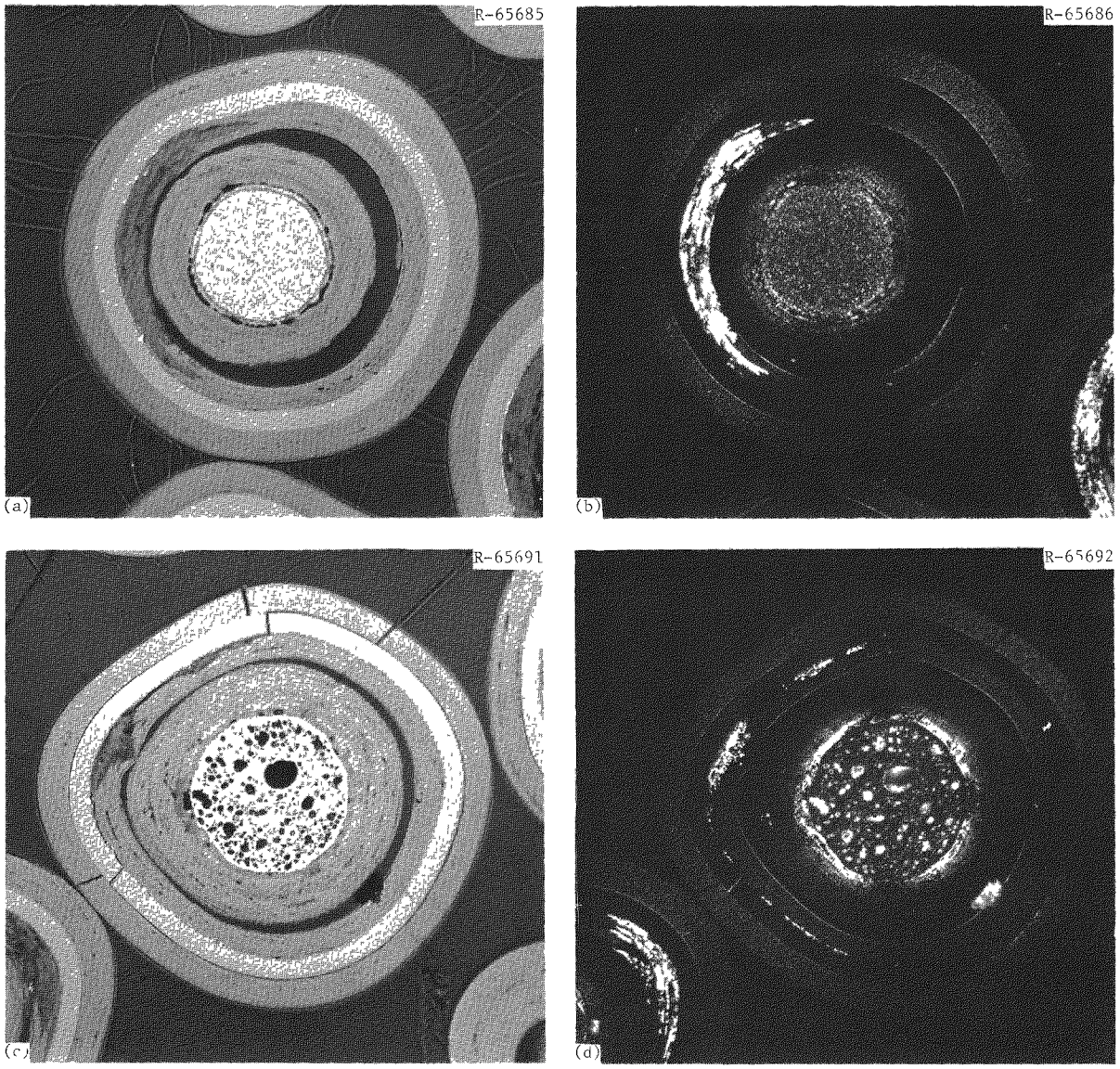

Fig. 4.16. Triso UC_2 Particles from RTE-2-3-1. 250×. (a) An intact particle. Bright field. (b) Same. Polarized light. (c) A failed particle. Bright field. (d) Same. Polarized light. Reduced 32.5%.

Table 5.1. Fuel-Loading Scheme for Recycle Test Element-5

Body	Hole	Fissile Fuel		Fertile Fuel		Carbonization Procedure for Fuel-Bed Bonded Rods
		Particle Type	Batch	Particle Type	Batch	
1,2,3,4	1,2	(4Th,U)O_2 Biso	PR-57-1	ThC_2 Biso	4000-225	CGT[a]
	3,4	(2Th,U)O_2 Biso	PR-61	ThO_2 Biso	PR-51	PGF[b]
	5,6	UC_2 Triso	4000-307	ThC_2 Biso	4000-226	CGT
	7,8	UO_2 Biso	Mixed 1	ThO_2 Biso	PR-48[c]	PGF
5	1,2	UO_2 Biso	4000-274	ThC_2 Biso	4000-225	CGT
	3,4	UC_2 Biso	4000-309	ThC_2 Biso	4000-226	CGT
	5,6	UC_2 Biso	4000-309	ThO_2 Biso	PR-47	CGT
	7,8	(2Th,U)O_2 Biso	PR-60	ThC_2 Biso	4000-225	PGF
6	1,2	UO_2 Biso	4000-274	ThC_2 Biso	4000-226	CGT
	3,4	(2Th,U)O_2 Biso	PR-60	ThC_2 Biso	4000-225	PGF
	5,6	UC_2 Biso	4000-309	ThC_2 Biso	4000-226	CGT
	7,8	UC_2 Triso	4000-307	ThC_2 Triso	4000-306	CGT

[a] Carbonized in covered graphite tray.

[b] Carbonized in packed graphite flour.

[c] Stacks RTE-5-1-4 and RTE-5-4-8 actually used combinations of OR-1256, -1257, -1258, and PR-48.

Table 5.2. Description of Graphite Filler Samples in Recycle Test Element-5

Sample[a]	Matrix Filler			Fissile Particle Batch[c]	Fertile Particle Batch[d]
	Content[b] (%)	Particle Size (μm)	Material		
1A,1B	35	<40	TOZ Graphite	Mixed 3	Mixed A
2A,2B	50		Thermax Carbon Black	Mixed 3	Mixed A
3A,3B	40	<27	Robinson Graphite	Mixed 3	Mixed A
4A,4C	35	<27	Poco Graphite	Mixed 2	PR-51
5A,5C	40	<40	Santa Maria Graphite	Mixed 2	PR-51
6A,6B	35	<40	Asbury Graphite	Mixed 3	Mixed A

[a] Samples 1A, 2A, 3A, 4A, 5A, and 6A were located in body 2, all others in body 4.

[b] Weight percent of filler in matrix; the rest consisted of 15 V pitch.

[c] All fissile particles were Biso UO_2.

[d] All fertile particles were Biso ThO_2.

Table 5.3. Recycle Test Element-5 Power, Flow, and Flux History

Interval Reference Equivalent Full-Power Time		Thermal Analysis					Nuclear Analysis						
		Irradiation Interval[a]	Absolute Radial Power	Relative Radial Power	Coolant Relative Radial-Power Factor	TRICUSP Channel Flow	Real Time[b]	Gage Power	Flux in Groups[c] from Gage, n/m^2s				
From EFPD	To EFPD	(d)	(kW)			(kg/s)	(d)	(kW)	1A[d]	1B	2	3	4
0.00	26.99	28.84	109.54	0.839	1.022	0.0315	28.84	109.54	3.8398×10^{17}	0.6776×10^{17}	7.6528×10^{17}	1.2067×10^{17}	4.0640×10^{17}
26.99	62.71	38.84	110.06	0.843	1.027	0.0334	38.84	110.06	3.9680	0.7002	7.9480	1.3093	4.1530
62.71	68.57	7.50	91.73	0.841	1.024	0.0324	7.50	91.73	3.3463	0.5905	6.7055	1.1029	3.5469
68.57	202.06	140.94	111.38	0.843	1.027	0.0326	140.94	111.38	4.0397	0.7129	8.1200	1.3363	4.3280
202.06	252.41	53.62	110.04	0.840	1.024	0.0342	60.00	98.36	3.6269	0.6400	7.3545	1.2064	4.1434
252.41	252.41	0.00	109.91	0.839	1.023	0.0342	0.00	0.00	0.0000	0.0000	0.0000	0.0000	0.0000
252.41	298.00	48.99	106.05	0.817	1.002	0.0331	56.40	92.12	3.3392	0.5893	6.7642	1.1077	3.9475
298.00	342.95	50.19	102.58	0.821	1.008	0.0330	55.62	92.58	3.4404	0.6071	7.0167	1.1489	4.1123
342.95	385.44	44.83	108.56	0.821	1.008	0.0336	46.98	103.58	3.7676	0.6649	7.7106	1.2618	4.7400
385.44	385.44	0.00	108.56	0.821	1.008	0.0036	0.00	0.00	0.0000	0.0000	0.0000	0.0000	0.0000
385.44	499.59	141.93	92.36	0.823	1.010	0.0303	145.87	89.86	3.2586	0.5750	6.6798	1.0923	4.1875
499.59	564.07	72.69	102.70	0.830	1.019	0.0343	80.59	92.63	3.3761	0.5958	7.0021	1.1443	4.6973
564.07	610.25	49.63	108.12	0.833	1.024	0.0339	51.56	104.08	3.9093	0.6899	8.1762	1.3362	5.5858
610.25	701.23	98.73	107.64	0.837	1.030	0.0330	98.73	107.63	3.9172	0.6913	8.2578	1.3506	5.9857
701.23	701.23	0.00	107.12	0.833	1.024	0.0330	0.00	0.00	0.0000	0.0000	0.0000	0.0000	0.0000
701.23	748.00	50.74	107.25	0.834	1.025	0.0336	50.74	107.24	3.9229	0.6923	8.3117	1.3583	6.3233
748.00	788.00	50.00	92.86	0.832	1.024	0.0283	50.00	92.85	3.5272	0.6225	7.5295	1.2309	5.7814
788.00	818.00	39.20	88.49	0.829	1.020	0.0288	37.50	92.52	3.5339	0.6236	7.5755	1.2386	5.9781
818.00	835.00	30.00	66.11	0.832	1.022	0.0239	30.00	66.08	2.4640	0.4348	5.2758	0.8620	4.3249
835.00	858.00	29.00	91.57	0.825	1.015	0.0313	29.00	91.57	3.4658	0.6116	7.4760	1.2230	6.1038
858.00	889.00	47.00	77.10	0.820	1.008	0.0297	47.00	77.11	2.9277	0.5167	6.3494	1.0394	5.2752
889.00	897.30	12.00	68.18	0.817	1.005	0.0285	12.00	68.19	2.5990	0.4587	5.6527	0.9254	4.8053
Sum/Time-Weighted Average		1034.67	100.64	0.831	1.019	0.0319	1068.11	97.49	3.5769	0.6312	7.3949	1.2113	4.8240
Root Mean Square			11.52	0.008	0.008	0.0023		11.14	0.3807	0.672	0.7408	0.1224	0.7971

[a] Time at nonzero power used in thermal analysis.

[b] Real calendar days used in nuclear analysis. Some short-term zero-power periods are included.

[c] The energy ranges for the flux groups follow:

Group 1A: 14.96 MeV ≥ E ≥ 0.18 MeV or 2.40 pJ ≥ E ≥ 28.84 fJ
Group 1B: 0.18 MeV ≥ E ≥ 8.65×10^4 eV or 28.84 fJ ≥ E ≥ 13.86 fJ
Group 2: 8.65×10^4 eV ≥ E ≥ 17.60 eV or 13.86 fJ ≥ E ≥ 2.82 aJ
Group 3: 17.60 eV ≥ E ≥ 2.38 eV or 2.82 aJ ≥ E ≥ 0.38 aJ
Group 4: 2.38 eV ≥ E ≥ 0 or 0.38 aJ ≥ E ≥ 0

[d] Group 1A, the fast-flux group, has been modified from the Gage output by a factor of 0.85. This accounts for the Peach Bottom energy cut-off of 8.65×10^4 eV instead of 0.18 MeV.

Table 5.4. Fissions per Initial Metal Atom for Recycle Test Element-5

Fuel Body	Fuel Rod	Core Height (mm)	Fertile FIMA (%)	Fissile FIMA (%)	Mixed FIMA (%)
1	1	687	0.287	17.643	2.834
	2	741	0.537	26.060	4.282
	3	795	0.790	33.998	5.663
	4	849	1.044	41.698	7.010
	5	903	1.298	46.081	7.871
	6	957	1.552	49.876	8.644
Mean		822	0.918	35.892	6.051
Range/RMS		324	0.433	11.302	2.024
2	1	1081	1.791	51.910	9.146
	2	1135	2.015	53.740	9.606
	3	1189	2.194	54.995	9.943
	4	1243	2.341	56.049	10.223
	5	1297	2.451	56.877	10.439
	6	1351	2.541	57.460	10.601
Mean		1216	2.222	55.172	9.993
Range/RMS		324	0.258	1.899	0.498
3	1	1477	2.621	57.913	10.736
	2	1531	2.683	58.312	10.847
	3	1585	2.738	58.682	10.949
	4	1639	2.748	58.738	10.965
	5	1693	2.746	58.679	10.955
	6	1747	2.705	58.265	10.859
Mean		1612	2.707	58.432	10.885
Range/RMS		325	0.045	0.297	0.081
4	1	1896	2.653	57.803	10.746
	2	1950	2.586	57.279	10.612
	3	2004	2.512	56.737	10.470
	4	2058	2.435	56.185	10.324
	5	2112	2.354	55.496	10.153
	6	2166	2.270	54.772	9.975
Mean		2031	2.468	56.379	10.380
Range/RMS		324	0.131	1.030	0.263
5	1	2266	2.140	53.723	9.710
	2	2320	2.003	52.573	9.425
	3	2374	1.844	51.055	9.066
	4	2428	1.683	49.344	8.677
	5	2482	1.522	47.364	8.249
	6	2536	1.356	45.361	7.814
Mean		2401	1.758	49.903	8.824
Range/RMS		324	0.270	2.899	0.655
6	1	2662	1.186	43.324	7.370
	2	2717	1.020	41.137	6.908
	3	2772	0.855	38.912	6.440
	4	2827	0.684	36.748	5.977
	5	2882	0.512	34.593	5.514
	6	2937	0.339	32.450	5.051
Mean		2800	0.766	37.861	6.210
Range/RMS		331	0.289	3.717	0.792
Grand Mean		1814	1.807	48.940	8.724
Grand Range/RMS		2305	0.788	10.270	2.159

Table 5.5. Recycle Test Element-5 Fast- and Thermal-Neutron Fluences

Fuel Body	Fuel Rod	Core Height (mm)	Fluence, n/m^2	
			Fast, >0.18 MeV	Thermal, <2.38 eV
1	1	687	1.308×10^{25}	1.741×10^{25}
	2	741	1.817	2.190
	3	795	2.217	2.635
	4	849	2.581	3.077
	5	903	2.890	3.516
	6	957	3.143	3.937
Mean		822	2.326	2.849
Range/RMS		324	0.627	0.751
2	1	1081	3.367	4.339
	2	1135	3.548	4.682
	3	1189	3.703	4.965
	4	1243	3.837	5.205
	5	1297	3.924	5.343
	6	1351	3.999	5.464
Mean		1216	3.730	5.000
Range/RMS		324	0.219	0.390
3	1	1477	4.056	5.563
	2	1531	4.097	5.632
	3	1585	4.127	5.688
	4	1639	4.139	5.725
	5	1693	4.136	5.742
	6	1747	4.125	5.748
Mean		1612	4.114	5.683
Range/RMS		325	0.029	0.067
4	1	1896	4.102	5.733
	2	1950	4.067	5.692
	3	2004	4.020	5.627
	4	2058	3.957	5.524
	5	2112	3.890	5.401
	6	2166	3.818	5.247
Mean		2031	3.976	5.537
Range/RMS		324	0.099	0.170
5	1	2266	3.720	5.056
	2	2320	3.610	4.848
	3	2374	3.486	4.618
	4	2428	3.346	4.376
	5	2482	3.195	4.125
	6	2536	3.019	3.848
Mean		2401	3.396	4.479
Range/RMS		324	0.239	0.413
6	1	2662	2.824	3.564
	2	2717	2.609	3.273
	3	2772	2.356	3.017
	4	2827	2.067	2.783
	5	2882	1.724	2.581
	6	2937	1.252	2.420
Mean		2800	2.139	2.940
Range/RMS		331	0.533	0.394
Total Mean		1814	3.280	4.415
Total Range/RMS		2305	0.856	1.219

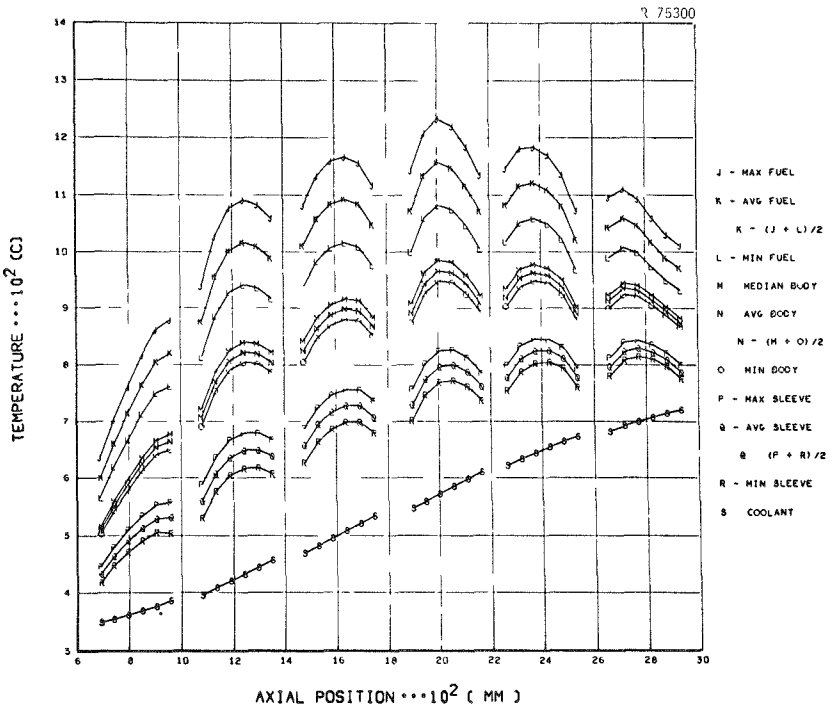

Fig. 5.1. Recycle Test Element-5 Time-Averaged Temperatures: Bodies 1–6, Holes 1–2.

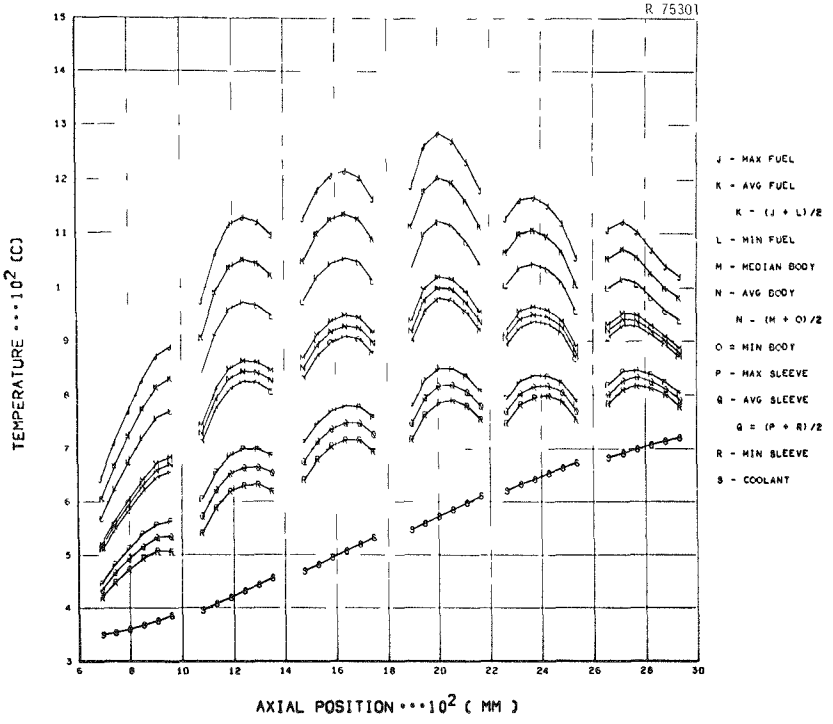

Fig. 5.2. Recycle Test Element-5 Time-Averaged Temperatures: Bodies 1–6, Holes 3–4.

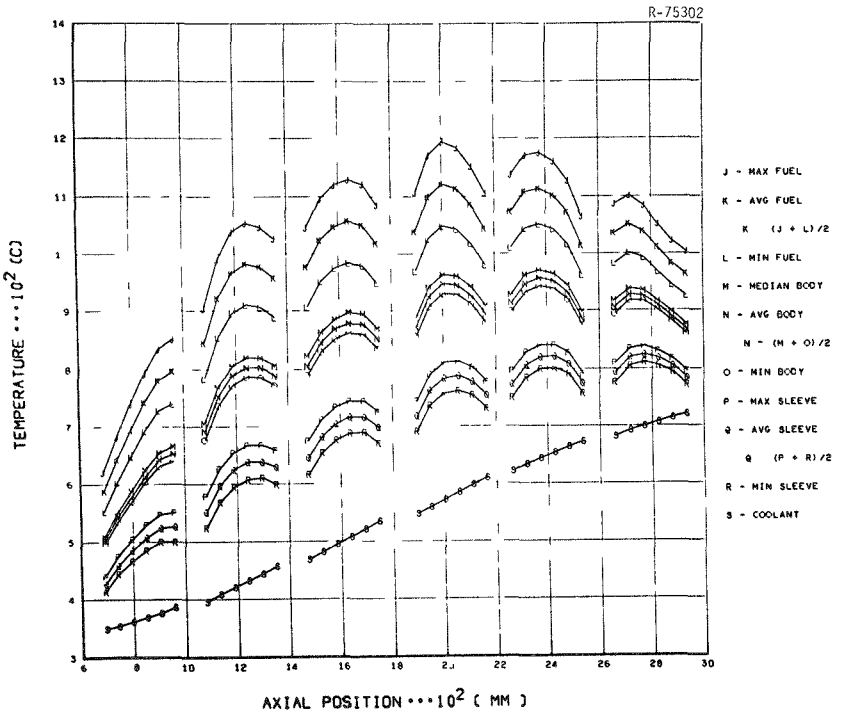

Fig. 5.3. Recycle Test Element-5 Time-Averaged Temperatures: Bodies 1–6, Holes 5–6.

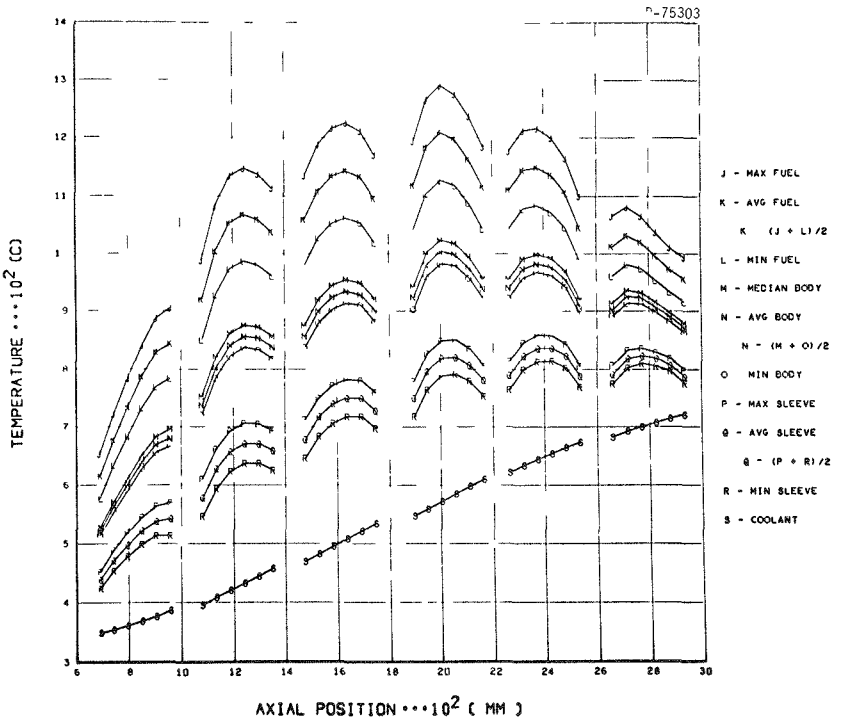

Fig. 5.4. Recycle Test Element-5 Time-Averaged Temperatures: Bodies 1–6, Holes 7–8.

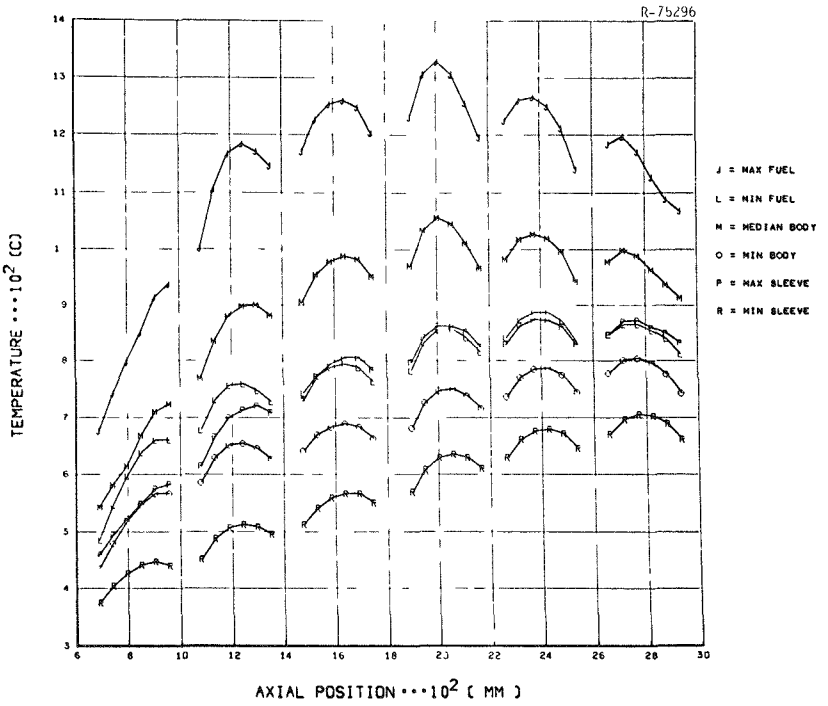

Fig. 5.5. Recycle Test Element-5 Temperature Envelope: Bodies 1–6, Holes 1–2.

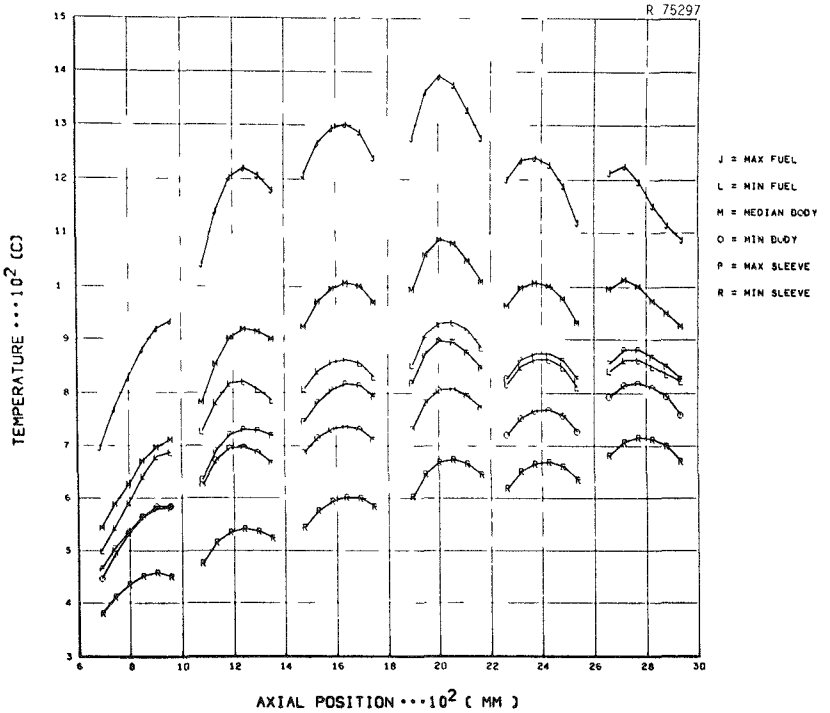

Fig. 5.6. Recycle Test Element-5 Temperature Envelope: Bodies 1–6, Holes 3–4.

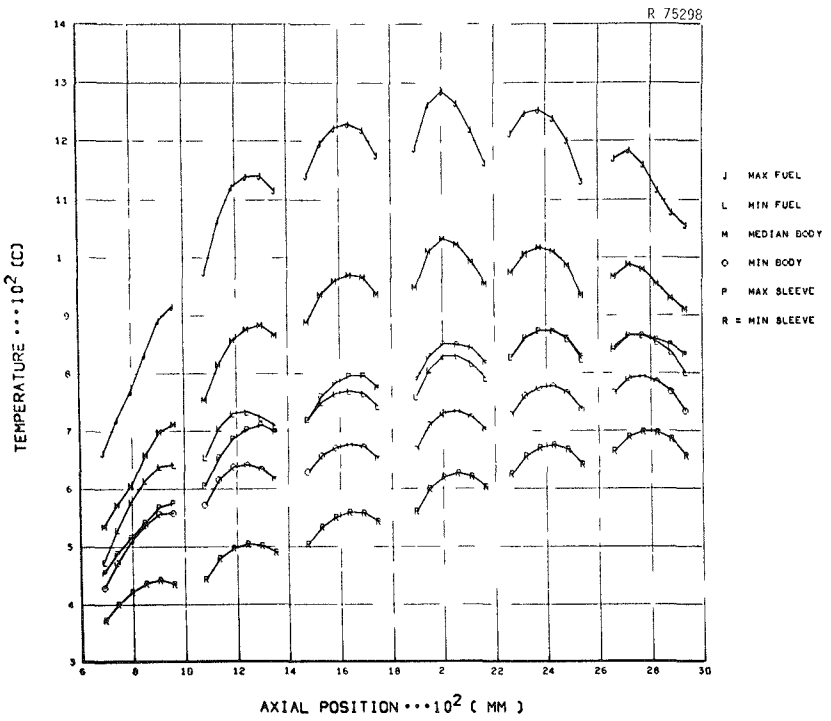

Fig. 5.7. Recycle Test Element-5 Temperature Envelope: Bodies 1—6, Holes 5—6.

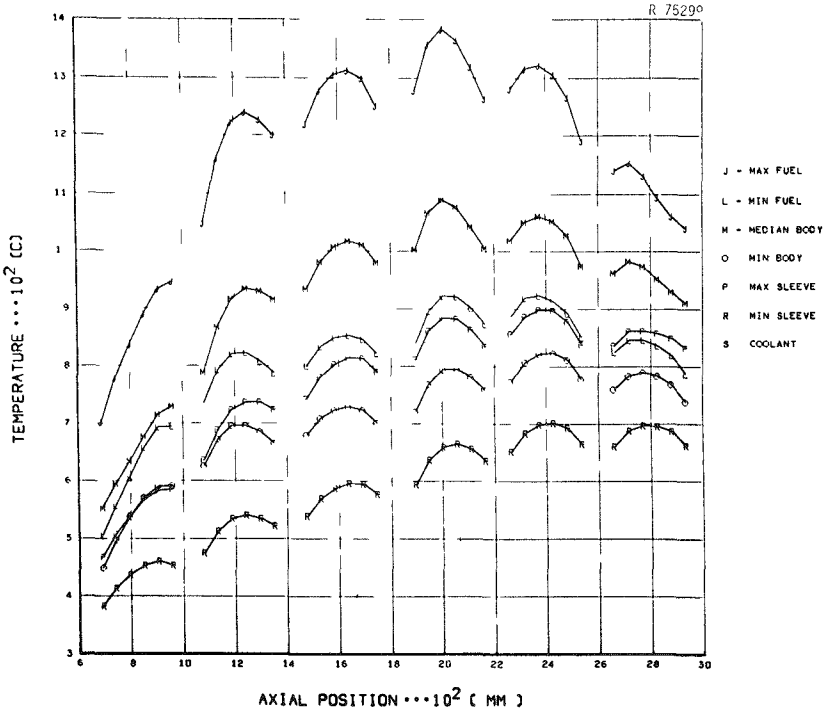

Fig. 5.8. Recycle Test Element-5 Temperature Envelope: Bodies 1—6, Holes 7—8.

holes 1 and 2, 3 and 4, 5 and 6, and 7 and 8 varied within each fuel body, a set of temperatures is reported for each section of the test element containing one of these pairs of fuel holes. Temperatures for the spine samples were not calculated.

Maximum burnups were 58.7 and 2.7% FIMA for the fissile and fertile particles, respectively. The highest fuel temperature and fast-fluence exposure (E >0.18 MeV) achieved were 1663 K (1390°C) and 4.1 x 10^{25} n/m^2, respectively. These irradiation conditions were more severe than those for the last recycle test element discussed.

Like that of the other test elements, the overall appearance of RTE-5 was normal, with no unexpected features. The fission-product trap and end fittings were cut off and the six fuel bodies were removed from the graphite sleeve. The appearance of the bodies was excellent with no evidence of surface corrosion.

Fuel rods were removed from all holes in body 3 and from holes 1, 3, 5, and 7 in bodies 1, 2, 4, 5, and 6 by core drilling upward from the bottom of the body and pushing the stack out the top. The two spine samples were also removed. The rods appeared to be in good condition, but showed some debonding. Seen on many rods were broken particles attributed to abrasion during rod removal from the bodies. Cracked coatings were observed on many of the rods containing UC_2 Triso (batch 4000-307), which showed much oLTI failure from fast-neutron damage.

Fuel representing all fuel types was selected from the fuel bodies for metallographic examination. Because many fuel types were duplicated in the element, fuel rods from the highest fluence regions were examined. Bodies 1, 2, 3, and 4 contained the same fuel types, so of these, only the fuel from body 3 was examined. The graphite filler samples were also examined metallographically.

Examination of the polished cross section from fuel rod RTE-5-3-1-6 containing Biso $(4Th,U)O_2$ from batch PR-57-1 and Biso ThC_2 showed no failures. The particles appeared in good condition with no observable amoeba migration. Typical fissile particles are shown in Fig. 5.9. They had an appearance typical of mixed oxides with fission gas

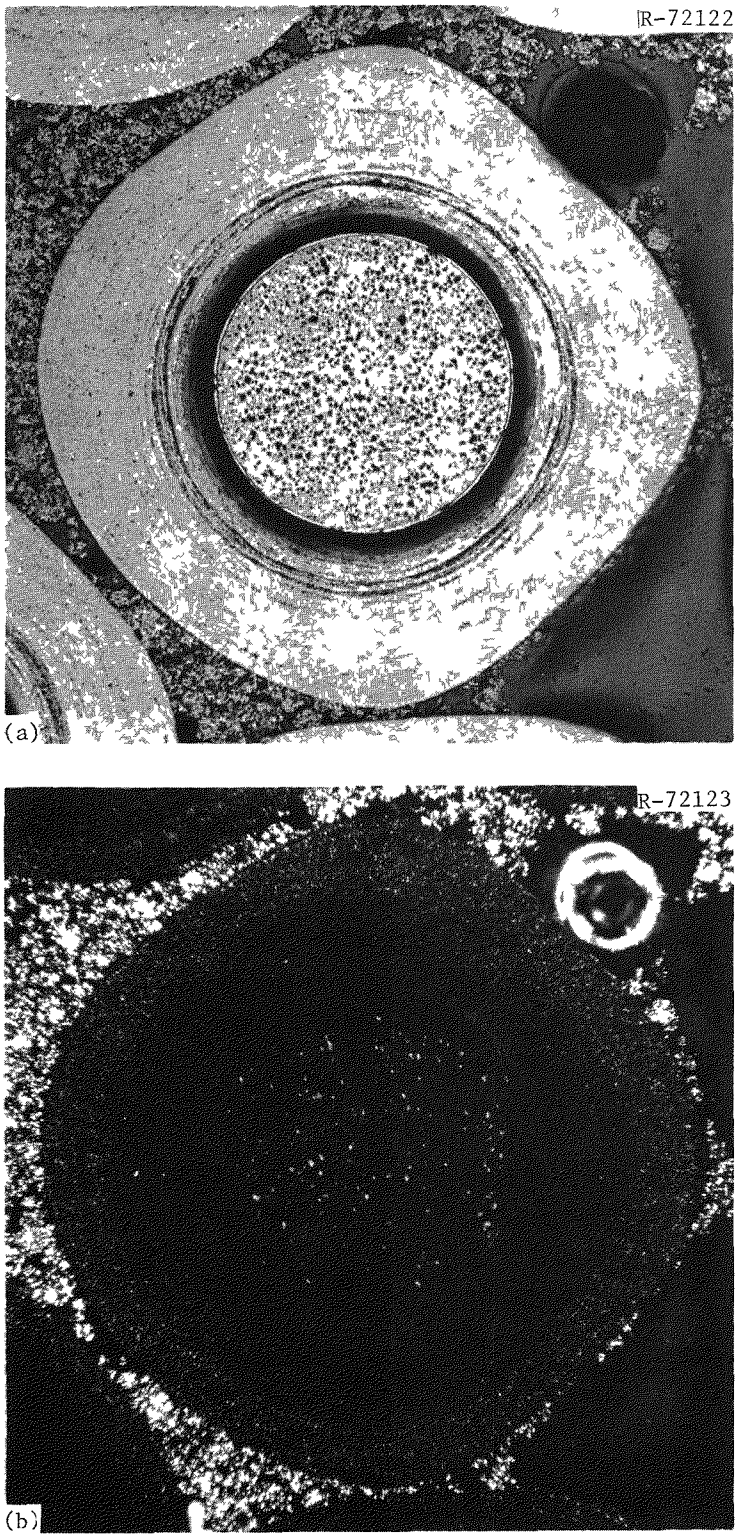

Fig. 5.9. Typical Biso $(4Th,U)O_2$ Fissile Particle from RTE-5-3-1-6. 125×. (a) Under bright field. (b) Under polarized light. Reduced 15%.

bubbles and metallic inclusions present. The fissile and fertile particles achieved maximum burnups of 10.9 and 2.7% FIMA, respectively, and had a maximum time-averaged fuel temperature of 1393 K (1120°C).

The Biso $(2Th,U)O_2$ particles from fuel rod RTE-5-3-3-6 were observed to be in good condition and no failures were found. Slight amoeba migration — less than 5 μm — of the $(2Th,U)O_2$ kernels up the temperature gradient was seen, while the ThO_2 kernels showed none. Typical particles are shown in Fig. 5.10. One fissile particle was observed to have a torn coating (Fig. 5.11). Under polarized light illumination the tears clearly appear to extend through a dense "band" in the oLTI coating. The tears are attributable to fast-neutron damage and not to matrix-particle interaction. The fissile and fertile particles in this fuel rod achieved maximum burnups of 21.2 and and 2.7% FIMA, respectively. The maximum time-averaged temperature was 1433 K (1160°C).

A metallographic cross section was made from fuel rod RTE-5-3-5-7, which contained Triso UC_2 from batch 4000-307 and Biso ThC_2 from batch 4000-226. The fissile particles appeared to be in fair condition; graphitization of the iLTI coating had occurred in virtually every particle. The graphitization of the iLTI, associated with migration of the rare earths, is very temperature-dependent. The average time-averaged fuel temperature was 1293 K (1020°C). Similar behavior was observed in RTE-2. Fast-neutron-induced shrinkage caused oLTI coatings to break in approximately 5% of the fissile particles observed. Particles from the same batch and in the other recycle test elements behaved the same way. The Biso ThC_2 fertile particles appeared to be in good condition with no failures or amoeba effect. Typical particles are shown in Fig. 5.12.

Biso UO_2 (batch Mixed 1) and Biso ThO_2 (see Table 5.1 for batch details) particles were contained in fuel rod RTE-5-3-7-6. The Biso UO_2 particles were in poor condition. Amoeba migration of the kernel up the temperature gradient and through the buffer appeared in over half the 208 particles observed (Fig. 5.13). The kernels of particles at the rod thermal center [1175°C (1448 K) maximum time-averaged

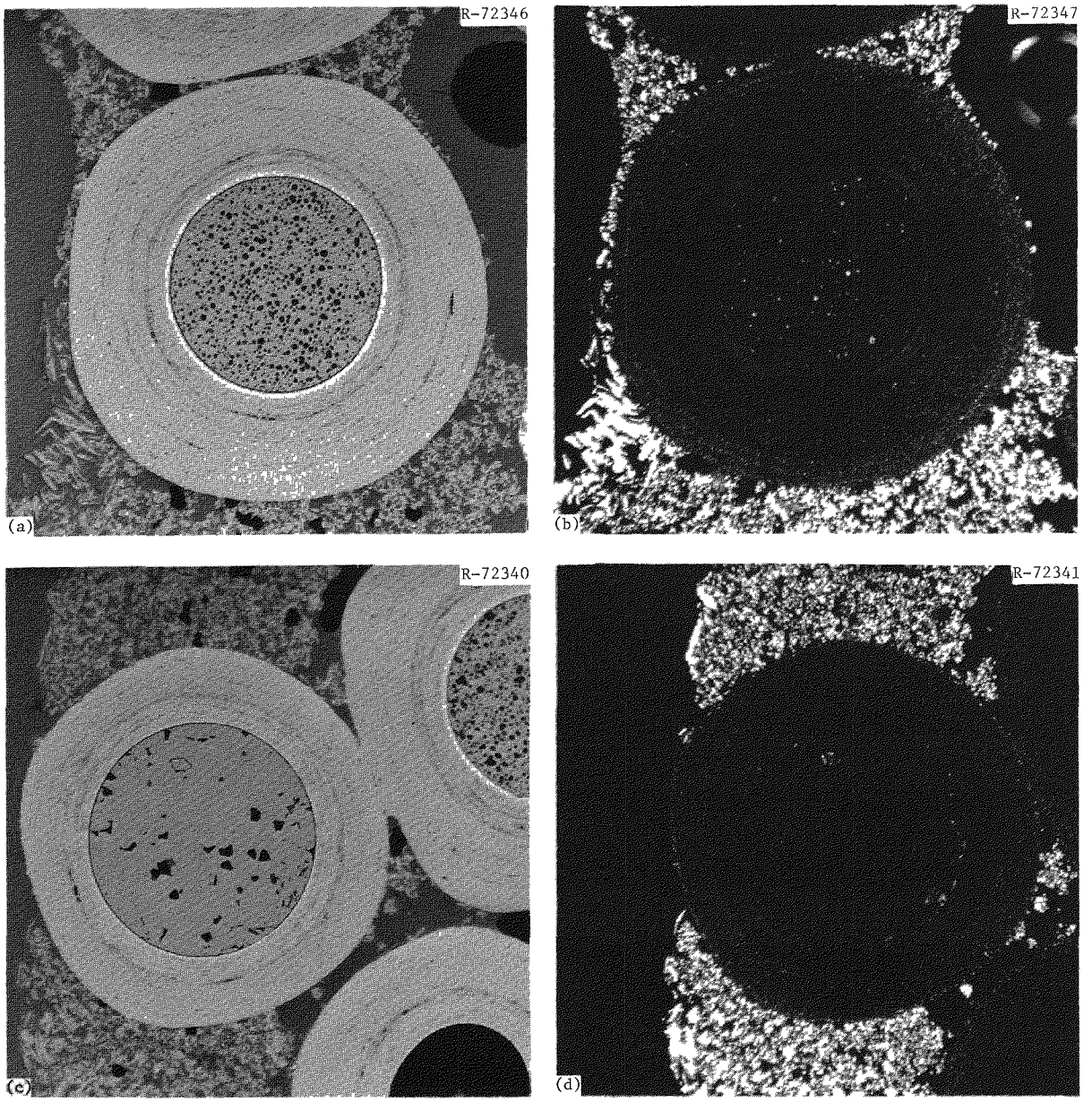

Fig. 5.10. Typical Particles from RTE-5-3-3-6. 125×. (a) Biso $(2Th,U)O_2$ fissile particle. Bright field. (b) Same. Polarized light. (c) Biso ThO_2 fertile particle. Bright field. (d) Same. Polarized light. Reduced 32%.

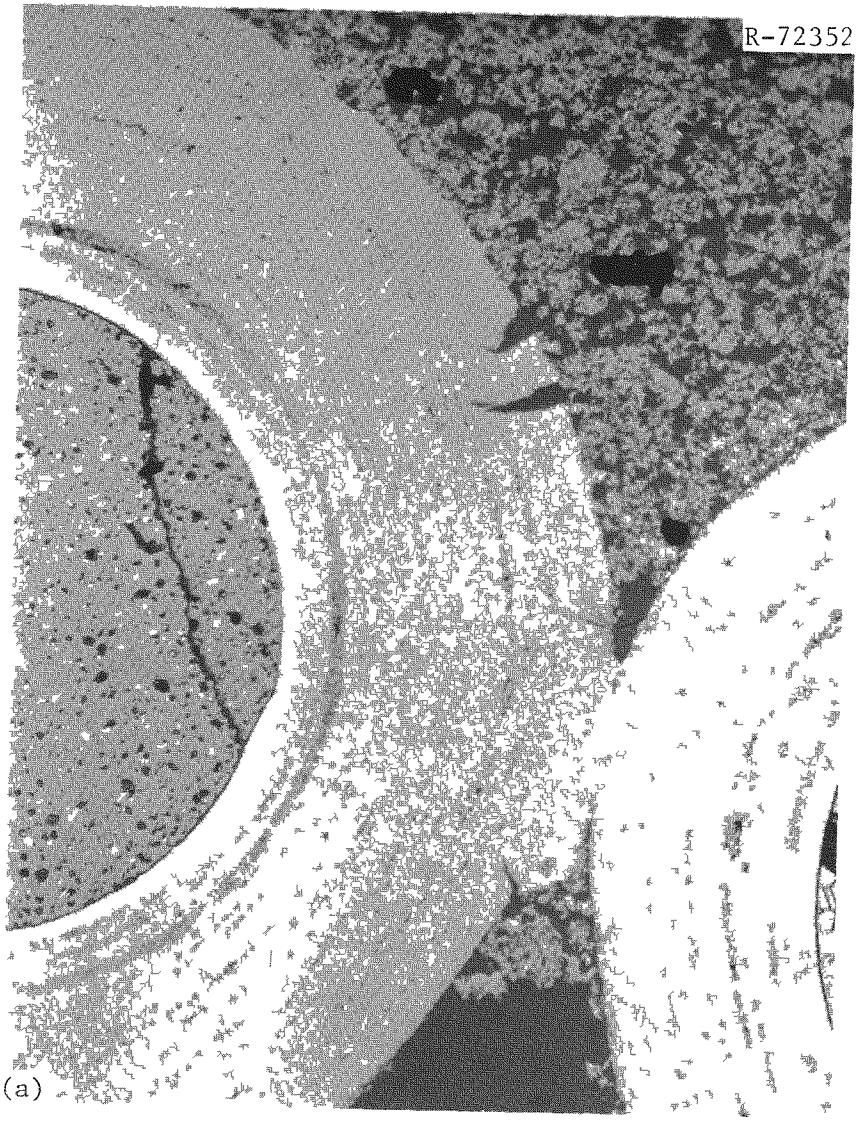

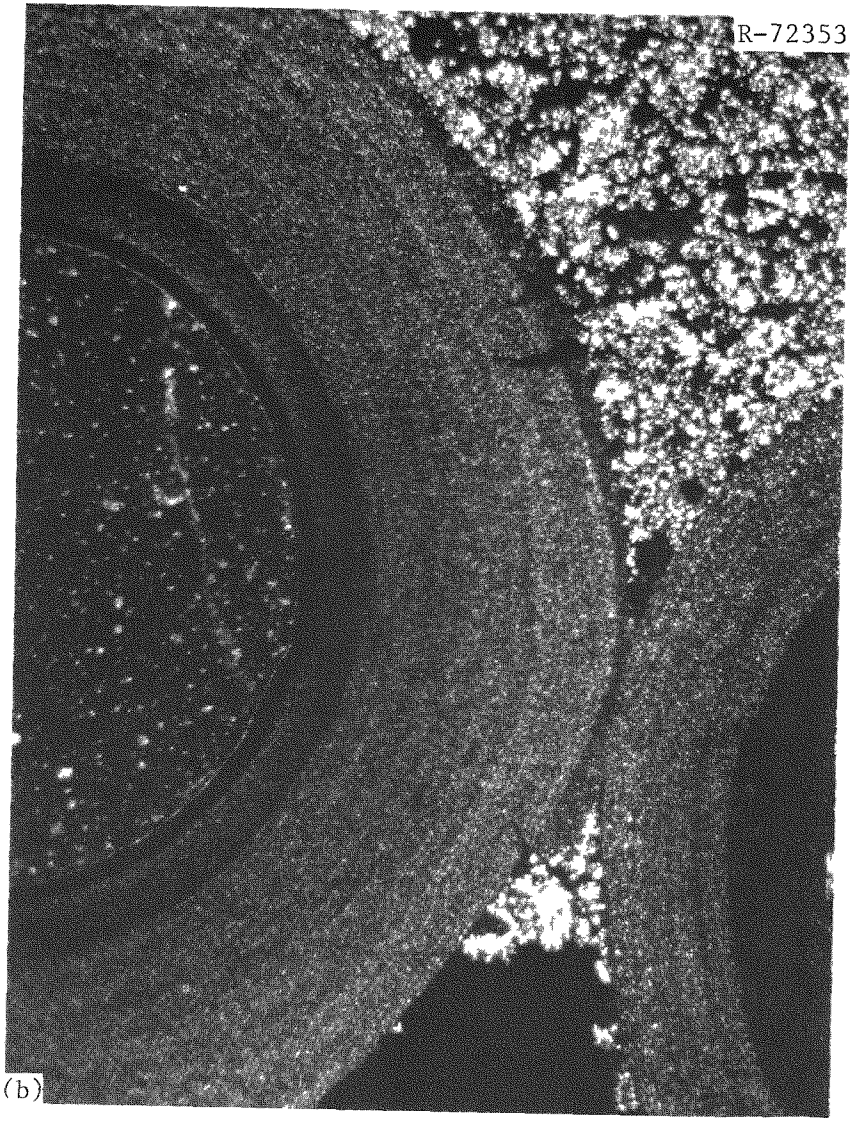

Fig. 5.11. Tearing of the oLTI Coating. 250×. (a) Bright field. (b) Polarized light. Note tears extend through dense band in oLTI coating.

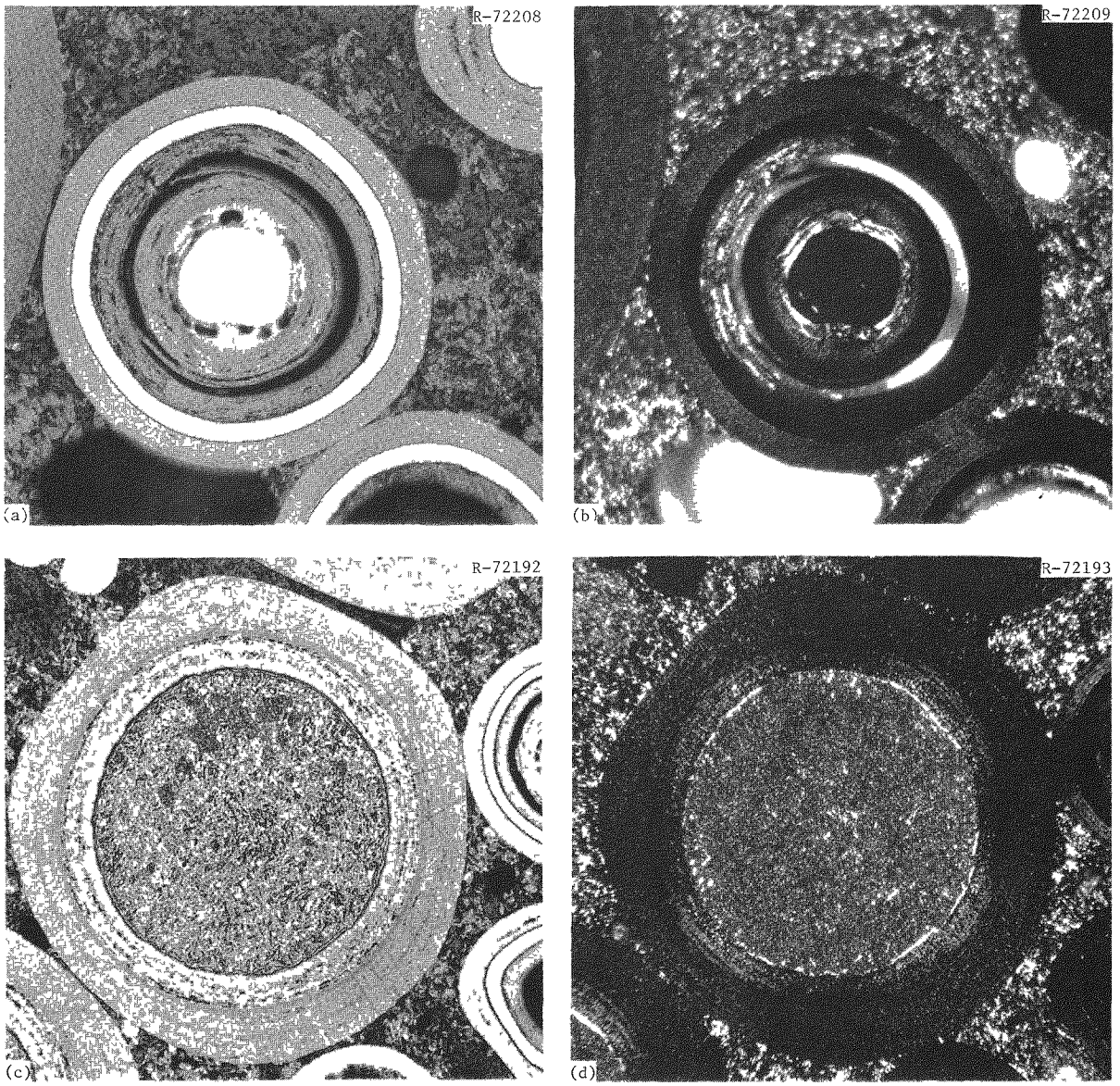

Fig. 5.12. Typical Particles From RTE-5-3-5-7. (a) Triso UC_2 Fissile particle. 250×. Bright field. (b) Same. Polarized light. (c) Biso ThC_2 fertile particle. 150×. Bright field. (d) Same. Polarized light. Reduced 32.5%.

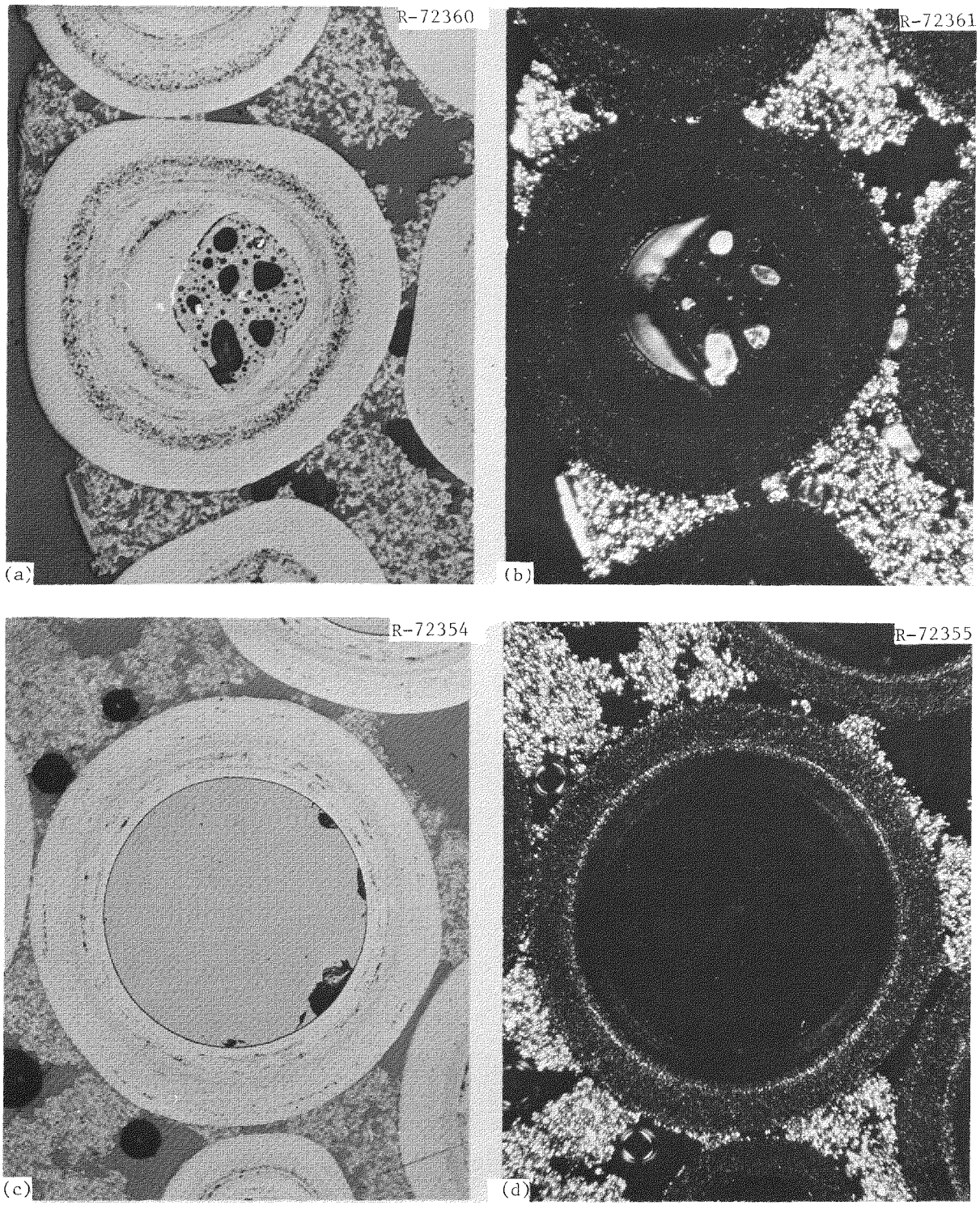

Fig. 5.13. Typical Particles from RTE-5-3-7-6. (a) Biso UO_2 fissile particle. 200×. Bright field. (b) Same. Polarized light. (c) Biso ThO_2 fertile particle. 125×. Bright field. (d) Same. Polarized light. Reduced 14%.

temperature] appeared broken into parts (Fig. 5.14). The Biso ThO_2 fertile particles appeared in good condition with no failures or amoeba effect (Fig. 5.13). Under polarized light illumination, a dense anisotropic band is visible in the oLTI coating. The band was also observed in the particles before irradiation. This coating defect caused no observable harm.

The Biso UO_2 particles from batch-4000-274 and contained in fuel rod RTE-5-5-1-1 performed poorly. Amoeba migration of the kernel through the buffer had occurred in virtually all the 310 particles in the metallographic cross section. The particles resembled the Biso UO_2 in RTE-5-3-7-6 (Fig. 5.14), where the kernels appear to have broken into separate parts and migrated up the temperature gradient (Fig. 5.15). While this behavior was seen only at high temperatures in RTE-5-3-7-6 (>1100°C), in RTE-5-5-1-1 the entire cross section was affected, because there, the minimum time-averaged fuel temperature was 1025°C. Apparently the UO_2 kernels were extremely plastic during irradiation. The Biso ThC_2 particles from batch 4000-225 appeared to be in good condition with no failures or amoeba effect (Fig. 5.15).

Examination of 425 UC_2 Biso fissile particles (batch 4000-309) from fuel rod RTE-5-5-3-1 revealed no failures. As observed in RTE-2, the buffers of these particles densified, while their optical anisotropy increased (Fig. 5.16). The maximum time-averaged temperature for these particles was 1125°C. We observed slight amoeba migration — less than 5 μm — in some, but no failures in any of the Biso ThC_2 fertile particles from batch 4000-226.

A metallographic cross section was made of fuel rod RTE-5-5-5-1. It contained the same batch of fissile particles as described in RTE-5-5-3-1. These 234 particles and the particles in RTE-5-5-3-1 were identical. The Biso ThO_2 fertile particles (batch PR-47) appeared in good condition. No failures were observed, but two fabrication defects were noted. A typical fertile particle is shown in Fig. 5.17.

Observations were made on Biso $(2Th,U)O_2$ (batch PR-60) and Biso ThC_2 (batch 4000-225) particles in RTE-5-5-7-1. Typical particles are shown in Fig. 5.18. No failures or amoeba migrations were

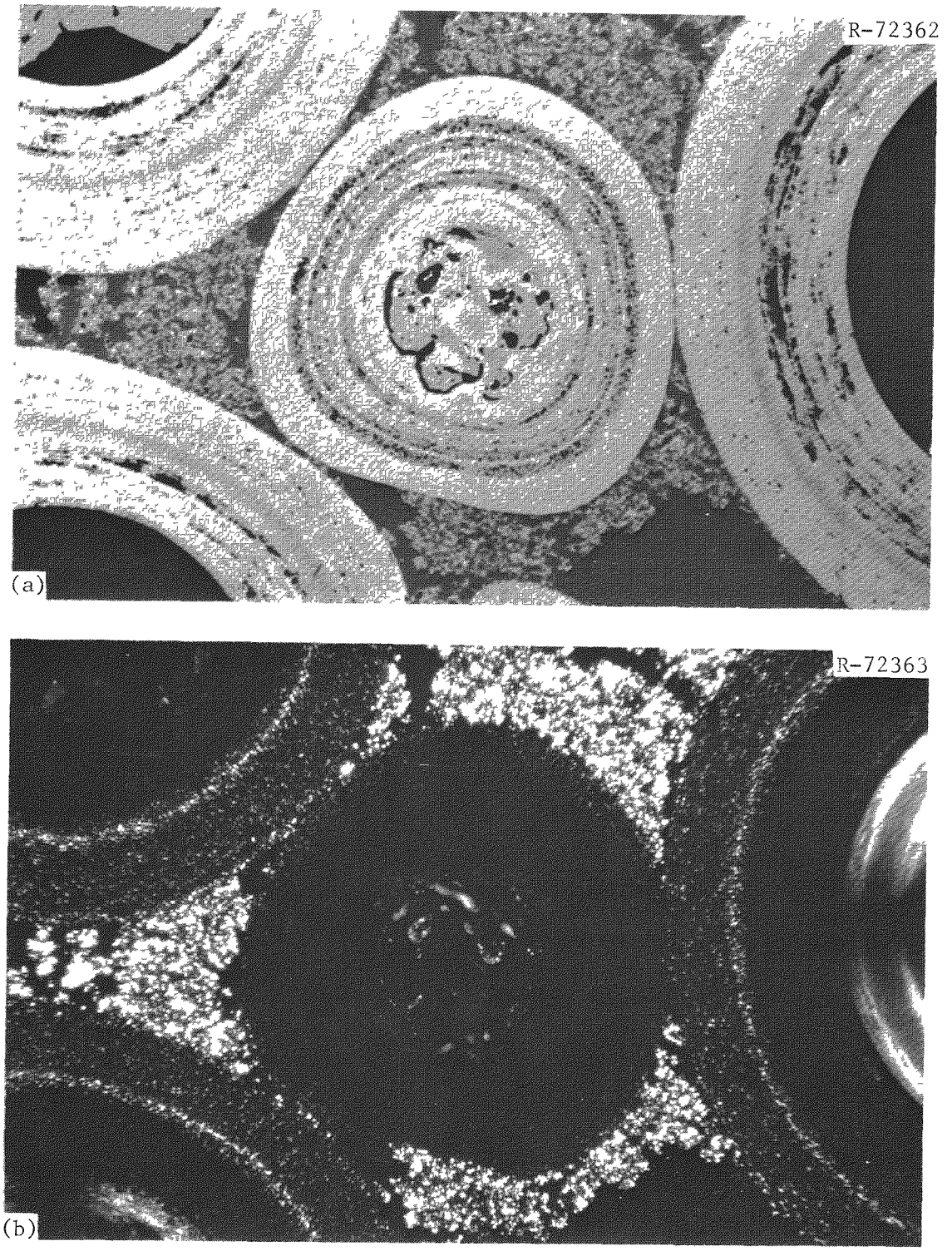

Fig. 5.14. Biso UO_2 Fissile Particle from the Thermal Center of RTE-5-3-7-6. 200×. (a) Under bright field. (b) Under polarized light. Note kernel has broken into separate parts.

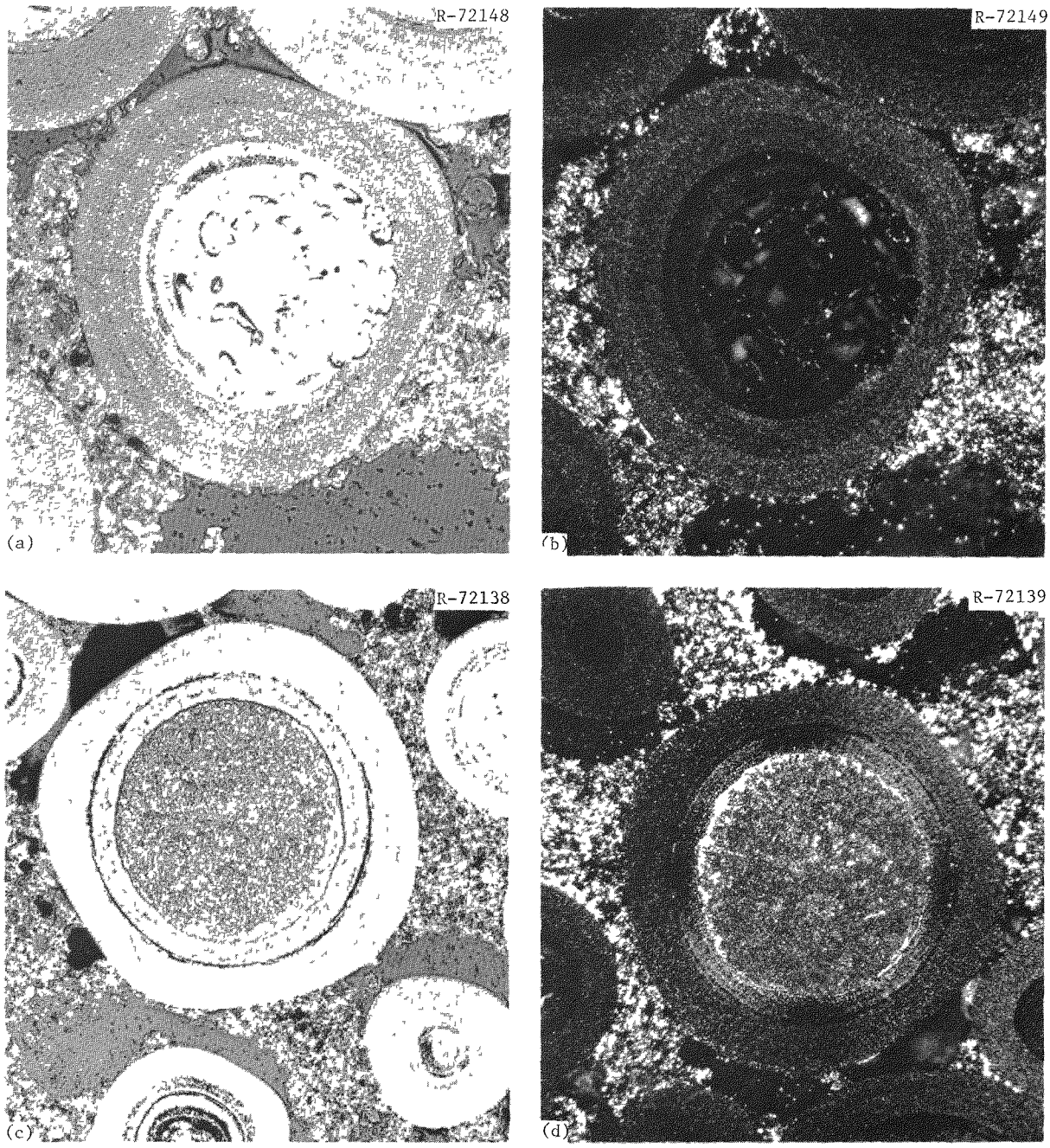

Fig. 5.15. Typical Particles from RTE-5-5-1-1. (a) Biso UO_2 fissile particle. 250×. Bright field. (b) Same. Polarized light. (c) Biso ThC_2 fertile particle. 125×. Bright field. (d) Same. Polarized light. Reduced 23.5%.

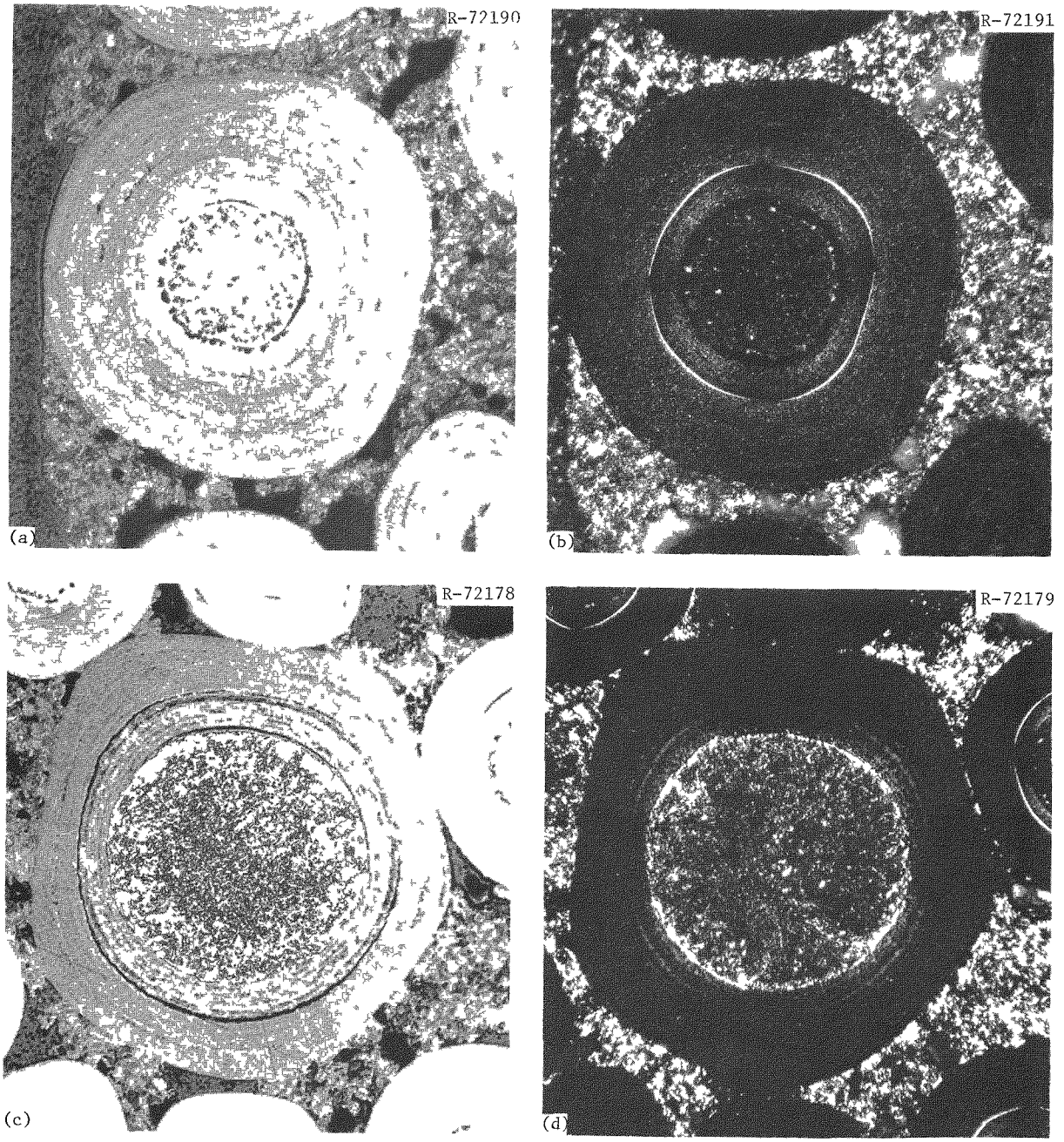

Fig. 5.16. Typical Particles from RTE-5-5-3-1. (a) Biso UC_2 fissile particle. 250×. Bright field. (b) Same. Polarized light. (c) Biso ThC_2 fertile particle. 125×. Bright field. (d) Same. Polarized light. Reduced 24%.

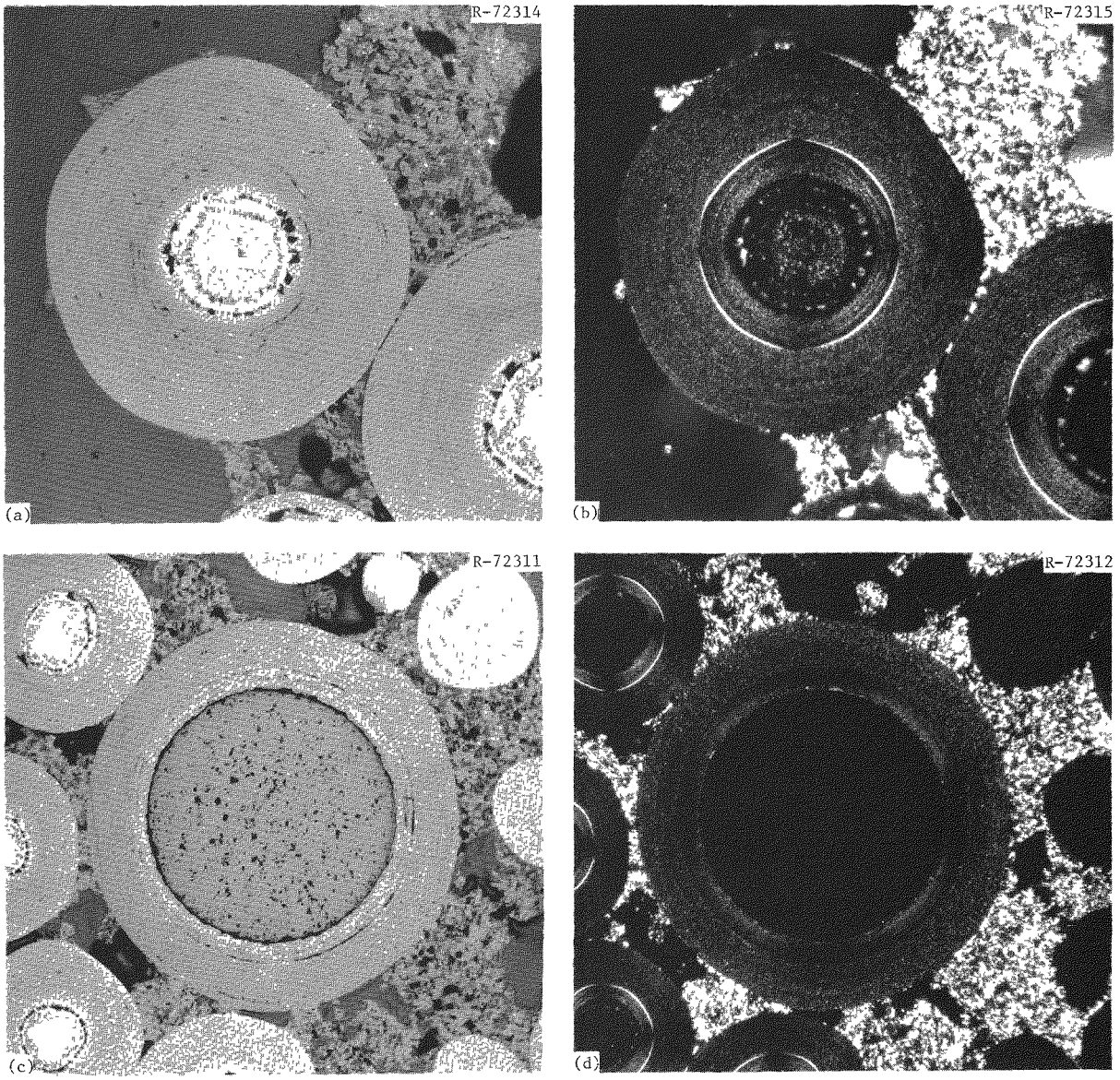

Fig. 5.17. Typical Particles from RTE-5-5-5-1. (a) Biso UC_2 fissile particle. 250×. Bright field. (b) Same. Polarized light. (c) Biso ThO_2 fertile particle. 125×. Bright field. (d) Same. Polarized light. Reduced 32.5%.

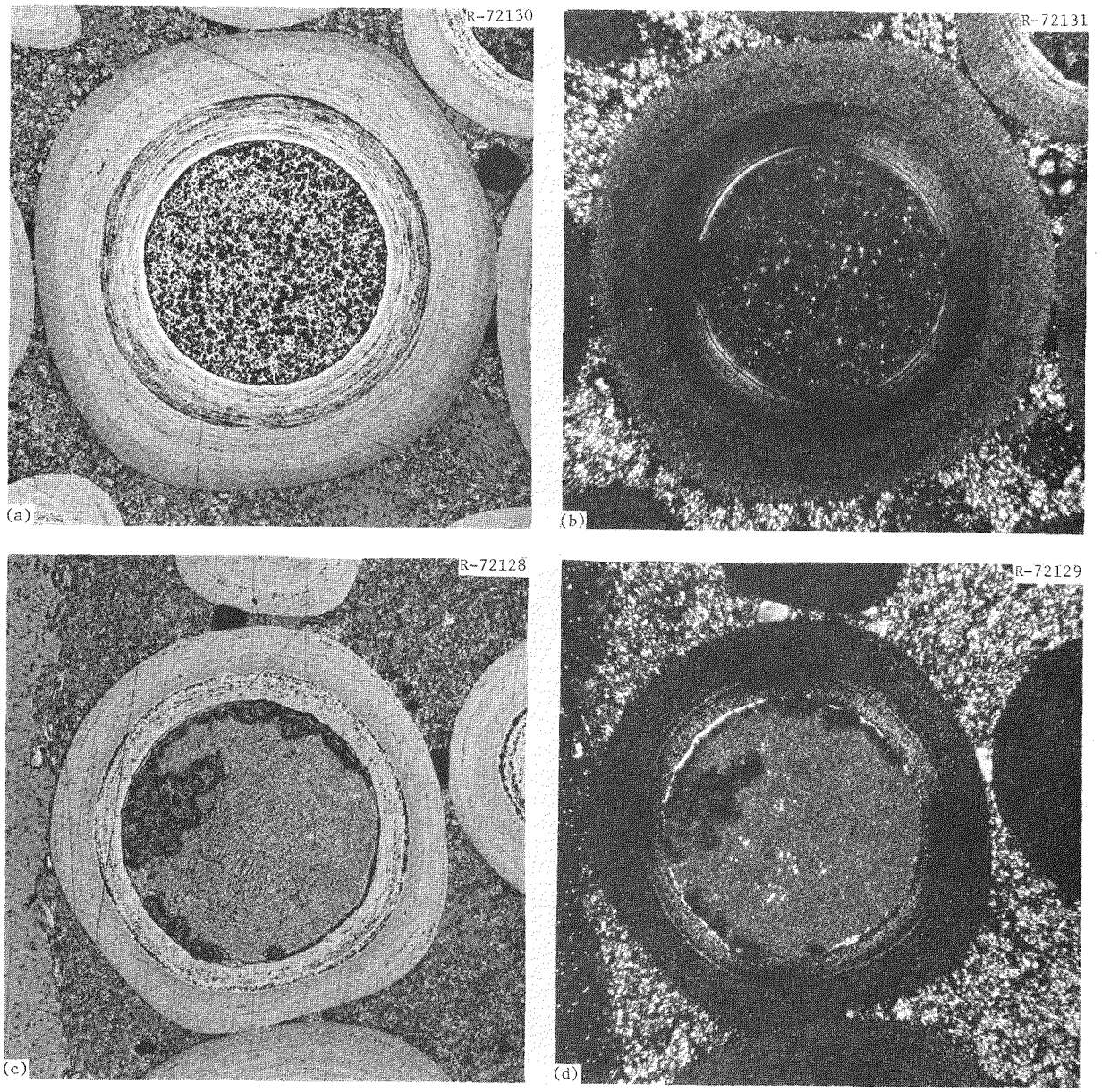

Fig. 5.18. Typical Particles from RTE-5-5-7-1. 125×. (a) Biso $(2Th,U)O_2$ fissile particle. Bright field. (b) Same. Polarized light. (c) Biso ThC_2 fertile particle. Bright field. (d) Same. Polarized light. Reduced 32.5%.

observed. The fissile particles had an appearance typical of mixed oxides, with fission gas bubbles and metallic inclusions present in the kernels.

Because all fuel types were duplicated in the other fuel bodies, the only fuel rod used from body 6 for metallography was from stack 7 (RTE-5-6-7-1). The Triso UC_2 (batch 4000-307) particles appeared to be in fair condition with some graphitization of the iLTI. The average time-averaged fuel temperature was 1283 K (1010°C). The same particle batch behaved similarly in the other recycle test elements. Damage by fast neutrons broke oLTI coatings in approximately 20% of the fissile and 25% of the fertile particles. The buffers had separated from the iLTI and had densified around the kernel in nearly all the fertile particles. Typical particles are shown in Fig. 5.19.

The matrix filler samples in the spines of bodies 2 and 4 appeared to be in good condition after irradiation. Section 9 of this report will refer to the dimensional changes of these samples. Although the matrix samples were not thermally analyzed, the particles from body 4 — Biso UO_2 and ThO_2 from various batches — appeared to have been at high temperatures (Fig. 5.20). In RTE-1 these particles appeared similar (see Sect. 8): their time-averaged temperatures exceeded 1723 K (1450°C). Metallographic sections were prepared from all the samples from body 4; the matrices are shown in Figs. 5.21 through 5.26. No matrix-particle interaction was observed in any of the samples. The densest matrix was obviously the one with 50% thermax carbon black (Fig. 5.22).

6. POSTIRRADIATION EXAMINATION OF RECYCLE TEST ELEMENT-6

Recycle Test Element-6 was irradiated in core position D10-06* from 0 to 897.4 Effective Full-Power Days of Peach Bottom Core 2. The fuel loadings are presented in Table 6.1.

Tables 6.2, 6.3, and 6.4 present summaries of the nuclear and thermal analyses by GA of RTE-6: its power history, heavy-metal

*See ref. 6 for core location.

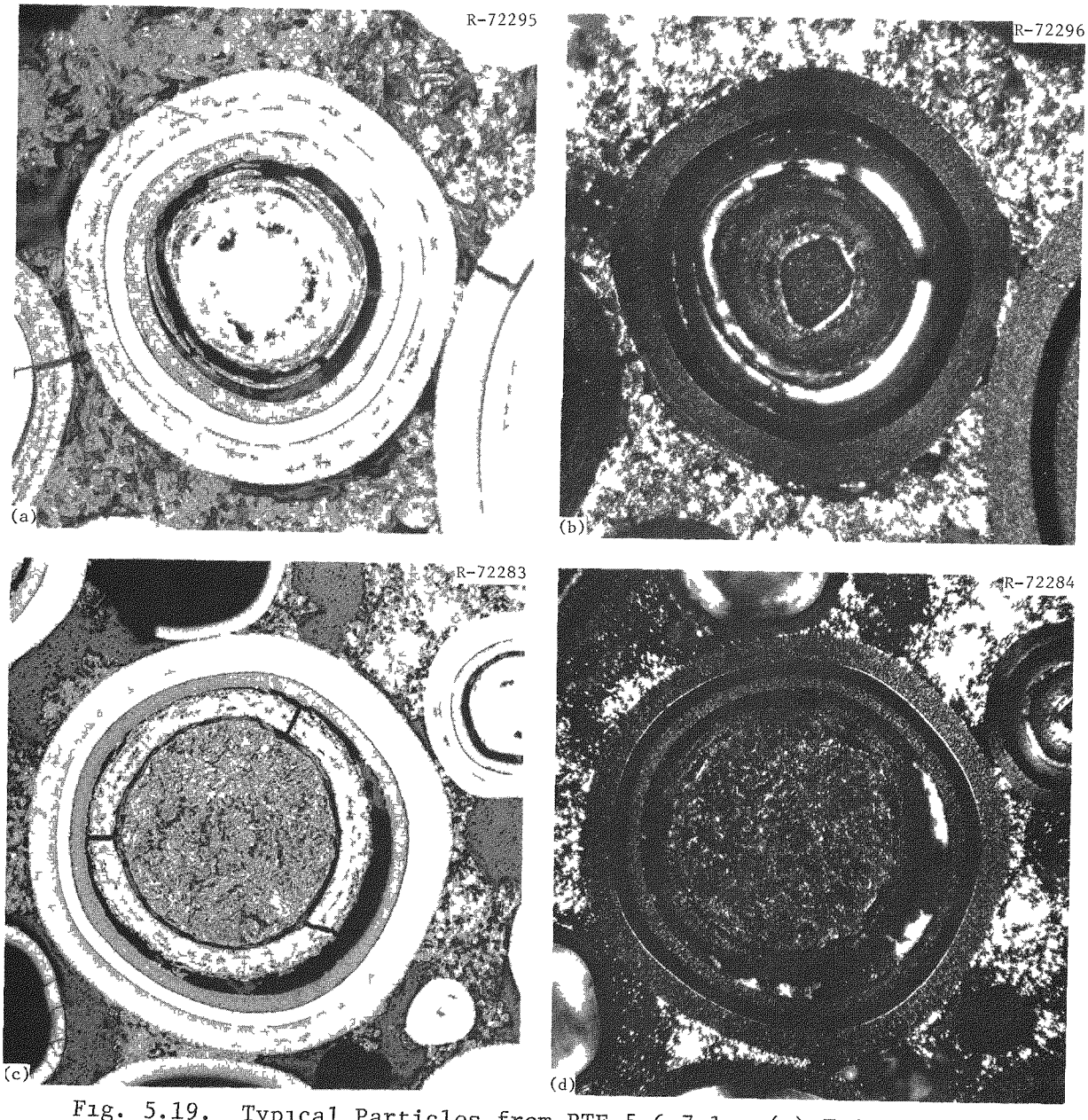

Fig. 5.19. Typical Particles from RTE-5-6-7-1. (a) Triso UC_2 fissile particle. 250×. Bright field. (b) Same. Polarized light. (c) Triso ThC_2 fertile particle. 125×. Bright field. (d) Same. Polarized light. Reduced 28%.

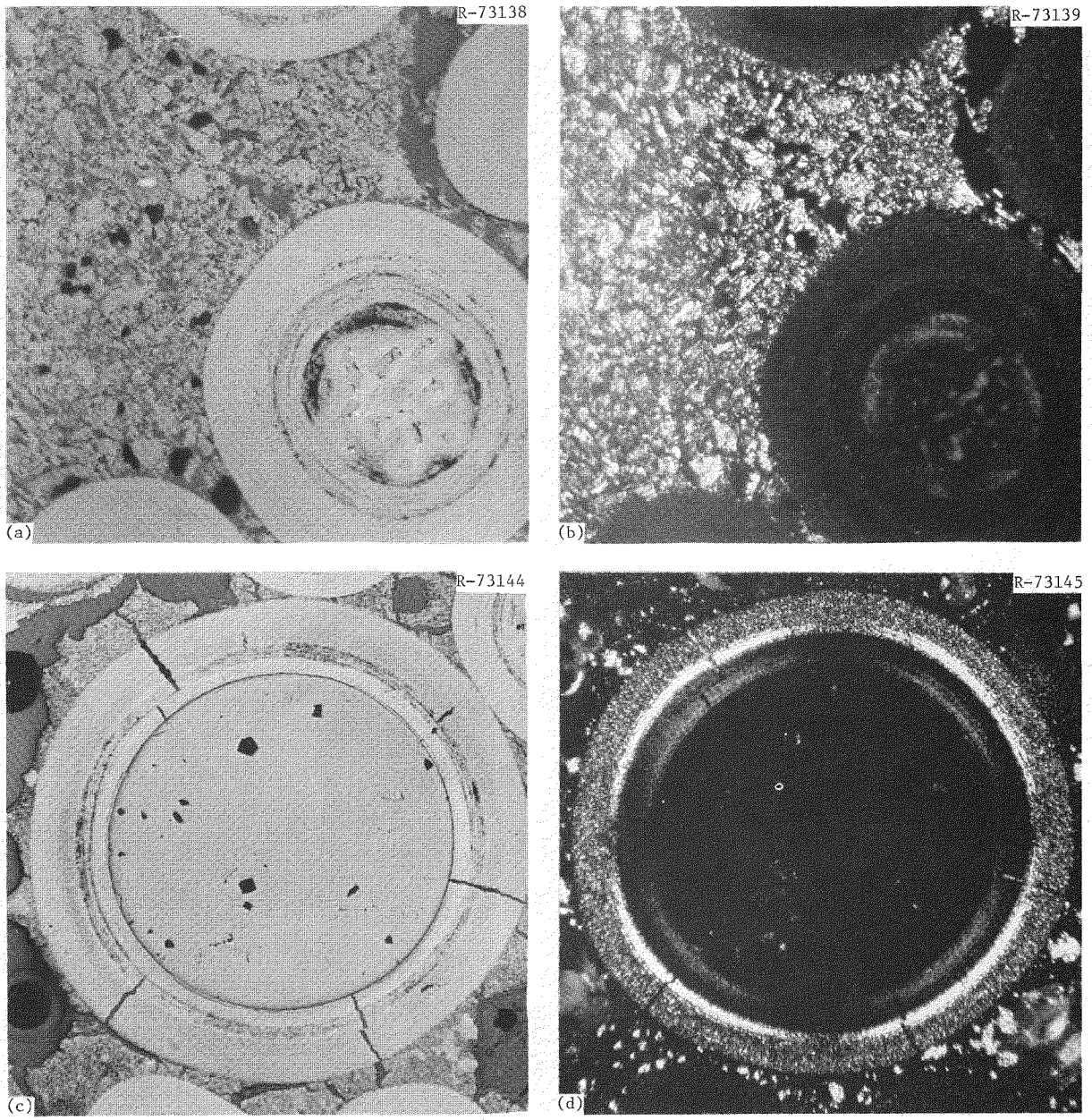

Fig. 5.20. Typical Particles from RTE-5-4-1B [(a) and (b)], and RTE-5-4-2B [(c) and (d)]. (a) Biso UO_2 fissile particle. 250×. Bright field. (b) Same. Polarized light. (c) Biso ThO_2 fertile particle. Bright field. (d) Same. Polarized light. Appearance of particles indicates matrix-filler samples operated at time-averaged temperatures exceeding 1723 K (1450°C). Reduced 30%.

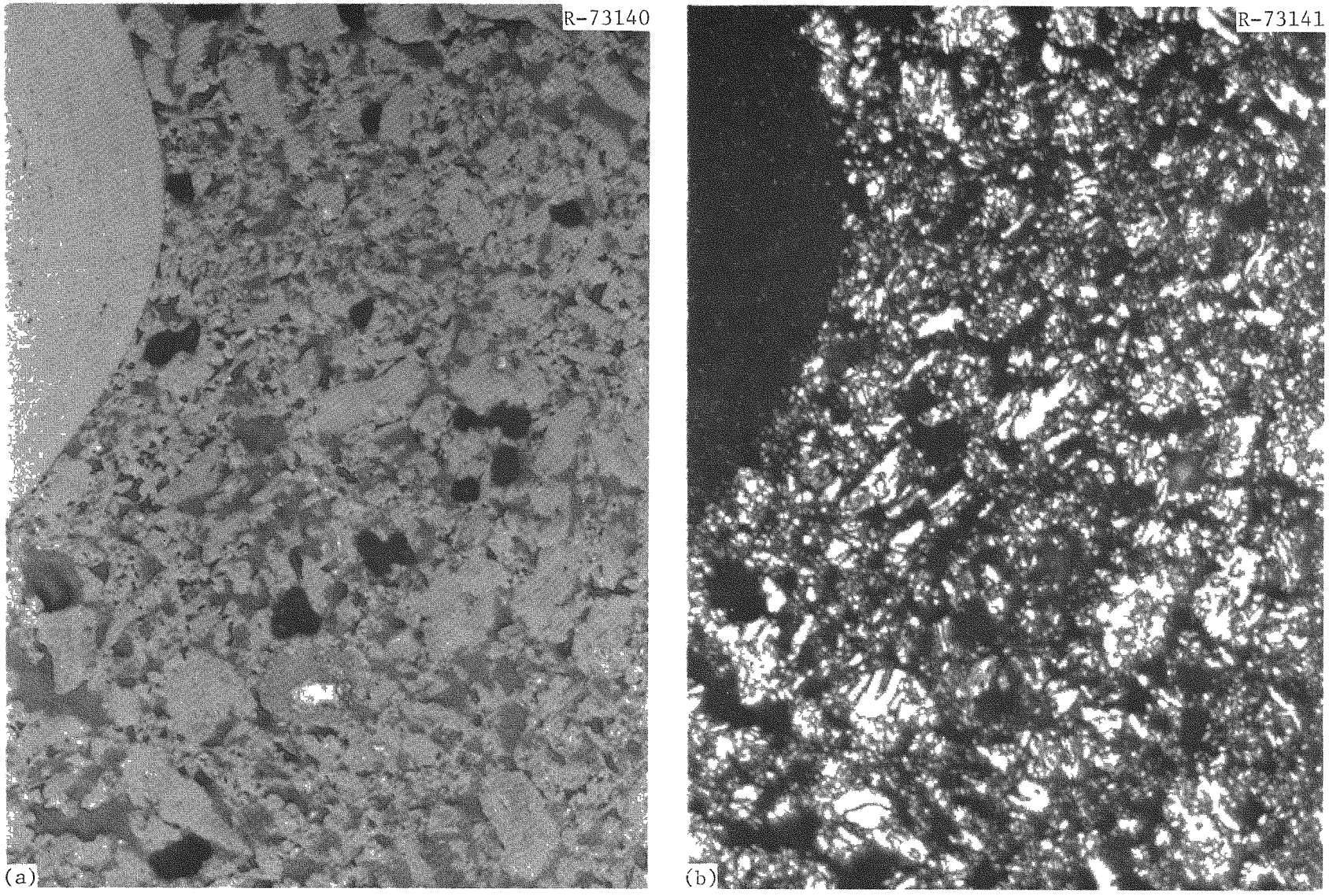

Fig. 5.21. Typical Appearance of Matrix from RTE-5-4-1B. 500×. Matrix contains 35 wt % JOZ graphite filler with particle size <40 μm. (a) Under bright field. (b) Under polarized light.

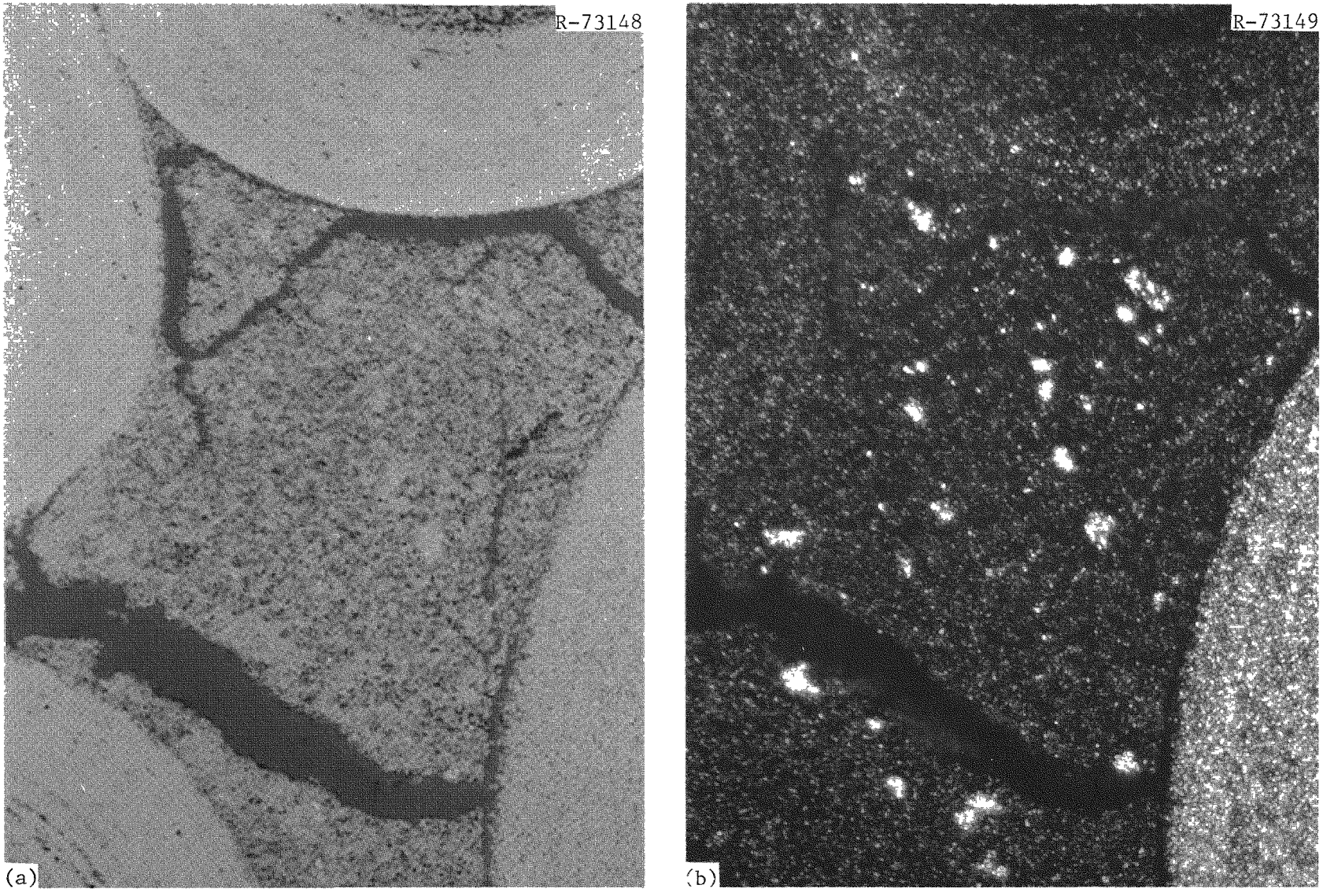

Fig. 5.22. Typical Appearance of Matrix from RTE-5-4-1B. 500×. Matrix contains 50 wt % Thermax carbon black. (a) Under bright field. (b) Under polarized light.

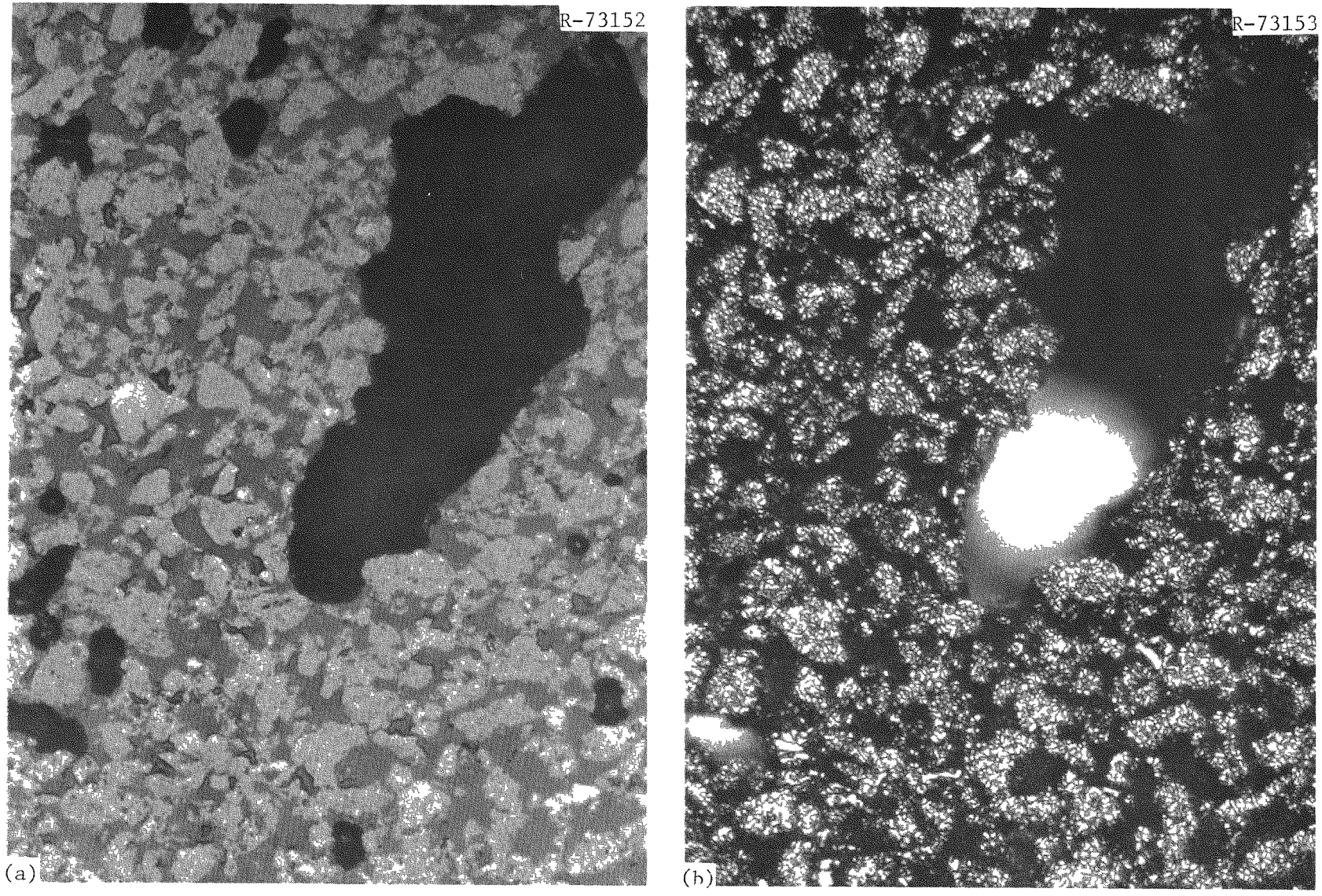

Fig. 5.23. Typical Appearance of Matrix from RTE-5-4-3B. 500×. Matrix contains 40 wt % Robinson graphite filler with particle size <27 μm. (a) Under bright field. (b) Under polarized light.

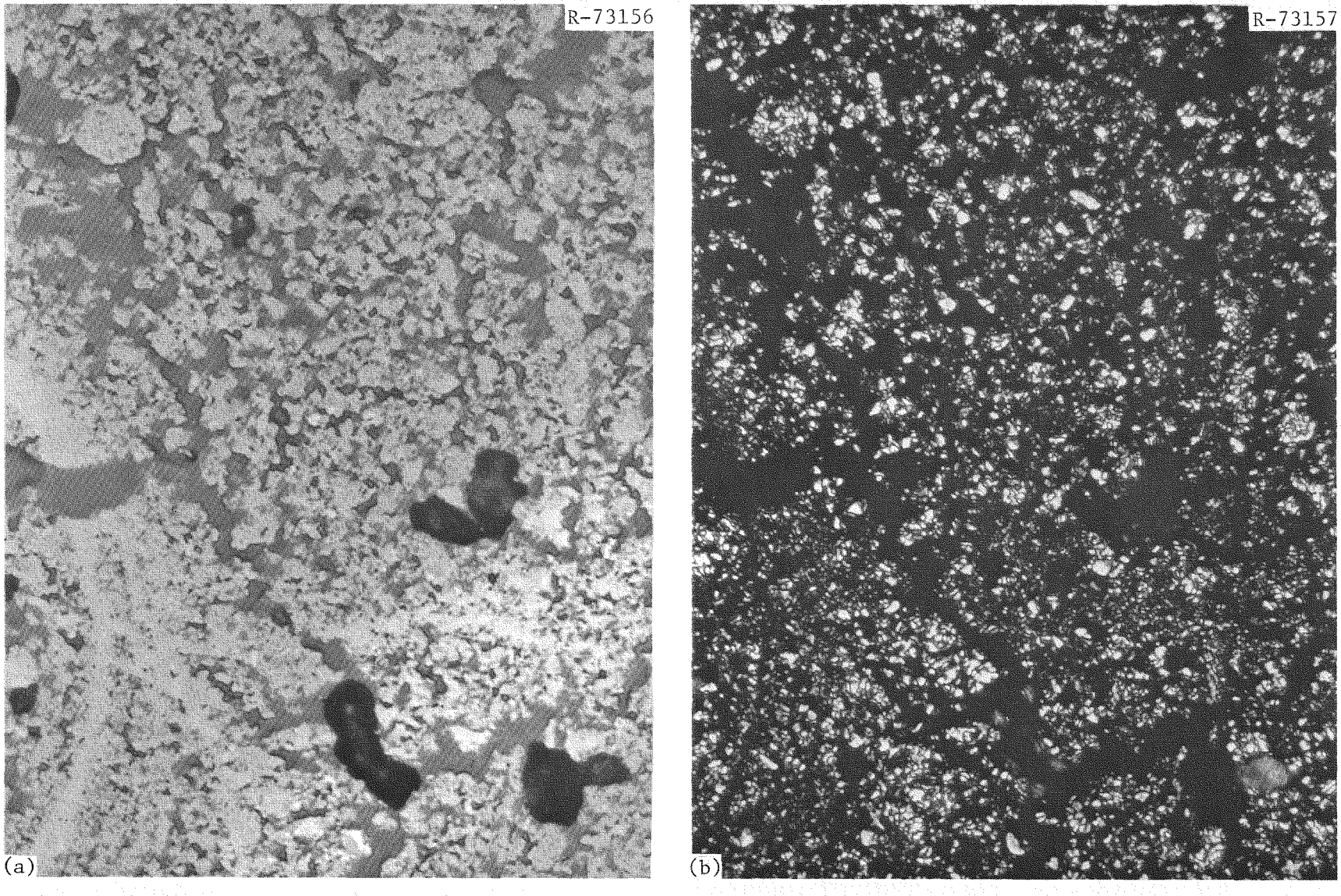

Fig. 5.24. Typical Appearance of Matrix from RTE-5-4-4C. 500×. Matrix contains 35 wt % Poco graphite filler with particle size <27 μm. (a) Under bright field. (b) Under polarized light.

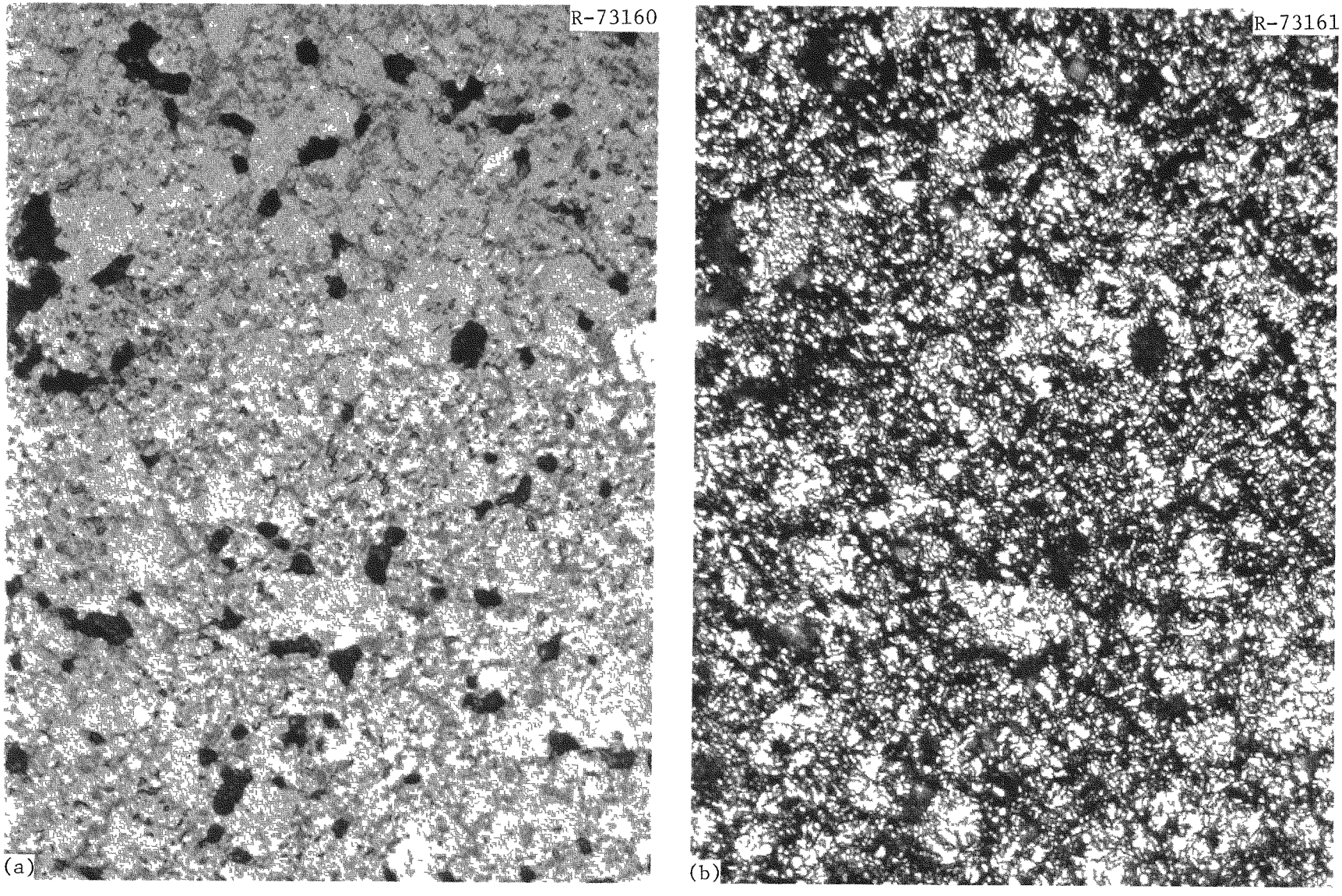

Fig. 5.25. Typical Appearance of Matrix from RTE-5-4-5C. 500×. Matrix contains 40 wt % Santa Maria graphite filler with particle size <40 μm. (a) Under bright field. (b) Under polarized light.

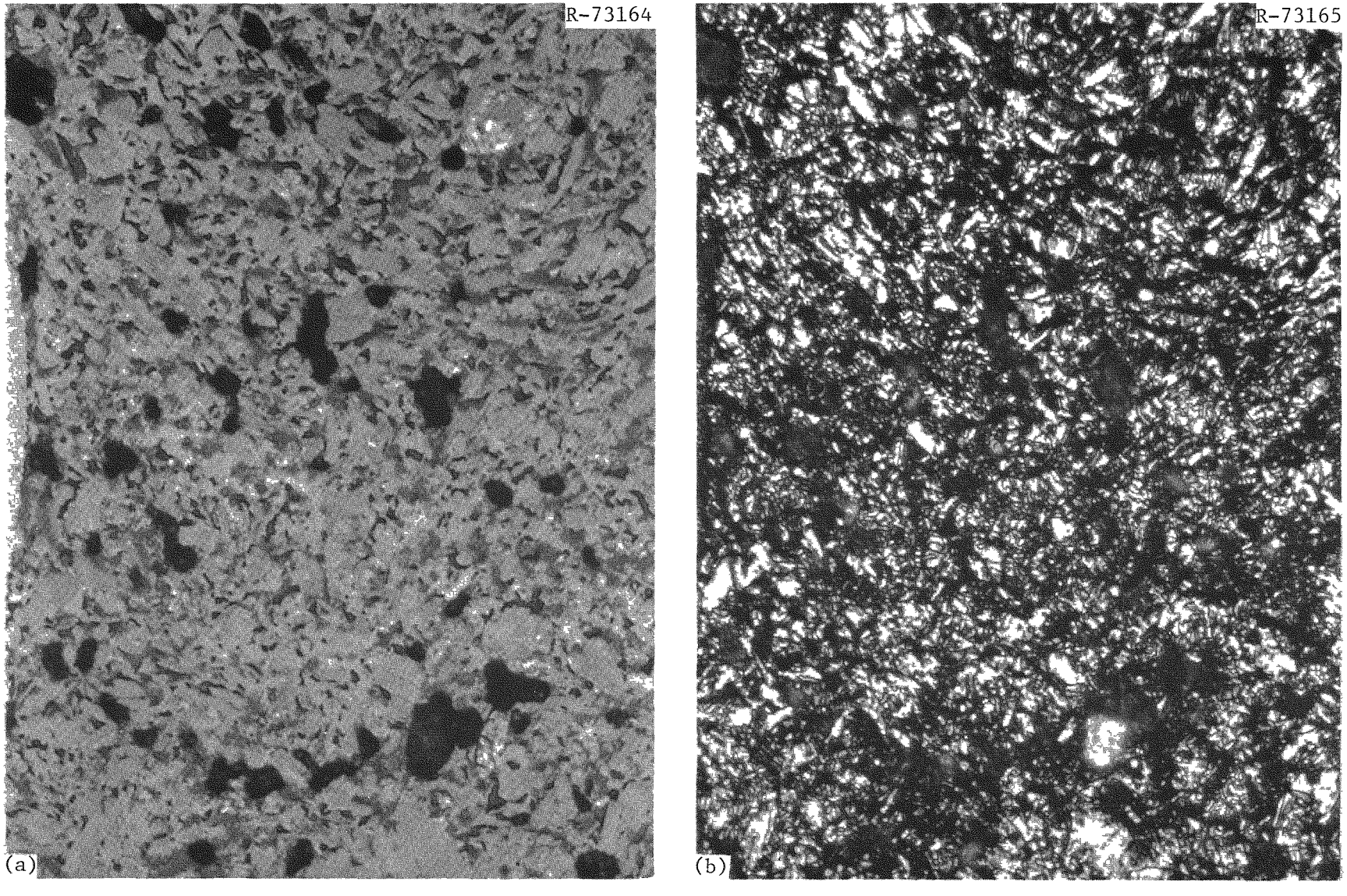

Fig. 5.26. Typical Appearance of Matrix from RTE-5-4-6B. 500×. Matrix contains 35 wt % Asbury graphite filler with particle size <40 μm. (a) Under bright field. (b) Under polarized light.

Table 6.1. Fuel-Loading Scheme for Recycle Test Element-6

Body	Fissile Fuel		Fertile Fuel		Carbonization[a] Mode
	Particle Type	Batch	Particle Type	Batch	
1	UC_2 Biso	4000-309	ThC_2 Biso	4000-226	Fuel Body
2	UC_2 Triso	4000-307	ThC_2 Biso	4000-226	Fuel Body
3	$(2Th,U)O_2$ Biso	PR-60	ThC_2 Biso	4000-225	Packed Graphite Flour
4	UC_2 Triso	4000-307	ThC_2 Biso	4000-226	Fuel Body
5	UC_2 Triso	4000-307	ThC_2 Biso	4000-226	Fuel Body
6	UO_2 Biso	Mixed 1	ThO_2 Biso	PR-48	Packed Graphite Flour

[a]All fuel particles were contained in bonded rods.

burnups, and neutron fluences. The time-averaged temperatures and temperature envelopes for the entire element are presented in Figs. 6.1 and 6.2.

The overall appearance of the element was excellent and had no unusual or unexpected features. The fission-product trap and end fittings were cut off and the six fuel bodies were easily removed from the graphite sleeve. The bodies appeared to be in good condition and showed no signs of surface corrosion. Dimensional measurements of the graphite components of the fuel element were taken; they included the sleeve, fuel bodies, and fuel rods. These results will be reported later.

Fuel rods were removed from holes 1, 5, and 7 in bodies 1, 2, 4, 5, and 6 and holes 1, 3, 5, and 7 in body 3. As in previous recycle test elements, the fuel rods carbonized in the graphite bodies, that is, in bodies 1, 2, 4, and 5, were more difficult to remove than those carbonized before being loaded in the graphite bodies, that is, in bodies 3 and 6. The rods appeared to be in good condition, except some particles on the surfaces incurred abrasion damage during removal from the fuel bodies. Many of the rods carbonized in the bodies were bonded together. This behavior had been observed in previous recycle test elements. Some failed particles — UC_2 Biso and ThC_2 Biso — were observed on the surface of rods from body 6. They appeared as bare

Table 6.2. Recycle Test Element-6 Power, Flow, and Flux History

Interval Reference Equivalent Full-Power Time		Thermal Analysis					Nuclear Analysis						
		Irradiation Interval[a]	Absolute Radial Power	Relative Radial Power	Coolant Relative Radial-Power Factor	TRICUSP Channel Flow	Real Time[b]	Gage Power	Flux in Groups[c] from Gage, n/m^2s				
From EFPD	To EFPD	(d)	(kW)			(kg/s)	(d)	(kW)	1A[d]	1B	2	3	4
0.00	26.99	28.84	115.41	0.884	1.064	0.0313	28.84	115.41	3.9027×10^{17}	0.6887×10^{17}	7.7083×10^{17}	1.2694×10^{17}	4.2169×10^{17}
26.99	62.71	38.84	115.41	0.884	1.064	0.0333	38.84	115.41	4.0195	0.7093	7.9864	1.3152	4.2920
62.71	68.57	7.50	95.76	0.878	1.059	0.0323	7.50	95.76	3.3824	0.5969	6.7260	1.1060	3.6570
68.57	202.06	140.94	116.40	0.881	1.062	0.0325	140.94	116.40	4.0852	0.7209	8.1505	1.3409	4.4437
202.06	252.41	53.62	113.31	0.865	1.049	0.0341	60.00	101.28	3.6434	0.6430	7.3507	1.2056	4.2392
252.41	252.41	0.00	112.66	0.860	1.044	0.0341	0.00	0.00	0.0000	0.0000	0.0000	0.0000	0.0000
252.41	298.00	48.99	111.37	0.858	1.042	0.0329	56.40	96.75	3.4139	0.6024	6.8858	1.1273	4.1337
298.00	342.95	50.19	106.82	0.855	1.040	0.0329	55.62	96.41	3.4986	0.6174	7.1142	1.1647	4.2798
342.95	385.44	44.83	112.53	0.851	1.038	0.0335	46.98	107.36	3.8241	0.6748	7.8084	1.2777	4.9208
385.44	385.44	0.00	112.00	0.847	1.034	0.0335	0.00	0.00	0.0000	0.0000	0.0000	0.0000	0 0000
385.44	499.59	141.93	95.61	0.852	1.041	0.0302	145.87	93.02	3.3169	0.5853	6.7882	1.1099	4.3572
499.59	564.07	72.69	105.06	0.849	1.043	0.0342	80.59	94.75	3.4196	0.6034	7 0928	1.1593	4.8569
564.07	610.25	49.63	110.20	0.849	1.045	0.0338	51.56	106.08	3.9576	0.6984	8.2842	1.3543	5.7685
610.25	701 23	98.73	109.44	0.851	1.051	0.0329	98.73	109.44	3.9625	0.6993	8.3634	1.3684	6.1781
701.23	701.23	0.00	108.02	0.840	1.040	0.0330	0.00	0.00	0.0000	0.0000	0.0000	0.0000	0.0000
701.23	748.00	50.74	108.15	0.841	1.042	0.0335	50.74	108.15	3.9600	0.6988	8.4073	1.3746	6.5097
748.00	788.00	50.00	93.64	0.839	1.042	0.0283	50.00	93.64	3.5701	0.6300	7.6381	1.2495	5.9653
788.00	818.00	39.20	88.91	0.833	1.036	0.0288	37.50	92.96	3.5731	0.6305	7.6786	1.2563	6.1614
818.00	835.00	30.00	66.27	0.834	1.039	0.0239	30.00	66.27	2.4920	0.4398	5.3496	0.8747	4.4580
835.00	858.00	29.00	91.57	0.825	1.028	0.0313	29.00	91.57	3.4972	0.6172	7.5644	1.2384	6.2773
858.00	889.00	47.00	76.92	0.818	1.020	0.0297	47.00	76.92	2.9500	0.5206	6.4160	1.0511	5.4169
889.00	897.30	12.00	67.84	0.813	1.015	0.0285	12.00	67.84	2.6170	0.4618	5.7088	0.9353	4.9304
Sum/Time-Weighted Average		1034.67	103.49	0.854	1.045	0.0318	1068.11	100.25	3.6228	0.6393	7.4755	1.2247	4.9829
Root Mean Square			12.78	0.018	0.011	0.0022		12.20	0.3829	0.0676	0.7359	0.1215	0.8134

[a] Time at nonzero power used in thermal analysis.

[b] Real calendar days used in nuclear analysis. Some short-term zero-power periods are included.

[c] The energy ranges for the flux groups follow:

Group 1A: 14.96 MeV $\geq$ E $\geq$ 0.18 MeV or 2.40 pJ $\geq$ E $\geq$ 28.84 fJ
Group 1B: 0.18 MeV $\geq$ E $\geq 8.65 \times 10^4$ eV or 28.84 fJ $\geq$ E $\geq$ 13.86 fJ
Group 2: 8.65×10^4 eV $\geq$ E $\geq$ 17.60 eV or 13.86 fJ $\geq$ E $\geq$ 2.82 aJ
Group 3: 17.60 eV $\geq$ E $\geq$ 2.38 eV or 2.82 aJ $\geq$ E $\geq$ 0.38 aJ
Group 4: 2.38 eV $\geq$ E $\geq$ 0 or 0.38 aJ $\geq$ E $\geq$ 0

[d] Group 1A, the fast-flux group has been modified from the Gage output by a factor of 0.85. This accounts for the Peach Bottom energy cut-off of 8.65×10^4 eV instead of 0.18 MeV.

Table 6.3. Fissions per Initial Metal Atom for Recycle Test Element-6

Fuel Body	Fuel Rod	Core Height (mm)	Fertile FIMA (%)	Fissile FIMA (%)	Mixed FIMA (%)
1	1	690	0.323	18.026	3.306
	2	744	0.596	26.379	4.940
	3	797	0.883	34.560	6.556
	4	851	1.171	42.513	8.136
	5	905	1.450	46.847	9.097
	6	959	1.737	50.768	9.997
Mean		824	1.027	36.515	7.005
Range/RMS		322	0.484	11.506	2.337
2	1	1084	2.009	52.870	10.577
	2	1138	2.261	54.740	11.102
	3	1192	2.457	55.987	11.475
	4	1245	2.624	57.075	11.797
	5	1299	2.749	57.927	12.044
	6	1353	2.850	58.519	12.228
Mean		1219	2.492	56.186	11.537
Range/RMS		324	0.289	1.932	0.565
3	1	1479	2.937	58.970	12.377
	2	1533	3.007	59.378	12.503
	3	1578	3.068	59.752	12.617
	4	1642	3.080	59.808	12.636
	5	1696	3.075	59.727	12.618
	6	1751	3.028	59.301	12.508
Mean		1613	3.032	59.490	12.543
Range/RMS		326	0.050	0.301	0.092
4	1	1875	2.967	58.818	12.376
	2	1929	2.891	58.279	12.222
	3	1983	2.807	57.719	12.058
	4	2037	2.723	57.171	11.896
	5	2091	2.630	56.451	11.697
	6	2144	2.530	55.676	11.483
Mean		2010	2.758	57.352	11.955
Range/RMS		323	0.149	1.064	0.303
5	1	2270	2.389	54.635	11.190
	2	2324	2.232	53.418	10.855
	3	2378	2.051	51.856	10.441
	4	2432	1.869	50.052	9.986
	5	2485	1.692	48.080	9.506
	6	2539	1.504	46.016	9.002
Mean		2405	1.956	50.676	10.163
Range/RMS		323	0.304	2.984	0.755
6	1	2660	1.314	43.942	8.495
	2	2714	1.130	41.717	7.967
	3	2768	0.952	39.557	7.456
	4	2822	0.762	37.370	6.929
	5	2876	0.571	35.191	6.404
	6	2931	0.379	33.033	5.880
Mean		2795	0.851	38.468	7.188
Range/RMS		325	0.319	3.724	0.893
Grand Mean		1811	2.019	49.781	10.065
Grand Range/RMS		2295	0.884	10.468	2.476

Table 6.4. Recycle Test Element-6
Thermal and Fast Fluence

Fuel Body	Fuel Rod	Core Height (mm)	Fluence, n/m^2	
			Fast, >0.18 MeV	Thermal, <2.38 eV
1	1	690	1.396×10^{25}	1.821×10^{25}
	2	744	1.916	2.285
	3	797	2.325	2.745
	4	851	2.688	3.202
	5	905	2.985	3.655
	6	959	3.222	4.089
Mean		824	2.422	2.966
Range/RMS		322	0.625	0.776
2	1	1084	3.435	4.502
	2	1138	3.613	4.857
	3	1192	3.761	5.145
	4	1245	3.889	5.388
	5	1299	3.972	5.531
	6	1353	4.043	5.654
Mean		1219	3.786	5.179
Range/RMS		324	0.210	0.399
3	1	1479	4.101	5.756
	2	1533	4.135	5.825
	3	1588	4.161	5.881
	4	1642	4.175	5.920
	5	1696	4.170	5.935
	6	1751	4.157	5.939
Mean		1615	4.150	5.876
Range/RMS		326	0.025	0.066
4	1	1875	4.134	5.923
	2	1929	4.095	5.874
	3	1983	4.046	5.805
	4	2037	3.982	5.696
	5	2091	3.916	5.563
	6	2144	3.846	5.403
Mean		2010	4.003	5.711
Range/RMS		323	0.100	0.181
5	1	2270	3.887	5.199
	2	2324	3.829	4.981
	3	2378	3.555	4.743
	4	2432	3.383	4.490
	5	2485	3.239	4.227
	6	2539	3.082	3.940
Mean		2405	3.496	4.597
Range/RMS		323	0.294	0.430
6	1	2660	2.912	3.647
	2	2714	2.730	3.351
	3	2768	2.523	3.094
	4	2822	2.281	2.860
	5	2876	2.001	2.653
	6	2931	1.609	2.493
Mean		2795	2.343	3.016
Range/S.D.		325	0.440	0.397
Total Mean		1811	3.367	4.558
Total Range/RMS		2295	0.804	1.259

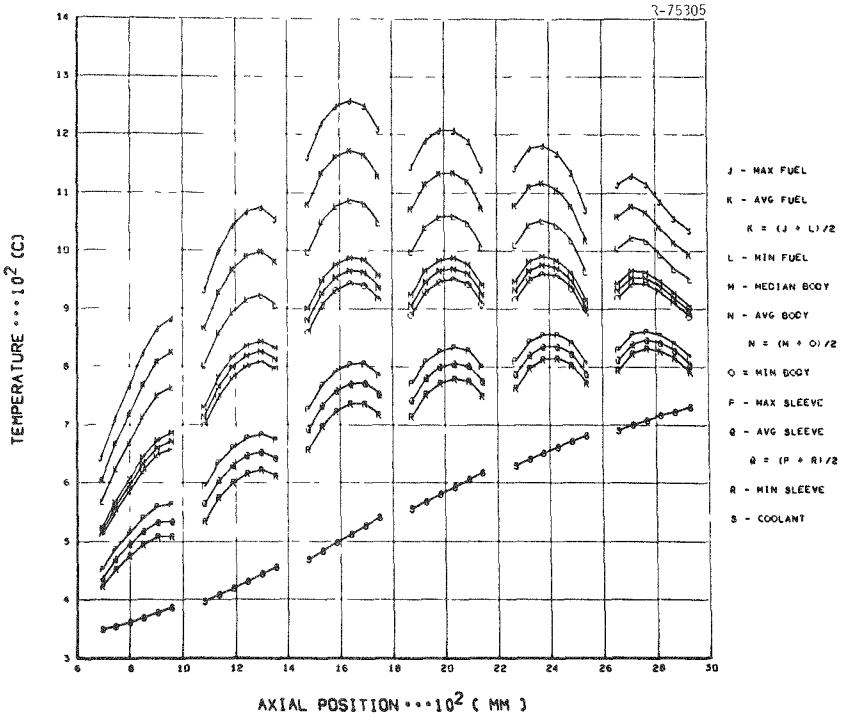

Fig. 6.1. Recycle Test Element-6 Time-Averaged Temperatures: Bodies 1–6.

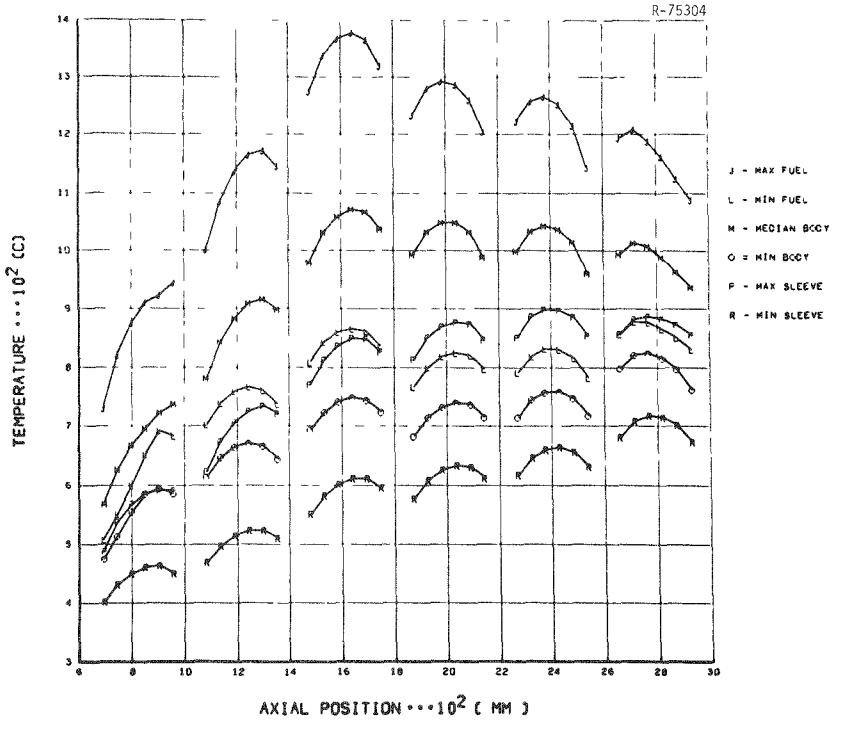

Fig. 6.2. Recycle Test Element-6 Temperature Envelope: Bodies 1–6.

kernels surrounded by a black sooty region (Fig. 6.3), evidently resulting from the fission products released. Metallographic examination could not isolate these failed particles.

Metallographic sections were taken from fuel rods RTE-6-1-1-5 and RTE-6-1-1-6, which both contained Biso UC_2 (batch 4000-309) and Biso ThC_2 (batch 4000-226). These particle batches were also irradiated in the recycle test elements previously discussed. Of the 583 fissile and 198 fertile particles observed, no failure or amoeba migration was seen. Typical particles are shown in Fig. 6.4. The maximum time-averaged temperature for these rods was 880°C and the maximum burnups achieved were 50.7 and 1.7% FIMA for the fissile and fertile particles, respectively. The behavior of the fissile particles was as in RTE-4. The irradiation temperatures were relatively low [(1173 K (<900°C)]; consequently, the buffer coatings did not exhibit the increased optical anisotropy observed at higher irradiation temperatures.

Triso-coated UC_2 (batch 4000-307) and Biso ThC_2 (batch 4000-226) particles were contained in bodies 2, 4, and 5. Metallographic sections of fuel rods from these bodies offered a side-by-side comparison of the performance of these particle types. Samples were taken from fuel rods RTE-6-2-7-6, RTE-6-4-1-1, and RTE-6-5-5-2. The range of burnups in the fissile particles was relatively small (53.4–58.5% FIMA), but the temperature range was wide [(1173–1453 K (900–1180°C) time-averaged temperatures].

The cross section from RTE-6-2-7-6 revealed little graphitization of the iLTI coatings of Triso UC_2 particles, even in the particles in the center of the fuel rod (Fig. 6.5). The maximum time-averaged temperature for this rod was 1323 K (1050°C). In the other test elements we observed such temperatures to cause greater iLTI-coating graphitization than observed in the Triso UC_2 particles in RTE-6-2-7-6. The increased temperatures were expected to increase the release of rare-earth fission products from the kernel.

On the other hand, the iLTI coating of the fissile particles across the entire diameter of fuel rod RTE-6-5-5-2 showed graphitization (Fig. 6.6). Here the minimum time-averaged temperature typical of the particles on the outer surface was 1323 K (1050°C). In

Fig. 6.3. Surface of RTE-6-1-1-6 Showing Black Sooty Regions Surrounding Failed Fuel Particles. 10×.

addition, adjacent to the graphitized iLTI coatings in some particles, slight attack of the SiC was noted.

Most fissile particles — about 90% — in fuel rod RTE-6-4-1-1 showed graphitization of the iLTI on the cold side of the particle, as well as slight attack of the SiC (Fig. 6.7). These particles operated at an average time-averaged temperature of 1348 K (1075°C). Thus, as the Triso UC_2 fissile particles in all three of these bodies indicate, the behavior of the rare-earth fission products depends heavily on the irradiation temperature. Furthermore, temperatures above 1323 K (1050°C) evidently promote migration of the rare-earth fission products, while below 1273 K (1000°C) the rare earths do not migrate to the SiC in sufficient amounts to cause graphitization of the iLTI coating.

The Biso ThC_2 particles (batch 4000-226) contained in bodies 2, 4, and 5 all appeared to be in good condition; no failures or amoeba

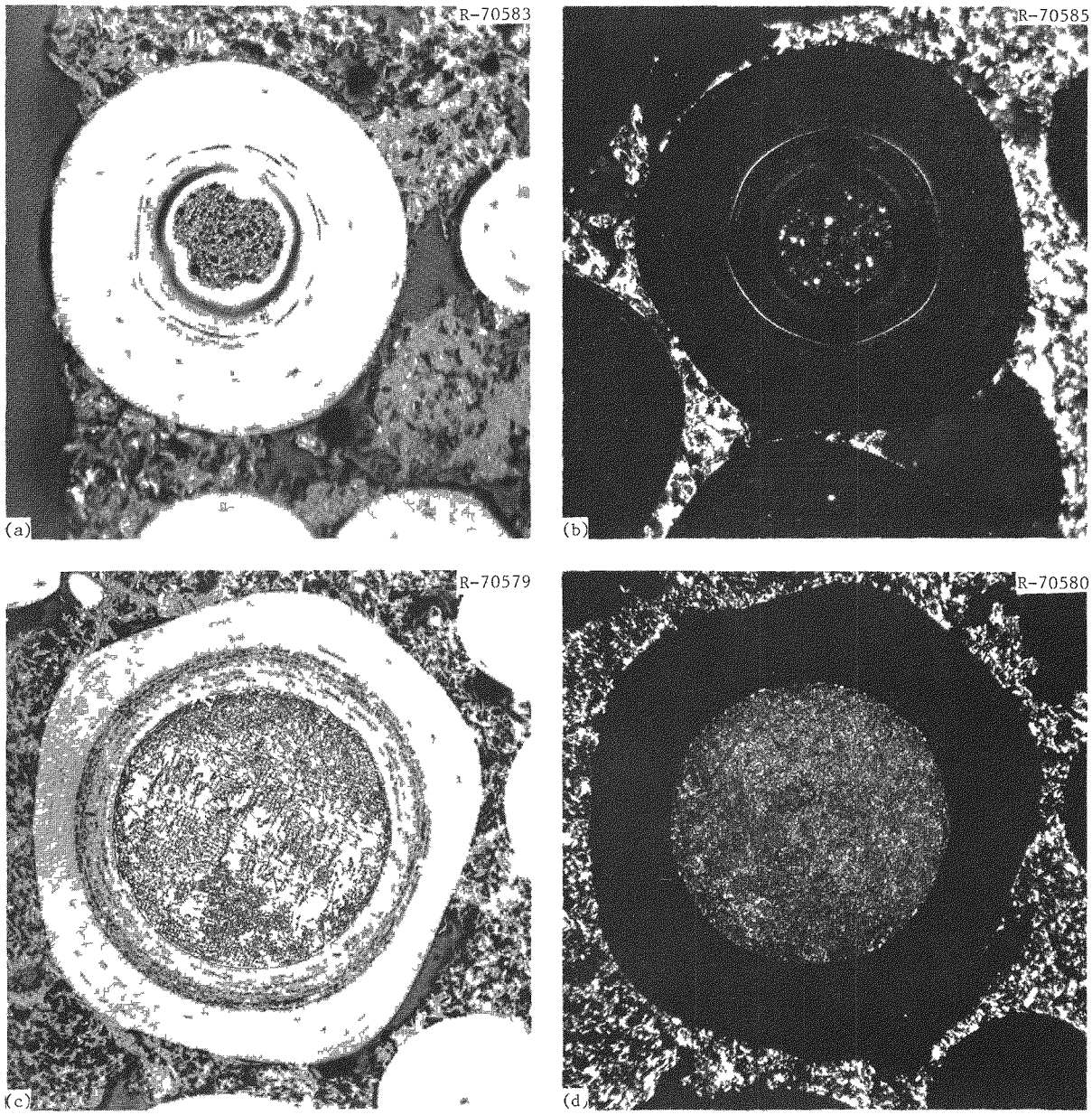

Fig. 6.4. Typical Particles from RTE-6-1-1-5. (a) Biso UC_2 fissile particle. 250×. Bright field. (b) Same. Polarized light. (c) Biso ThC_2 fertile particle. 150×. Bright field. (d) Same. Polarized light. Reduced 28.5%.

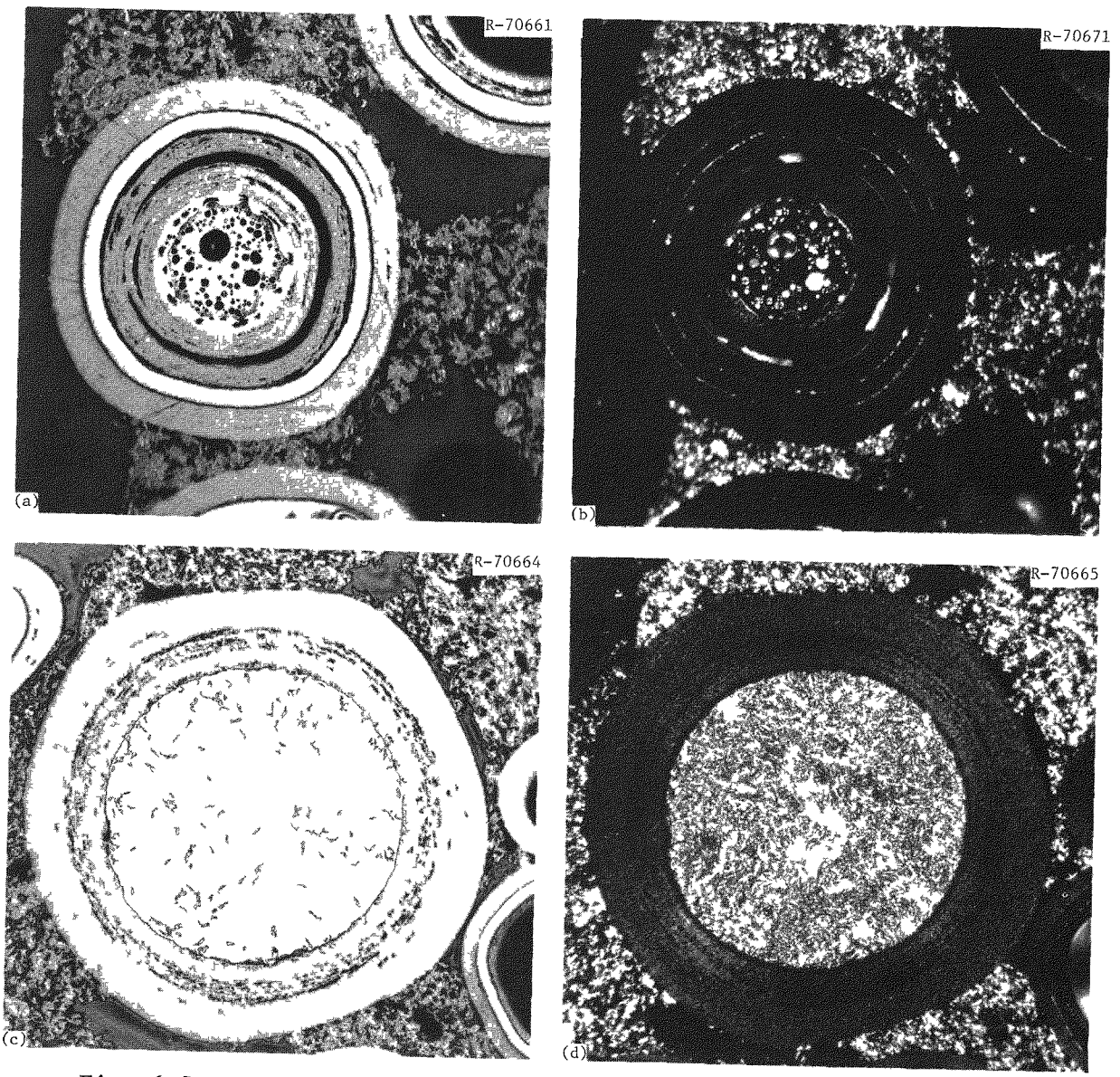

Fig. 6.5. Typical Particles from RTE-6-2-7-6. (a) Triso UC_2 fissile particle. 250×. Bright field. (b) Same. Polarized light. (c) Biso ThC_2 fertile particle. 150×. Bright field. (d) Same. Polarized light.

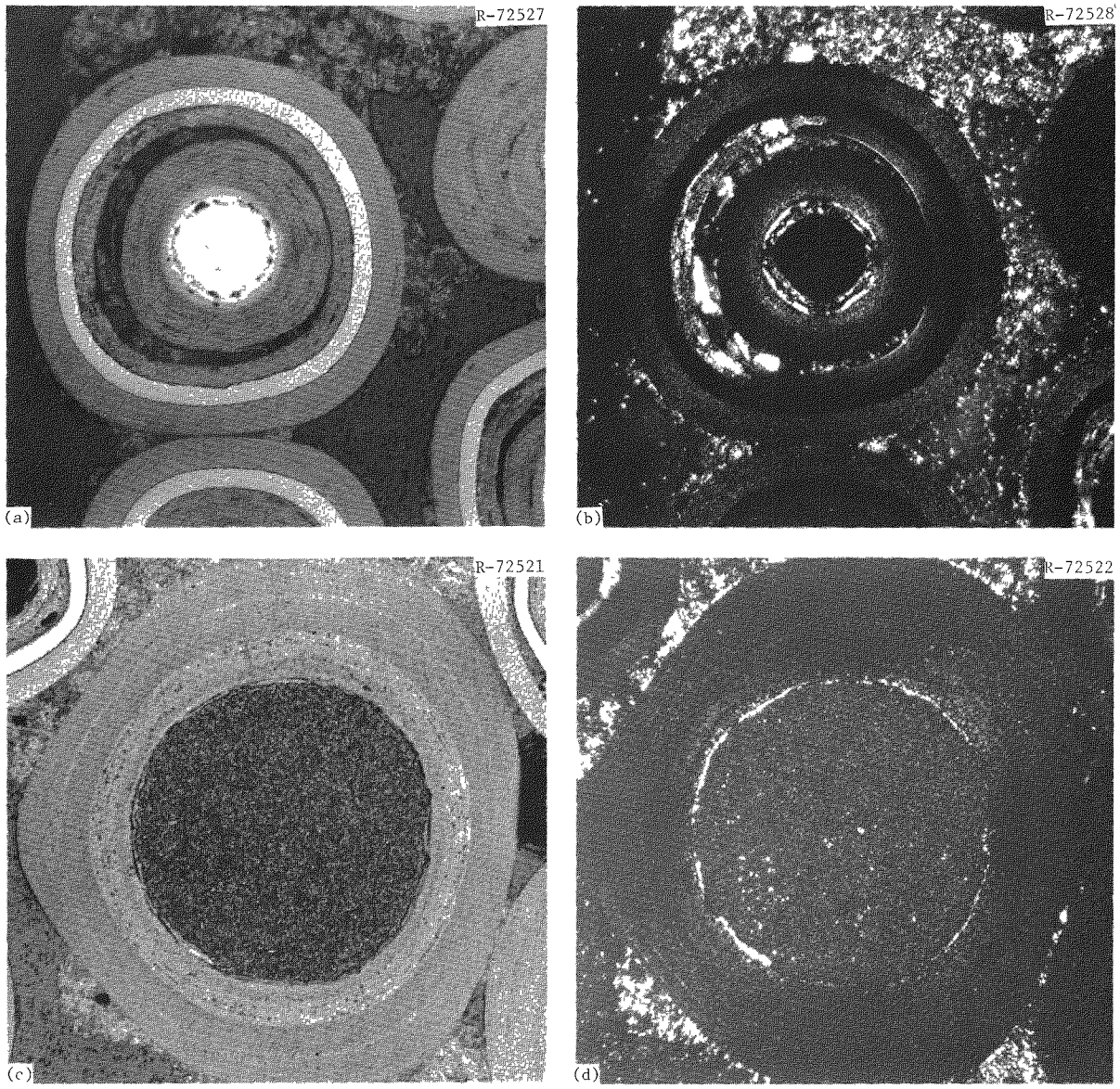

Fig. 6.6. Typical Particles from RTE-6-5-5-2. (a) Triso UC_2 fissile particle. 250×. Bright field. (b) Same. Polarized light. (c) Biso ThC_2 fertile particle. 200×. Bright field. (d) Same. Polarized light. Reduced 32.5%.

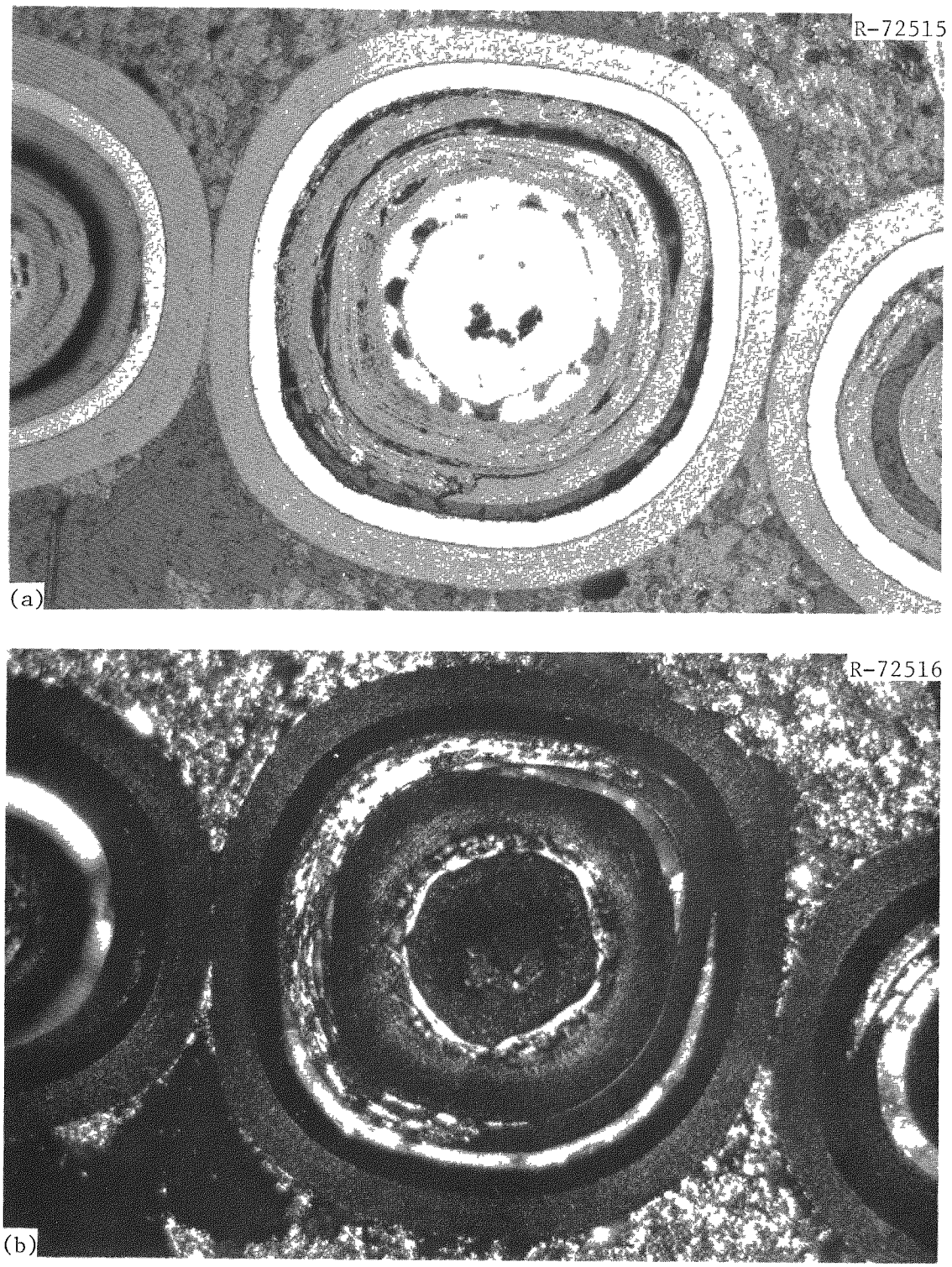

Fig. 6.7. Typical Triso UC_2 Fissile Particle from RTE-6-4-1-1. 250×. (a) Under bright field. (b) Under polarized light.

migration were visible. The particles underwent burnups of up to 2.9% FIMA and reached temperatures as high as 1523 K (1250°C).

Examination of the Biso $(2Th,U)O_2$ and the Biso ThC_2 particles in body 3 (from batches PR-60 and 4000-226, respectively) revealed no failures, although many had faceted coatings (Fig. 6.8). Additionally, no amoeba migration of the $(2Th,U)O_2$ kernels occurred, although very slight amoeba — less than 5 μm — was seen in the ThC_2 particles. The $(2Th,U)O_2$ fissile particles resembled the mixed-oxide particles from accelerated irradiation tests:[16,18] in both cases fission gas bubbles and metallic inclusions were observed.

Biso UO_2 fissile particles (batch Mixed 1) and Biso ThO_2 fertile particles (batch PR-48) were contained in fuel rods from body 6. A metallographic section was taken from fuel rod RTE-6-6-1-1, which experienced a burnup of 43.9 and 1.3% FIMA in the fissile and fertile particles, respectively, with a maximum time-averaged temperature of 1383 K (1110°C). Amoeba migration of the kernels up to 25 μm was seen in many fissile UO_2 particles (Fig. 6.9). The coatings of approximately 4% of the fissile particles had failed (Fig. 6.10), and two minor cases of matrix-particle interaction were observed. The Biso ThO_2 particles were in good condition with no failures or amoeba effect (Fig. 6.9).

7. POSTIRRADIATION EXAMINATION OF RECYCLE TEST ELEMENT-8

Recycle Test Element-8 was irradiated in core position F10-06 from 0 to 897.4 Effective Full-Power Days of Peach Bottom Core 2. The varieties of fuel contained in the element are shown in Table 7.1. All fuel types were irradiated in the recycle test elements previously discussed.

Summaries of the power history, heavy-metal burnup, and neutron fluence calculated by GA are presented in Tables 7.2, 7.3, and 7.4, respectively. The time-averaged temperatures and temperature envelopes for the entire element are presented in Figs. 7.1 and 7.2. This element achieved the highest burnup and neutron fluence of any element in the recycle test element series.

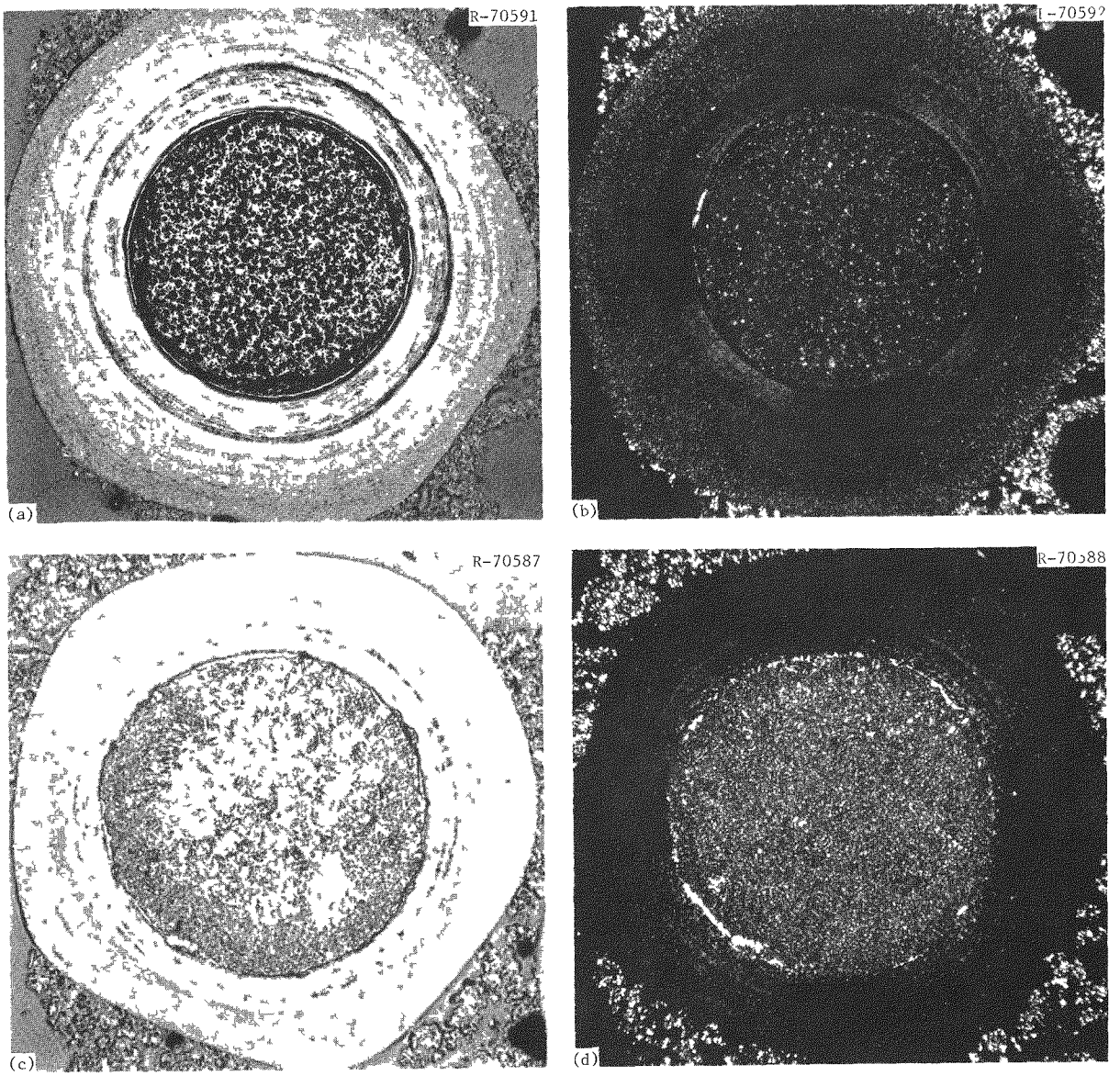

Fig. 6.8. Typical Particles from RTE-6-3-1-6. (a) Biso $(2Th,U)O_2$ fissile particle. 150×. Bright field. (b) Same. Polarized light. (c) Biso ThC_2 fertile particle. 200×. Bright field. (d) Same. Polarized light. Reduced 32.5%.

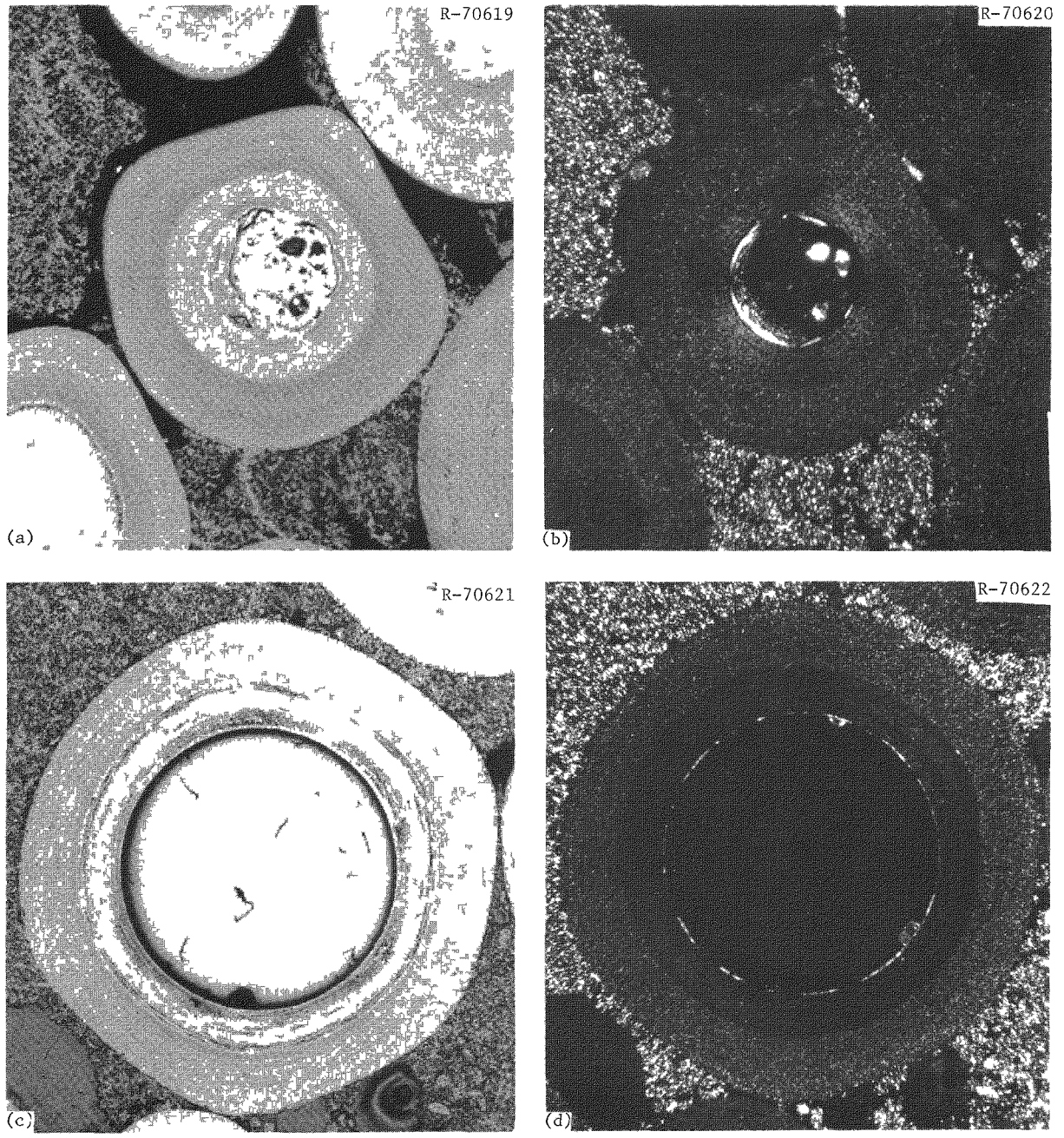

Fig. 6.9. Typical Particles from RTE-6-6-1-1. (a) Biso UO_2 fissile particle. 200×. Bright field. (b) Same. Polarized light. (c) Biso ThO_2 fertile particle. 150×. Bright field. (d) Same. Polarized light. Reduced 24%.

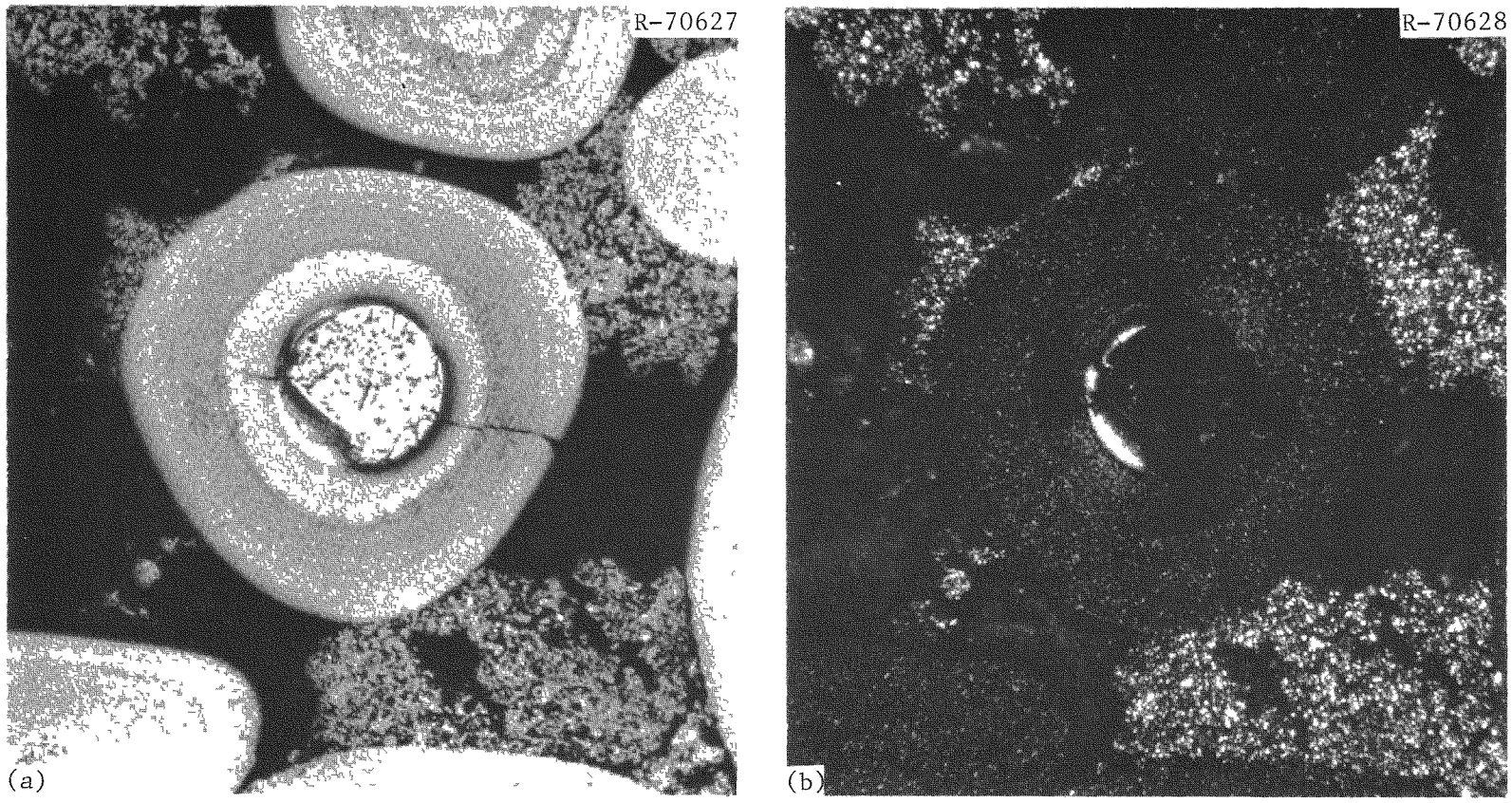

Fig. 6.10. Failed Biso UO_2 Fissile Particle from RTE-6-6-1-1. 200×. (a) Under bright field. (b) Under polarized light.

Table 7.1. Fuel-loading Scheme for Recycle Test Element-8

Body	Fissile Fuel		Fertile Fuel		Fuel-Bed Type
	Particle Type	Batch	Particle Type	Batch	
1	UC_2 Triso	4000-307	ThC_2 Biso	4000-225	Blended Bed
2	UC_2 Triso	4000-307	ThC_2 Triso	4000-306	Bonded Rod[a]
3	UC_2 Biso	4000-309	ThC_2 Biso	4000-226	Bonded Rod[a]
4	$(2Th,U)O_2$ Biso	PR-60	ThC_2 Biso	4000-225	Bonded Rod[b]
5	UC_2 Triso	4000-307	ThC_2 Triso	4000-306	Bonded Rod[a]
6	UC_2 Triso	4000-307	ThC_2 Biso	4000-226	Bonded Rod[a]

[a]Carbonized in fuel body.

[b]Carbonized in packed graphite flour.

The RTE-8 element was shipped from the Peach Bottom Reactor site to ORNL in March 1975. The overall appearance of the element was normal with no unusual or unexpected features. The fission trap and end fittings were cut off and the six fuel bodies removed from the graphite sleeve. The bodies appeared to be in good condition.

Fuel rods were removed from holes 1, 5, and 7 in bodies 2, 3, 5, and 6 and holes 1, 3, 5, and 7 in body 4. Loose particle samples were taken from hole 1 in body 1. The rods appeared to be in good condition with virtually no debonding. Particles with failed coatings were primarily observed on the rods containing UC_2 Triso (batch 4000-307). Previous metallographic examination showed that this batch of particles suffered oLTI failure from fast-neutron damage.

Metallographic sections were prepared from rods from each fuel body. Every fuel-particle type was included in the test elements previously discussed and many observations were identical.

The same batch of UC_2 Triso fissile particles (batch 4000-307) was irradiated in bodies 2, 5, and 6. The metallographic section from fuel rod RTE-8-2-7-7 showed that the fissile particles were in good condition with no graphitization of the iLTI coating (Fig. 7.3). As in previous test elements, fast-neutron damage had caused the oLTI coatings of many particles to break. However, because this element was

Table 7.2. Recycle Test Element-8 Power, Flow, and Flux History

Interval Reference Equivalent Full-Power Time		Thermal Analysis					Nuclear Analysis						
		Irradiation Interval[a]	Absolute Radial Power	Relative Radial Power	Coolant Relative Radial Power Factor	TRICLSP Channel Flow	Real Time[b]	Gage Power	Flux in Groups[c] from Gage, n/m^2s				
From EFPD	To EFPD	(d)	(kW)			(kg/s)	(d)	(kW)	1A[d]	1B	2	3	4
0 00	26 99	28 84	115 94	0 888	1 087	0 0312	28 84	115 94	4 0355 × 10^{17}	0 7121 × 10^{17}	7 9754 × 10^{17}	1 3128 × 10^{17}	4 3431 × 10^{17}
26 99	62 71	38 84	115 55	0 885	1 086	0 0332	38 84	115 55	4 1494	0 7322	8 2496	1 3579	4 4130
62 71	68 57	7 50	95 87	0 879	1 080	0 0322	7 50	95 87	3 4910	0 6161	6 9466	1 1417	3 7601
68 57	202 06	140 94	116 27	0 880	1 081	0 0324	140 94	116 27	4 2083	0 7426	8 4018	1 3816	4 5809
202 06	252 41	53 62	99 77	0 858	1 062	0 0341	60 00	100 46	3 7344	6590	7 5409	1 2362	4 3312
252 41	252 41	0 00	111 22	0 849	1 054	0 0341	0 00	0 00	0 0000	0 0000	0 0000	0 0000	0 0000
252 41	298 00	48 99	110 72	0 853	1 059	0 0328	56 40	96 18	3 5164	0 6205	7 1012	1 1621	4 2424
298 00	342 95	50 19	105 70	0 846	1 053	0 0329	55 62	95 39	3 5869	0 6330	7 3028	1 1952	4 3724
342 95	385 44	44 83	111 07	0 840	1 048	0 0335	46 98	105 97	3 9128	0 6905	8 0001	1 3086	5 0190
385 44	385 44	0 00	110 15	0 833	1 042	0 0335	0 00	0 00	0 0000	0 0000	0 0000	0 0000	0 0000
385 44	499 59	141 93	92 81	0 827	1 035	0 0303	145 87	90 29	3 3425	0 5899	6 8523	1 1201	4 3764
499 59	564 07	72 69	101 47	0 820	1 033	0 0342	80 59	91 51	3 4329	0 6058	7 1333	1 1657	4 8616
564 07	610 25	49 63	106 05	0 817	1 032	0 0339	51 56	102 08	3 9606	0 6989	8 3053	1 3575	5 7573
610 25	701 23	98 73	105 19	0 818	1 036	0 0330	98 73	105 19	3 9631	0 6995	8 3792	1 3707	6 1597
701 23	701 23	0 00	103 65	0 806	1 025	0 0330	0 00	0 00	0 0000	0 0000	0 0000	0 0000	0 0000
701 23	748 00	50 74	103 91	0 808	1 028	0 0330	50 74	103 90	3 9713	0 7008	8 4493	1 3814	6 4935
748 00	788 00	50 00	89 73	0 804	1 024	0 0283	50 00	89 73	3 5647	0 6291	7 6431	1 2502	5 9250
788 00	818 00	39 20	85 18	0 798	1 019	0 0288	37 50	93 05	3 5675	0 6296	7 6834	1 2570	6 1196
818 00	835 00	30 00	63 63	0 798	1 020	0 0239	30 00	63 38	2 4865	0 4388	5 3500	0 8747	4 4257
835 00	858 00	29 00	87 68	0 790	1 011	0 0313	29 00	87 69	3 4927	0 6163	7 5701	1 2392	6 2358
858 00	889 00	47 00	73 63	0 783	1 003	0 0297	47 00	73 63	2 9468	0 5200	6 4226	1 0521	5 3825
889 00	897 30	12 00	64 92	0 788	0 998	0 0285	12 00	64 94	2 6143	0 4614	5 7153	0 9363	4 8998
Sum/Time-weighted Average		1034 67	100 50	0 833	1 044	0 0318	1068 11	98 12	3 6715	0 6479	7 5845	1 2422	5 0223
Root Mean Square			13 36	0 031	0 024	0 002		12 85	0 4083	0 0720	0 7631	0 1262	0 7665

[a] Time at nonzero power used in thermal analysis

[b] Real calendar days used in nuclear analysis. Some short term zero-power periods are included

[c] The energy ranges for the flux groups follow

Group 1A 14 96 MeV ≥ E ≥ 0 18 MeV or 2 40 pJ ≥ E > 28 84 fJ
Group 1B 0 18 MeV ≥ E ≥ 8 65 × 10^{4} eV or 28 84 fJ ≥ E ≥ 13 86 fJ
Group 2 8 65 × 10^{4} eV ≥ E ≥ 17 60 eV or 13 86 fJ ≥ E ≥ 2 82 aJ
Group 3 17 60 eV ≥ E ≥ 2 38 eV or 2 82 aJ ≥ E ≥ 0 38 aJ
Group 4 2 38 eV ≥ E ≥ 0 or 0 38 aJ ≥ E ≥ 0

[d] Group 1A, the fast-flux group has been modified from the Cage output by a factor of 0 85. This accounts for the fixed Bettis energy cut-off of 8 65 × 10^{4} eV instead of 0 18 MeV

Table 7.3. Fissions per Initial Metal Atom for Recycle Test Element-8

Fuel Body	Fuel Rod	Core Height (mm)	Fertile FIMA (%)	Fissile FIMA (%)	Mixed FIMA (%)
1	1	687	0.326	18.019	3.372
	2	741	0.608	26.537	5.072
	3	794	0.895	34.612	6.699
	4	847	1.182	42.432	8.283
	5	900	1.470	46.984	9.305
	6	953	1.757	50.922	10.221
Mean		820	1.040	36.584	7.159
Range/RMS		319	0.489	11.528	2.386
2	1	1083	2.030	53.011	10.807
	2	1137	2.288	54.920	11.349
	3	1191	2.494	56.210	11.742
	4	1245	2.666	57.312	12.074
	5	1298	2.792	58.162	12.324
	6	1352	2.896	58.773	12.516
Mean		1218	2.528	56.398	11.802
Range/RMS		323	0.297	1.970	0.585
3	1	1477	2.988	59.239	12.671
	2	1531	3.058	59.645	12.800
	3	1584	3.123	60.035	12.921
	4	1638	3.135	60.092	12.940
	5	1691	3.134	60.053	12.933
	6	1745	3.088	59.631	12.822
Mean		1611	3.088	59.782	12.848
Range/RMS		321	0.053	0.308	0.096
4	1	1873	3.029	59.159	12.692
	2	1927	2.952	58.617	12.535
	3	1981	2.868	58.057	12.369
	4	2036	2.779	57.487	12.197
	5	2090	2.684	56.775	11.996
	6	2144	2.587	56.021	11.786
Mean		2008	2.816	57.686	12.262
Range/RMS		326	0.151	1.066	0.309
5	1	2267	2.437	54.936	11.475
	2	2321	2.279	53.736	11.138
	3	2375	2.096	52.172	10.717
	4	2430	1.911	50.388	10.256
	5	2484	1.725	48.341	9.750
	6	2538	1.534	46.274	9.237
Mean		2403	1.997	50.975	10.429
Range/RMS		325	0.311	3.004	0.774
6	1	2663	1.341	44.191	8.718
	2	2717	1.154	41.966	8.180
	3	2771	0.968	39.724	7.640
	4	2826	0.775	37.534	7.103
	5	2880	0.581	35.353	6.567
	6	2934	0.386	33.191	6.034
Mean		2798	0.867	38.660	7.373
Range/SD		325	0.326	3.759	0.917
Grand		1810	2.056	50.014	10.312
Grand	Range/RMS	2301	0.901	10.539	2.537

Table 7.4. Thermal- and Fast-Neutron Fluences for Recycle Test Element-8

Fuel Body	Fuel Rod	Core Height (mm)	Fluence, n/m^2s	
			Fast, >0.18 MeV	Thermal, <2.38 eV
1	1	687	1.393×10^{25}	1.815×10^{25}
	2	741	1.915	2.279
	3	794	2.332	2.738
	4	847	2.704	3.195
	5	900	3.003	3.648
	6	953	3.247	4.083
Mean		820	2.432	2.960
Range/RMS		319	0.635	0.776
2	1	1083	3.465	4.504
	2	1137	3.646	4.862
	3	1191	3.801	5.162
	4	1244	3.934	5.414
	5	1298	4.019	5.560
	6	1352	4.093	5.687
Mean		1218	3.826	5.198
Range/RMS		323	0.217	0.411
3	1	1477	4.151	5.790
	2	1531	4.188	5.862
	3	1584	4.215	5.921
	4	1638	4.229	5.959
	5	1691	4.227	5.978
	6	1745	4.217	5.985
Mean		1611	4.204	5.916
Range/RMS		321	0.027	0.070
4	1	1873	4.193	5.969
	2	1927	4.157	5.927
	3	1981	4.107	5.859
	4	2036	4.043	5.751
	5	2090	3.976	5.621
	6	2144	3.904	5.459
Mean		2008	4.063	5.764
Range/RMS		326	0.101	0.179
5	1	2267	3.935	5.256
	2	2321	3.903	5.037
	3	2375	3.624	4.796
	4	2430	3.437	4.540
	5	2484	3.292	4.275
	6	2538	3.132	3.984
Mean		2403	3.554	4.648
Range/RMS		325	0.298	0.435
6	1	2663	2.959	3.688
	2	2717	2.776	3.388
	3	2771	2.565	3.127
	4	2826	2.324	2.889
	5	2880	2.039	2.681
	6	2934	1.647	2.517
Mean		2798	2.385	3.048
Range/SD		325	0.444	0.403
Total Mean		1810	3.411	4.589
Total Range/RMS		2300	0.817	1.272

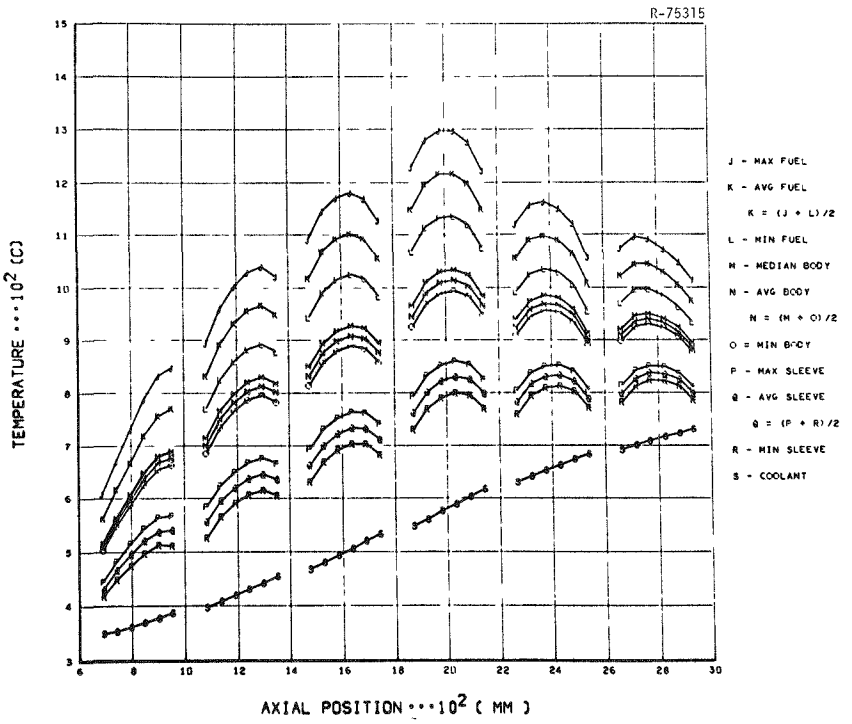

Fig. 7.1. Recycle Test Element-8 Time-Averaged Temperatures: Bodies 1–6.

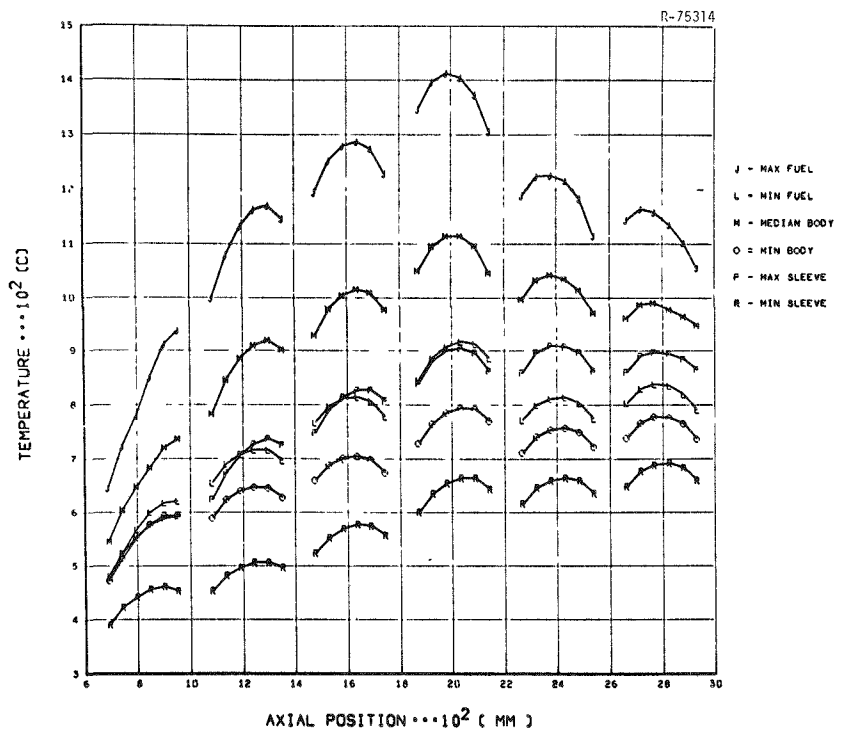

Fig. 7.2. Recycle Test Element-8 Temperature Envelope: Bodies 1–6.

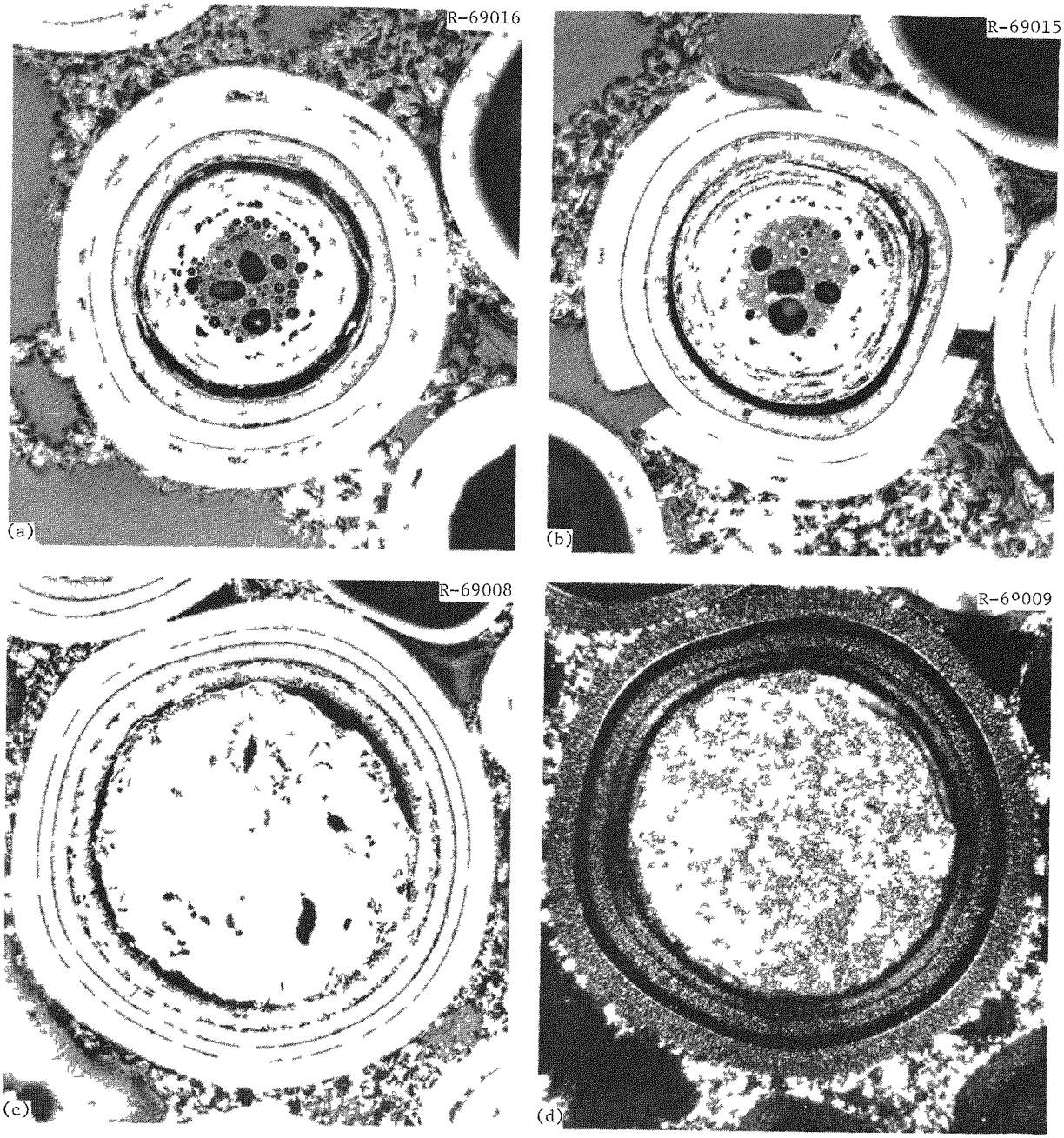

Fig. 7.3. Typical Fuel Particles From RTE-8-2-7-7. (a) Triso UC_2 fissile particle with intact oLTI. 250×. (b) Same. With failed oLTI. (c) Triso ThC_2 fertile particle. 150×. Bright field. (d) Same. Polarized light. Reduced 24%.

irradiated to a higher exposure, the cracks appeared to be larger, indicating that when the oLTI is unrestrained by the SiC, its shrinkage depends on the fast-neutron exposure.

Whereas no graphitization of the iLTI was observed in RTE-8-2-7-7, most of the UC_2 Triso particles (about 90%) in fuel rod RTE-8-5-8-1 showed graphitization of the iLTI on the cold side of the particle, with evidence of slight SiC attack (about 5 μm) (Fig. 7.4). A significant temperature difference between the two rods was noted: RTE-8-2-7-7 had a maximum time-averaged temperature of 1293 K (1020°C), while that of RTE-8-5-7-1 was 1393 K (1120°C). In addition many broken oLTI coatings were observed; the reason is the same as for body 2.

In fuel rod RTE-8-6-7-1 the UC_2 Triso particles appeared to be in good condition with little graphitization of the iLTI coating (Fig. 7.5). The maximum time-averaged temperature for this rod was 1348 K (1075°C). These observations agree with those from the other test elements, which indicate that the iLTI of Triso UC_2 particles irradiated at temperatures above 1373 K (1100°C) shows graphitization caused by migration of the rare-earth fission products. At irradiation temperatures below 1273 K (1000°C) very little rare earth migration occurs, while between 1273 K (1000°C) and 1373 K (1100°C), a transition range exists, in which some migration occurs. Many broken oLTI coatings were observed in RTE-8-6-7-1 also.

The fertile particles in the three metallographic samples just discussed included Biso ThC_2 (batch 4000-226) and Triso ThC_2 (batch 4000-306). The Biso ThC_2 particles in RTE-8-6-7-1 were in good condition with no amoeba, though some had faceted coatings (Fig. 7.5). The Triso ThC_2 particles in the other two samples were both in good condition with no amoeba observed (Figs. 7.3 and 7.4). In both cases the buffers separated from the iLTI and densified around the kernel in some particles. Although no oLTI failure was observed in RTE-8-2-7-7, the oLTI on about half the Triso ThC_2 particles in RTE-8-5-7-1 failed from fast-neutron damage. Surprisingly, fuel rod RTE-8-2-7-7 received the higher fast-neutron fluence: 3.9×10^{25} n/m^2 versus 4.1×10^{25} n/m^2, although the rod operated at lower fuel temperatures: 1323 K (1050°C) versus 1223 K (950°C), respectively.

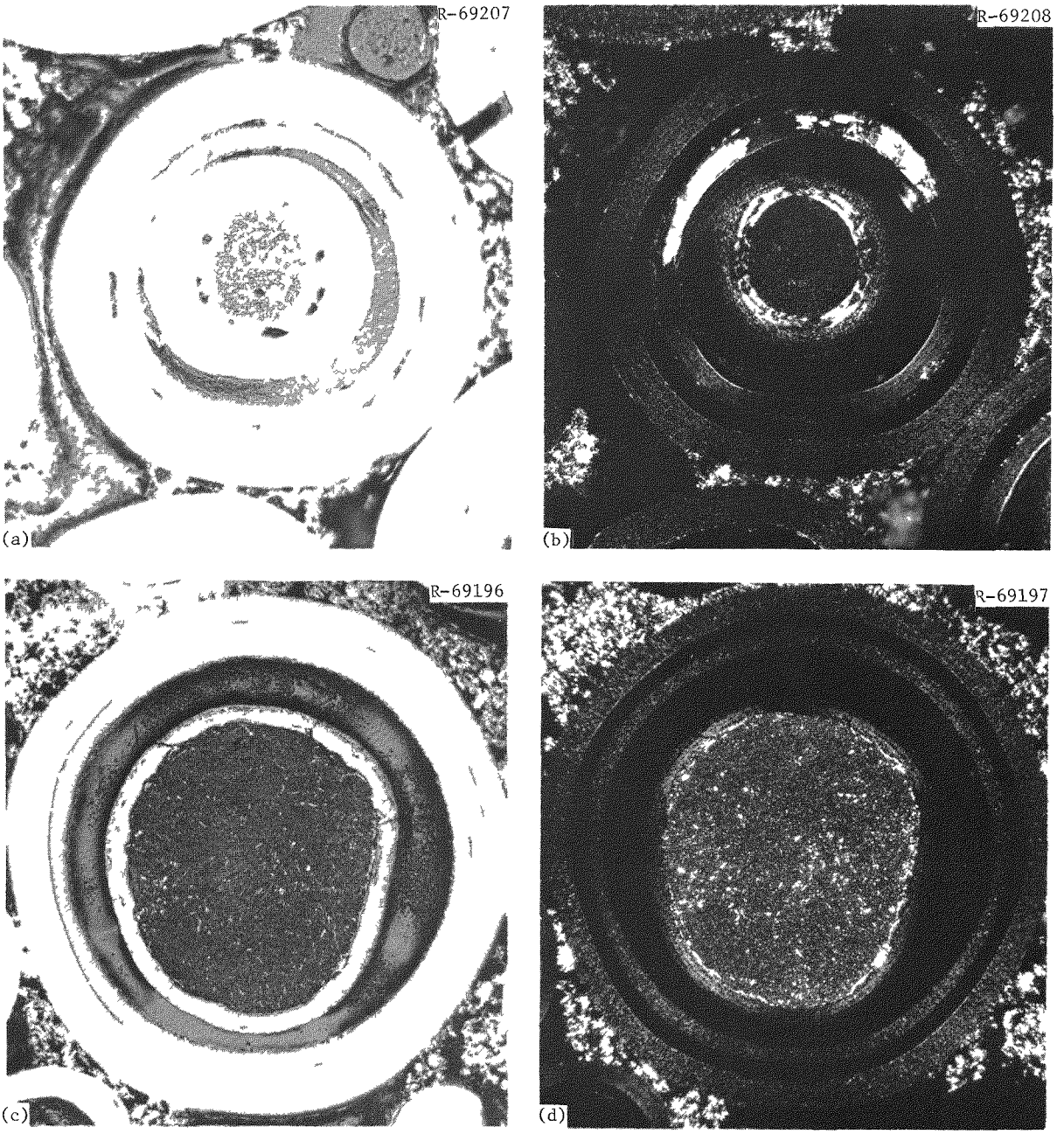

Fig. 7.4. Typical Fuel Particles from RTE-8-5-7-1. (a) Triso UC_2 fissile particle. 250×. Bright field. (b) Same. Polarized light. (c) Triso ThC_2 fertile particle. 150×. Bright field. (d) Same. Polarized light. Reduced 23.5%.

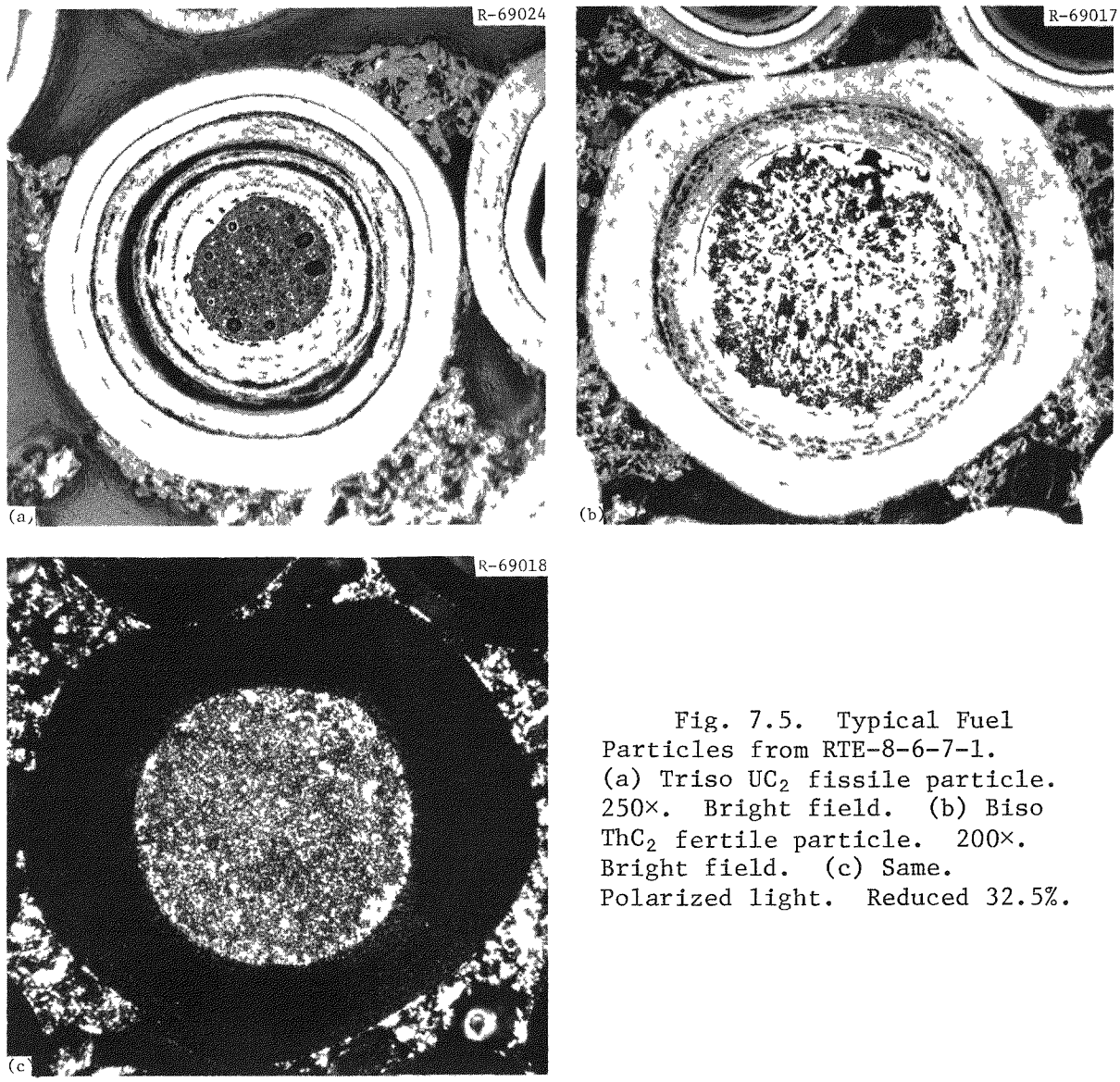

Fig. 7.5. Typical Fuel Particles from RTE-8-6-7-1. (a) Triso UC_2 fissile particle. 250×. Bright field. (b) Biso ThC_2 fertile particle. 200×. Bright field. (c) Same. Polarized light. Reduced 32.5%.

Examination of the metallographic section made from fuel rod RTE-8-3-1-7 showed no failed Biso UC_2 (batch 4000-309) or failed Biso ThC_2 (batch 4000-226). No graphitization, matrix-particle interaction, or amoeba was seen in either particle type. Generally the particles were in good condition, though some had faceted coatings or misshapen kernels. Typical particles are shown in Fig. 7.6. Their behavior resembled that of particles from the same batch in RTE-6. In RTE-2, the buffer densified and optical anisotropy increased in the Biso UC_2 particles from the same batch. However, the buffer of the Biso UC_2 particles in RTE-8-3-1-7 did not show this density increase or high optical anisotropy. The irradiation temperature [1398 K (1125°C), time-averaged] was 100 K less than that in the fuel rod in RTE-2, where the anisotropy had been observed. We had hypothesized that migration of the rare-earth fission products might have induced the change in the buffer properties. However, the irradiation temperature was sufficiently high to cause substantial release of the rare earths from the kernel. Evidently the rare earths do not cause buffer densification or optical anisotropy.

No failed particles or matrix-particle interactions were observed in the metallographic cross sections from fuel rods RTE-8-4-1-6 and RTE-8-4-5-1 that contained Biso $(2Th,U)O_2$ and Biso ThC_2 particles. The particles were in good condition though some had faceted coatings. Typical particles are shown in Fig. 7.7. Slight amoeba — less than 5 μm — of the $(2Th,U)O_2$ kernels up the temperature gradient was observed.

8. POSTIRRADIATION EXAMINATION OF RECYCLE TEST ELEMENT-1 (FUEL TEST ELEMENT-11)

Recycle Test Element-1 was irradiated in core location E10-06* from 252 to 897.4 Effective Full-Power Days of Peach Bottom Core 2. The original designation for this element was RTE-1, but it was renamed

*See ref. 6 for core location.

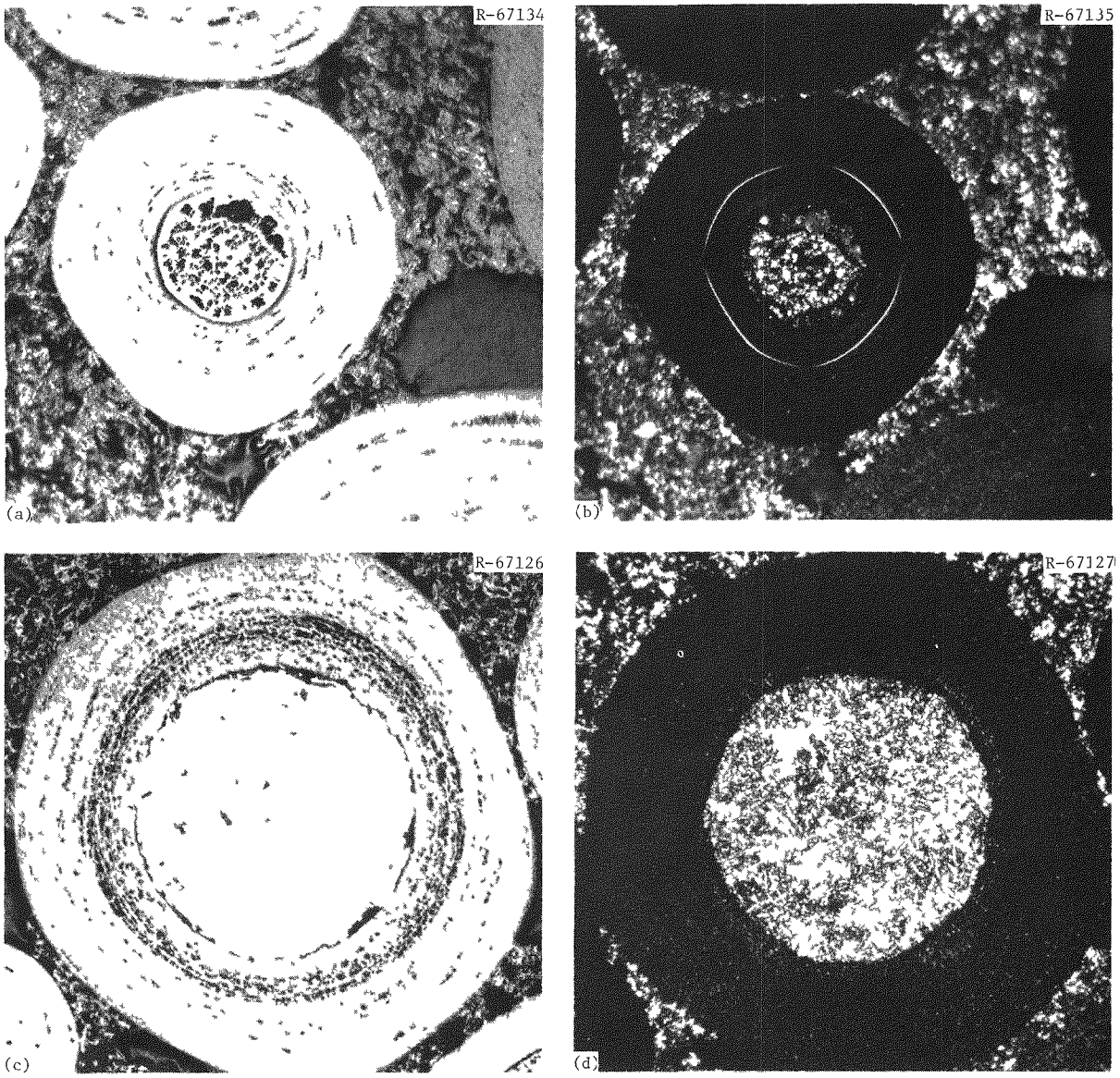

Fig. 7.6. Typical Fuel Particles from RTE-8-3-1-7. (a) Biso UC_2 fissile particle. 250×. Bright field. (b) Same. Polarized light. (c) Biso ThC_2 fertile particle. 200×. Bright field. (d) Same. Polarized light. Reduced 32.5%.

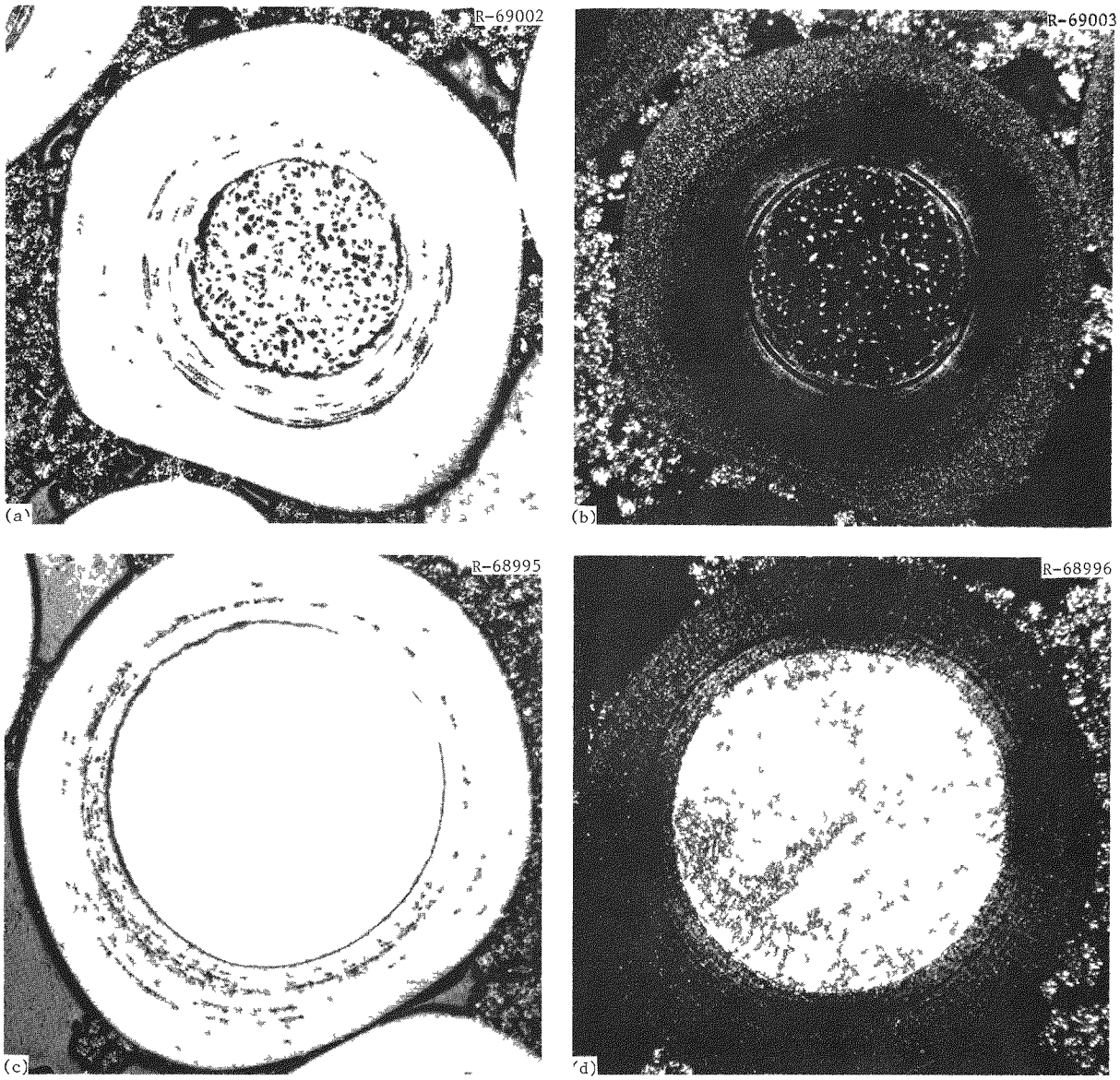

Fig. 7.7. Typical Particles from RTE-8-4-16. (a) Biso $(2Th,U)O_2$ fissile particle. 150×. Bright field. (b) Same. Polarized light. (c) Biso ThC_2 fertile particle. 200×. Bright field. (d) Same. Polarized light. Reduced 32%.

Fuel Test Element-11. Table 8.1 identifies the fuel-loading combinations in the element. All the fuel in RTE-1 was fabricated to duplicate the fuel used in the other recycle test elements. So although RTE-1 tested the same fuel types, new particle batches were irradiated.

The nuclear and thermal evaluations of this element were performed by GA. Summaries of the power history, heavy-metal burnup, and neutron fluence are given in Tables 8.2, 8.3, and 8.4, respectively. The time-averaged temperatures and temperature envelopes for the entire element are presented in Figs. 8.1 through 8.8. Since the heavy-metal loading and, therefore, the power production in fuel holes 1 and 5, 2 and 6, 3 and 7, and 4 and 8 varied within each fuel body, a set of temperatures is reported for each section of the test element containing one of these pairs of fuel holes.

Maximum burnups were 49.6 and 1.8% FIMA for the fissile and fertile particles, respectively. The highest fuel temperature and fast-fluence exposure (E >0.18 MeV) achieved were 1913 K (1640°C) and 3.0×10^{25} n/m^2, respectively. While the burnups and fast-fluence exposures were not as severe, the maximum fuel temperatures were significantly higher — above 200°C — than in the previous recycle test elements.

As in the other test elements, the overall appearance of the element was normal with no unexpected features. The fission-product trap and end fittings were cut off and the six fuel bodies removed from the graphite sleeve. The appearance of the bodies was excellent with no evidence of surface corrosion.

Fuel rods were removed from holes 1, 3, 6, and 8 in bodies 1, 2, and 3, and from all the holes in bodies 4, 5, and 6. On visual examination, most rods were in good condition, except for rods from fuel stacks RTE-1-2-6, -3-6, and -4-6, which had experienced severe debonding. All three contained the same particle batches. Fuel stack RTE-1-1-6, which also contained these particles, had only minor rod debonding. The surface of some rods from stack RTE-1-5-3 showed a rust-colored corrosion reaction believed attributable to iron contamination in the matrix material, as discussed in Sect. 10.

Table 8.1. Fuel-Loading Scheme for Recycle Test Element-1

Body	Hole	Fissile Fuel		Fertile Fuel		Carbonization Procedure for Bonded Rods
		Particle Type	Batch	Particle Type	Batch	
1,2,3,4	1,5	$(4Th,U)O_2$ Biso	PR-56[a]	ThC_2 Biso		PGF[d]
	2,6	UC_2 Triso	4000-325[b]	ThC_2 Biso	4000-323[b]	CGT[e]
	3,7	$(2Th,U)O_2$ Biso	PR-66[a]	ThO_2 Biso	Mixed A[a]	PGF
	4,8	UO_2 Biso	Mixed 3[a,c]	ThO_2 Biso	Mixed A[a]	PGF
5	1,5	$(2Th,U)O_2$ Biso	PR-66[a]	ThC_2 Biso	9T-980-BL[b]	PGF
	2,6	UC_2 Biso	4000-340[b]	ThC_2 Biso	4000-323[b]	CGT
	3,7	UC_2 Biso	4000-340[b]	ThO_2 Biso	4000-339[b]	CGT
	4,8	UO_2 Triso	4000-355[b]	ThO_2 Biso	4000-339[b]	CGT
6	1,5	$(2Th,U)O_2$ Biso	PR-66[a]	ThC_2 Biso	9T-980-BL[b]	PGF
	2,6	UC_2 Biso	4000-340[b]	ThC_2 Biso	4000-323[b]	CGT
	3,7	UC_2 Triso	4000-325[b]	ThC_2 Triso	4000-319[b]	CGT
	4,8	UO_2 Triso	4000-355[b]	ThO_2 Biso	4000-339[b]	CGT

[a] Fuel fabricated by Oak Ridge National Laboratory.

[b] Fuel fabricated by 6A General Atomic Company.

[c] Fuel stack RTE-1-4-8 used batch Mixed 1.

[d] Carbonized in packed graphite flour.

[e] Carbonized in covered graphite tray.

Metallographic sections were prepared from the fuel rods to represent all fuel batches irradiated. Because many batches were duplicated, samples were prepared only from the regions of highest temperature and neutron fluence. Bodies 1, 2, 3, and 4 contained the same fuel batches, so fuel from bodies 3 and 4 were examined.

In the fuel rod RTE-1-4-1-6 no failures were seen in the Biso $(4Th,U)O_2$ fissile or Biso ThC_2 fertile particles. No amoeba migration was observed in the $(4Th,U)O_2$ particles (Fig. 8.9). However, because this rod exprienced high average temperatures (1373 K, $\geq$1100°C), amoeba migration might have been expected in particles of this type.

The Triso UC_2 and Biso ThC_2 particles examined in fuel rod RTE-1-3-6-6 behaved much as did particles of the same type from other batches. Graphitization of the iLTI coating occurred in all the fissile particles observed. In addition, the high average irradiation temperatures (1423 K, >1150°C) induced extensive corrosion of the SiC. Visible penetration of the SiC by fission products presumed to be rare

Table 8.2. Recycle Test Element-1 Power, Flow, and Flux History

Interval Reference Equivalent Full-Power Time		Irradiation Interval	Thermal Analysis					Nuclear Analysis				
			Absolute Radial Power	Relative Radial Power	Coolant Relative Radial-Power Factor	TRICE[a] Channel Flow	Real Time	Gage Power	Flux in Groups from Gage, n/cm²s			
From EFPD	To EFPD	(d)	(kW)			(kg/s)	(d)	(kW)	1A	1B	2	3	4
252.41	298.00	48.99	142.97	1.107	1.089	0.0327	56.40	124.15	3.4233×10^{7}	0.6052×10^{7}	6.8088×10^{6}	1.1122×10^{6}	3.8925×10^{5}
298.00	342.95	50.19	137.93	1.104	1.095	0.0327	55.62	124.49	3.5332	0.6235	7.0674	1.1543	4.0525
342.95	385.44	44.83	140.49	1.100	1.095	0.0333	46.98	138.78	3.8722	0.6833	7.7767	1.2693	4.6822
385.44	385.44	0.00	140.32	1.099	1.095	0.0333	0.00	0.00	0.0000	0.0000	0.0000	0.0000	0.0000
385.44	499.59	141.93	123.11	1.097	1.097	0.0301	145.87	119.77	3.3562	0.5923	6.7545	1.1016	4.1509
499.59	564.07	72.69	135.62	1.096	1.106	0.0340	80.59	122.31	3.4817	0.6144	7.0981	1.1568	4.6729
564.07	610.25	49.63	142.52	1.098	1.112	0.0336	51.56	137.20	4.0387	0.7127	8.3076	1.3539	5.5709
610.25	701.23	98.73	140.95	1.096	1.117	0.032	99.73	140.93	4.0452	0.7139	8.3923	1.3688	5.9789
701.23	701.23	0.00	138.60	1.079	1.107	0.0327	0.00	0.00	0.0000	0.0000	0.0000	0.0000	0.0000
701.23	748.00	50.74	139.27	1.083	1.132	0.0332	50.74	139.26	4.1008	0.7237	8.5464	1.3958	6.3685
748.00	788.00	50.00	120.34	1.080	1.132	0.0280	50.00	120.53	3.6940	0.6519	7.7589	1.2676	5.8350
788.00	818.00	39.20	114.21	1.070	1.12	0.0285	37.50	119.41	3.6970	0.6525	7.8029	1.2748	6.0358
818.00	835.00	30.00	84.55	1.064	1.124	0.0237	30.00	84.50	2.5759	0.4546	5.4343	0.8872	4.3728
835.00	858.00	29.00	116.63	1.051	1.112	0.0310	29.00	116.66	3.6120	0.6374	7.6788	1.2552	6.1537
858.00	889.00	47.00	97.79	1.040	1.102	0.0294	47.00	97.80	3.0452	0.5374	6.5104	1.0649	5.3116
889.00	897.30	12.00	86.04	1.031	1.095	0.0283	12.00	86.06	2.6999	0.4764	5.7915	0.9473	4.8382
Sum/Time-Weighted Average		764.93	127.96	1.087	1.109	0.0313	791.99	123.59	3.5841	0.6325	7.3638	1.2019	5.0292
Root Mean Square			10.38	0.019	0.014	0.0025		14.27	0.3788	0.0668	0.7985	0.1301	0.8512

[a] Time at nonzero power used in thermal analysis.

[b] Real calendar days used in nuclear analysis. Some short-term zero-power periods are included.

[c] The energy ranges for the flux groups follow:

Group 1A. 14.96 MeV ≥ E ≥ 0.18 MeV or 2.40 pJ ≥ F ≥ 28.84 fJ
Group 1B: 0.18 MeV ≥ E ≥ 8.65×10^{4} eV or 28.84 fJ ≥ E ≥ 13.86 fJ
Group 2: 8.65×10^{4} eV ≥ E ≥ 17.60 eV or 13.86 fJ ≥ E ≥ 2.82 aJ
Group 3: 17.60 eV ≥ E ≥ 2.38 eV or 2.82 aJ > E ≥ 0.38 aJ
Group 4: 2.38 eV ≥ E ≥ 0 or 0.38 aJ ≥ E ≥ 0

[d] Group 1A, the fast-flux group, has been modified from the Gage output by a factor of 0.85. This accounts for the Peach Bottom energy cut-off of 8.65×10^{4} eV instead of 0.18 MeV.

Table 8.3. Fissions per Initial Metal Atom for Recycle Test Element-1

Fuel Body	Fuel Rod	Core Height (mm)	Fertile FIMA (%)	Fissile FIMA (%)	Mixed FIMA (%)
1	1	688	0.179	22.225	4.562
	2	743	0.344	27.427	5.729
	3	798	0.515	31.743	6.723
	4	852	0.687	35.673	7.643
	5	907	0.856	38.573	8.355
	6	962	1.024	41.257	9.023
Mean		825	0.601	32.816	7.006
Range/RMS		329	0.290	6.518	1.526
2	1	1083	1.187	42.991	9.498
	2	1138	1.333	44.530	9.921
	3	1192	1.439	45.570	10.213
	4	1247	1.532	46.501	10.473
	5	1302	1.612	47.313	10.698
	6	1357	1.674	48.013	10.887
Mean		1220	1.463	45.820	10.282
Range/RMS		329	0.166	1.694	0.470
3	1	1478	1.727	48.660	11.058
	2	1533	1.768	49.108	11.180
	3	1588	1.806	49.502	11.283
	4	1643	1.811	49.594	11.311
	5	1697	1.808	49.613	11.313
	6	1752	1.783	49.427	11.255
Mean		1615	1.784	49.317	11.234
Range/RMS		330	0.030	0.338	0.091
4	1	1873	1.754	49.115	11.170
	2	1928	1.721	48.652	11.052
	3	1983	1.675	48.161	10.917
	4	2037	1.622	47.653	10.774
	5	2092	1.564	46.990	10.595
	6	2147	1.504	46.294	10.409
Mean		2010	1.640	47.811	10.820
Range/RMS		328	0.087	0.960	0.261
5	1	2268	1.422	45.479	10.181
	2	2323	1.335	44.517	9.921
	3	2379	1.237	43.115	9.563
	4	2434	1.131	41.627	9.182
	5	2489	1.017	40.038	8.775
	6	2545	0.903	38.252	8.329
Mean		2406	1.174	42.171	9.325
Range/RMS		333	0.178	2.502	0.640
6	1	2664	0.790	36.389	7.868
	2	2719	0.674	34.451	7.389
	3	2774	0.558	32.501	6.908
	4	2829	0.447	30.622	6.446
	5	2884	0.335	28.735	5.982
	6	2940	0.223	26.826	5.512
Mean		2802	0.504	31.587	6.684
Range/RMS		331	0.193	3.262	0.803
Grand Mean		1813	1.194	41.587	9.225
Grand Range/RMS		2307	0.522	7.713	1.948

Table 8.4. Recycle Test Element-1 Fast- and Thermal-Neutron Fluences

Fuel Body	Fuel Rod	Core Height (mm)	Fluence, n/m^2	
			Fast, >0.18 MeV	Thermal, <2.38 eV
1	1	688	0.971×10^{25}	1.292×10^{25}
	2	743	1.344	1.609
	3	798	1.628	1.945
	4	852	1.885	2.284
	5	907	2.104	2.627
	6	962	2.282	2.959
Mean		825	1.702	2.119
Range/RMS		329	0.447	0.572
2	1	1083	2.440	3.278
	2	1138	2.568	3.555
	3	1192	2.678	3.792
	4	1247	2.775	4.000
	5	1302	2.841	4.124
	6	1357	2.898	4.231
Mean		1220	2.700	3.830
Range/RMS		329	0.158	0.331
3	1	1478	2.946	4.319
	2	1533	2.982	4.384
	3	1588	3.011	4.438
	4	1643	3.026	4.476
	5	1697	3.031	4.498
	6	1752	3.031	4.511
Mean		1615	3.004	4.438
Range/RMS		330	0.031	0.068
4	1	1873	3.024	4.502
	2	1928	3.008	4.468
	3	1983	2.986	4.415
	4	2037	2.952	4.329
	5	2092	2.915	4.229
	6	2147	2.875	4.110
Mean		2010	2.960	4.342
Range/RMS		328	0.052	0.138
5	1	2268	2.812	3.955
	2	2323	2.740	3.785
	3	2379	2.657	3.595
	4	2434	2.558	3.396
	5	2489	2.450	3.192
	6	2545	2.323	2.965
Mean		2406	2.590	3.481
Range/RMS		333	0.167	0.339
6	1	2664	2.178	2.732
	2	2719	2.019	2.495
	3	2774	1.827	2.298
	4	2829	1.605	2.120
	5	2884	1.342	1.970
	6	2940	0.973	1.843
Mean		2802	1.657	2.243
Range/RMS		331	0.409	0.304
Total Mean		1813	2.436	3.409
Total Range/RMS		2307	0.614	0.983

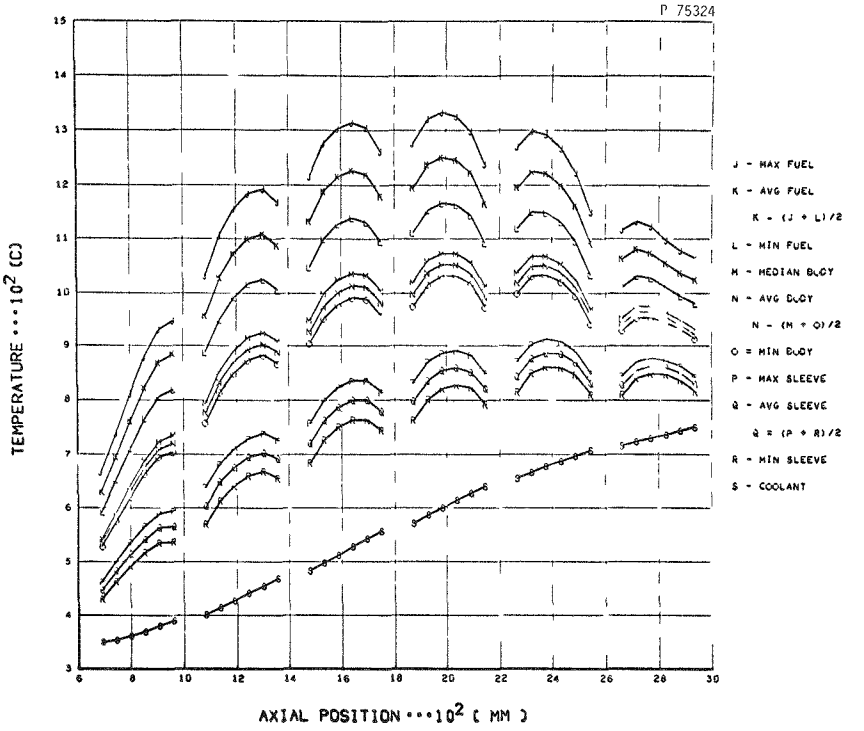

Fig. 8.1. Recycle Test Element-1 Time-Averaged Temperatures: Bodies 1–6, Holes 1–5.

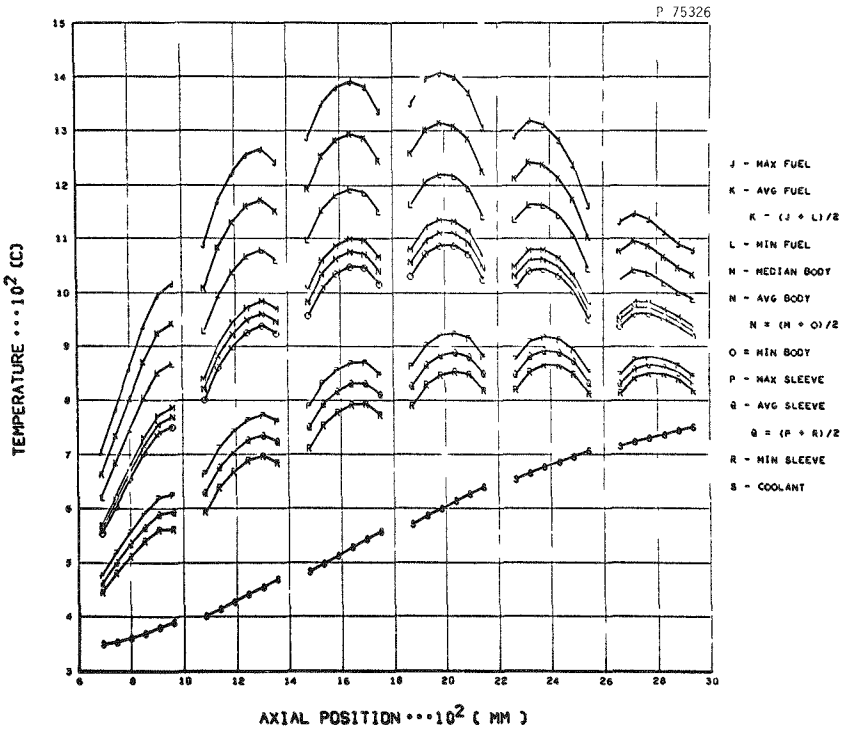

Fig. 8.2. Recycle Test Element-1 Time-Averaged Temperatures: Bodies 1–6, Holes 2–6.

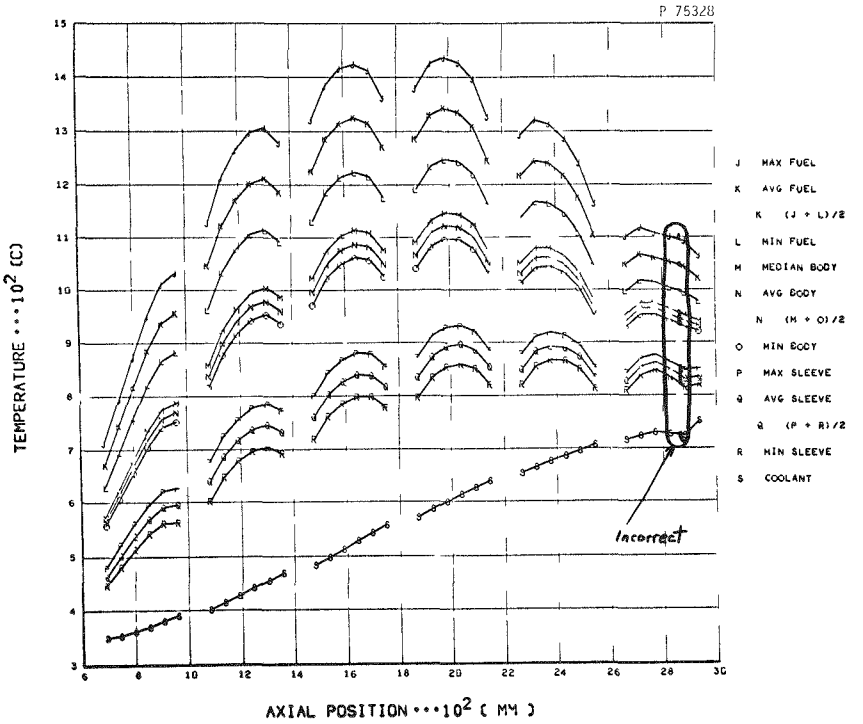

Fig. 8.3. Recycle Test Element-1 Time-Averaged Temperatures: Bodies 1–6, Holes 3,7. Reasonable estimates of the correct temperatures for rods 4 and 5 of body 6 can be obtained by interpolation of the data on either side of the incorrect values.

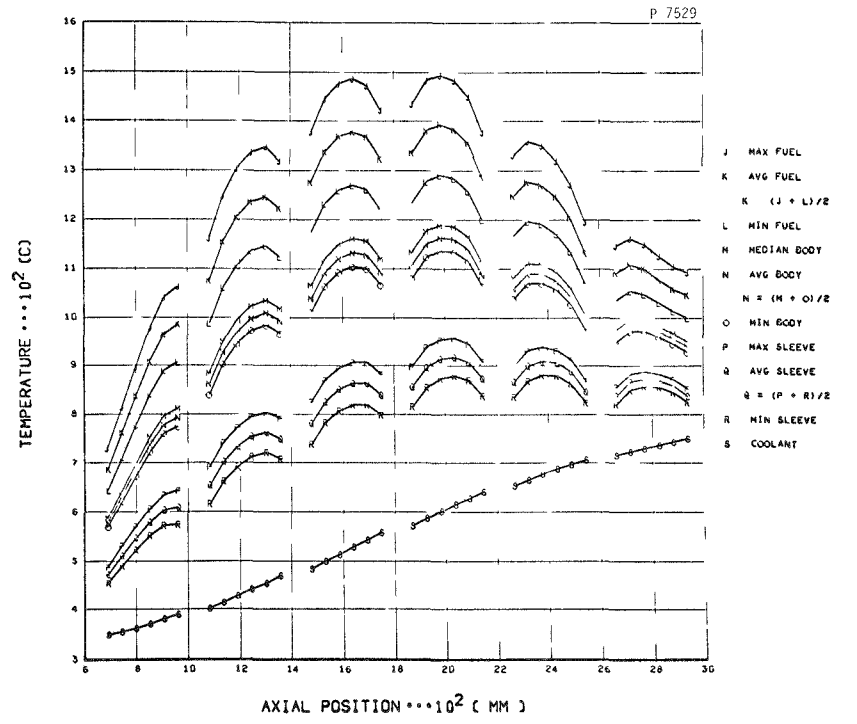

Fig. 8.4. Recycle Test Element-1 Time-Averaged Temperatures: Bodies 1–6, Holes 4,8.

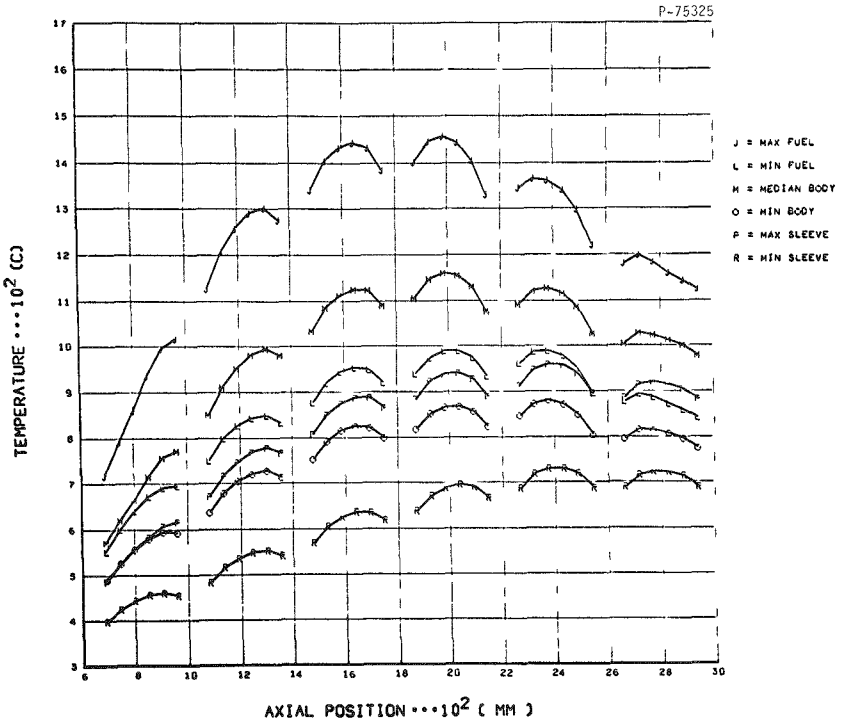

Fig. 8.5. Recycle Test Element-1 Temperature Envelope: Bodies 1–6, Holes 1,5.

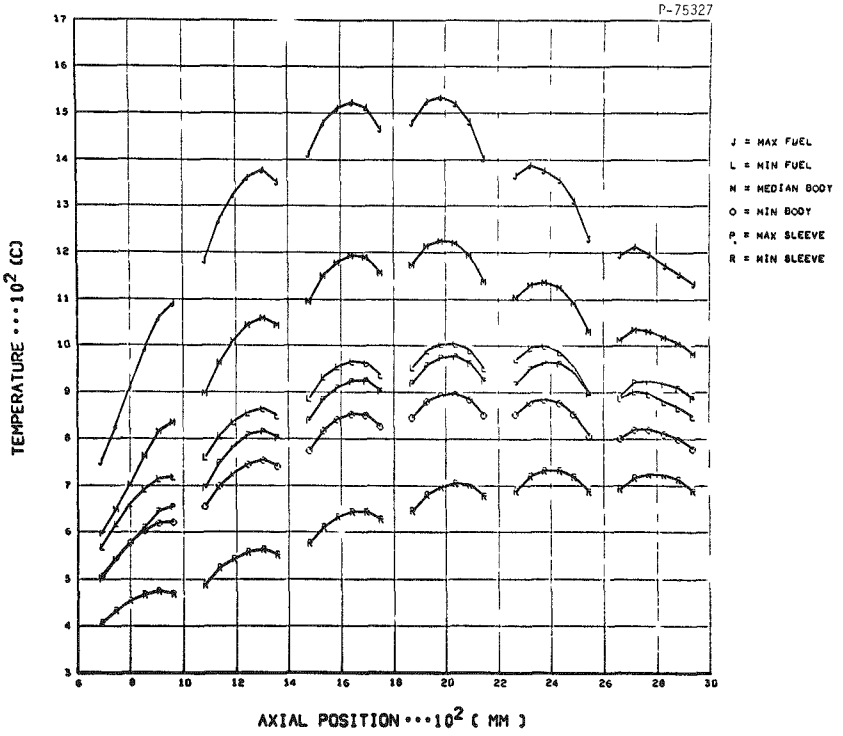

Fig. 8.6. Recycle Test Element-1 Temperature Envelope: Bodies 1–6, Holes 2,6.

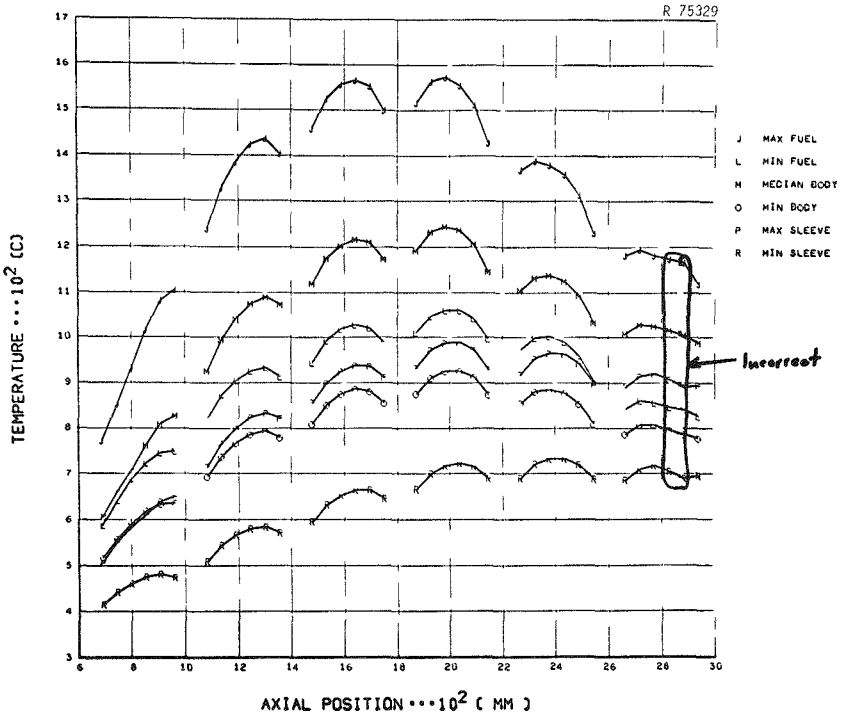

Fig. 8.7. Recycle Test Element-1 Temperature Envelope: Bodies 1–6, Holes 3,7. Reasonable estimates of the correct temperatures for rods 4 and 5 of body 6 can be obtained by interpolation of the data on either side of the incorrect values.

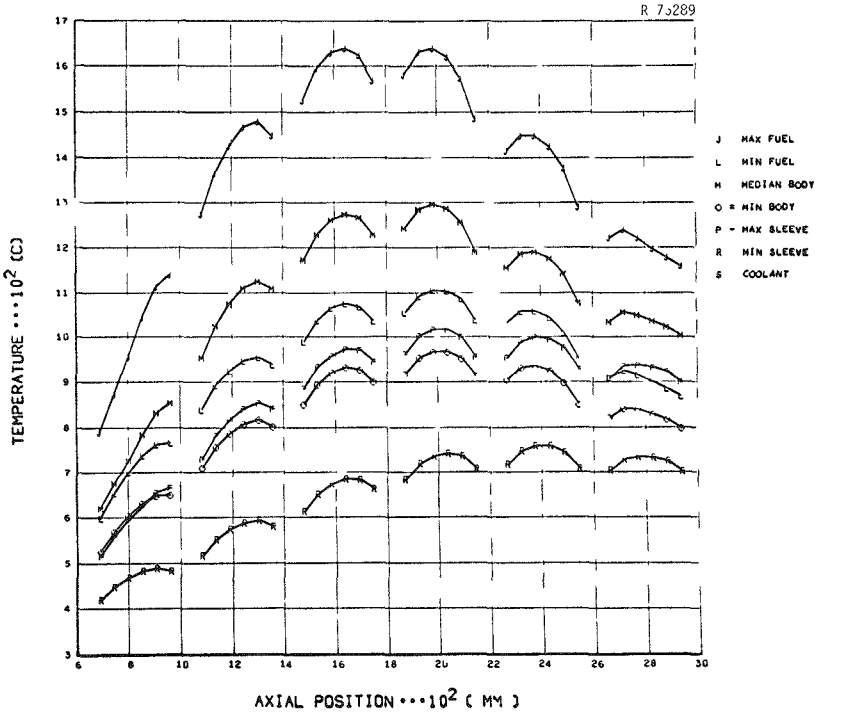

Fig. 8.8. Recycle Test Element-1 Temperature Envelope: Bodies 1–6, Holes 4,8.

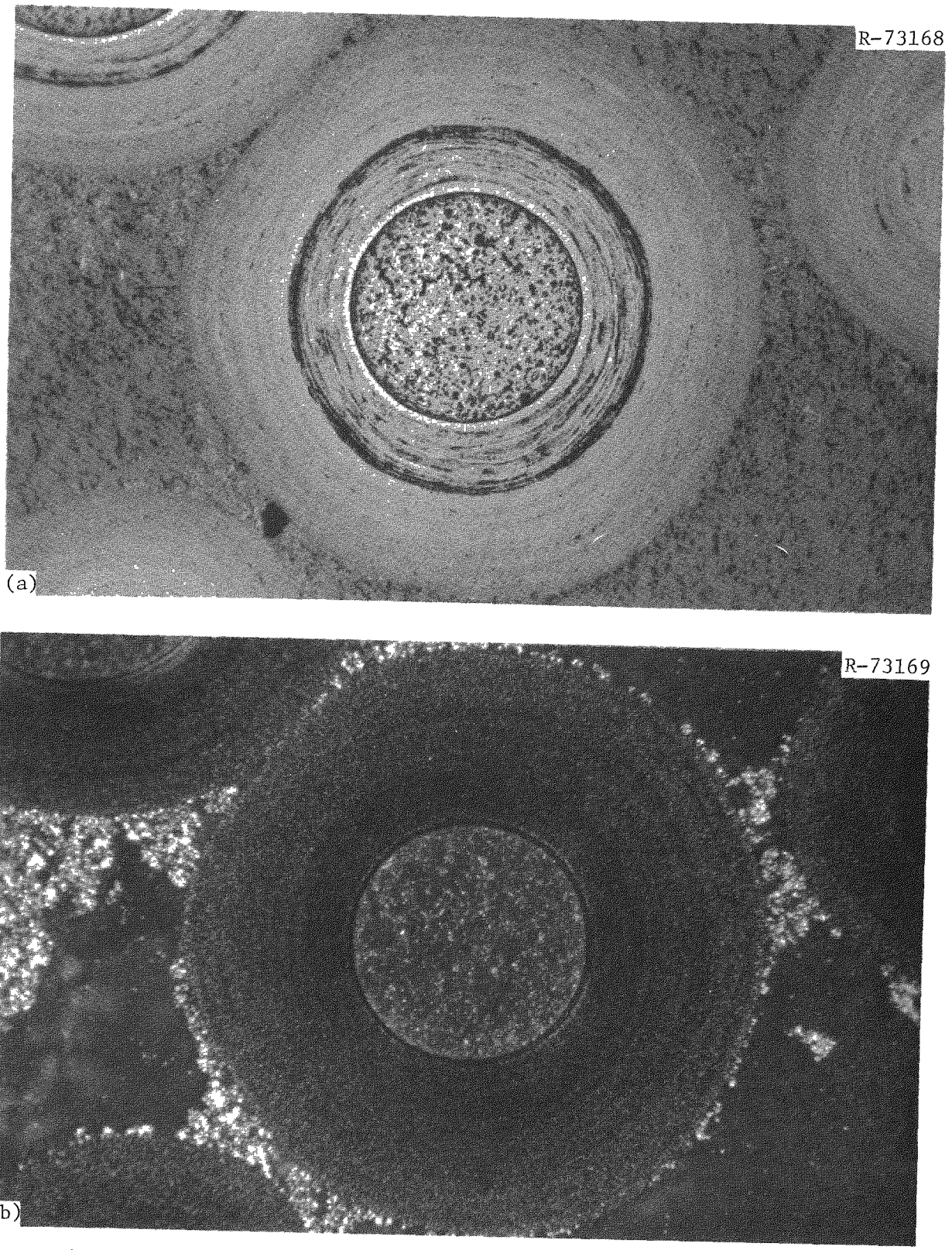

Fig. 8.9. Typical Fissile Biso (4Th,U)O_2 Particles from Fuel Rod RTE-1-4-1-6. Note absence of amoeba migration. (a) Bright field. (b) Polarized light. 125×.

earths was on the order of 5 μm. The kernel of the Biso ThC_2 particles, on the other hand, showed amoeba migration (5 μm) up the temperature gradient. Typical particles are shown in Fig. 8.10.

Examination of the transverse section from fuel rod RTE-1-4-3-6 showed no failures of any Biso $(2Th,U)O_2$ or Biso ThO_2 particles. No amoeba migration was observed. However, poor coatings were seen in both particle types. Typical particles are shown in Fig. 8.11. The oLTI coating of the fissile particles showed some tearing (Fig. 8.12). Polarized light showed the cracks to extend only through the area of high optical activity, which indicates high anisotropy, and has been known to cause coating fracture.[18,23] The Biso ThO_2 had dense buffer coatings, which also showed high optical activity under polarized light. However, no total fractures were associated with these coating defects.

The Biso UO_2 fissile particles from fuel rod RTE-1-4-8-6 exhibited gross amoeba migration and numerous particle failures. In addition to migrating, the kernels had also broken into separate parts (Fig. 8.13). Similar behavior was observed in RTE-5, where high temperatures had been achieved. The average fuel temperature for this rod had exceeded 1473 K (1200°C), so the kernel behavior was consistent with that in the other test elements. When the iLTI coating was breached, the UO_2 converted to UC_2 (Fig. 8.14). The observations on these Biso ThO_2 particles are identical to those from the preceding discussion on fuel rod RTE-1-4-3-6.

Triso UO_2 and Biso ThO_2 particles were contained in fuel rod RTE-1-5-8-1. The fissile particles were in poor condition with amoeba migration of the kernel (Fig. 8.15). Kernel migration through the buffer and iLTI coatings to the SiC had occurred in many particles (Fig. 8.16). Failure of the SiC, as evidenced by conversion of the UO_2 kernel to UC_2, was also observed (Fig. 8.17). The average fuel temperatures for this fuel rod exceeded 1448 K (>1175°C). The kernel migrations measured under RTE and accelerated conditions (similar temperature and temperature gradients) are comparable (Fig. 8.18).[16] The Biso ThO_2 particles appeared to be in good condition with no apparent kernel migration.

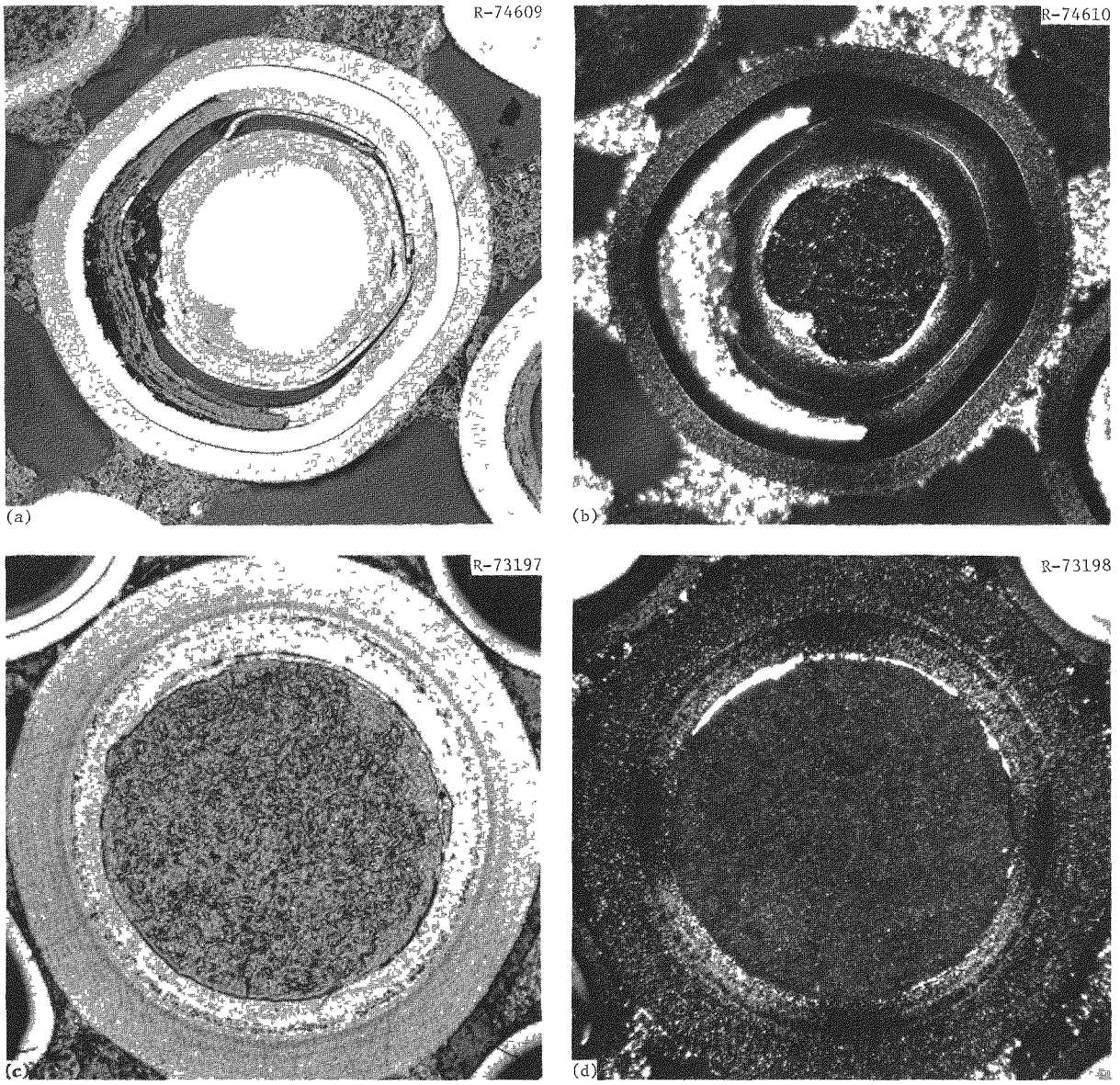

Fig. 8.10. Typical Particles from RTE-1-3-6-6. (a) Triso UC_2 fissile particle. 250×. Bright field. (b) Same. Polarized light. (c) Biso ThC_2 fertile particle. 200×. Bright field. (d) Same. Polarized light. Reduced 31.5%.

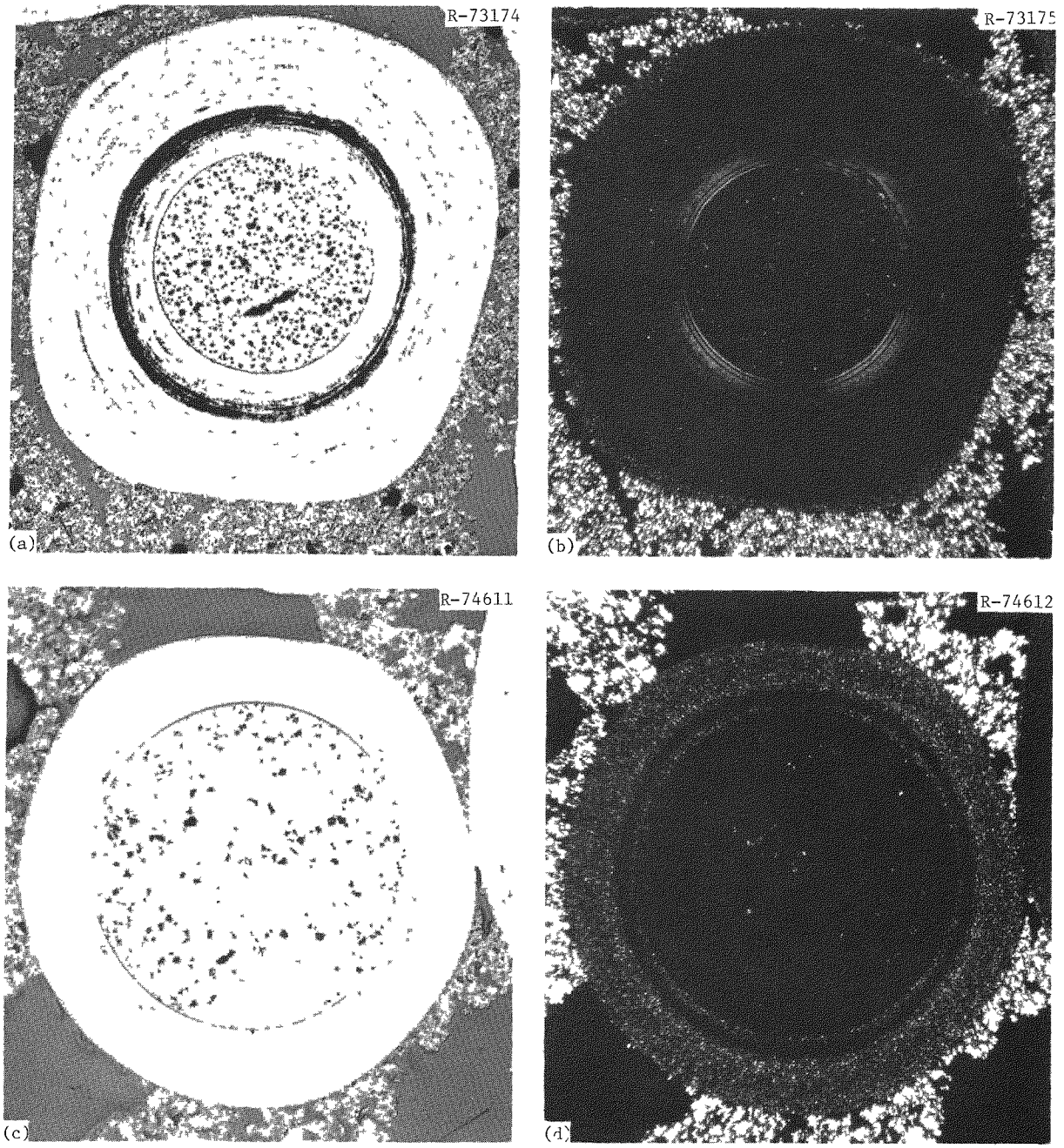

Fig. 8.11. Typical Fuel Particles from RTE-1-4-3-6. (a) Biso $(2Th,U)O_2$ fissile particle. 125×. Bright field. (b) Same. Polarized light. (c) Biso ThO_2 fertile particle. Bright field. (d) Same. Polarized light. Reduced 24%.

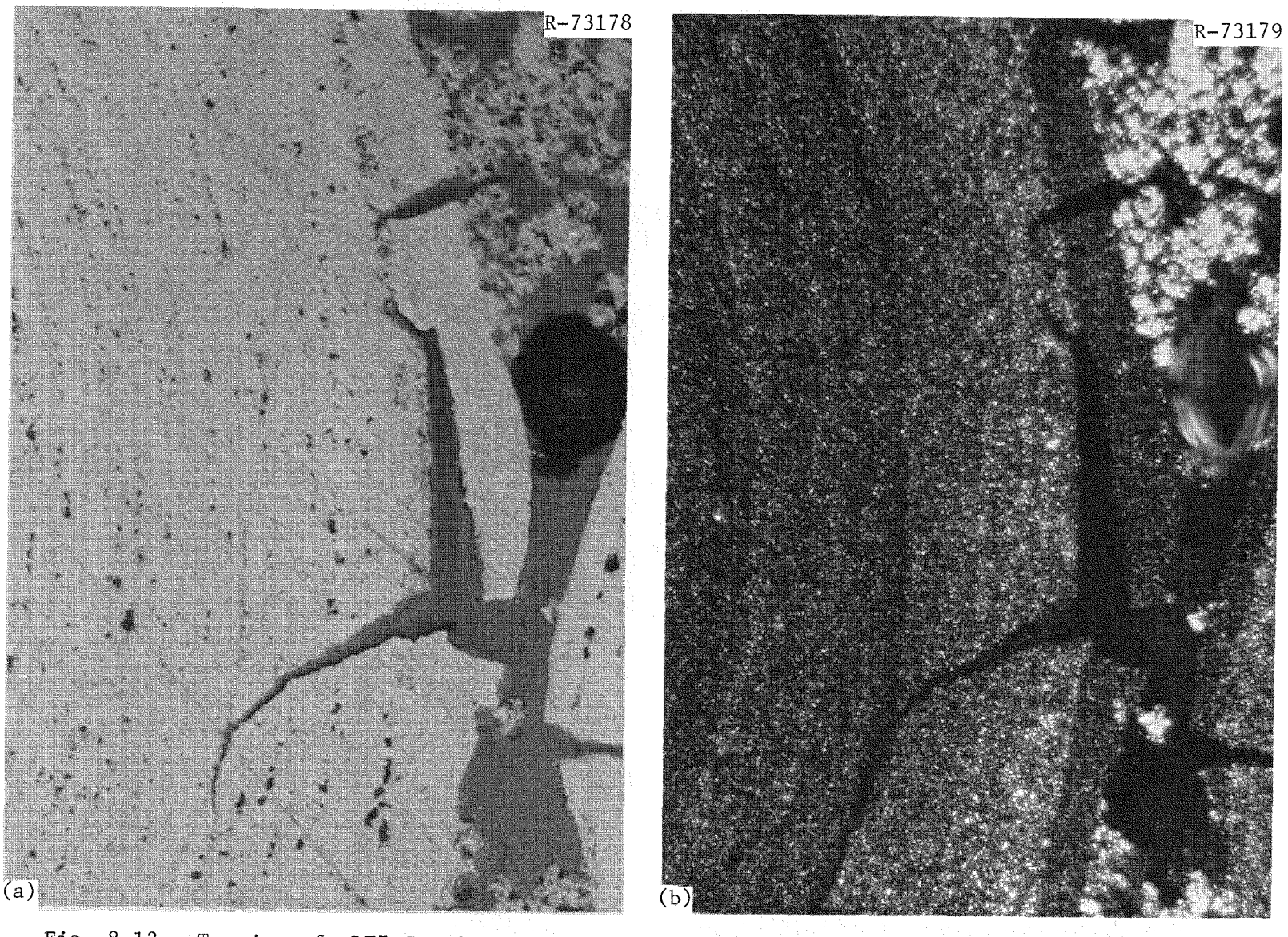

Fig. 8.12. Tearing of oLTI Coating as Observed in RTE-1-4-3-6. 500×. (a) Under bright field. (b) Under polarized light.

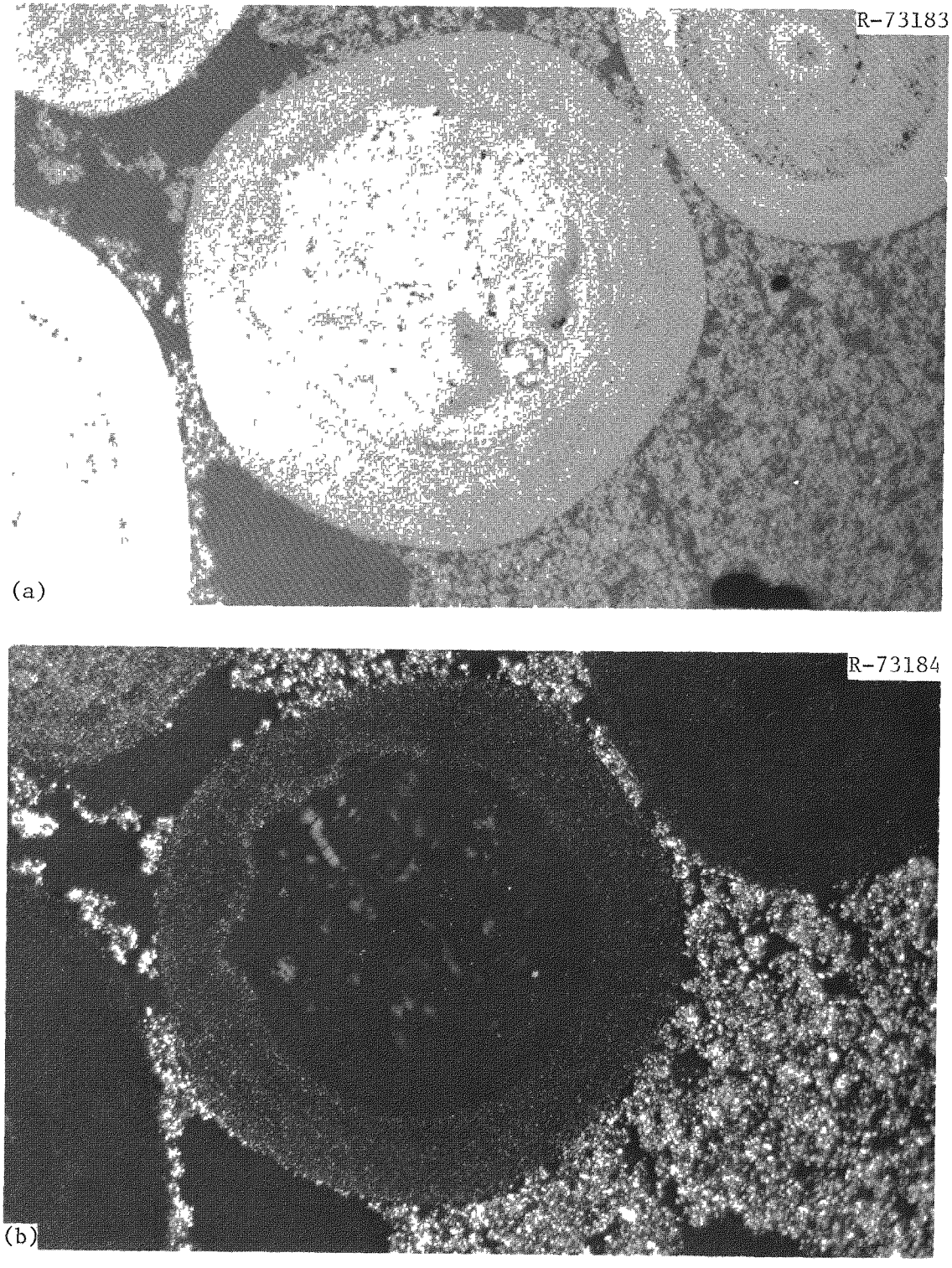

Fig. 8.13. Typical Biso UO_2 Fissile Particle from RTE-1-4-8-6. 250×. (a) Under bright field. (b) Under polarized light. This behavior is indicative of high temperatures.

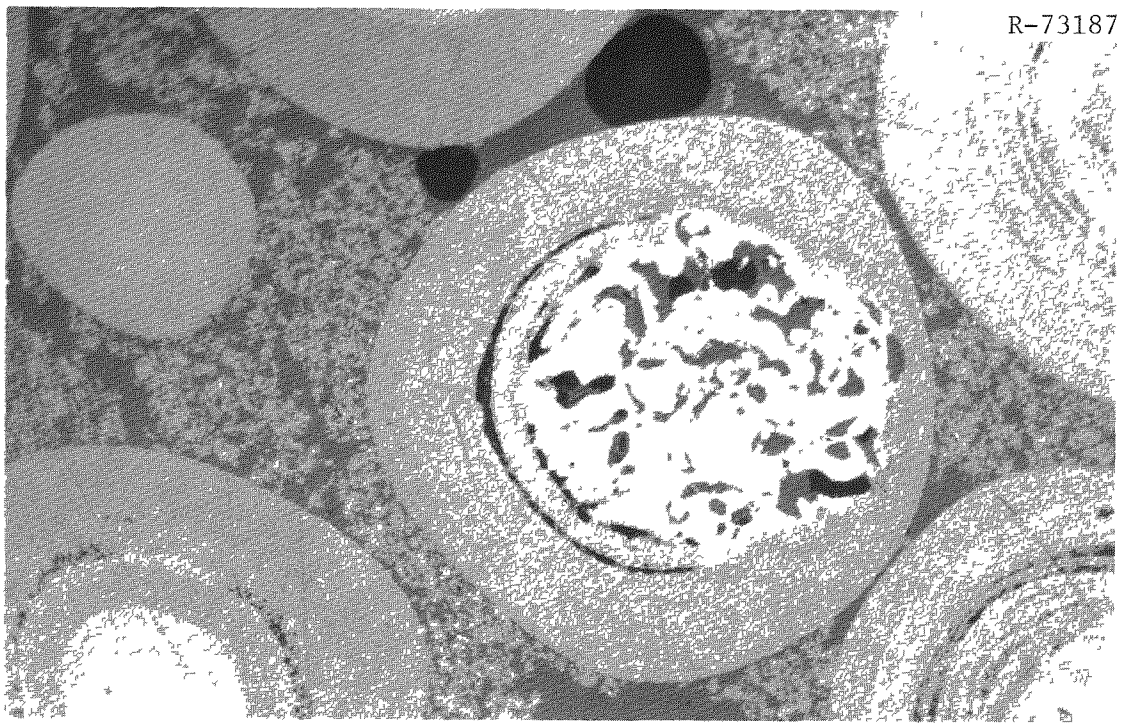

Fig. 8.14. Failed Biso UO_2 Fissile Particle from RTE-1-4-8-6. 250×.

The Biso UC_2 fissile and Biso ThO_2 fertile particles from fuel rod RTE-1-5-3-1 appeared to be in good condition (Fig. 8.19). No failures or amoeba migration had occurred. We presume that at average irradiation temperatures higher than 1423 K (1150°C), the rare-earth fission products migrated out of the Biso UC_2 particles. The fertile particles appeared identical to those from fuel rod RTE-1-5-8-1 discussed above.

9. DIMENSIONAL ANALYSIS

Because a large number of rods were irradiated under a variety of conditions, the recycle test elements provided much data on irradiation-induced dimensional changes. We inspected most fuel rods by measuring their diameters at the top, midlength, and bottom at 0 and 90° (these were arbitrary) with a dial gage comparator and V-block assembly. The dial gage comparator also determined maximum length for the fuel rod. Significant radial and axial shrinkage occurred in all the fuel rods.

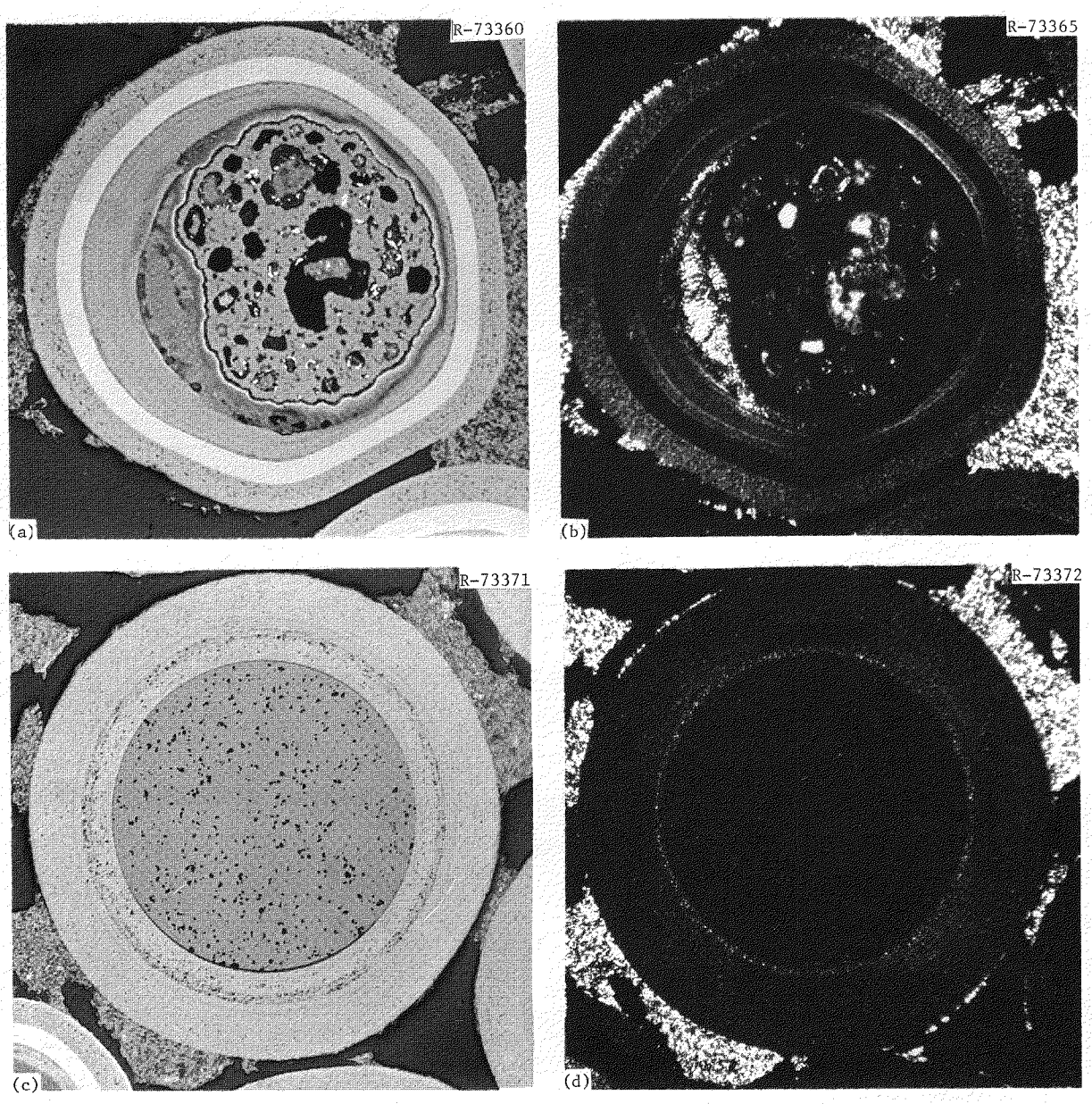

Fig. 8.15. Typical Fuel Particles from RTE-1-5-8-1. (a) Triso UO_2 fissile particle. 200×. Bright field. (b) Same. Polarized light. (c) Biso ThO_2 fertile particle. 150×. Bright field. (d) Same. Polarized light. Reduced 28.5%.

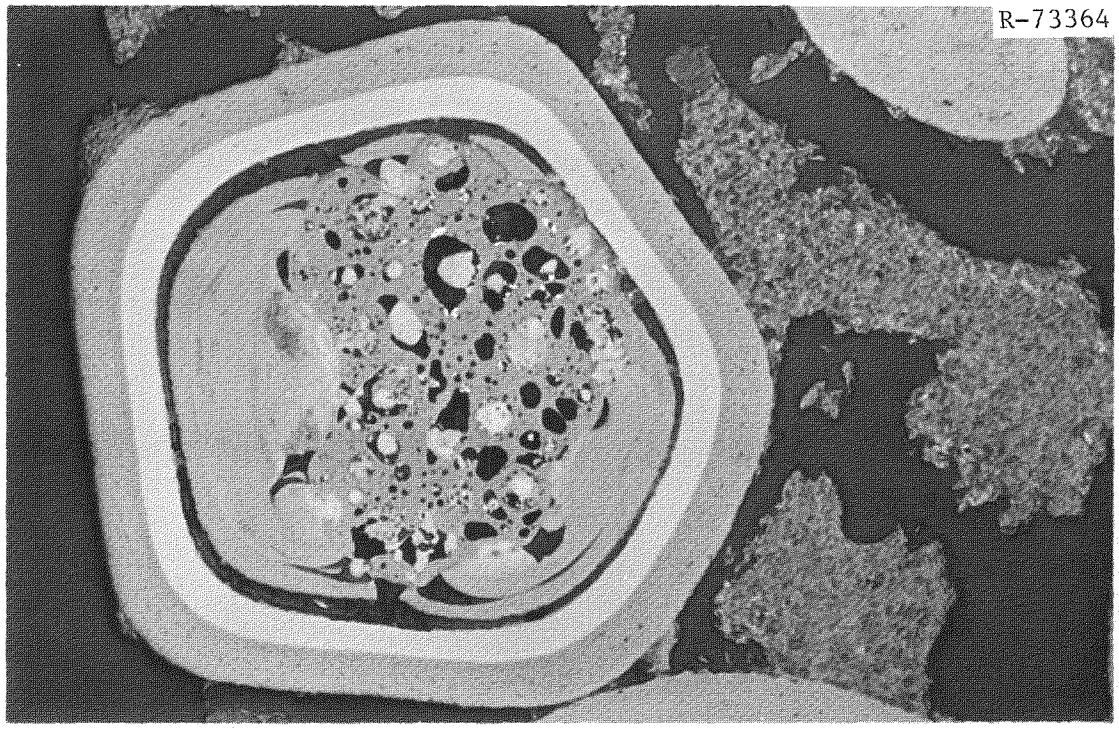

Fig. 8.16. Triso UO_2 Fissile Particle from RTE-1-5-8-1 Showing Amoeba Through Inner PyC Coatings to SiC. 200×.

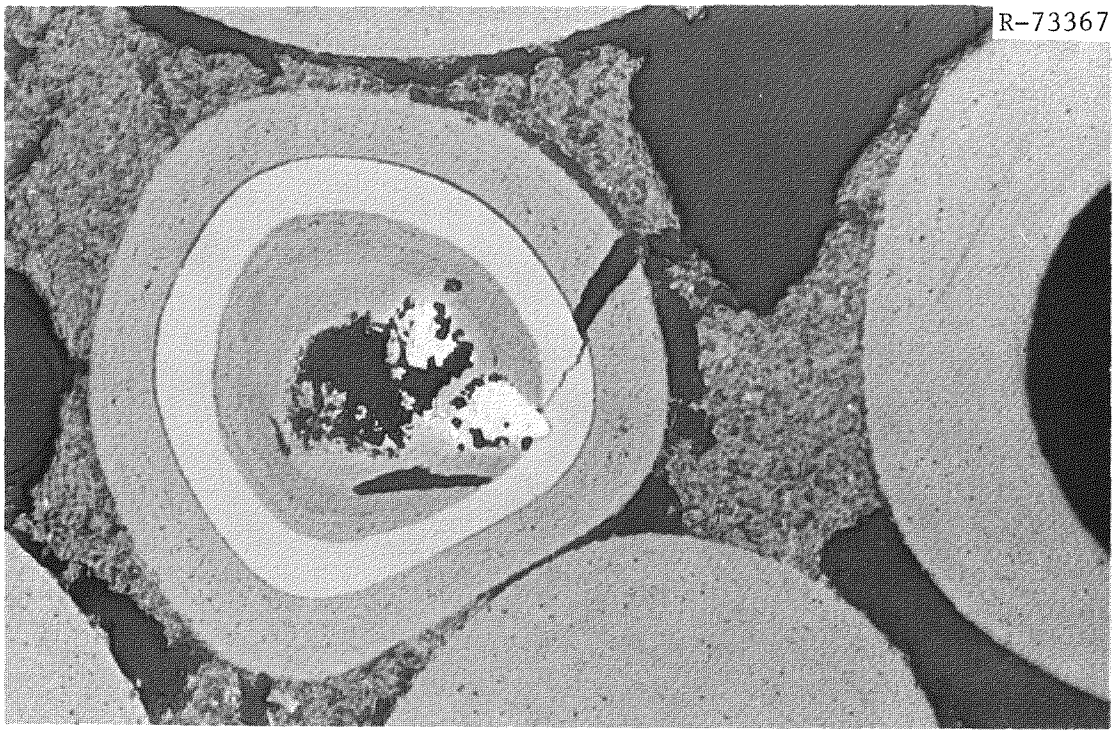

Fig. 8.17. Failed Triso UO_2 Fissile Particle from RTE-1-5-8-1. 200×.

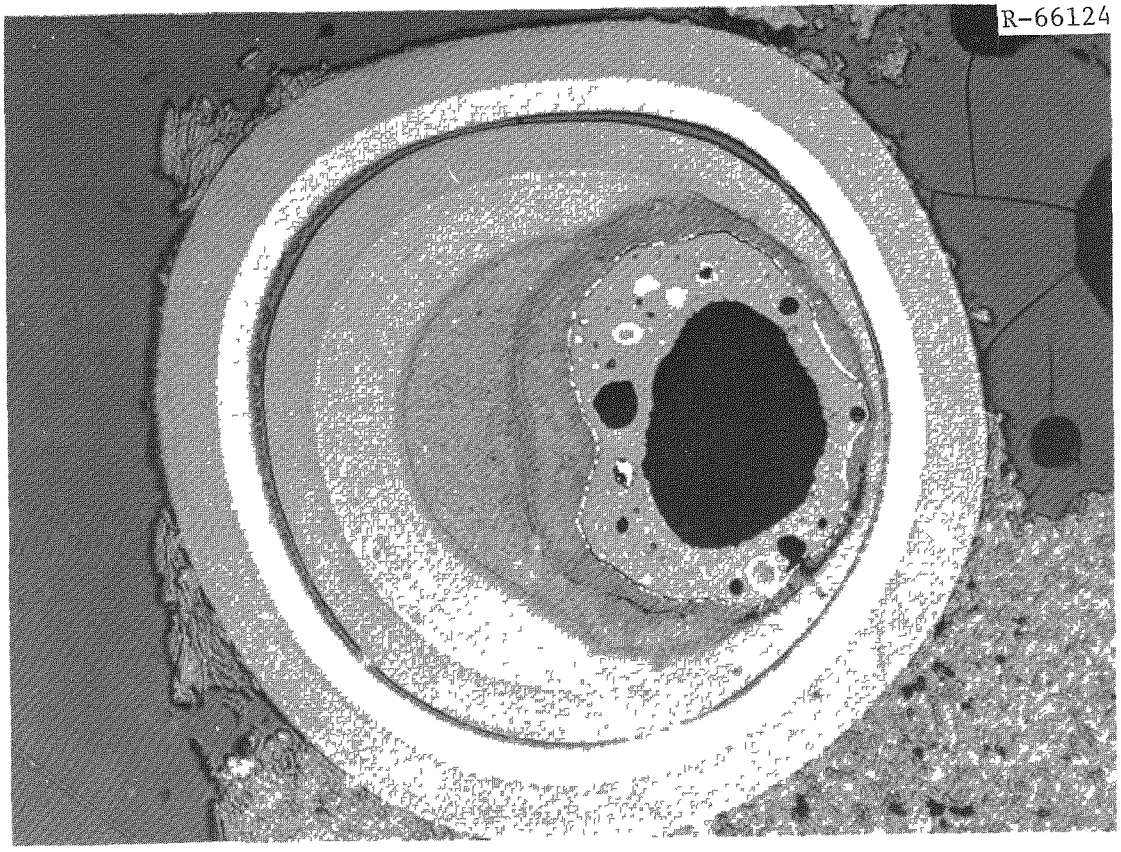

Fig. 8.18. A Triso UO_2 Particle Irradiated in an Accelerated Irradiation Test Showing Amoeba of the Kernel up the Temperature Gradient. The irradiation temperature and temperature gradient resemble those experienced by the particle in Fig. 8.15. 200×. Source: K. H. Valentine, F. J. Homan, E. L. Long, Jr., T. N. Tiegs, B. H. Montgomery, R. L. Hamner, and R. L. Beatty, *Irradiation Performance of HTGR Fuel Rods in HFIR Experiments HRB-7 and -8*, ORNL-5228 (May 1977).

The fuel rods fabricated by GA were not individually dimensioned before irradiation; only nominal dimensions were available. Thus, dimensional changes were difficult to interpret. The results showed the changes were consistent with each other but not with the data from the ORNL fuel rods.

The data from the ORNL rods were relatively consistent with the fuel rod shrinkage data from the accelerated tests. The results agreed with those of other studies, which showed that the dimensional changes of the fuel rods were a function of the physical properties of the particle coatings, the fast-neutron fluence (E >0.18 MeV), and the characteristics of the matrix.

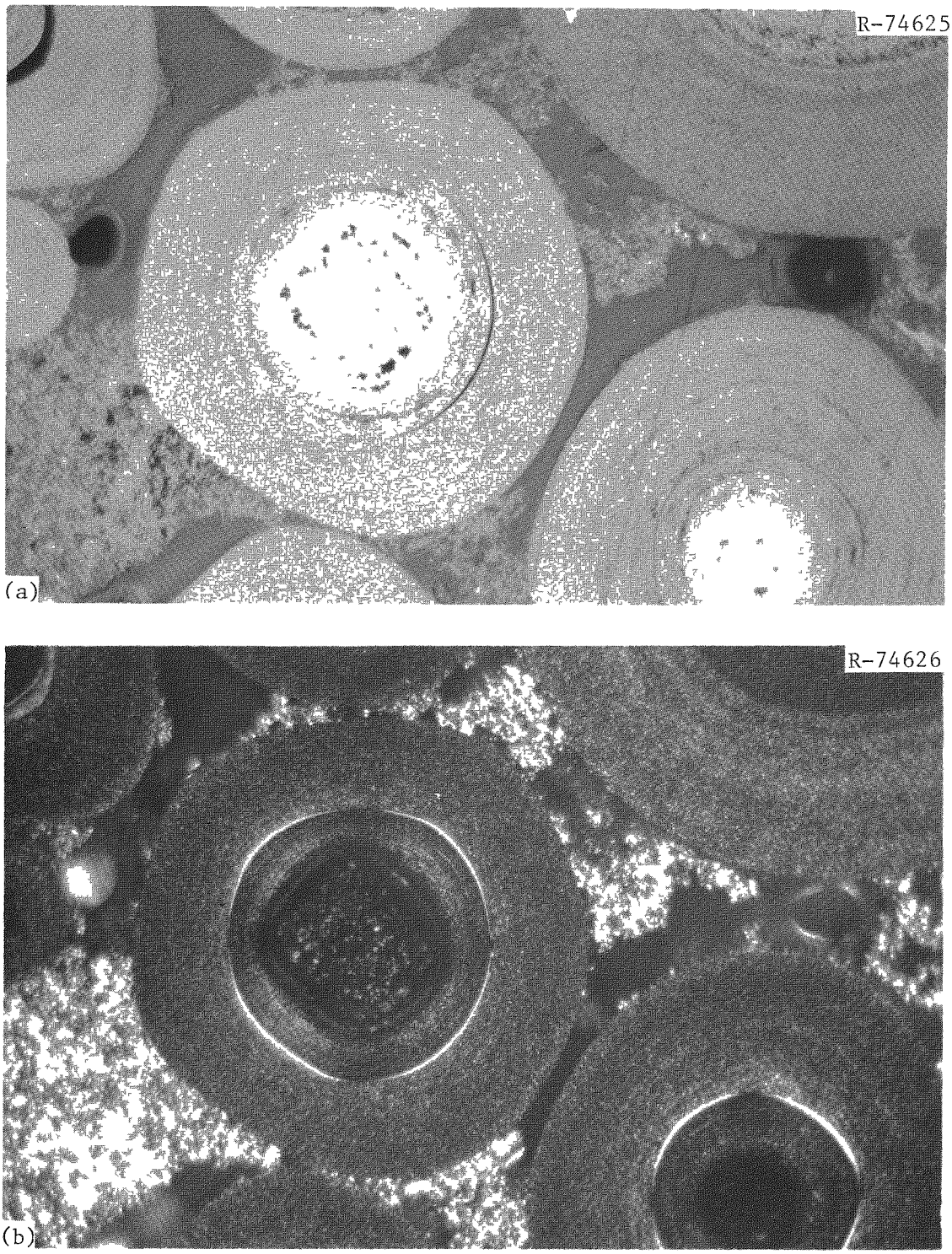

Fig. 8.19. Typical Biso UC_2 Fissile Particle from RTE-1-5-6-1. (a) Under bright field. (b) Under polarized light. 250×.

We felt that such massive data could be best presented in an addendum report dealing solely with the irradiation-induced dimensional changes.

10. PERFORMANCE OF NON-SPECIFICATION FUEL

In all situations in which a product is mass-produced, fabrication defects are manufactured along with the in-specification product. This is also true of HTGR fuel. Many types of fabrication defects were observed in the recycle test elements. We should emphasize, however, that these observations constituted only a minor fraction — less than 0.1% — of all the observations made.

Fabrication defects in HTGR fuel can arise during kernel preparation, during coating process, or during rod fabrication. Most defects impaired the performance of the particles, but some did not. This discussion addresses the following areas: odd-shaped kernels, coating defects, broken particles, and fuel rod defects.

Examples of odd-shaped kernels that have been coated and irradiated are shown in Fig. 10.1. This type of defect was found not to impair the performance of the particle. The only broken coatings observed on odd-shaped kernels were the buffer coatings on the Triso ThC_2. However, the buffer coatings of in-specification particles also broke (see section on RTE-8). We should also point out that most odd-shaped kernels were associated with the fertile ThC_2. The low burnup level achieved by such particles may explain why few failures were observed.

Many types of coating defects can occur to produce odd-shaped particles (Fig. 10.2), doublets (Fig. 10.3), and particles with missing coatings (Fig. 10.4). Odd-shaped particles result from variations in coating processes. Examples are the adherence of soot to the particles and overcoating of the particles. Doublets are created when two kernels are attached or when two particles are bound together as the buffer is being deposited. The defect of a missing coating most seriously impairs particle performance. The examples in Fig. 10.4 show

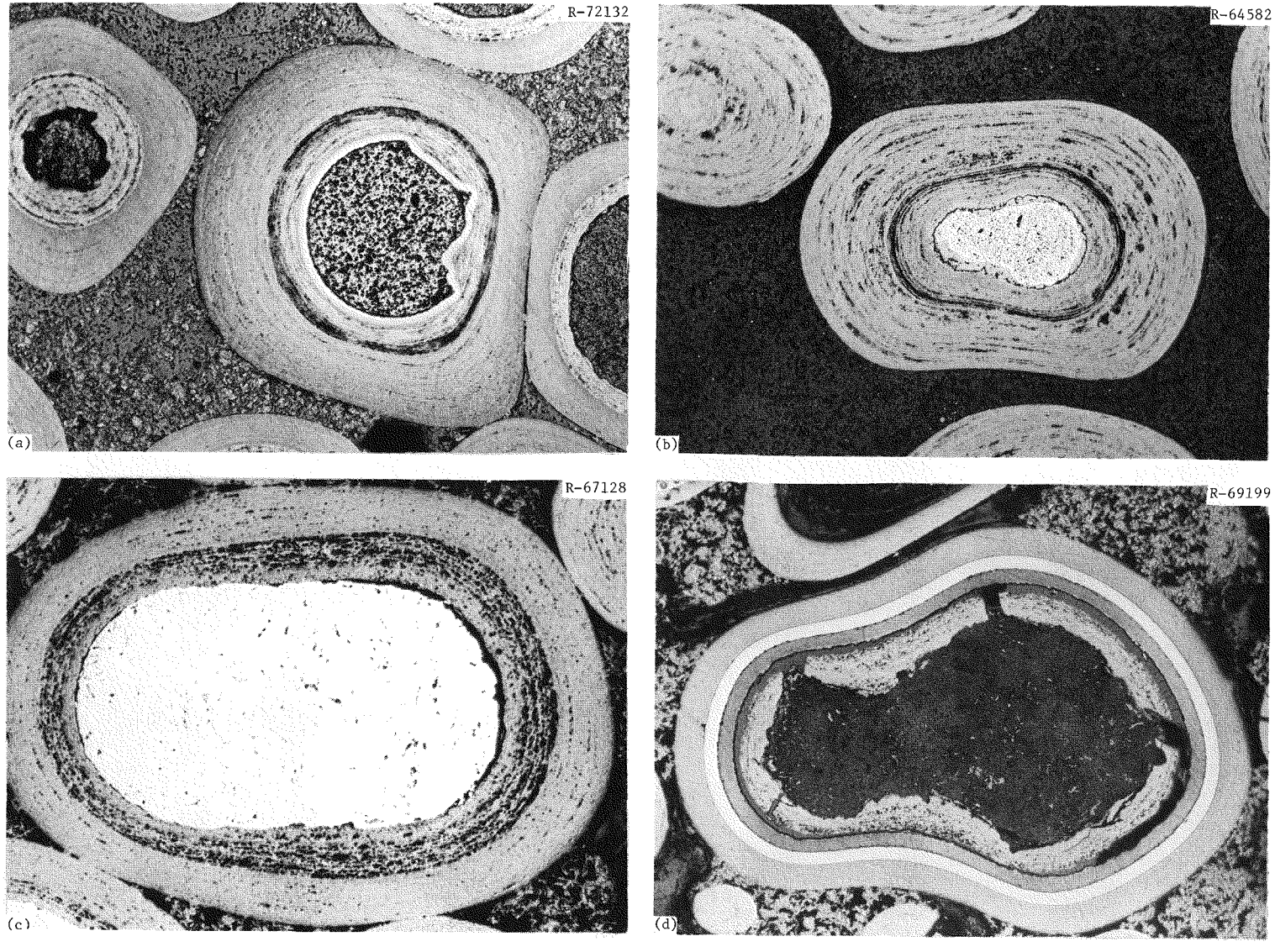

Fig. 10.1. Examples of Odd-Shaped Kernels That Were Coated and Irradiated. (a) Biso $(2Th,U)O_2$ particle from RTE-5-5-7-1. 125×. (b) Biso UC_2 particle from RTE-4-6-1. 250×. (c) Biso ThC_2 particle from RTE-8-3-1-7. 200×. (d) Triso ThC_2 particle from RTE-8-5-7-1. 150×. Reduced 34%.

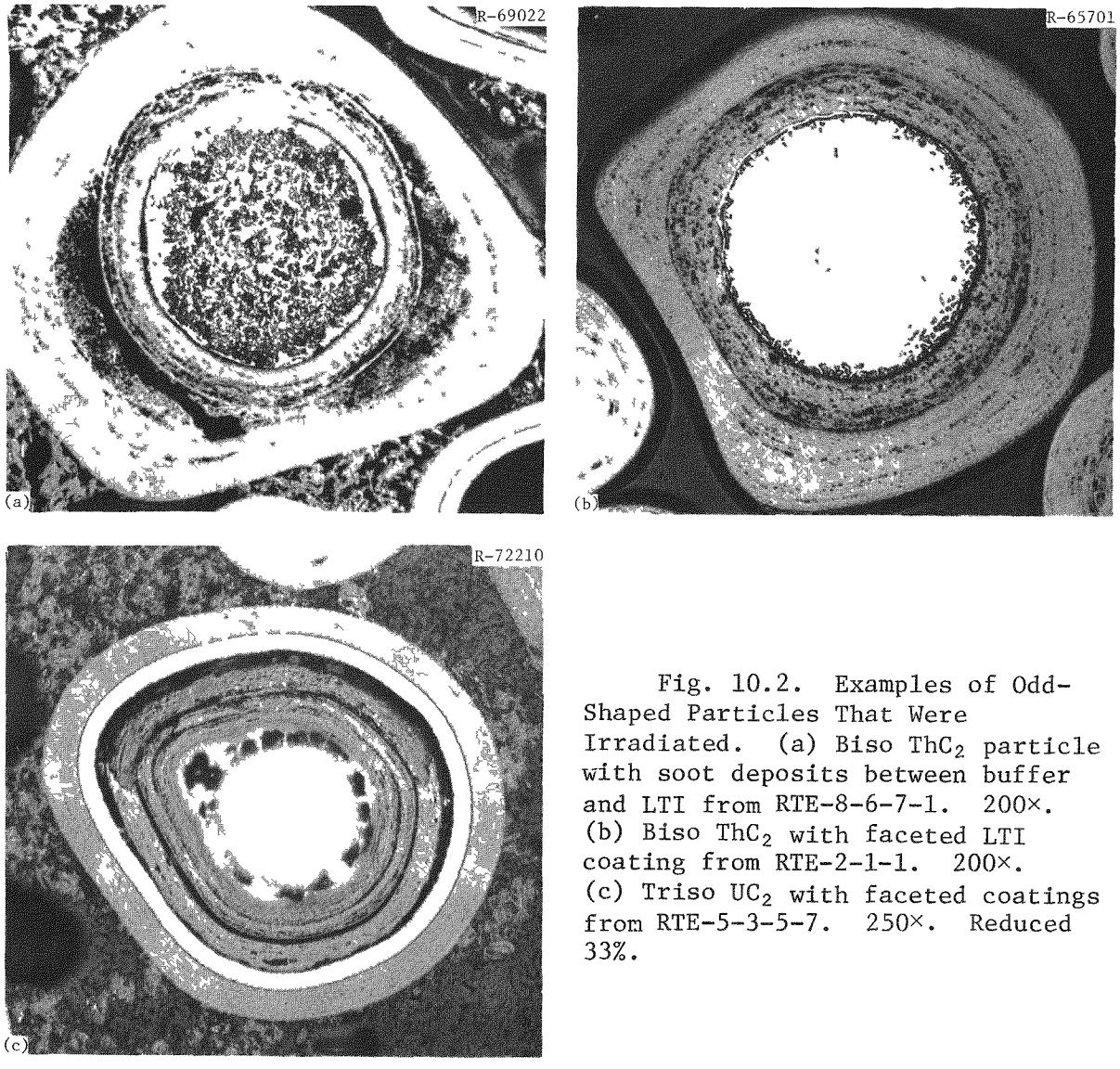

Fig. 10.2. Examples of Odd-Shaped Particles That Were Irradiated. (a) Biso ThC_2 particle with soot deposits between buffer and LTI from RTE-8-6-7-1. 200×. (b) Biso ThC_2 with faceted LTI coating from RTE-2-1-1. 200×. (c) Triso UC_2 with faceted coatings from RTE-5-3-5-7. 250×. Reduced 33%.

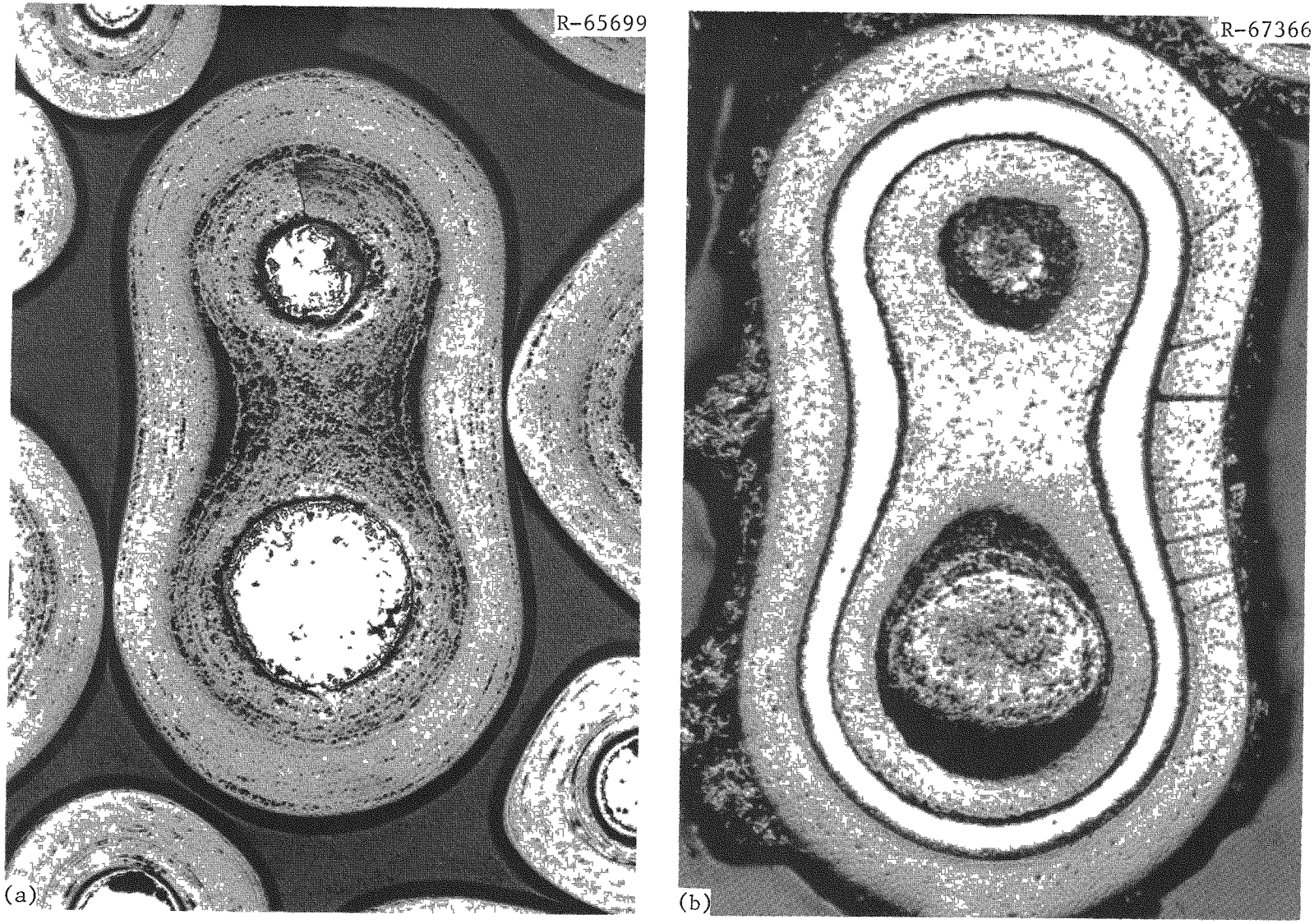

Fig. 10.3. Examples of Doublets. (a) Biso ThC_2 particle from RTE-2-1-1. 150×. (b) Triso ThC_2 particle from RTE-8-2-7-7. 200×.

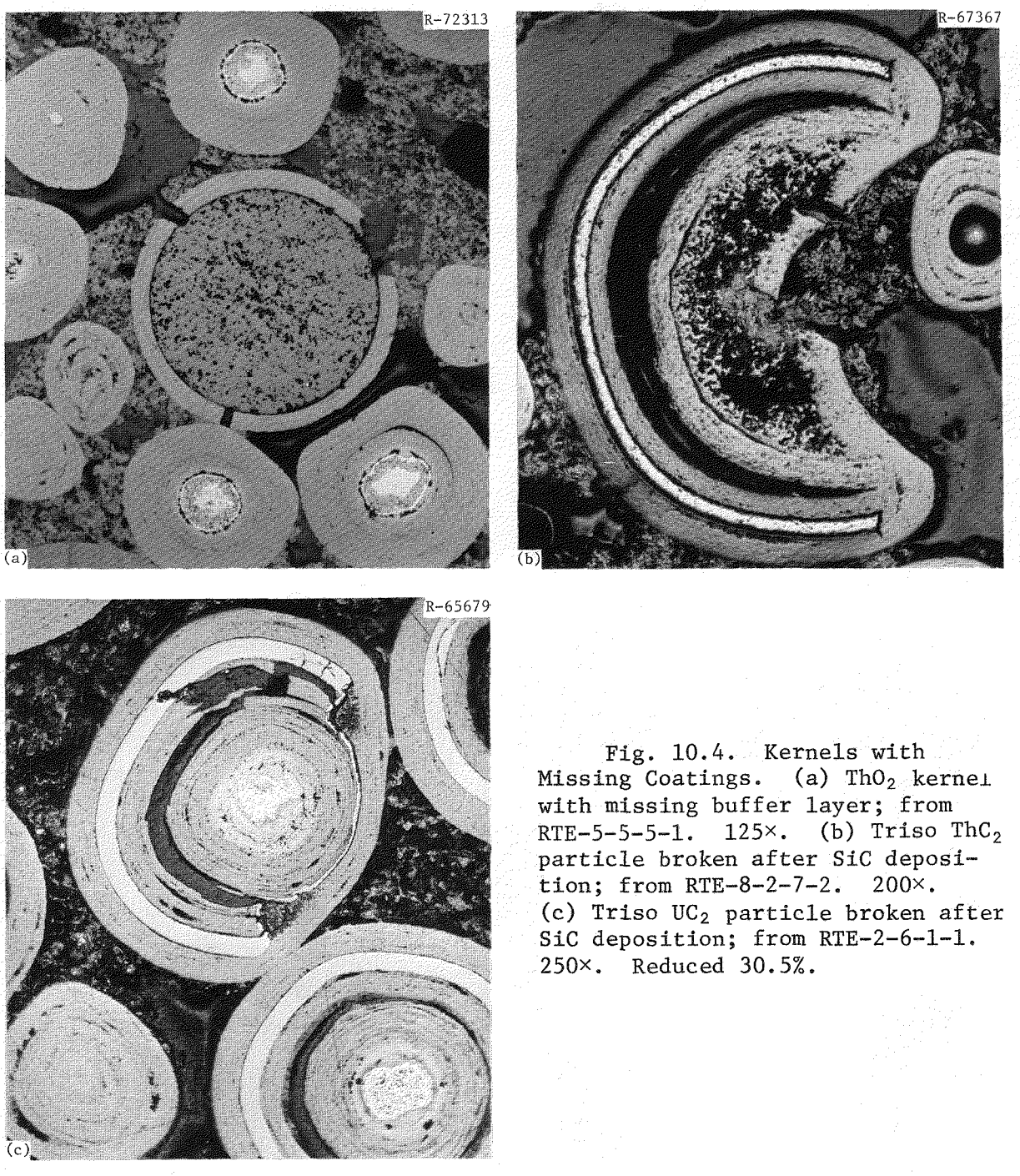

Fig. 10.4. Kernels with Missing Coatings. (a) ThO_2 kernel with missing buffer layer; from RTE-5-5-5-1. 125×. (b) Triso ThC_2 particle broken after SiC deposition; from RTE-8-2-7-2. 200×. (c) Triso UC_2 particle broken after SiC deposition; from RTE-2-6-1-1. 250×. Reduced 30.5%.

a ThO_2 kernel with only an LTI coating, apparently, and ThC_2 and UC_2 kernels with portions of the iLTI and SiC missing.

Defects also occurred during rod fabrication. One problem noted before irradiation[3] was the formation of a matrix cap at the ends of the rods. This cap formed on the injection end of the rod when the particles settled slightly during injection, leaving a cap of bonding material without particles. Fig. 10.5 shows the end of a fuel rod ground away, exposing some of the kernels and in area of matrix material with no particles.

Another defect observed in the recycle test elements was rod contamination by iron. As Fig. 10.6 shows, the coatings of the affected particles are seriously degraded. Electron microprobe analysis identified the affected areas as high in iron (Fig. 10.7). Apparently, iron in the form of rust flakes was introduced into the pitch during storage in metal containers.[21] The particle bed acted as a filter during injection molding, which resulted in the concentration of the rust on the top end of the fuel rods. The attack shown in Figs. 10.6 and 10.7 only occurred on the top region of the fuel rods.

11. GAMMA SCANNING

Gross gamma scans (0.55–0.75 MeV) were made along the bodies from RTE-1, RTE-5, and RTE-6. These scans measured the relative gamma activity of the fission-product isotopes listed in Table 11.1. A sodium iodide detector and a 0.25- by 425-mm (0.010- by 17.0-in.) collimator slit were both used on all scans. The bodies were moved past the collimator, and because of the "telephone dial" arrangement of the fuel stacks, the gamma activity of two opposite fuel stacks was measured simultaneously. This made the interpretation of the scans difficult.

The scans from the bodies are presented in Appendix A. They represent a relative measure of the heavy-metal burnup across the fuel rod stacks. The burnup depends on the neutron flux levels and the fuel rod loading. Scans from any given recycle test element show

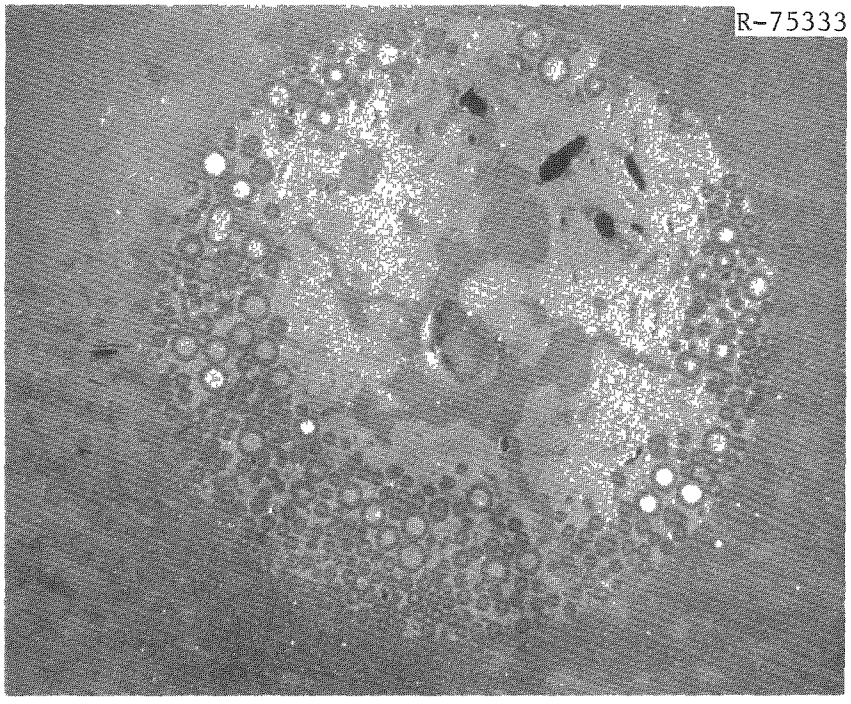

Fig. 10.5. End of Fuel Rod from RTE-6-1. Photomicrograph shows an area devoid of particles. 6×.

neutron flux levels to be relatively flat across the middle but steep at the ends, namely across bodies 1 and 6. The gaps or sharp decreases in gamma activity on the scans represent either fuel rod interfaces or breaks in the fuel rod itself.

Gamma activity from two fuel rod stacks interfered with determining the homogeneity of the fuel rod loadings. However, in cases in which the fuel rod stacks coincided axially — for example RTE-6-3, -4, and -5 — loading homogeneity could be estimated. The scans just mentioned show two levels of homogeneity. The scan from RTE-6-3 (Fig. A.29) shows relatively flat gamma activity across every fuel rod except rod 1 (higher activity in center than at ends) and rods 3 and 4 (activity peaks at fuel rod end). The scans (Figs. A.31 and A.33, respectively) from RTE-6-4 and -5, which both used the same fuel types, show very irregular gamma activity, which indicates fuel loading inhomogeneity. The visually observed rod breakage could not have produced the irregularities. Variations in the fuel loading can cause hot spots in the fuel during irradiation.[14]

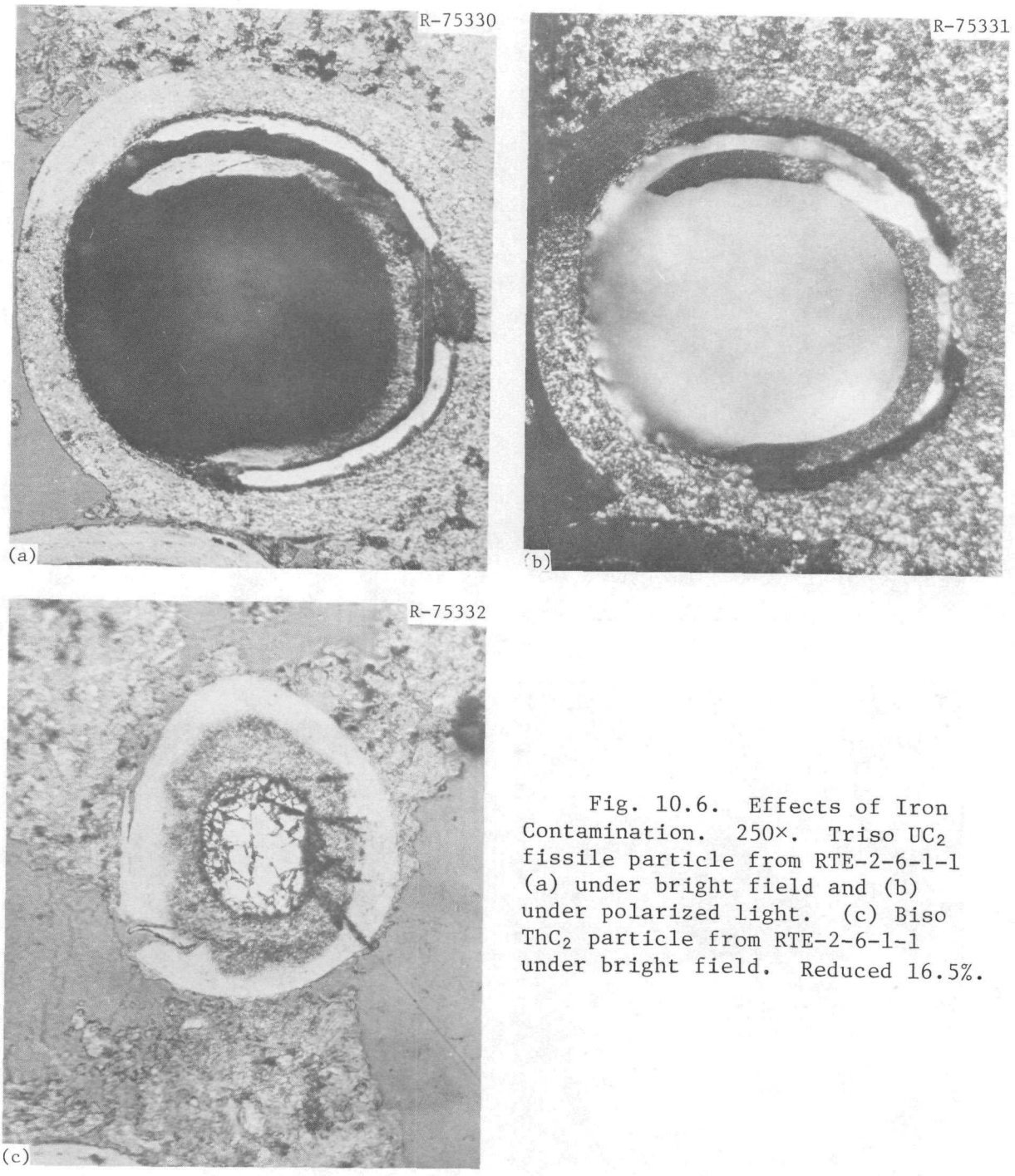

Fig. 10.6. Effects of Iron Contamination. 250×. Triso UC_2 fissile particle from RTE-2-6-1-1 (a) under bright field and (b) under polarized light. (c) Biso ThC_2 particle from RTE-2-6-1-1 under bright field. Reduced 16.5%.

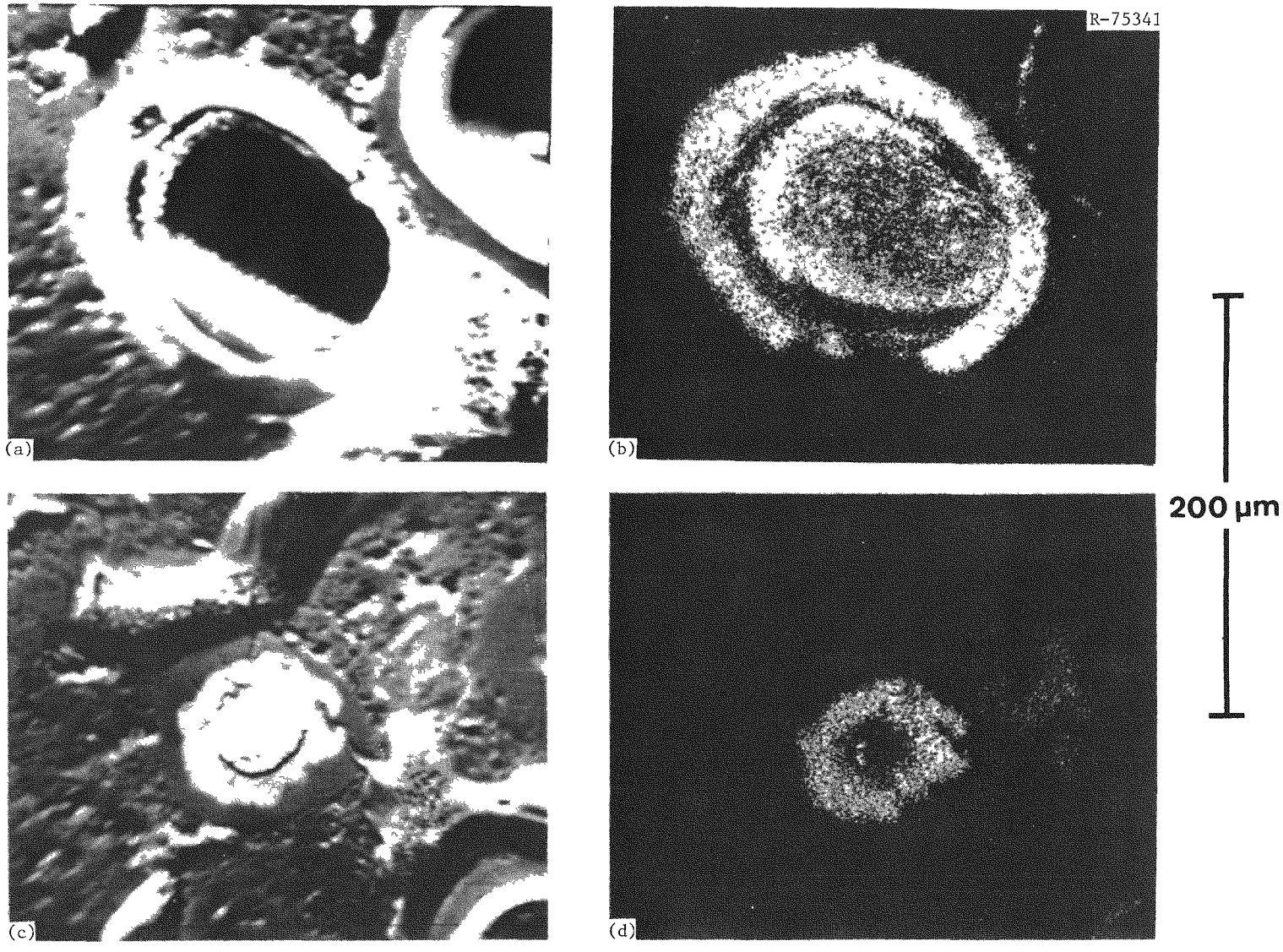

Fig. 10.7. Results from Electron Microprobe Examination of Particles from RTE-2-6-1-1. 200×. (a) Triso UC_2: backscattered electron image. (b) Same: iron x-ray display. (c) Biso ThC_2: backscattered electron image. (d) Same: iron x-ray display. Reduced 21.5%.

Table 11.1. Fission-Product Isotopes Measured by Recycle Test Element Gamma Scans

Isotope	Energy (keV)
^{134}Cs	603
^{103}Ru	609
^{137}Cs	661
^{144}Ce	695
^{95}Zr, ^{154}Eu	723

12. GAS SAMPLING OF RECYCLE TEST ELEMENT SHIPPING CONTAINERS

Peach Bottom Reactor elements examined at ORNL were shipped in sealed aluminum canisters. These included the recycle test elements, as well as the actual driver elements; and a plutonium-fueled element. As part of the postirradiation examination, the contents of some canisters were analyzed upon arrival at ORNL. A summary of the gas-sampling data gathered from the shipping canisters for seven elements is presented in Tables 12.1 and 12.2.

The canisters were supposedly backfilled with helium at Peach Bottom before sealing,[20] but evidently the backfilling was at best only moderately successful. All the canisters contained various mixtures of helium and air, except for the F03-01 canister, which contained no detectable helium. Personnel at the Peach Bottom reactor site said there was no way the canisters could have been filled with nitrogen.[22]

Figure 12.1 shows an interesting relationship between the helium and carbon monoxide plus nitrogen contents. We believe that between the time the canisters were backfilled with helium and the time they were sealed, some air leaked into the canisters. During storage in the canisters and shipment to ORNL, the oxygen in the air was gettered by reducing materials in the fuel elements such as ThC_2 and UC_2. This

would also explain why the gas volumes (STP) in the canisters were less than the void volumes of the canisters. The N_2/O_2 ratios superimposed on the same plot (Fig. 12.1), clearly show that most of the oxygen in the canisters was gettered by the elements (N_2/O_2 = 3.7 for air).

Table 12.1. Gas-Sampling Results from Peach Bottom Elements

Element	Date Sampled	Volume, m^3 at STP			
		Of Can Void	Of Gas in Can	Collected for	
				Mass Spectroscopy ($\times 10^{-6}$)	Gamma Counts ($\times 10^{-6}$)
F-03-01	6-23-75	0.0158	0.0128	4.005	
RTE-6	8-26-75	0.0163	0.0141	222	4.02
E-01-01	9-16-75	0.0150	0.0127	219	4.36
FTE-13	2-23-76	0.0161	0.0133	212	3.86
RTE-5	3-11-76	0.0163	0.0132	215	3.85
RTE-1	4-21-76	0.0160	0.0129	205	3.81
F-05-05	5-17-76	0.0154	0.0123	208	3.37

Table 12.2. Gas Analysis Results

Element	Total DPM[a] of Kr^{85} Sample ($\times 10^6$)	Total Curies of Kr^{85} in Can ($\times 10^{-3}$)	Mass Spectroscopy Analysis, wt %									
			H_2	He	H_2O	N_2 + CO	O_2	Ar	CO_2	Kr	Xe	T_2
F-03-01	N.D.[b]	N.D.	0.29	0.0	0.02	96.14	0.06	1.07	2.42	<0.01	<0.02	
RTE-6	3.03	4.8	0.16	39.40	0.06	57.70	0.05	0.66	2.00	0.0004	0.001	
E-01-01	36.1	47.4	0.174	65.96	0.03	33.37	0.041	0.376	0.026	0.004	0.006	
FTE-13	0.227	0.4	0.014	50.20	0.02	48.34	0.18	0.66	0.59	<0.0005	<0.0005	
RTE-5	2.68	4.2	0.101	45.99	0.005	51.31	0.028	0.62	2.04	<0.001	<0.001	0.003
RTE-1	5.27	8.0	0.16	35.97	0.08	60.39	0.12	0.77	2.51	<0.01	<0.001	<0.01
F-05-05	8.36	13.7	0.02	45.07	0.04	52.29	0.08	0.69	1.80	<0.002	<0.002	

[a] Disintegrations per minute.
[b] Not determined.

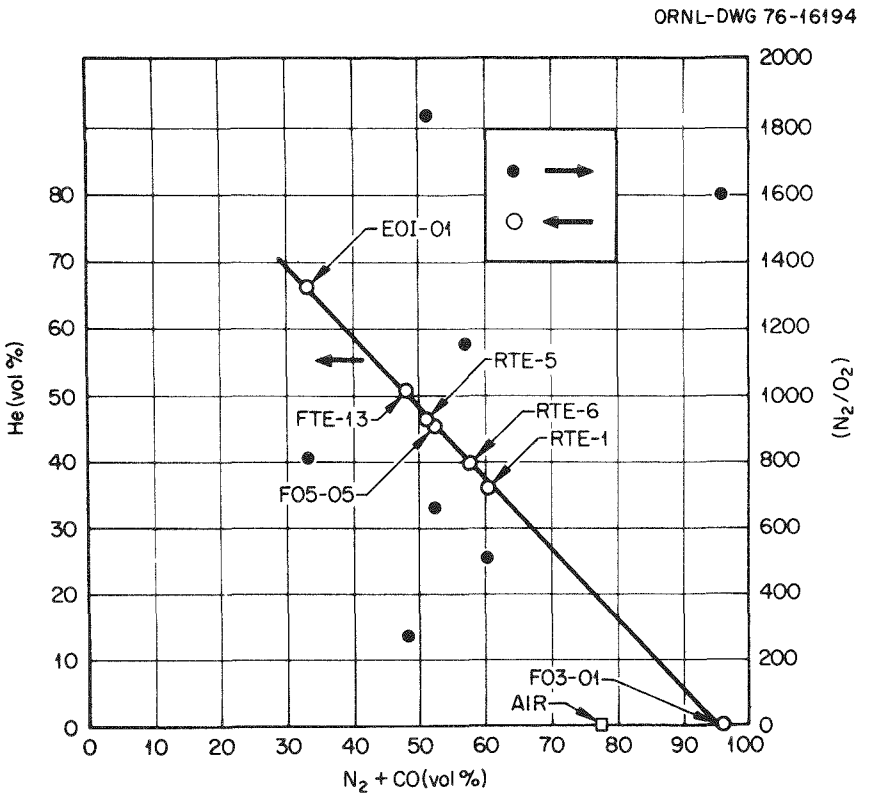

Fig. 12.1. Correlation of Helium, Oxygen, and Nitrogen-Plus-Carbon Monoxide Contents in Peach Bottom Shipping Canisters.

On the positive side of these results, the magneform seals on the canisters remained leaktight during shipment, as the void and gas volumes show. The ^{85}Kr contained in the canisters ranged from less than 1 to 47 mCi.

13. DISCUSSION AND CONCLUSIONS

The Recycle Test Element series tested a variety of fuel types in an actual HTGR environment. The information obtained from these tests and from accelerated tests[16,17,18] influenced the development of the HTGR recycle fuel concept. The present reference recycle design consists of a Triso-coated fissile particle whose kernel is uranium oxide-carbide and the fertile particle is a Biso-coated thorium dioxide

kernel. All the candidate fissile recycle particle types tested in the RTE series are no longer of interest as HTGR recycle fuel because of performance problems demonstrated in accelerated tests and confirmed by real-time tests.

Particles with kernels made of uranium carbide showed no thermal migration in any of the elements examined. In the Triso-coated UC_2 particles rare-earth fission products migrated out of the kernel core and down the temperature gradient. The result was an accumulation at the inner surface of the SiC, which caused graphitization of the iLTI coating. In Biso UC_2 particles, no graphitization of the LTI was observed because no barrier, such as SiC, existed. Rare-earth migration occurred in particles with burnups as low as 13.7% FIMA (Rod RTE-7-5-5-5). However, the migration behavior depended very much on temperature. At temperatures below 1000°C no significant rare-earth migration occurred, while above 1100°C massive migration took place. Between 1000°C and 1100°C appreciable migration was observed.

Kernels made of UO_2 showed an unacceptable amount of migration up the temperature gradient. In Biso-coated particles migration occurred at average temperatures as low as 1025°C and at burnups of 53.7% FIMA (Rod RTE-5-5-1-1). At temperatures above 1100°C the UO_2 kernels were observed to be extremely plastic with multidirectional amoeba. The only Triso UO_2 irradiated was in RTE-1, where amoeba had also occurred. However, the rod examined had experienced relatively severe conditions (an average temperature higher than 1175°C and a burnup of 45.5% FIMA).

Slight amoeba was observed in the $(2Th,U)O_2$ kernels, which had been irradiated at an average temperature of 1150°C and at 21.7% FIMA (Rod RTE-8-4-5-1). However, at comparable temperatures but lower burnups (<20% FIMA) no amoeba was detectable (Rod RTE-5-5-7-1). In the particles more highly diluted with thorium, such as $(4Th,U)O_2$, no amoeba was observed in any of the recycle test elements, although such particles encountered average temperatures up to 1240°C and burnups of 10.4% FIMA (Rod RTE-1-4-1-6). We should note that all the mixed Th-U particles were Biso-coated. Thermal migration has been shown to increase in Triso-coated particles because of an increase in the carbon monoxide pressure.[19]

The ThC_2 particles performed adequately at moderate temperatures and low burnups. However, amoeba migration was observed in RTE-1-3-6-6, which experienced average temperatures exceeding 1250°C and a burnup of 1.7% FIMA, as well as in RTE-6-3-1-6, which had an average fuel temperature of 1150°C but a burnup of 3.0% FIMA.

On the other hand, the ThO_2 kernels performed very well. No amoeba migration was observed in any of the samples, including those with average temperatures of 1425°C and burnups of 3.1% FIMA.

Biso coatings appear useable only for fertile particles. In the RTE series metallic fission products like cesium were released from the kernels at low fuel temperatures (<900°C) and migrated through the pyrocarbon coatings. A layer of SiC is thus necessary to prevent further migration of these fission products.

A problem associated with Triso-coated particles is the potential failure of their oLTI coating. In the RTE series oLTI failures occurred in the Triso UC_2 particles (batch 4000-307). Failure was attributed to fast-neutron damage (E >0.18 MeV) at fluences as low as 1.16×10^{25} n/m^2 (RTE-7-3-7-3). These particles had an oLTI density of 1.73 Mg/m^3 and a Bacon Anisotropic Factor (as determined by optical methods) of 1.03. Recent studies have shown that the density of the oLTI must be at least 1.85 Mg/m^3 for the particle to perform well.[23]

The results from accelerated tests agreed well with those from the real-time tests. Migration of the rare-earth fission products limits the use of UC_2 and amoeba migration of the UO_2 kernels similarly restricts the use of UO_2. These results stimulated the development of the current reference particle. The Triso-coated uranium oxide-carbide particle shows neither of the performance problems, rare-earth migration and amoeba, that affect the UC_2 and UO_2 particles, respectively.

Because these real-time and accelerated tests agreed so well on particle behavior, accelerated tests may now be used for product development. If all testing had to be under real-time conditions, product development would be very slow and cumbersome. Although proof

tests for fuel licensing must be carried out under actual irradiation conditions, the results from the recycle test element show the validity of information obtained about HTGR fuel under accelerated conditions.

14. ACKNOWLEDGMENTS

The authors wish to acknowledge the efforts of the many people who made significant contributions in the postirradiation examination and evaluation of the test elements. The postirradiation examination was done by the staff of the High Radiation Level Examination Laboratory, R. B. Fitts, and E. L. Ryan. Metallography was performed by N. M. Atchley, L. G. Shrader, and E. R. Boyd; and the electron microprobe examination by T. J. Henson. The authors also acknowledge the editorial work by N. Richards and the assistance of C. L. Harrison, K. A. Witherspoon, and M. R. Hill of the Reports Office in the preparation of this report.

15. REFERENCES

1. Oak Ridge National Laboratory and Gulf General Atomic, *National HTGR Fuel Recycle Development Program Plan*, ORNL-4702 (August 1971).
2. R. P. Morissette and K. P. Steward, *Recycle Test Element Program Design, Fabrication, and Assembly*, GA-10109 (September 1971).
3. E. L. Long, Jr., R. B. Fitts, and F. J. Homan, *Fabrication of ORNL Fuel Irradiated in the Peach Bottom Reactor and Postirradiation Examination of Recycle Test Elements 7 and 4*, ORNL/TM-4477 (September 1974).
4. J M Robbins and J. H. Coobs, *Gas-Cooled Reactor Programs Semiannu. Prog. Rep. March 31, 1970*, ORNL-4589, pp. 10–15.
5. R. S. Lowrie and V.C.A. Vaughen, *Gas-Cooled Reactor Programs Semiannu. Prog. Rep. Sept. 30, 1970*, ORNL-4637, pp. 97–99; J. D. Sease, F. J. Furman, P. A. Haas, C. B. Pollock, and J M Robbins, same source pp. 104–09.

6. W. J. Scheffel, N. L. Baldwin, and R. W. Tomlin, *Operating History Report for the Peach Bottom HTGR; Vol. 1 Reactor Operating History*, GA-A13907 (Aug. 31, 1976); W. J. Scheffel and C. B. Scott, *Irradiation Experience with HTGR Fuels in the Peach Bottom Reactor*, GA-A12897 (Nov. 1, 1974).
7. R. B. Fitts, *Gas-Cooled Reactors-Thorium Utilization Programs Annu. Prog. Rep. Sept. 30, 1971*, ORNL-4760, pp. 65–67.
8. R. B. Fitts, *Metals and Ceramics Div. Annu. Prog. Rep. June 30, 1972*, ORNL-4820, pp. 138–39 (January 1973).
9. *ORNL Gas-Cooled Reactor Programs Annu. Prog. Rep. Oct. 1, 1971–Dec. 31, 1972*, ORNL-4911 (March 1974).
10. *ORNL Gas-Cooled Reactor Programs Annu. Prog. Rep. Dec. 31, 1973*, ORNL-4975 (April 1976).
11. F. J. Homan, "HTGR Fuel Qualification," *HTGR Base Program Prog. Rep. Jan. 1, 1974–Dec. 31, 1975*, ORNL-5108, Chap. 6.
12. F. S. Dyer et al., "Post Irradiation Examination of Special Peach Bottom Element RTE-7," *ORNL Nuclear Safety Research Development Program Bi-monthly Rep. March–April 1972*, ORNL/TM-3831, p. 79.
13. E. L. Long, Jr., and T. N. Tiegs, "Peach Bottom Irradiations," *Gas-Cooled Reactor Programs: Thorium Utilization Program Prog. Rep. Jan. 1, 1974–June 30, 1975*, ORNL-5128, pp. 278–304.
14. T. N. Tiegs, E. L. Long, Jr., and E. L. Ryan, "Peach Bottom Irradiation," pp. 252–65 in *Gas-Cooled Reactor Programs: Thorium Utilization Program Prog. Rep. July 1, 1975–Sept. 30, 1976*, ORNL-5266.
15. T. N. Tiegs and T. J. Henson, *Fission Product Behavior in HTGR Fuel Particles Made From Weak-Acid Resins* (report in preparation).
16. K. H. Valentine, F. J. Homan, E. L. Long, Jr., T. N. Tiegs, B. H. Montgomery, R. L. Hamner, and R. L. Beatty, *Irradiation Performance of HTGR Fuel Rods in HFIR Experiments HRB-7 and -8*, ORNL-5228 (May 1977).
17. F. J. Homan, E. L. Long, Jr., B. H. Montgomery, T. N. Tiegs, M. J. Kania, R. L. Hamner, R. L. Beatty, and B. A. Thiele, *Irradiation Performance of HTGR Fuel Rods in HFIR Experiments HRB-9 and -10*, ORNL-5254 (in press).

18. T. N. Tiegs, E. L. Long, Jr., M. J. Kania, K. R. Thoms, and E. J. Allen, *ORR Irradiation Experiment OF-1: Accelerated Testing of HTGR Fuel*, ORNL-5234 (August 1977).

19. T. B. Lindemer and R. L. Pearson, *Kernel Migration for HTGR Fuels from the Th-U-C-O-N System*, ORNL/TM-5207 (April 1976).

20. D. P. Harmon and C. B. Scott, *Development and Irradiation Performance of HTGR Fuel*, GA-A-13173 (Oct. 31, 1975).

21. Personal Communication with D. P. Harmon, General Atomic Company, San Diego, Calif., November 1975.

22. Personal Communication with W. Birely at Peach Bottom, Pa., June, 1976.

23. D. P. Harmon and C. B. Scott, *Properties Influencing HTGR Coated Fuel Particle Performance*, GA-A-14105 (March 1977).

APPENDIX A

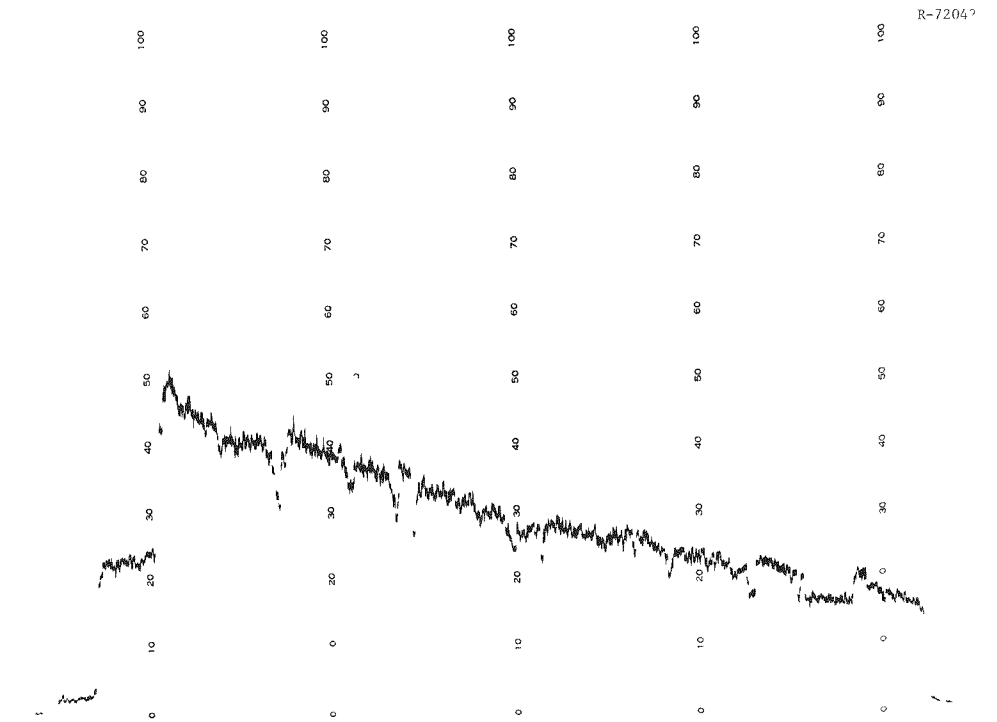

Fig. A.1. Recycle Test Element-1; Body 1; Across Hole 1. Top to bottom from left to right; 5000 counts/s full scale; 0.55—0.75 MeV; standard deviation — 2.0%.

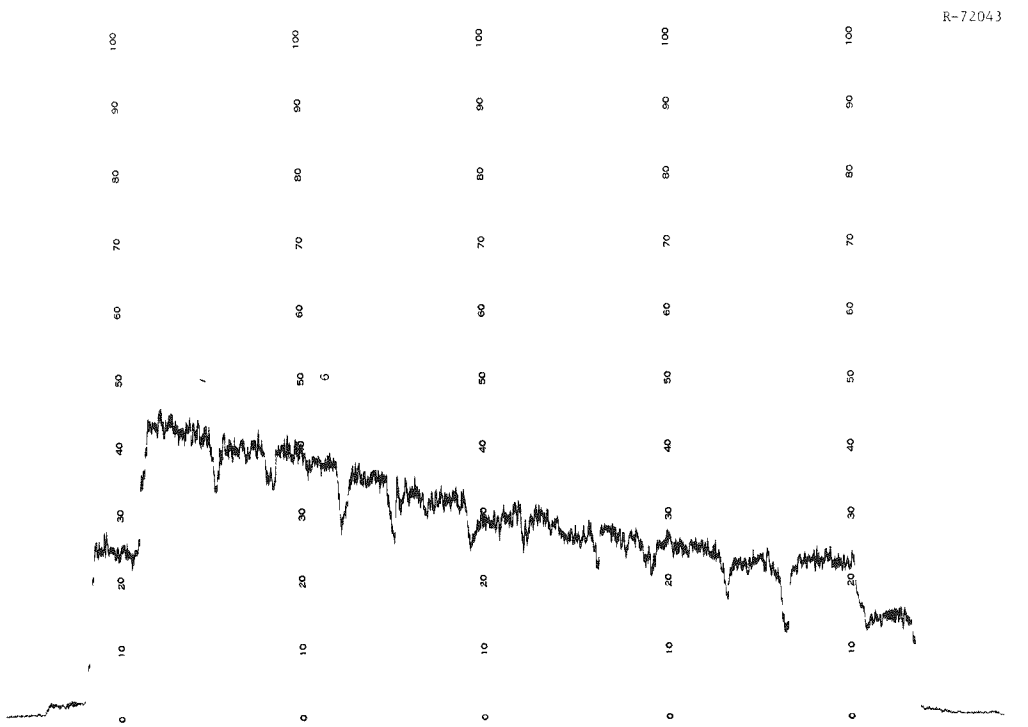

Fig. A.2. Recycle Test Element-1; Body 1; Across Hole 3. Top to bottom from left to right; 5000 counts/s full scale; 0.55—0.75 MeV; standard deviation — 2.0%.

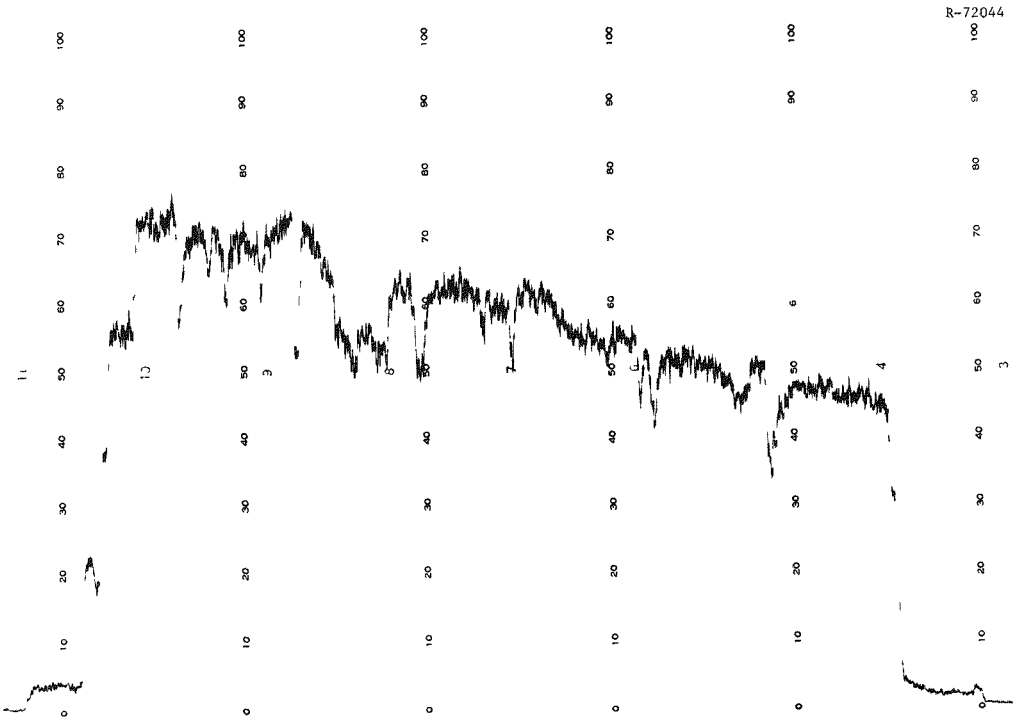

Fig. A.3. Recycle Test Element-1; Body 2; Across Hole 1. Top to bottom from left to right; 5000 counts/s full scale; 0.55—0.75 MeV; standard deviation — 2.0%.

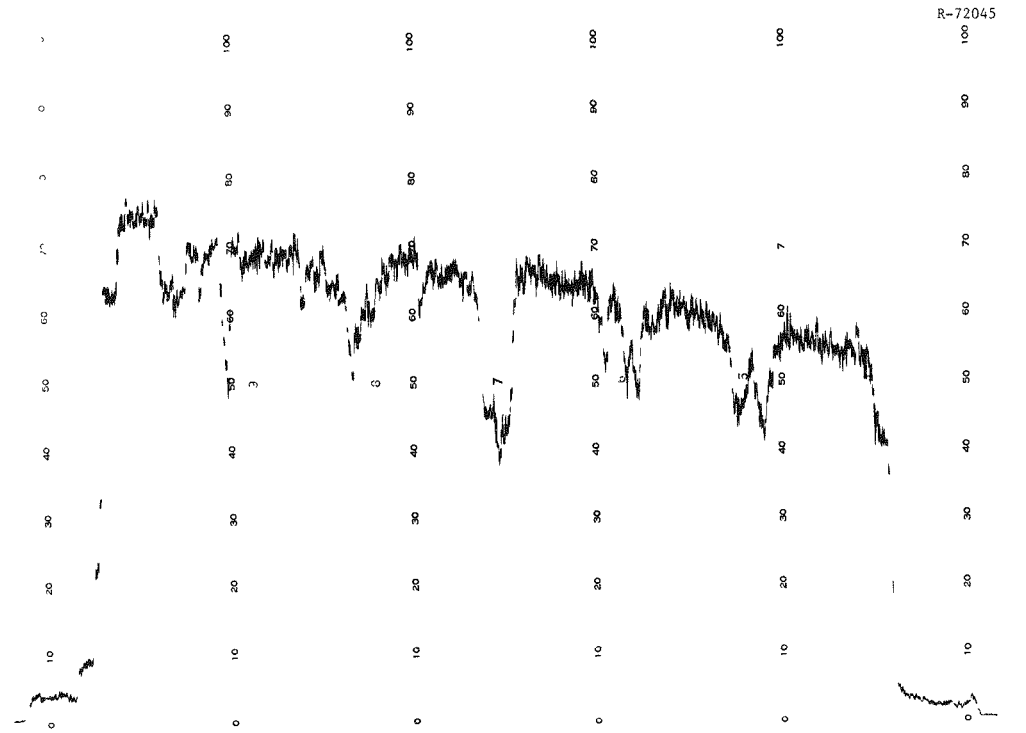

Fig. A.4. Recycle Test Element-1; Body 2; Across Hole 3. Top to bottom from left to right; 5000 counts/s full scale; 0.55—0.75 MeV; standard deviation — 2.0%.

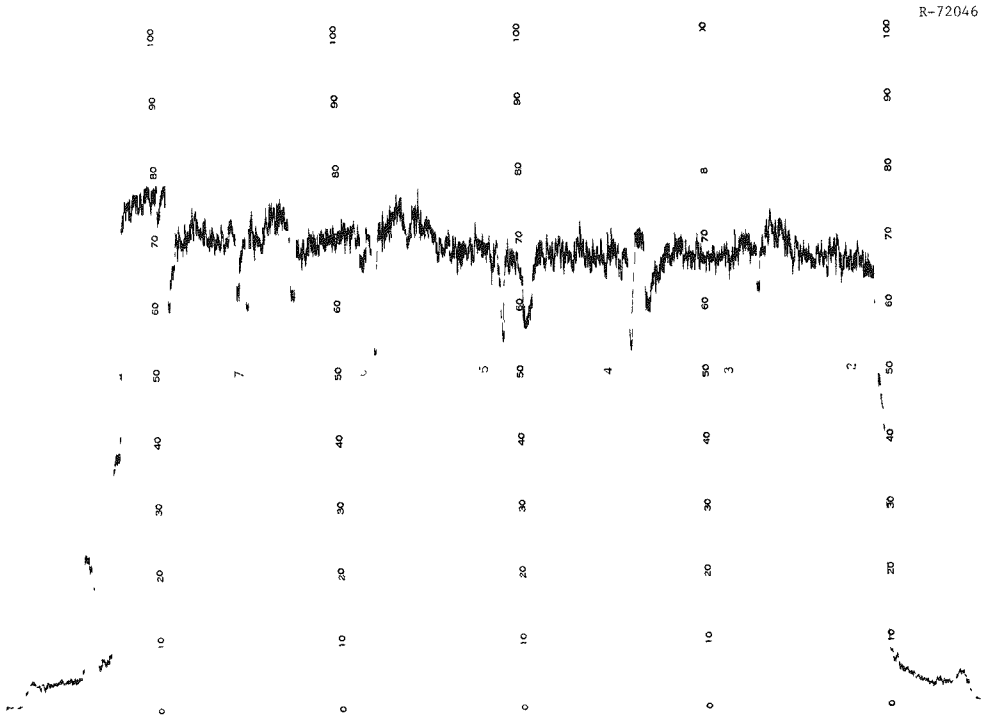

Fig. A.5. Recycle Test Element-1; Body 3; Across Hole 1. Top to bottom from left to right; 5000 counts/s full scale; 0.55–0.75 MeV; standard deviation — 2.0%.

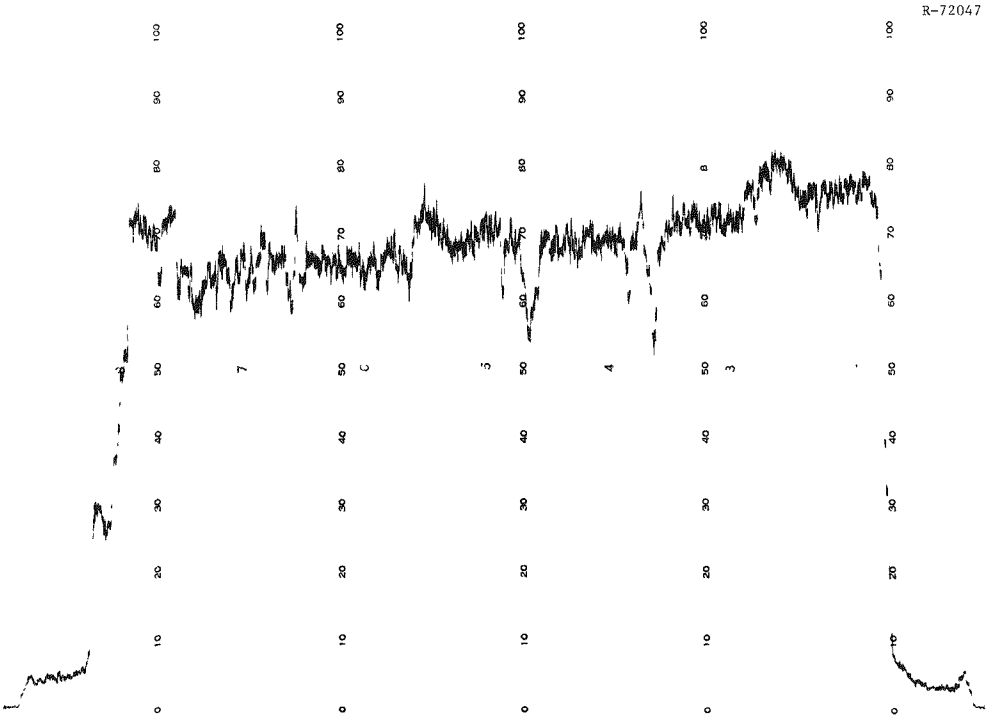

Fig. A.6. Recycle Test Element-1; Body 3; Across Hole 3. Top to bottom from left to right; 5000 counts/s full scale; 0.55–0.75 MeV; standard deviation — 2.0%.

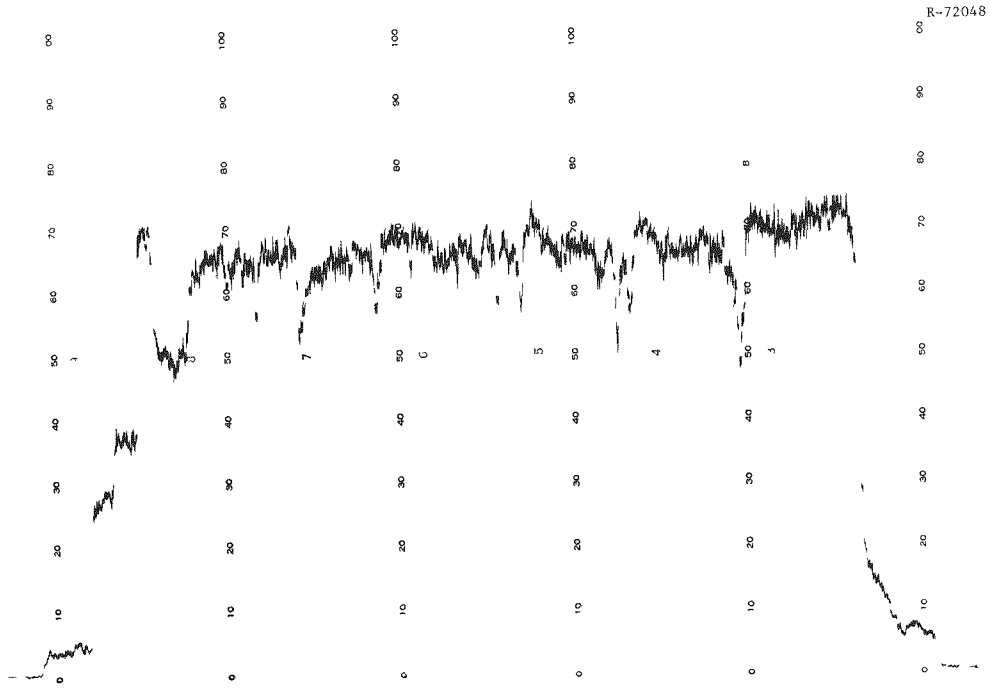

Fig. A.7. Recycle Test Element-1; Body 4; Across Hole 1. Top to bottom from left to right; 5000 counts/s full scale; 0.55–0.75 MeV full scale; standard deviation — 2.0%.

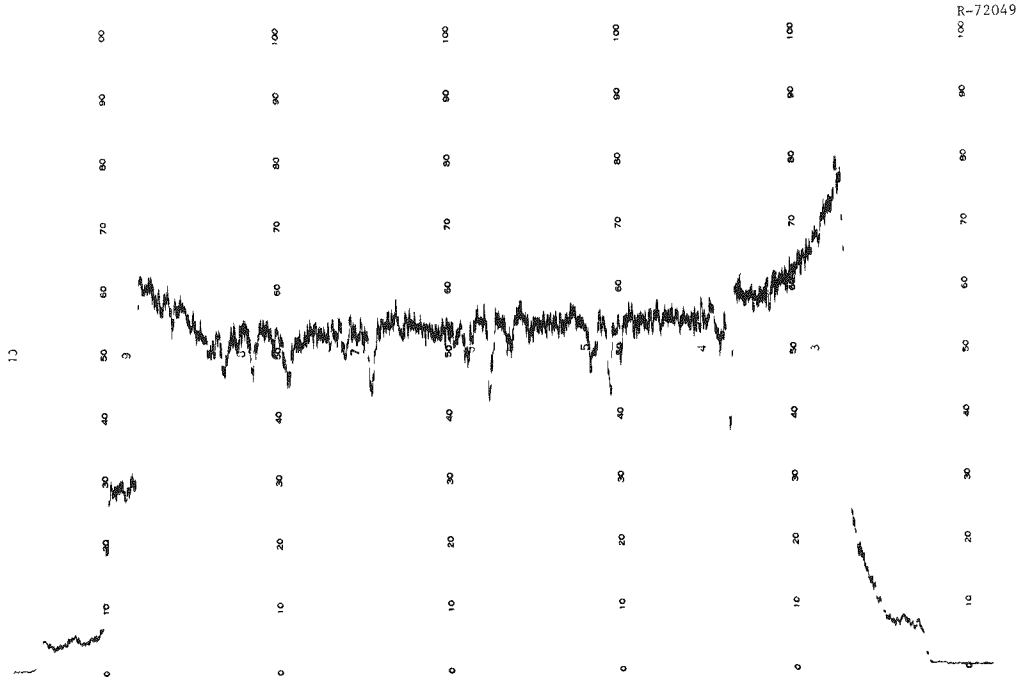

Fig. A.8. Recycle Test Element-1; Body 4; Across Hole 3. Top to bottom from left to right; 5000 counts/s full scale; 0.55–0.75 MeV; standard deviation — 2.0%.

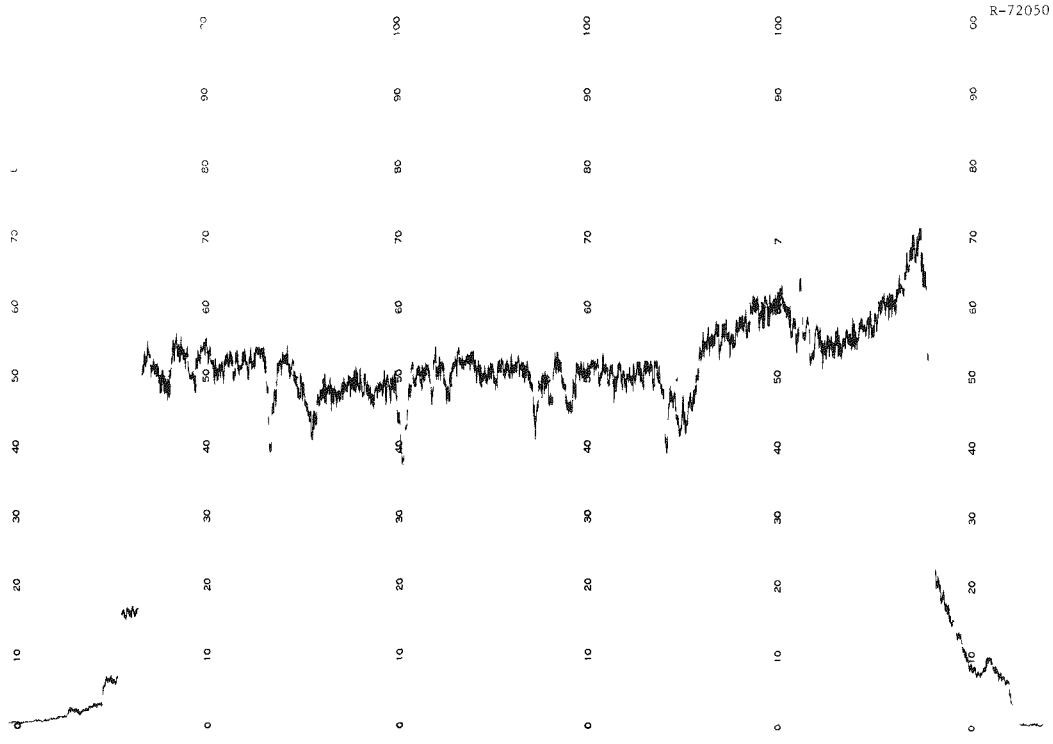

Fig. A.9. Recycle Test Element-1; Body 5; Across Hole 1. Top to bottom from left to right; 5000 counts/s full scale; 0.55—0.75 MeV; full scale; standard deviation — 2.0%.

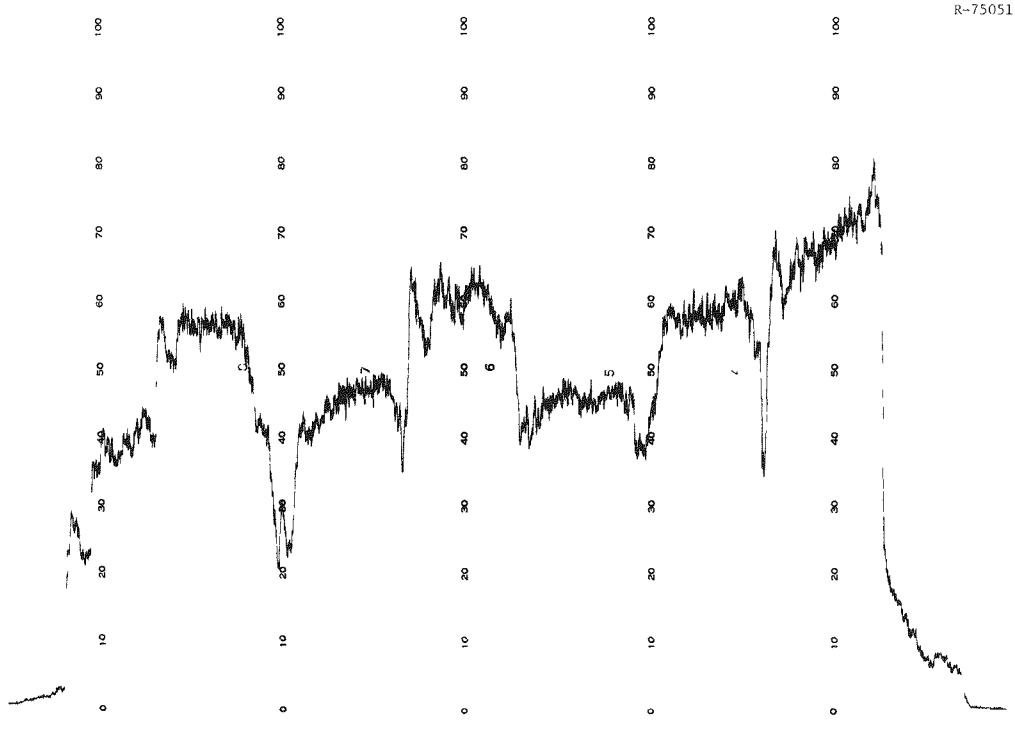

Fig. A.10. Recycle Test Element-1; Body 5; Across Hole 3. Top to bottom from left to right; 5000 counts/s full scale; 0.55—0.75 MeV full scale; standard deviation — 2.0%.

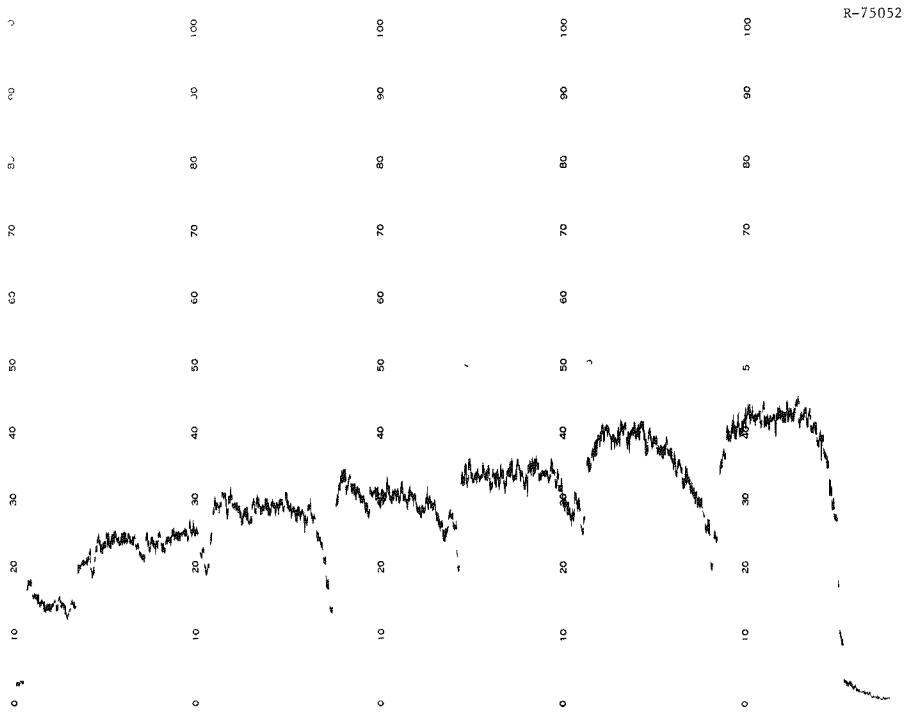

Fig. A.11. Recycle Test Element-1; Body 6; Across Hole 1. Top to bottom from left to right; 5000 counts/s full scale; 0.55–0.75 MeV full scale; standard deviation — 2.0%.

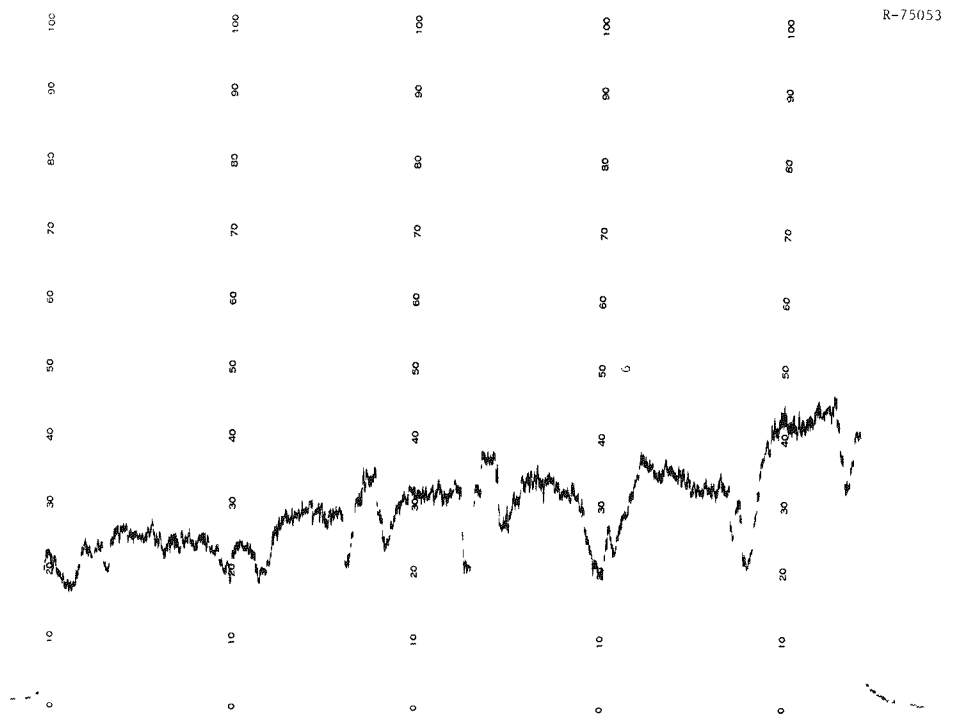

Fig. A.12. Recycle Test Element-1; Body 6; Across Hole 3. Top to bottom from left to right; 5000 counts/s full scale; 0.55–0.75 MeV full scale; standard deviation — 2.0%.

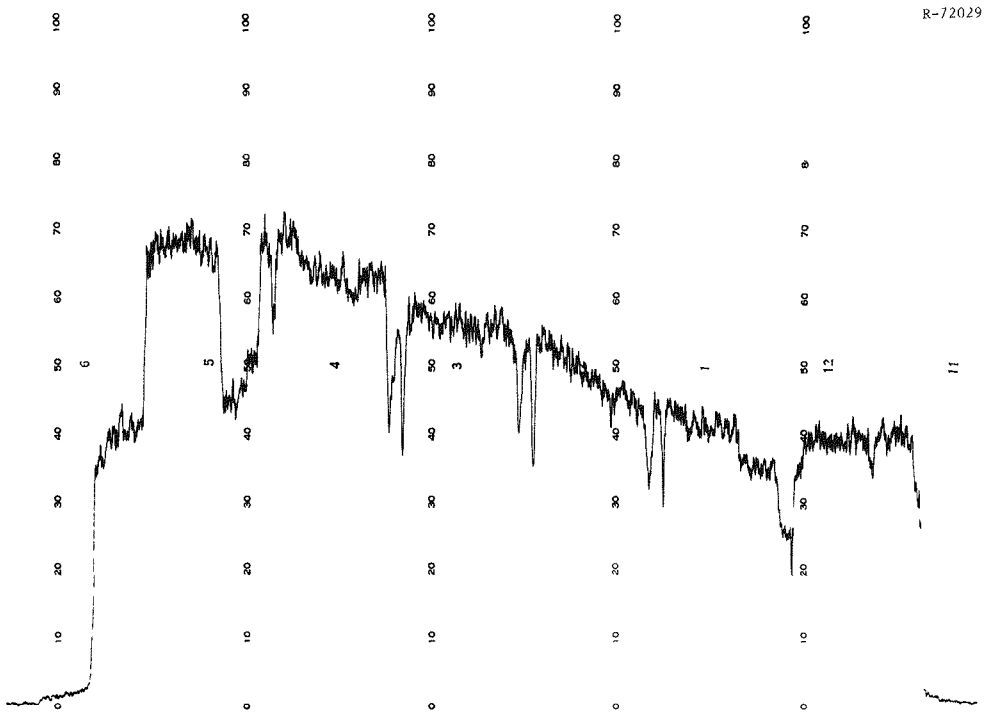

Fig. A.13. Recycle Test Element-5; Body 1; Across Holes 1 and 5. Top to bottom from left to right; 2500 counts/s full scale; 0.55–0.75 MeV full scale; standard deviation — 2.0%.

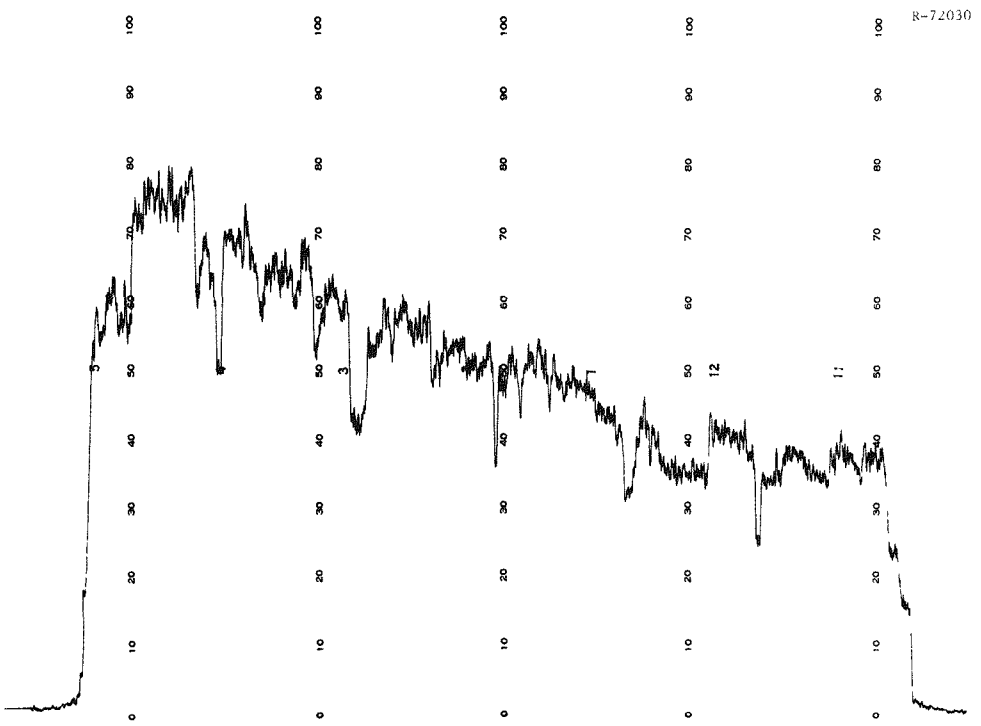

Fig. A.14. Recycle Test Element-5; Body 1; Across Hole 3. Top to bottom from left to right; 2500 counts/s full scale; 0.55–0.75 MeV full scale; standard deviation — 2.0%.

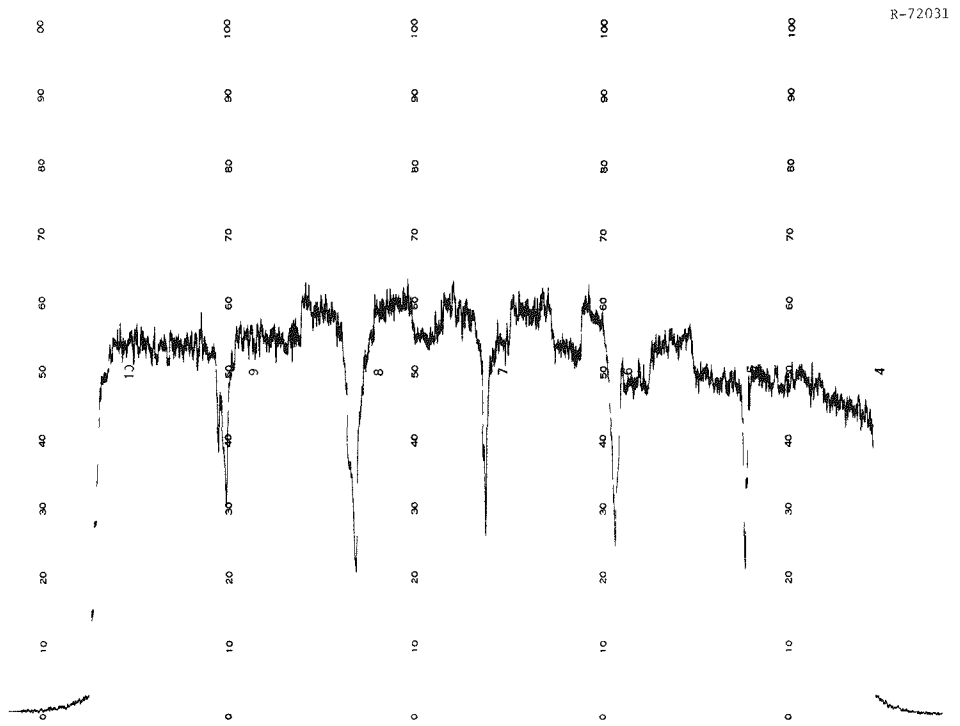

Fig. A.15. Recycle Test Element-5; Body 2; Across Hole 1. Top to bottom from left to right; 5000 counts/s full scale; 0.55–0.75 MeV full scale; standard deviation — 2.0%.

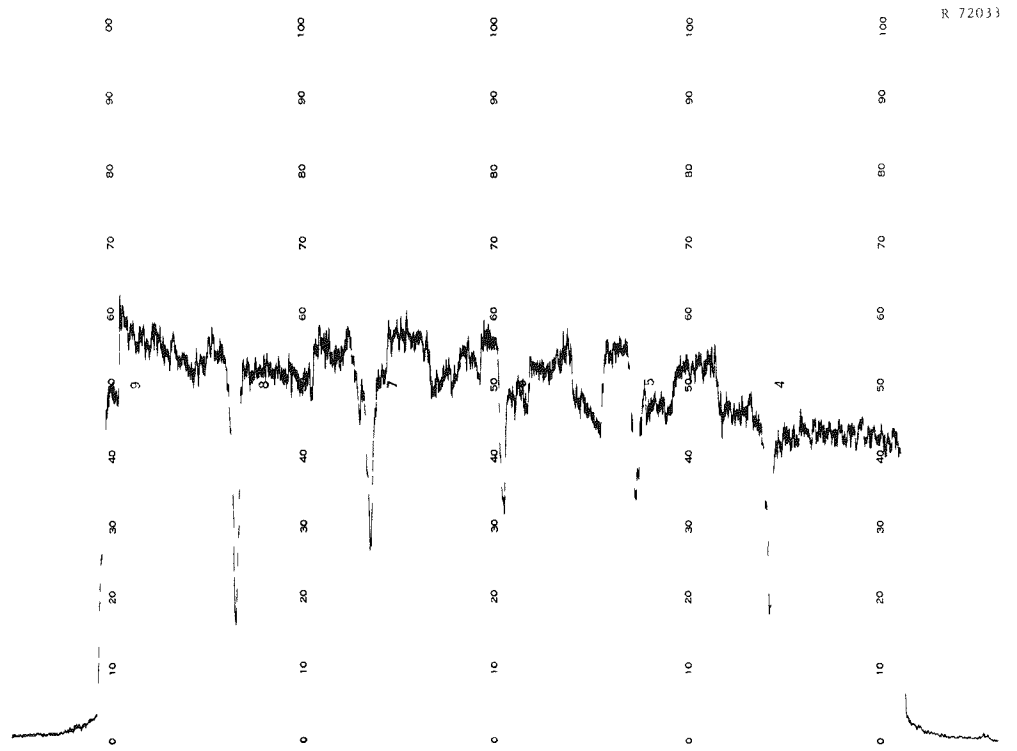

Fig. A.16. Recycle Test Element-5; Body 2; Across Hole 3. Top to bottom from left to right; 5000 counts/s full scale; 0.55–0.75 MeV full scale; standard deviation — 2.0%.

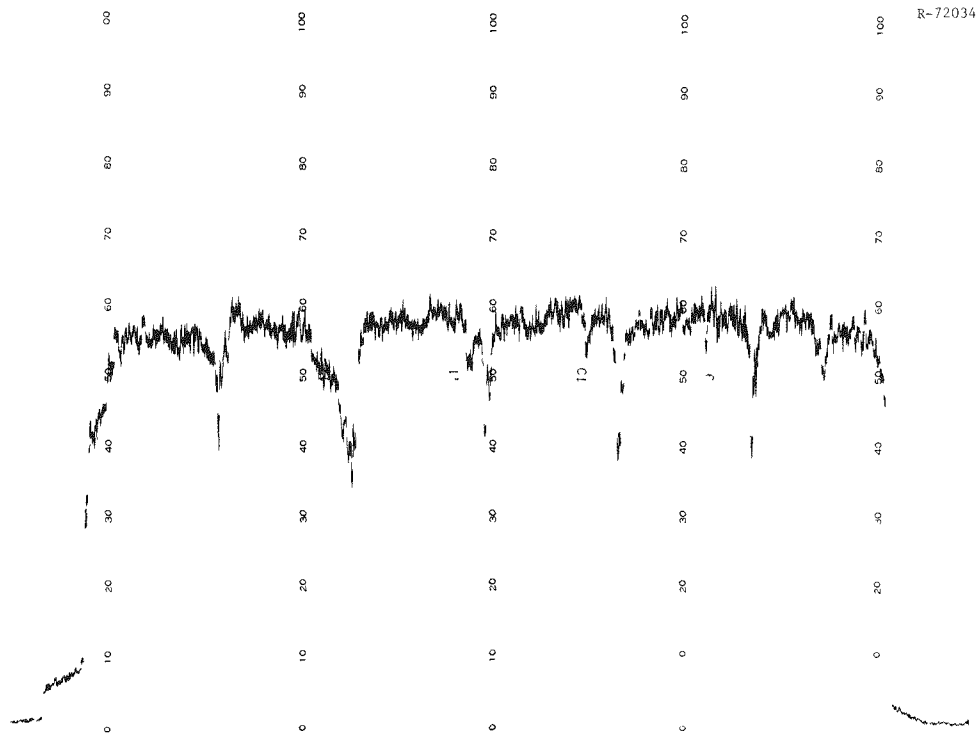

Fig. A.17. Recycle Test Element-5; Body 3; Across Hole 1. Top to bottom from left to right; 5000 counts/s full scale; 0.55–0.75 MeV full scale; standard deviation — 2.0%.

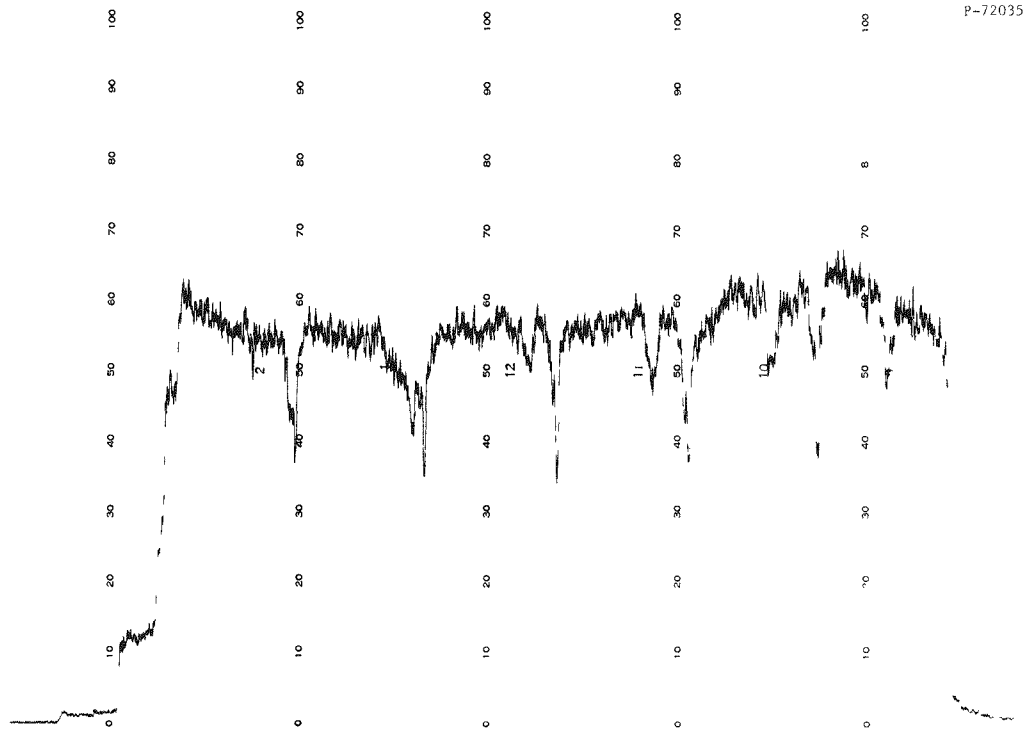

Fig. A.18. Recycle Test Element-5; Body 3; Across Hole 3. Top to bottom from left to right; 5000 counts/s full scale; 0.55–0.75 MeV full scale; standard deviation — 2.0%.

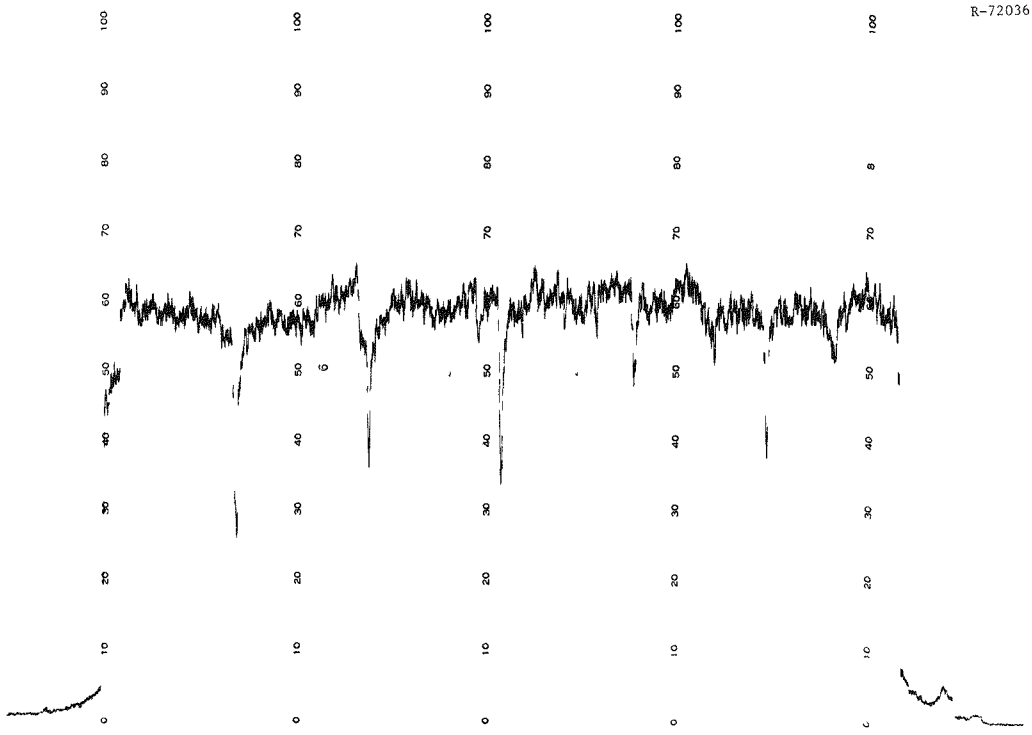

Fig. A.19. Recycle Test Element-5; Body 4; Across Hole 1. Top to bottom from left to right; 5000 counts/s full scale; 0.55–0.75 MeV full scale; standard deviation — 2.0%.

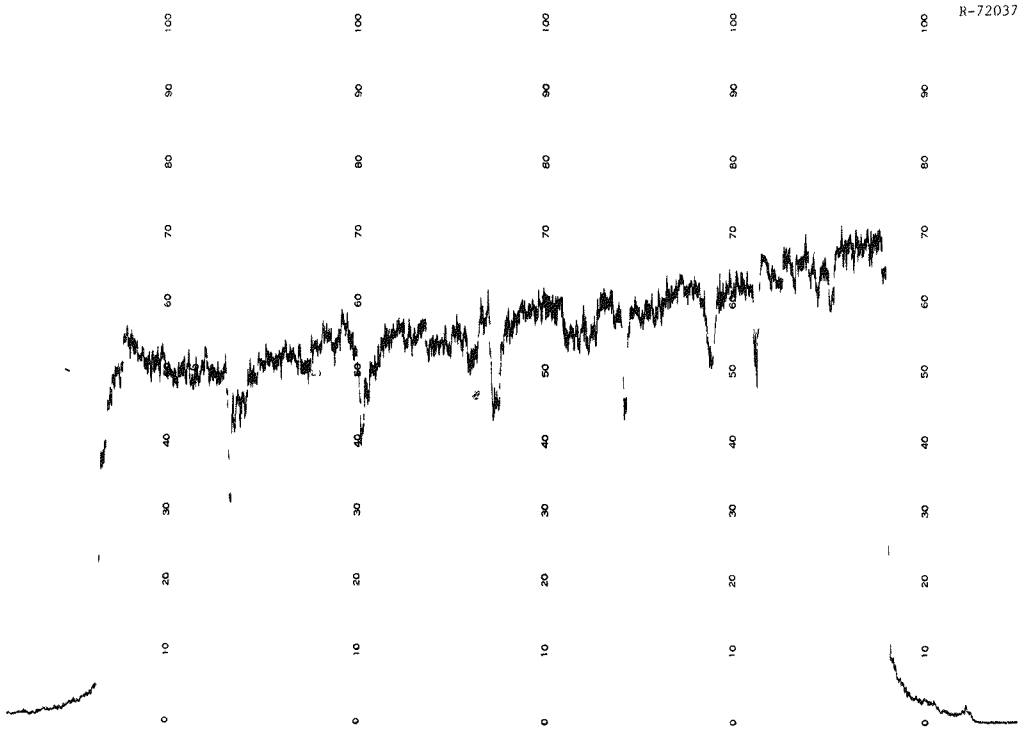

Fig. A.20. Recycle Test Element-5; Body 4; Across Hole 3. Top to bottom from left to right; 5000 counts/s full scale; 0.55–0.75 MeV full scale; standard deviation — 2.0%.

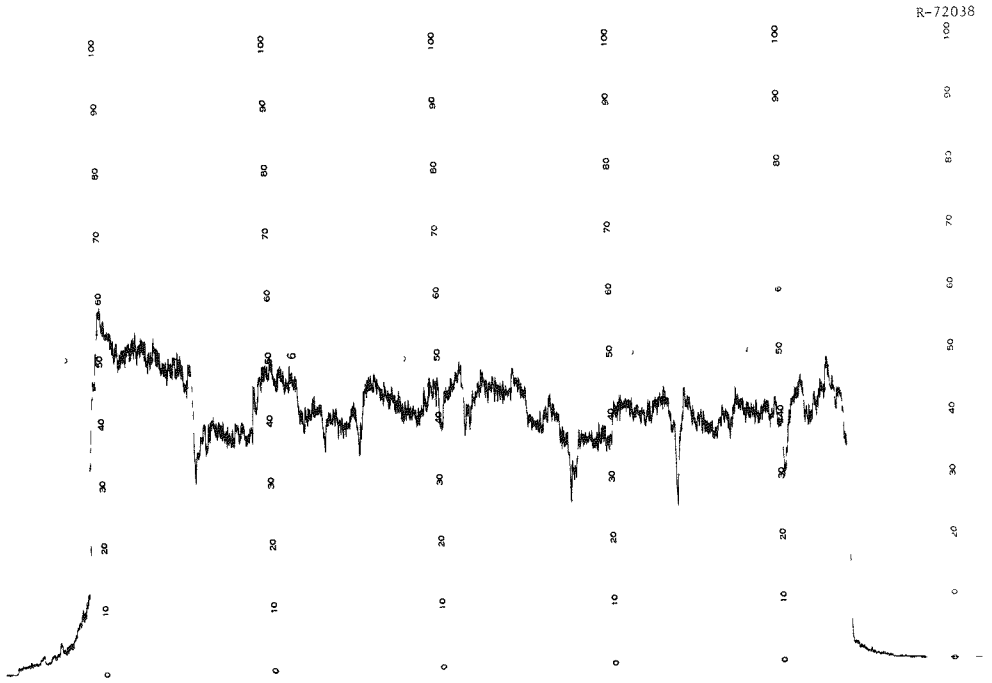

Fig. A.21. Recycle Test Element-5; Body 5; Across Hole 1. Top to bottom from left to right; 5000 counts/s full scale; 0.55–0.75 MeV full scale; standard deviation — 2.0%.

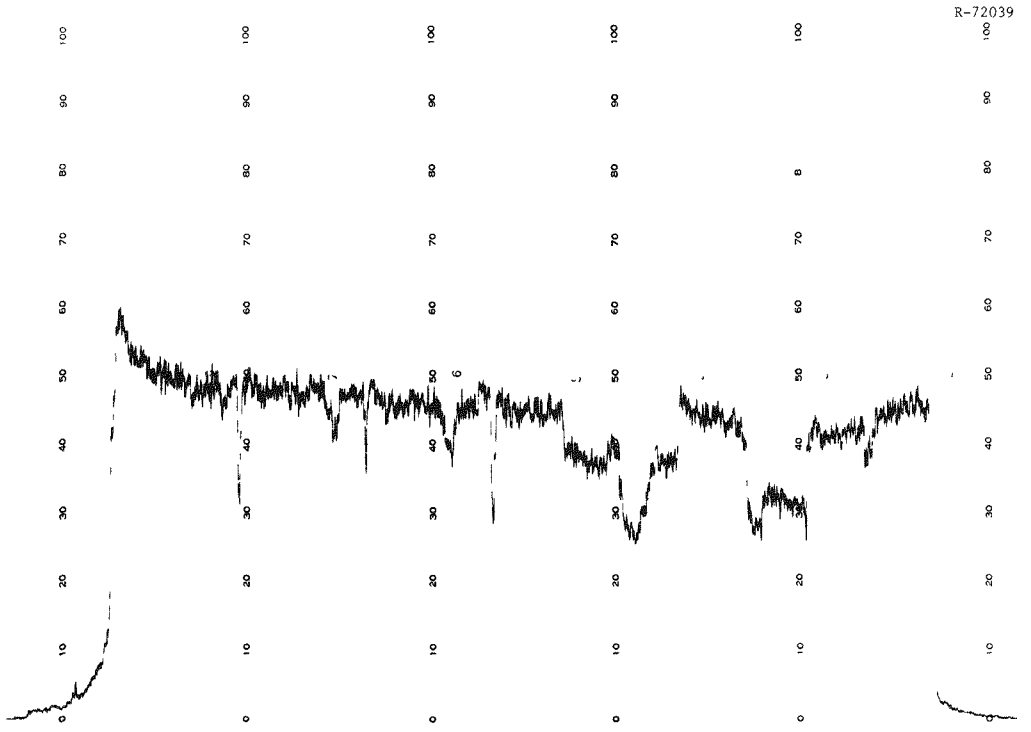

Fig. A.22. Recycle Test Element-5; Body 5; Across Hole 3. Top to bottom from left to right; 5000 counts/s full scale; 0.55–0.75 MeV full scale; standard deviation — 2.0%.

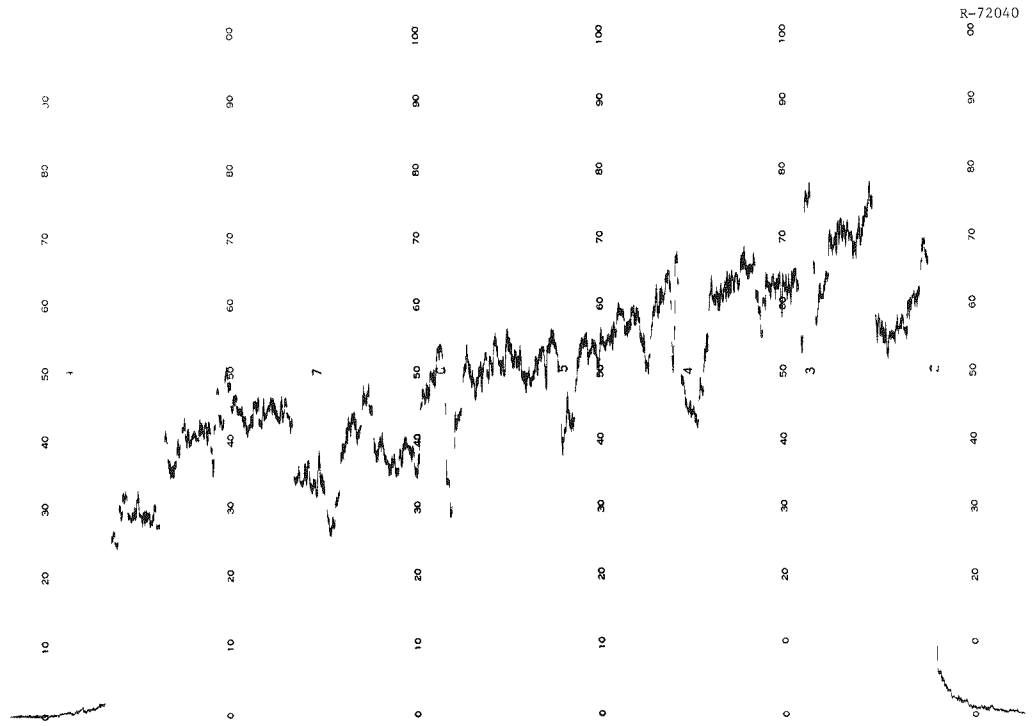

Fig. A.23. Recycle Test Element-5; Body 6; Across Hole 1. Top to bottom from left to right; 2500 counts/s full scale; 0.55–0.75 MeV full scale; standard deviation — 2.0%.

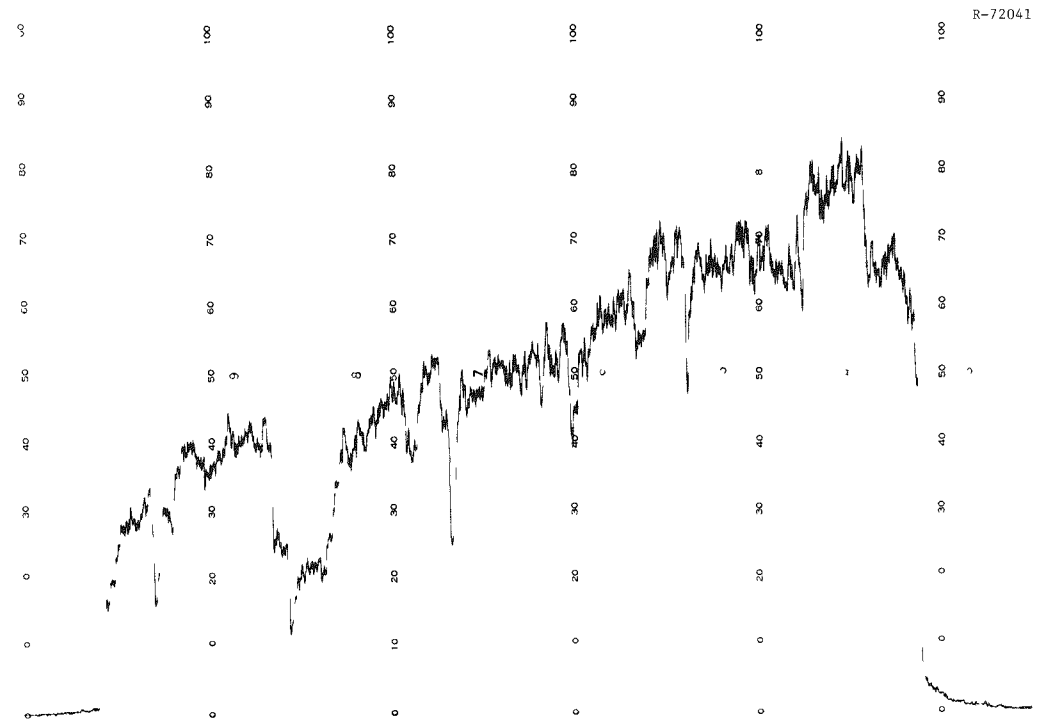

Fig. A.24. Recycle Test Element-5; Body 6; Across Hole 3. Top to bottom from left to right; 2500 counts/s full scale; 0.55–0.75 MeV full scale; standard deviation — 2.0%.

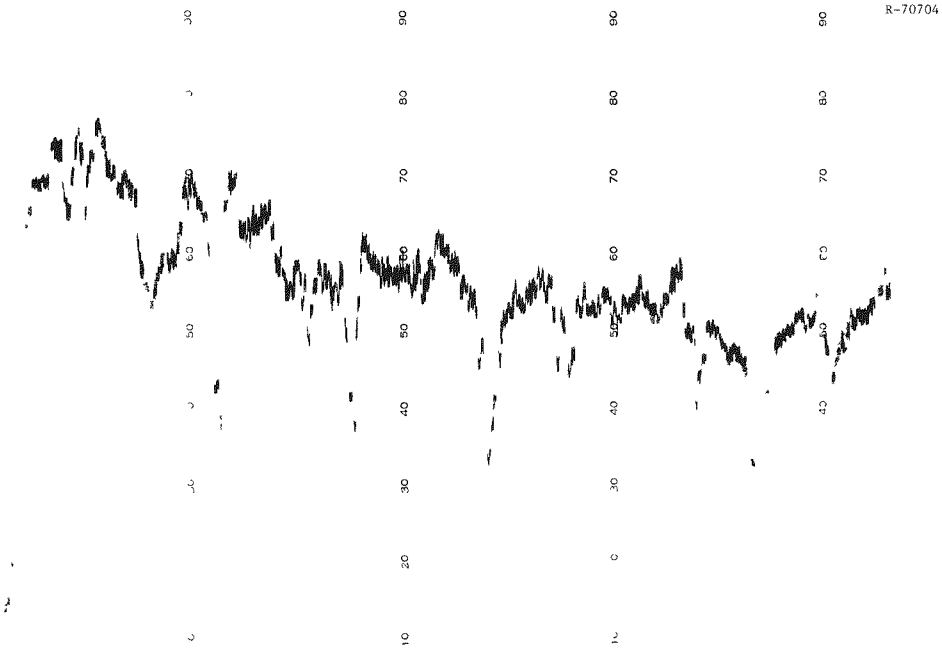

Fig. A.25. Recycle Test Element-6; Body 1; Across Hole 1. Top to bottom from left to right; 2500 counts/s full scale; 0.55–0.75 MeV full scale; standard deviation — 2.0%.

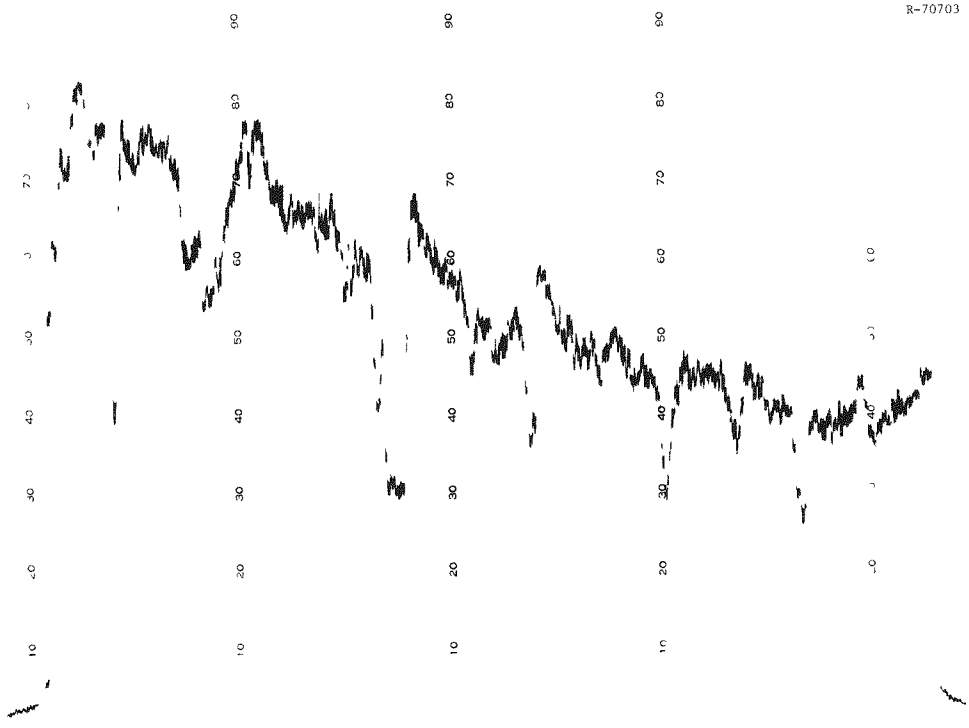

Fig. A.26. Recycle Test Element-6; Body 1; Across Hole 3. Top to bottom from left to right; 2500 counts/s full scale; 0.55–0.75 MeV full scale; standard deviation — 2.0%.

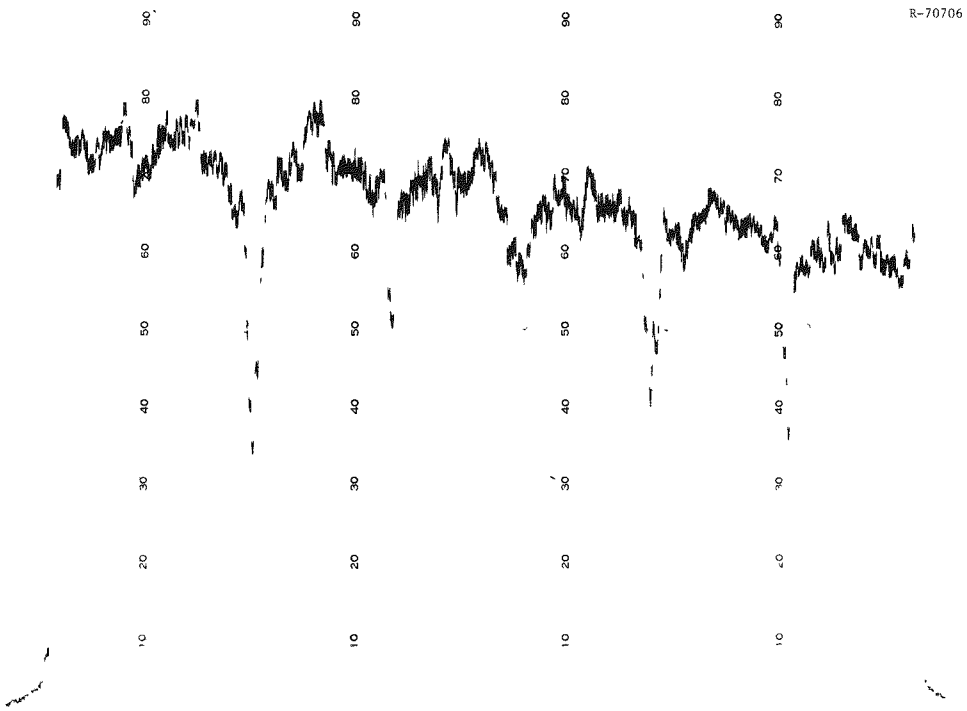

Fig. A.27. Recycle Test Element-6; Body 2; Across Hole 1; Top to bottom from left to right; 5000 counts/s full scale; 0.55—0.75 MeV full scale; standard deviation — 2.0%.

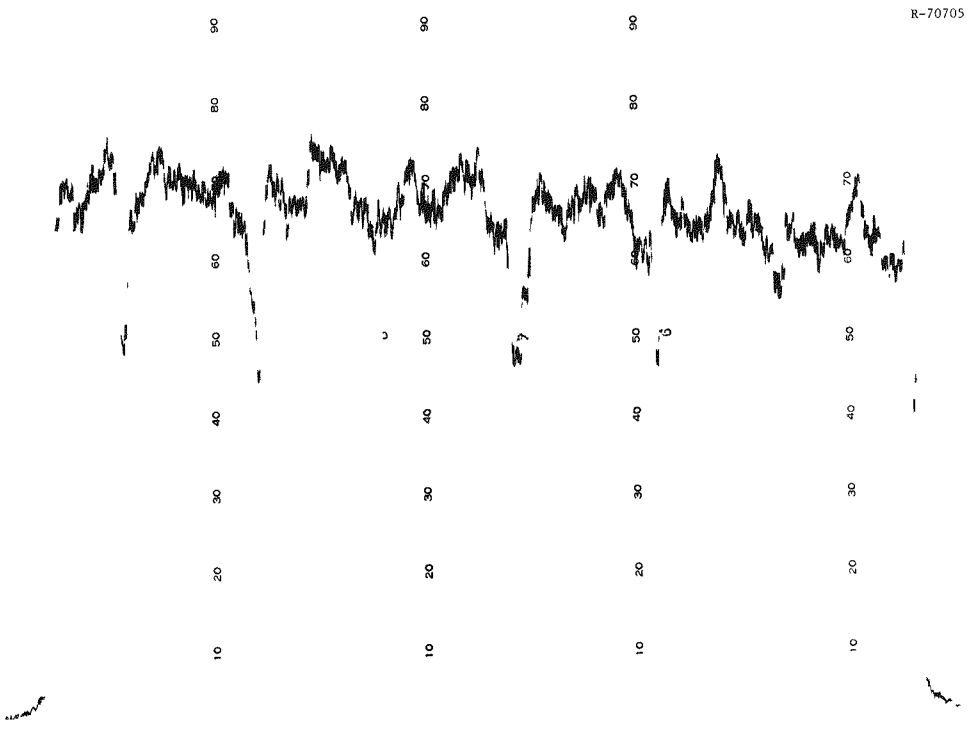

Fig. A.28. Recycle Test Element-6; Body 2; Across Hole 3. Top to bottom from left to right; 5000 counts/s full scale; 0.55—0.75 MeV full scale; standard deviation — 2.0%.

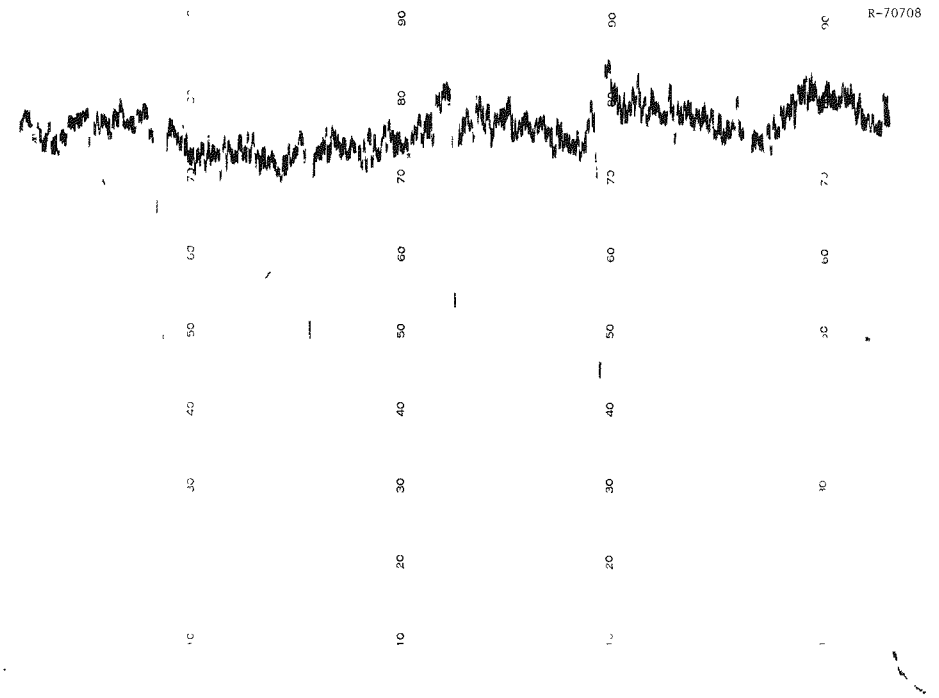

Fig. A.29. Recycle Test Element-6; Body 3; Across Hole 1. Top to bottom from left to right; 5000 counts/s full scale; 0.55—0.75 MeV full scale; standard deviation — 2.0%.

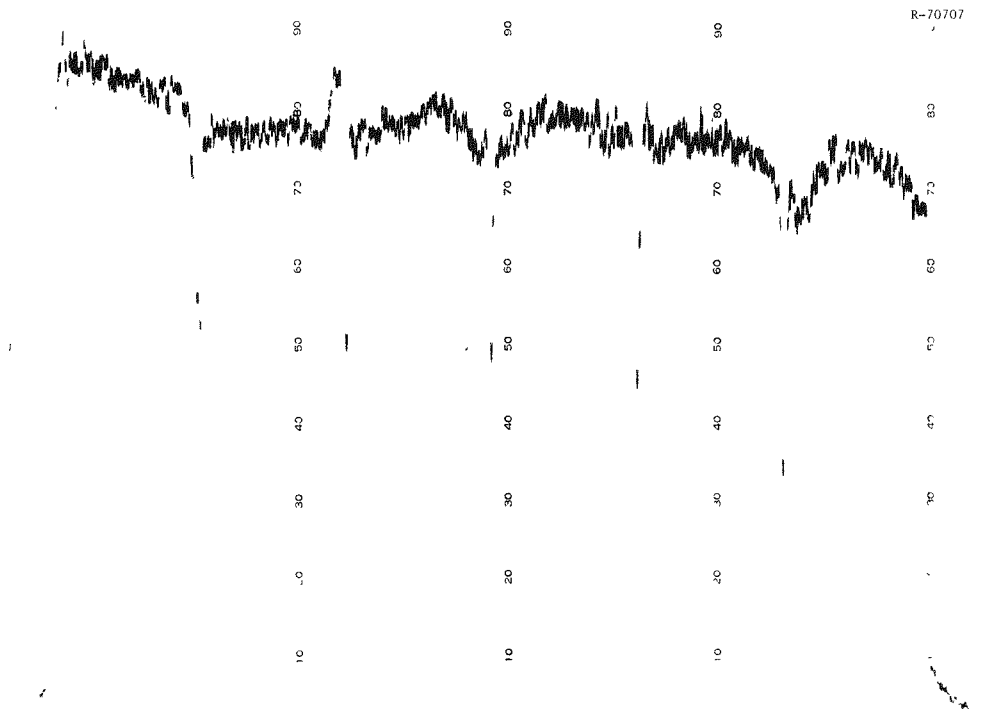

Fig. A.30. Recycle Test Element-6; Body 3; Across Hole 3. Top to bottom from left to right; 5000 counts/s full scale; 0.55—0.75 MeV full scale; standard deviation — 2.0%.

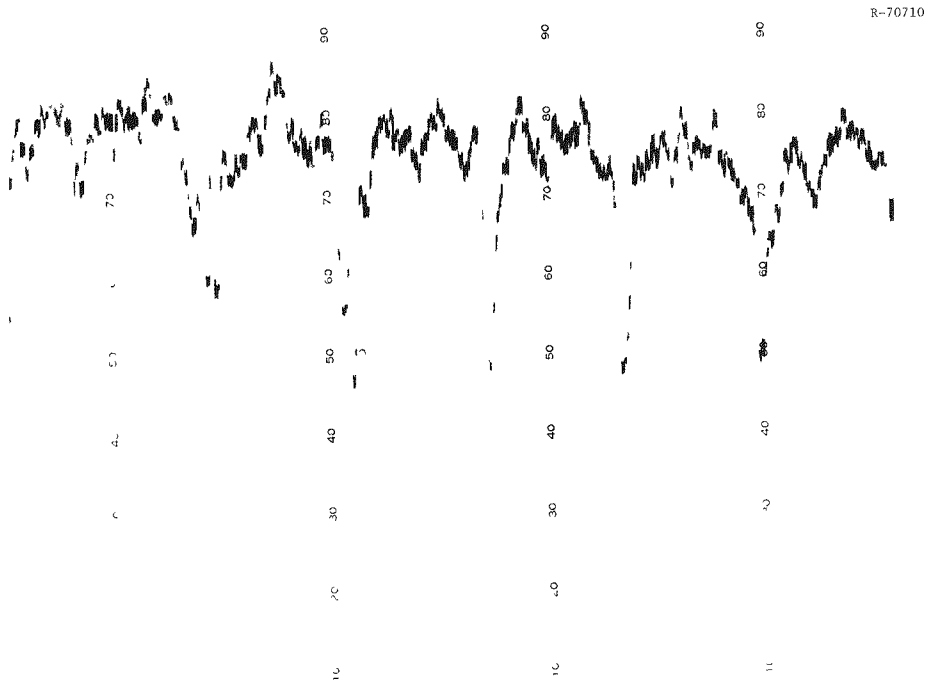

Fig. A.31. Recycle Test Element-6; Body 4; Across Hole 1. Top to bottom from left to right; 5000 counts/s full scale; 0.55–0.75 MeV full scale; standard deviation — 2.0%.

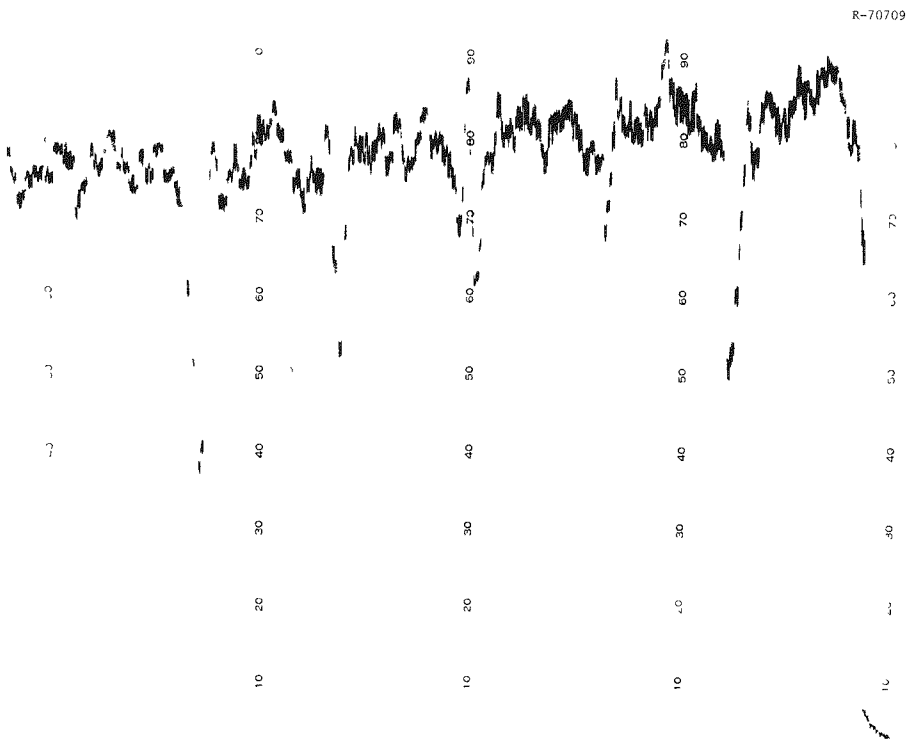

Fig. A.32. Recycle Test Element-6; Body 4; Across Hole 3. Top to bottom from left to right; 5000 counts/s full scale; 0.55–0.75 MeV full scale; standard deviation — 2.0%.

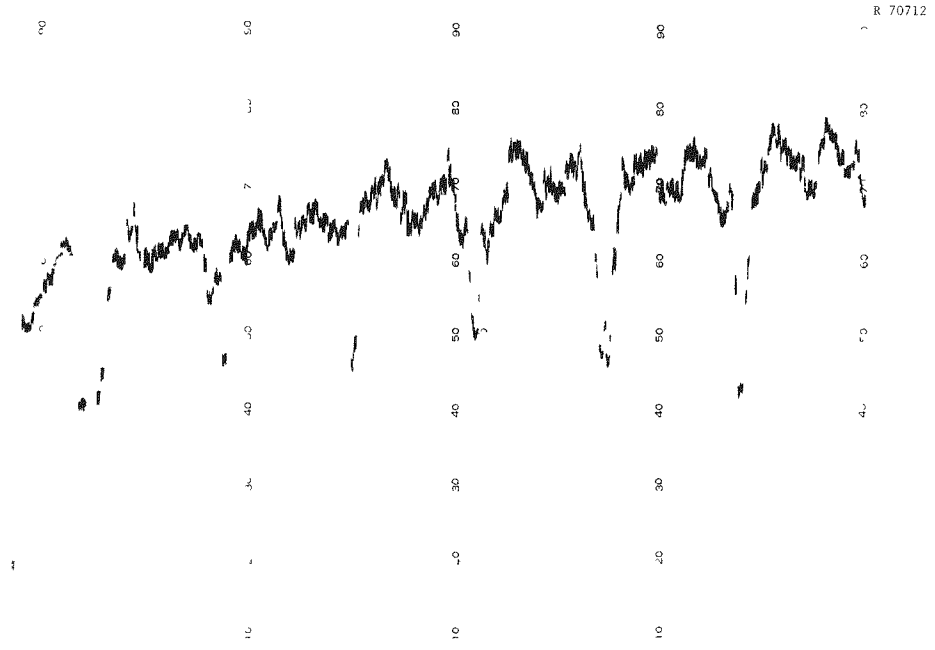

Fig. A.33. Recycle Test Element-6; Body 5; Across Hole 1. Top to bottom from left to right; 5000 counts/s full scale; 0.55—0.75 MeV full scale; standard deviation — 2.0%.

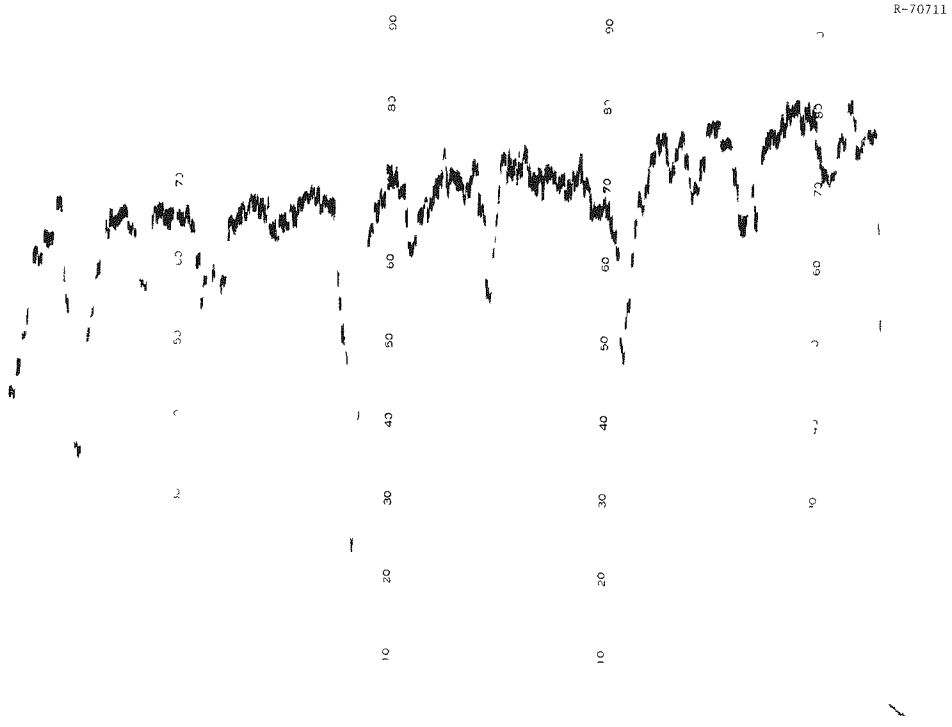

Fig. A.34. Recycle Test Element-6; Body 5; Across Hole 3. Top to bottom from left to right; 5000 counts/s full scale; 0.55—0.75 MeV full scale; standard deviation — 2.0%.

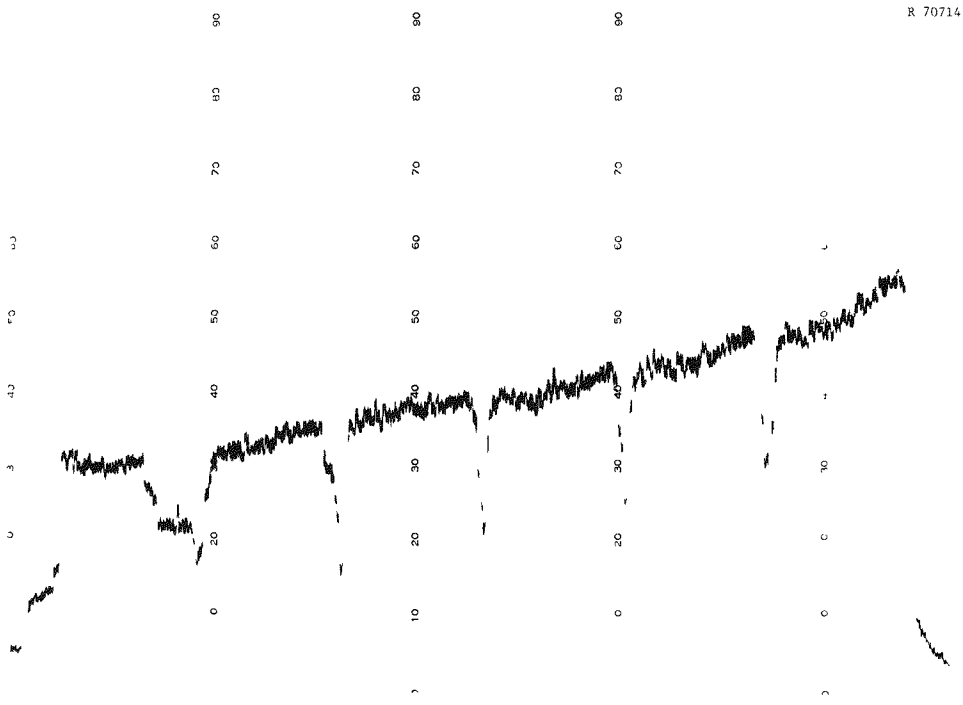

Fig. A.35. Recycle Test Element-6; Body 6; Across Hole 1. Top to bottom from left to right; 5000 counts/s full scale; 0.55—0.75 MeV full scale; standard deviation — 2.0%.

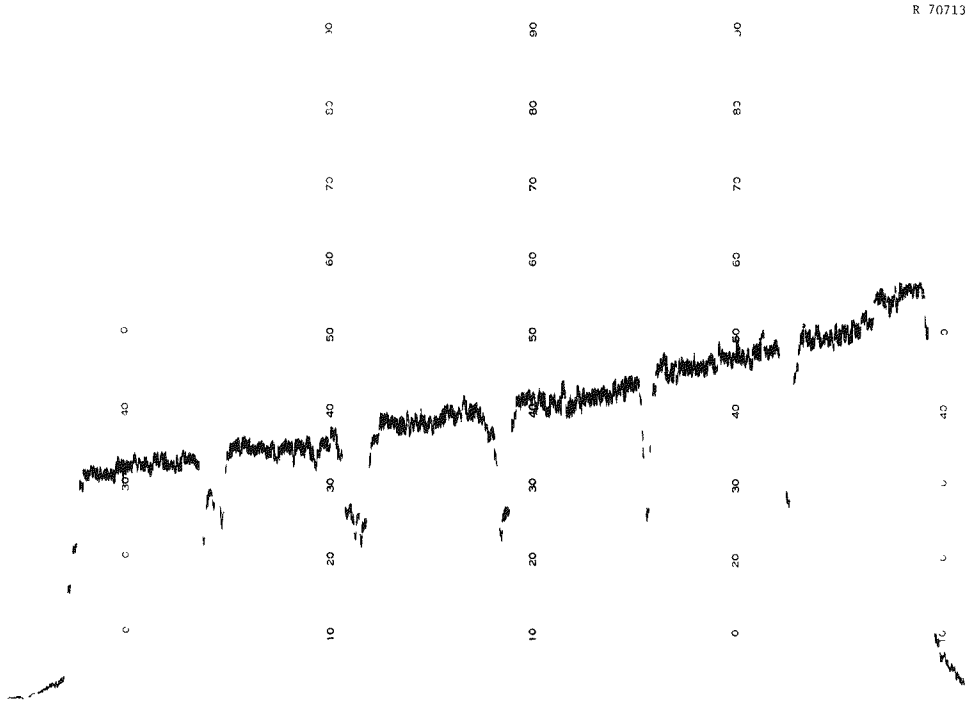

Fig. A.36. Recycle Test Element-6; Body 6; Across Hole 3. Top to bottom from left to right; 5000 counts/s full scale; 0.55—0.75 MeV full scale; standard deviation — 2.0%.

ORNL-5422
Distribution
Category UC-77

INTERNAL DISTRIBUTION

1–2. Central Research Library
3. Document Reference Section
4–6. Laboratory Records Department
7. Laboratory Records, ORNL RC
8. ORNL Patent Office
9. R. L. Beatty
10. B. J. Bolfing
11. R. A. Bradley
12. A. J. Caputo
13. R. S. Crouse
14. F. F. Dyer
15. C. L. Fitzgerald
16. R. F. Hibbs
17–19. M. R. Hill
20. F. J. Homan
21. J. A. Horak
22. R. R. Judkins
23. M. J. Kania
24–33. P. R. Kasten
34. W. J. Lackey
35. C. E. Lamb
36. B. C. Leslie
37. K. H. Lin
38. T. B. Lindemer
39–40. E. L. Long, Jr.
41. A. L. Lotts
42. J. E. Mack
43. A. D. Mitchell
44. K. J. Notz
45. A. R. Olsen
46. R. L. Pearson
47. J. P. Renier
48. J M Robbins
49. T. F. Scanlan
50. J. E. Selle
51. C. J. Sparks, Jr.
52. D. P. Stinton
53. S. M. Tiegs
54–58. T. N. Tiegs
59. V.C.A. Vaughen
60. D. R. Vondy
61. R. W. Balluffi (Consultant)
62. P. M. Brister (Consultant)
63. W. R. Hibbard, Jr. (Consultant)
64. M. J. Mayfield (Consultant)
65. N. E. Promisel (Consultant)
66. J. T. Stringer (Consultant)

EXTERNAL DISTRIBUTION

67–68. DOE DIVISION OF NUCLEAR POWER DEVELOPMENT, Washington, DC 20545

Director

69. DOE IDAHO OPERATIONS OFFICE, P.O. Box 2108, Idaho Falls, ID 83401

Barry Smith

70. DOE OFFICE OF PROGRAM MANAGEMENT, RESEARCH AND SPACE PROGRAMS, P.O. Box 81325, San Diego, CA 92138

J. B. Radcliffe

71. DOE SAN FRANCISCO OPERATIONS OFFICE, 1333 Broadway, Wells Fargo Building, Oakland, Ca 94612

Manager

72. DOE OAK RIDGE OPERATIONS OFFICE, P.O. Box E, Oak Ridge, TN 37830

Assistant Manager, Energy Research and Development

73–249. DOE TECHNICAL INFORMATION CENTER, Office of Information Services, P.O. Box 62, Oak Ridge, TN 37830

For distribution as shown in TID-4500 Distribution Category, UC-77 (Gas-Cooled Reactor Technology)

☆ U.S. GOVERNMENT PRINTING OFFICE: 1978-748-189/310